Charged ligands for direct ESI-MS analysis of catalytic reactions

by

Danielle Marie Chisholm
B. Sc., St. Francis Xavier University, 2004

A Dissertation Submitted in Partial Fulfillment
of the Requirements for the Degree of

DOCTOR OF PHILOSOPHY

in the Department of Chemistry

Supervisory Committee

Charged ligands for direct ESI-MS analysis of catalytic reactions

by

Danielle Marie Chisholm
B. Sc., St. Francis Xavier University, 2010

Supervisory Committee

Dr. J. Scott McIndoe, Department of Chemistry
Supervisor

Dr. Robin G. Hicks, Department of Chemistry
Departmental Member

Dr. Matthew Moffitt, Department of Chemistry
Departmental Member

Dr. Kevin Telmer, Department of Earth and Ocean Sciences
Outside Member

Abstract

Supervisory Committee

Dr. J. Scott McIndoe, Department of Chemistry
Supervisor

Dr. Robin G. Hicks, Department of Chemistry
Departmental Member

Dr. Matthew Moffitt, Department of Chemistry
Departmental Member

Dr. Kevin Telmer, Department of Earth and Ocean Sciences
Outside Member

Electrospray ionization mass spectrometry (ESI-MS) is well-established in the detection of large fragile organic molecules such as polymers, peptides and proteins. The study of catalysis by transition metal complexes is complicated by difficulties including ligand lability, complex neutrality and air- and moisture-sensitivity. This work is focused on establishing methods to solve these problems and to apply them to well-understood systems in order to establish credibility before applying them to new systems.

Attempts to synthesize a 2,2'-bipyridine (bipy)-type ligand designed to have proton sponge-like properties after binding to a metal are presented. The synthesis of 3,3'-*N,N'*-bis(dimethylamino)-2,2'-bipyridine was stymied by the formation of two strong intramolecular hydrogen bonds, which are clearly evident in the X-ray crystal structure of the isolated dimethylated 3,3'-bis(methylamino)-2,2'-bipyridine.

A simple, one step synthesis of a charge-tagged phosphine from commercially available precursors was developed. Monoalkylation of bisphosphines is a highly convenient

approach to such ligands, avoiding the multi-step routes demanded for phosphine/ammonium ligands. 4-diphenylphosphino-1-benzyldiphenylphosphonium-butane tetrafluoroborate was used for the investigation of hydrogenation of olefins by $RhCl(PPh_3)_3$ (Wilkinson's catalyst) by ESI-MS. The results obtained by ESI-MS and ESI-MS/MS on the speciation of the reaction as well as the potential reactivity of select species are in agreement with results obtained by traditional techniques. This work serves as a proof of principle that the methodology employed in our lab is suited to these investigations. The same ligand was used to examine the poorly understood dehydrocoupling of di(*n*-hexyl)silane by the same catalyst. Continuous monitoring of the reaction over 48 minutes added the time dimension to the data, and insight into the dynamics of the reaction was obtained. Key intermediates were observed, along with decomposition products and circumstantial evidence supporting the formation of a silylene intermediate was also obtained.

Lastly, some collaborative work is presented in which some of the techniques and methods developed in our laboratory were applied to problems of interest to other scientists. The formation of a heteronuclear ruthenium-gold cluster is monitored by ESI-MS and further analyzed by ESI-MS/MS. The characteristics that affect the surface activity of an ion are discussed and solutions of a dication with two different anions are examined. Biologically active ruthenium trimers were studied by EDESI-MS/MS, and their fragmentation behaviour shown to be analogous to their properties as CO-releasing molecules.

Table of Contents

List of Tables

List of Figures

List of Schemes

List of Abbreviations

BF_4^- – tetrafluoroborate

bipy – 2,2'-bipyridine

bmim – butylmethylimidazole

BPh_4^- – tetraphenylborate

CI – Chemical Ionization

CID – Collision Induced Dissociation

cod – cyclooctadiene

CORMs – Carbon monOxide Releasing Molecules

CRM – Charge Residue Model

dba – dibenzylideneacetone

DCM – dichloromethane

DMSO – dimethylsulfoxide

dppe – 1,2-bis(diphenylphosphino)ethane

EDESI – Energy Dependant Electrospray Ionization

EI – Electron Impact

ESI-MS – Electrospray Ionization Mass Spectrometry

hex – hexyl

IEM – Ion Evaporation Model

LAB – lithium-amino-borane reagent

m/z – mass to charge ratio

MALDI – Matrix Assisted Laser Desorption Ionization

MCP – microchannel plate

nbd – norbornene

nbs – *N*-bromosuccinimde

NMR – Nuclear Magnetic Resonance

PEEK - polyetheretherketone

PF_6^- – hexafluorophosphate

PPN^+ – bis(triphenylphosphoranylidene)ammonium

PPNCl – bis(triphenylphosphoranylidene)ammonium chloride

Tf_2N^- – bistriflimide

THF – tetrahydrofuran

ToF – Time of Flight

List of Structures

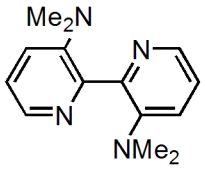

2.1

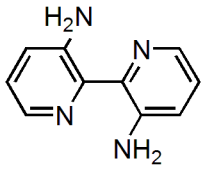

2.2

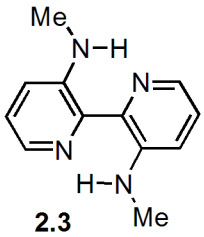

2.3

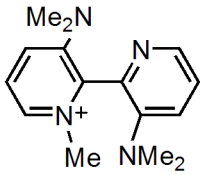

[2.4]$^+$

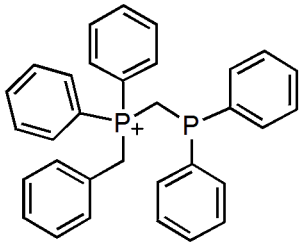

[3.1]$^+$

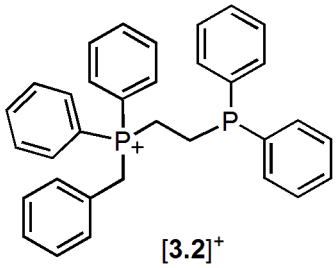

[3.2]$^+$

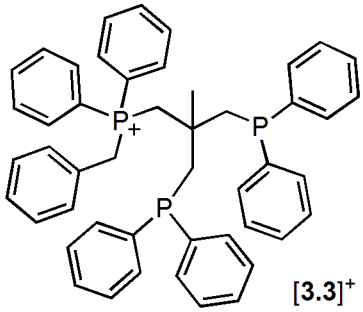

[3.3]$^+$

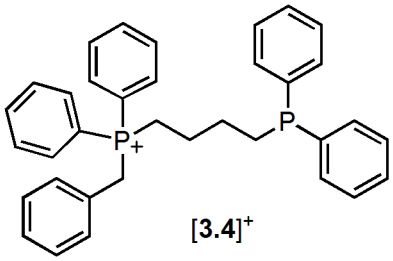

[3.4]$^+$

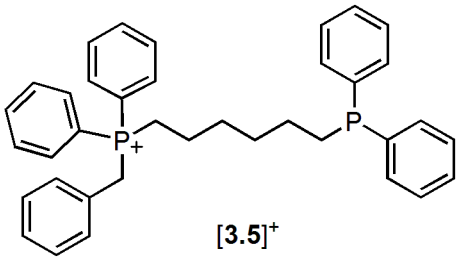

[3.5]$^+$

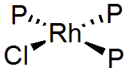

A

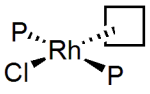

B

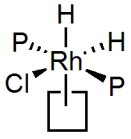

C

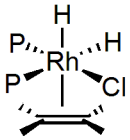

D

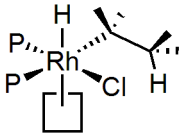

E

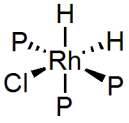

F

G

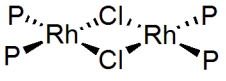

H

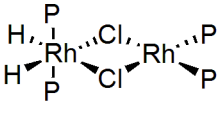

I

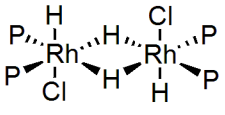

J

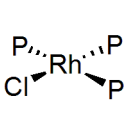

4.1

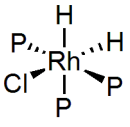

4.2

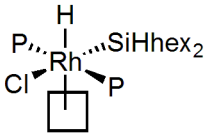

4.3

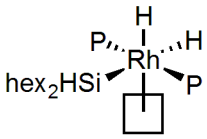

4.5

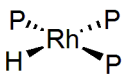

4.6

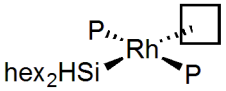

4.4

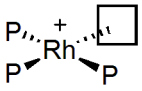

4.7

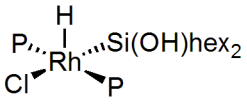

4.8

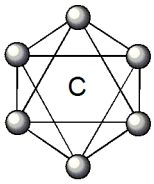

[**5.1**]$^{2-}$

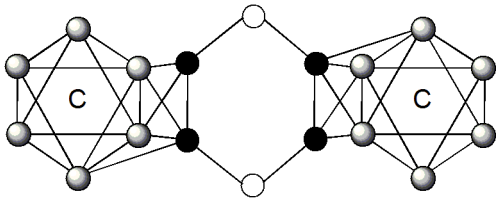

[{**5.1**Ag_2X}$_2$]$^{2-}$

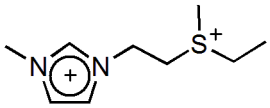

[**5.2**]$^{2+}$

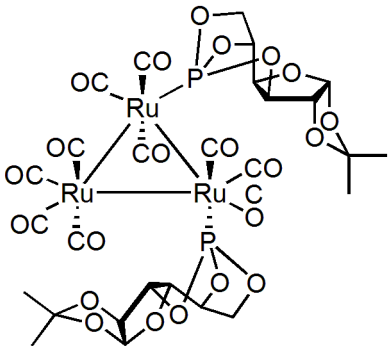

5.3

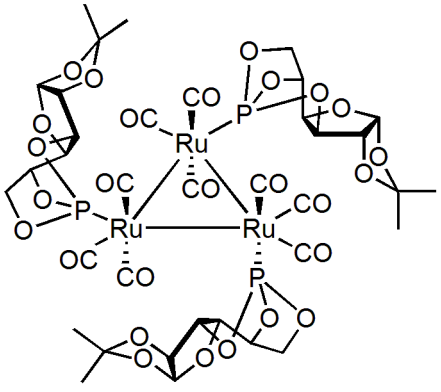

5.4

Acknowledgments

First off I would like to thank Scott for all of his guidance, support, encouragement and patience with my extremely neurotic tendencies. I have been lucky enough to come to school every day and work with my friends. Thank you to all past and present members of the McIndoe group (Nicky, Matt, Keri, Krista, Jen, Zohrab and Jingwei) and my fellow past and present graduate students across the department, for making every day enjoyable. Nicky and Keri, you are missed. Krista, thanks for listening. Matt, it's been a lot quieter these last 10 months. I've missed the noise.

I want to thank UVic faculty and staff for all their technical support and expertise, Dr. Robert MacDonald (University of Alberta) and Dr. Allen Oliver (University of Notre Dame) for X-ray crystallography.

Hardly anyone does anything important without the support of their family and friends. Thank you to Nichole, who got a lot more than she bargained for when she took me on as a T.A. Thank you to my family and friends at home who offered me support and encouragement every step of the way, even when I didn't know I needed it. Thank you to Mom and Dad who raised me to know that a little bit of hard work never really hurt anybody, and for their endless support. Lastly, and absolutely not least, thank you to Brendan. Helping me through this was more than I could have asked of anyone.

Dedication

For Brendan, Mom and Dad

Chapter 1. Electrospray Ionization Mass Spectrometry (ESI-MS)

1.1 Introduction

Mass spectrometry is an essential tool for the characterization of molecules. It involves the separation of ions in the gas phase by their mass-to-charge (*m/z*) ratio using electric (and sometimes magnetic) fields. Different types of mass spectrometers are defined as much by the way in which ions are formed in the source as by the way in which they are separated, and different types of sources will be dealt with first here.

The oldest and most well known mass spectrometer source is electron impact (EI).[1-3] A sample is introduced into the gas phase where it encounters a beam of energetic electrons. Energy is transferred from these electrons to the sample causing release of an electron from the analyte (producing a molecular ion $[M]^{\bullet+}$) and fragmentation of the newly energized molecule. Information is obtained from the fragmentation pattern of the analyte and the intensity of the molecular ion is often just a fraction of the spectrum's base peak. In an effort to retain molecular weight information, "soft ionization" techniques were developed. Chemical ionization (CI)[4,5] involves much the same process as EI with the exception that the energized electrons first make contact with a reagent gas which is present in high concentration with respect to the analyte. Proton transfer from this reagent gas to an analyte molecule gives the analyte a charge. Because collisions with the analyte are less energetic than in EI much less fragmentation is seen. The spectrum consists mainly of pseudomolecular ions in the form $[M + H]^+$.

Matrix-assisted laser desorption ionization (MALDI)[6,7] is another soft ionization technique. Tanaka[8] first described the analysis of high molecular weight molecules using a matrix. In MALDI, analyte molecules which have been co-crystallized with an organic matrix are energized with a laser. The sample is rapidly vaporized into the gas phase with the bulk of the energy being absorbed by the matrix. Once in the gas phase, the analyte becomes charged through interactions with the matrix to give mainly singly charged molecular ions. However, it has been the aromatic acids used by Karas and Hillenkamp that have proved more popular as matrices in modern MALDI-MS.[6] This development led Tanaka to share in the Nobel Prize for Chemistry in 2002, for developing soft ionization methods, with John Fenn who developed electrospray ionization (ESI).

ESI was developed in the late 1960s by Dole and co-workers[9] but was not applied to mass spectrometry until the early 1980s when it was coupled to a quadrupole mass analyser by Fenn and Yamashita.[10] Of all the soft ionization techniques ESI transfers the least amount of energy to the analyte molecules and minimal fragmentation is observed.[11] The common observation of cation-anion aggregates that have been transferred from solution into the gas phase is good evidence of this characteristic. Due to the gentle nature of ESI it quickly became popular in the study of large, fragile molecules such as polypeptides and proteins.[12,13]

1.2 Mechanism of formation of gas phase ions in ESI

Electrochemistry is fundamental to the mechanism of ESI. The capillary (through which the sample is introduced into the source) acts as one electrode and other components of the instrument (the baffle, the cone, mass analyzers, the detector) act as the other. Oxidation

(positive ion mode) or reduction (negative ion mode) of species will occur to generate excess charge[14] (cations in positive mode, anions in negative mode) due to a voltage applied to the capillary (Figure 1-1). The ions to be detected in ESI-MS must be pre-existing in solution and the species most likely to undergo this oxidation or reduction are counterions, solvent molecules or the capillary itself. The sample then exits the capillary in a Taylor cone[15] that has a surface enriched in cations if the instrument is operating in positive mode. When the repulsions due to charge density at the surface of the cone overcomes the surface tension of the solvent[16] droplets are formed, made up primarily of the surface of the cone, and therefore containing high concentrations of excess cations. Once a droplet is formed the excess charge is again found on the surface and the interior of the droplet is made up of ion-paired, charge-neutral species.[17,18] The droplets are surrounded by a warm bath gas (N_2) that in combination with a sheath gas surrounding the capillary (also N_2) promotes desolvation of the droplets.

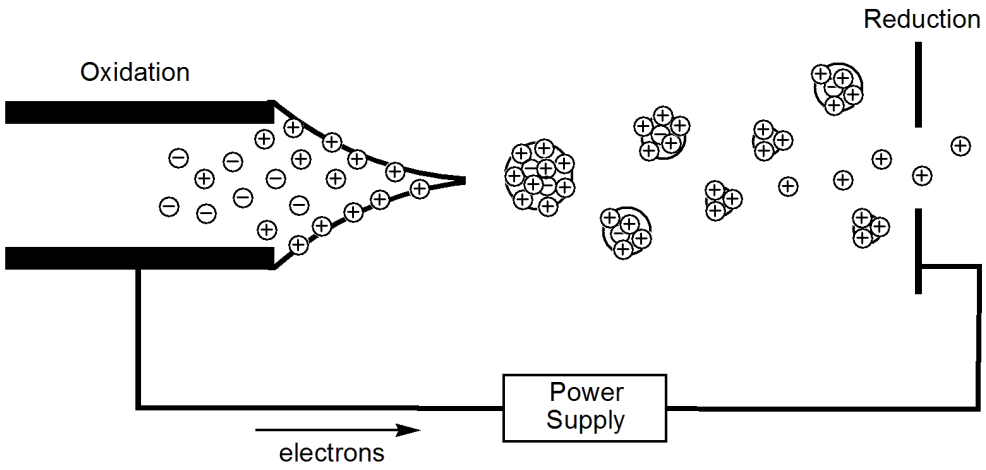

Figure 1-1. Schematic of an ESI source in positive ion mode. The solution is drawn out of the capillary into a Taylor cone. Droplets containing solvent, neutral molecules and enriched in cations are formed from the tip of the cone. The droplets are continually desolvated until they are bare gas-phase ions which then travel to the inside of the instrument to be analyzed. Redrawn from reference 17.

The mechanism of arriving at bare, gas phase ions from these charged droplets has been an ongoing topic of discussion. As the droplets decrease in size due to solvent evaporation the ions on the droplet surface are forced closer together and the repulsion between them increases. In order to relieve this concentration of charge two different processes are possible (Figure 1-2). The charge residue model (CRM)[9,19] describes continued fission of the droplet until the offspring droplets contain a single ion. The ion evaporation model (IEM)[20,21] states that at a certain charge density, a single ion is emitted from the surface of the droplet. Previous work in our group has shown direct observation of a solvated ion evaporating from a droplet.[22] Kebarle proposes that the IEM dominates when the ions in question are small (such as hydronium) and that the CRM is predominant for much larger molecules (such as proteins).[23] It seems most likely that both processes are occurring to some degree to arrive at fully desolvated species and that under certain conditions one mechanism may be more prominent that the other.

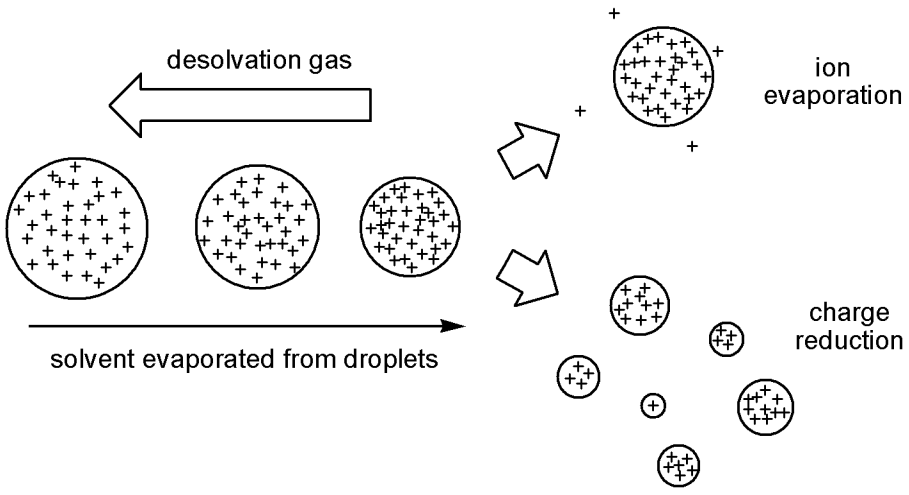

Figure 1-2. The desolvation process in ESI may occur through either ion evaporation or charge reduction. Redrawn from reference 24.

1.3 Factors influencing ESI response

The ESI–MS peak intensities for different species present at the same concentration in a single solution are not necessarily a reliable measure of their relative concentrations as the molecules may have different ionization efficiencies (the effectiveness with which ions are transferred from solution to gas phase during the ESI process). The determining factor is the surface activity of an ion; those that have a propensity to concentrate at the surface of a droplet will most efficiently make it into the gas phase. Surface activity is determined by a combination of factors[11,17,18,23,25] including concentration, the presence of other electrolytes, lipophilicty, acidity or basicity, charge density, ion pairing and solvent polarity. Investigations on the issues of ion pairing and solvent polarity are described in Chapter 5.

1.4 ESI as a means to monitor reaction progress

There are several factors that make ESI especially suitable to the study of reaction mixtures.

1.4.1 Detection of charged species

Generally, only species that carry a charge in solution are detected. Unlike other ionization sources, the ions detected in ESI-MS must be pre-existing in solution. Usually this means that the species is permanently charged or contains acidic or basic sites. Essentially only molecular ions ($[M]^+$) or adducts of molecular ions (e.g. $[M + H]^+$, $[M - H]^-$) are observed. Neutral molecules are not observed, an important fact when considering that the solvent is usually by far the most abundant compound in a reaction. Since interferences from the solvent are not problematic the use of expensive deuterated solvents, as with NMR, are not necessary. ESI-MS also allows for selectivity through design of permanently charged species. For example, if

metal-containing species are of particular interest an ESI-active ligand can be designed that will also make the metal complex ESI-active and neutral species that are not associated with the metal will not appear in the spectrum.

1.4.2 Minimal fragmentation

The particularly gentle nature of ESI coupled with the necessity of an already charged species provides simple spectra. This feature is especially beneficial when studying reaction mixtures. Again using NMR as an example, one analyte can have many peaks and monitoring reactions involving several species can generate spectra that quickly become complicated. In techniques such as IR, UV-Vis and NMR, similar types of species can generate overlapping signals. In ESI even structurally similar species will have only one (in most cases distinct) signal. The identity of a species can be confirmed by its mass-to-charge ratio (*m/z*), its isotopic distribution, its exact mass and through MS/MS techniques (MS/MS is described further in Section 1.5.1 .

1.4.3 The high sensitivity of ESI

The electrospray process is extremely efficient at transferring ions into the gas phase, with detection limits in the range of 10^{-6} to 10^{-9} molar. High sensitivity is an incredible advantage as it means that species can be monitored at the concentrations normally utilized in catalytic reactions, beneficial when dealing with expensive catalysts. Confirmation of identity of even the smallest peaks can be obtained by analysis of the isotope patterns and MS/MS experiments.

1.4.4 Continuous injection

The continuous flow of analyte provided by a syringe pump (and therefore continuous collection of data) is highly amenable to in-situ monitoring. It has become commonplace in our laboratory to monitor a reaction from beginning to end directly on the mass spectrometer. A reaction profile can be obtained by extracting a volume out of the reaction flask *via* syringe at time zero and monitoring the entire process as it proceeds in the syringe. The lag time between injection and detection is short and the initial moments of a reaction are easily captured; data that can easily be missed in other standard techniques. Real time information on the system is readily obtainable. While ESI-MS is not a reliable tool for discerning absolute concentrations in the absence of standards (see Section 1.3) the relative changes in peak intensity will reflect the progress of a reaction and may provide information on how species are related to one another.

1.5 Quadrupole-Time of Flight (Q-ToF)

In our laboratory, an ESI source is connected to a quadrupole-time-of-flight (Q-ToF) mass spectrometer (Figure 1-4).[24,26] Once the ions are sprayed into the source at atmospheric pressure (Figure 1-3) they are drawn into the instrument, perpendicular to the direction of the spray, through the sample (Figure 1-3, C) and extraction cone (Figure 1-3, E) by a pressure and voltage differential. Only a fraction of the ions actually make it into the instrument as much of the sample ends up on a baffle (Figure 1-3, B) located directly in line with the spray and after the cone. Inside this first chamber the remaining solvent is pumped away and the ions are drawn at a right angle into the main part of the instrument into a hexapole ion guide. This particular configuration is found in Waters/Micromass ESI instruments and is known as a Zspray™ source. It ensures that a minimum of neutral molecules enter the analyzer.[27]

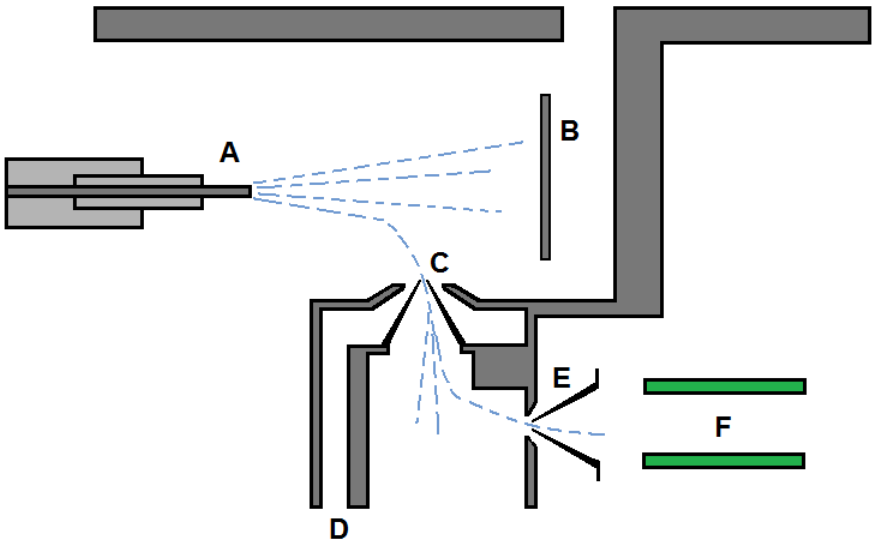

Figure 1-3. Schematic of the source in an ESI-MS. **A**: ESI capillary; **B**: baffle; **C**: sampling cone; **D**: inlet for cone gas; **E**: extraction cone; **F**: hexapole ion guide. (Not drawn to scale.) Redrawn from reference 27.

Once the ions leave the source they enter the mass spectrometer proper. The first section is a hexapole ion guide (Figure 1-4, C) where the ions are focused into a beam so that they all travel a similar path to the detector. The ions then enter a quadrupole mass analyser (Figure 1-4, D). Here, ions of specific *m/z* can be isolated through control of the applied voltage and all other ions will collide with the quadrupole and be dissipated. Those ions that have been selected travel to the collision cell (Figure 1-4, E) to undergo further analysis through fragmentation (Section 1.5.1). If fragmentation analysis is not desired the quadrupole and collision cell simply act as ion guides on the path to the detector.

After the ions pass through the collision cell a section of the beam is subjected to an electric pulse by the pusher (Figure 1-4, F) which redirects the group of ions towards the reflectron (Figure 1-4, G), positioned parallel to the beam. All of the ions in the beam do not travel

precisely the same path nor carry exactly the same kinetic energy. The pusher imparts a large amount of kinetic energy perpendicular to the ion beam so that the differences in directionality are relatively quite small. When ions reach the reflectron, (essentially an ion mirror) the ions with more kinetic energy travel further into the device (and consequently take longer to return to the detector) than those with less kinetic energy. Because of this, a group of ions entering the reflectron with the same *m/z* but differing kinetic energies will be focused with respect to time, arrive at the detector in a shorter time frame and result in sharper peak shape and higher resolution. The microchannel plate detector (MCP, Figure 1-4, H) is an electrified plate containing an array of electron multipliers that generate a current when an ion arrives at any of these multipliers. Many thousands of spectra are collected each second and are summed to give high signal to noise ratios.

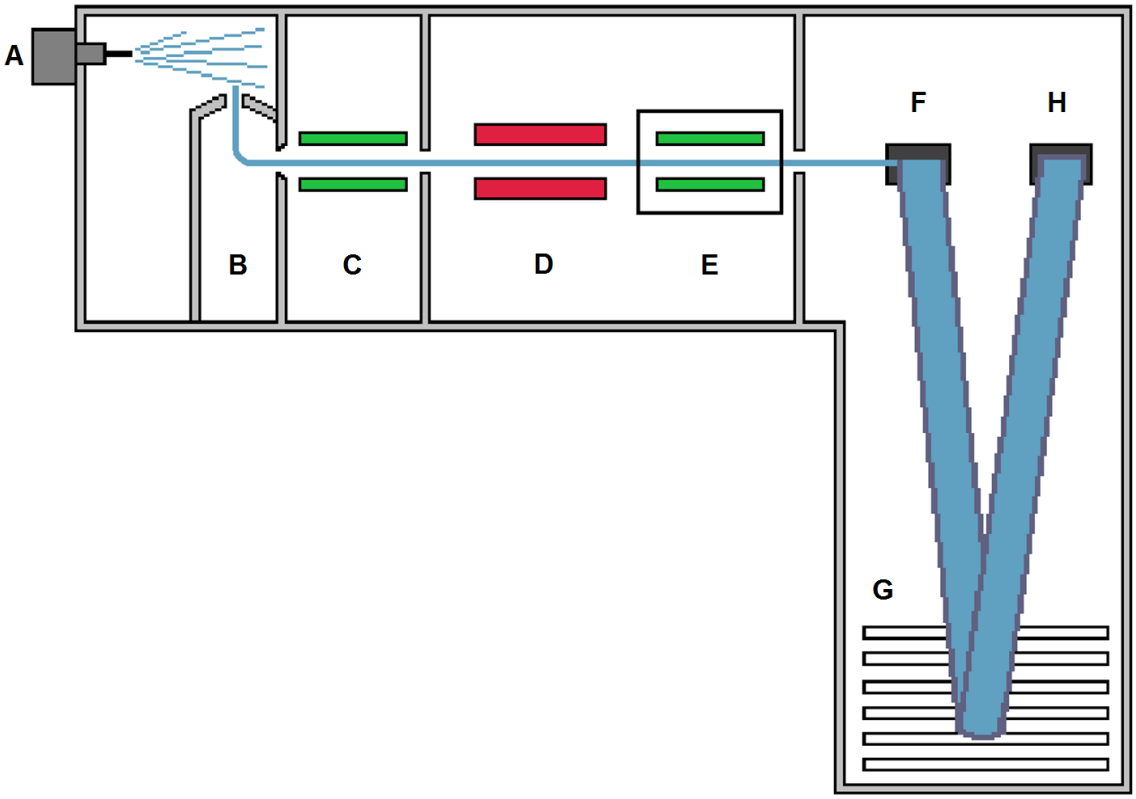

Figure 1-4. Cartoon of a Q-ToF Micro instrument. **A**: ESI source; **B**: cone; **C**: hexapole ion guide; **D**: quadrupole mass analyser; **E**: hexapole collision cell; **F**: pusher; **G**: reflectron; **H**: MCP detector.

In simple experiments the ions essentially travel unchanged from the first hexapole ion guide until they reach the ToF detector where they are separated based on their *m/z* (ESI-MS). In more in-depth analyses the ions can undergo mass selection in the quadrupole and fragmentation in the collision cell (ESI-MS/MS).

1.5.1 Collision Induced Dissociation (CID)

Sometimes a peak is not easily identifiable from its *m/z* and isotope pattern or definitive confirmation is needed and in these cases the molecule can be further studied through fragmentation. The way a molecule fragments can give clues to the functional groups that make up a compound and putting the pieces back together can help in identification of unknown

species. Organometallic and coordination complexes typically fragment through loss of L-type ligands (charge-neutral ligands), lost as stable neutral molecules (e.g. CO, PPh_3). If CID analysis is desired the species of interest is usually isolated by its *m/z* in the quadrupole and arrives in the collision cell without complication from other species in the sample (ESI-MS/MS). However, collision induced dissociation (CID)[24] can be carried out in two locations within the ESI-QToF instrument.

The collision cell is typically filled with a neutral, inert gas (e.g. argon). The ions of interest are accelerated into contact with the inert gas. Upon contact there is transfer of translational energy into vibrational energy of the bonds of the ion. If the ion collides with sufficient energy the resulting vibrations will be enough to cause fragmentation of the selected ions. Not only can CID provide structural information but also information on relative bond strengths within a given system. Larger, heavier ions (such as proteins or polymers) and stronger bonds will require greater acceleration (higher voltages) to promote fragmentation. Information of this type is useful in catalytic investigations because it provides a way to assess the relative strength of association of a metal to a set of ligands or substrates.[28] Once data has been collected at a series of voltages the spectra can be combined to give a fragmentation profile of the analyte.

Fragmentation of ions can also occur in the source of the instrument, if so desired. The area behind the sampling cone is under reduced pressure so sufficient acceleration is possible and the neutral molecules involved in the collisions are residual solvent or desolvation gas. It is possible to induce dissociation of the analyte molecule by careful control of the voltage applied to the cone within the source[29] (Figure 1-4, B). In this way it is possible to generate reactive fragments

before they pass into the quadrupole mass filter so that they may be mass-selected then exposed to a reactive gas in the collision cell. Other implications of operating at high cone voltage are discussed in Chapter 3.

Use of non-reactive gas (e.g. argon) in the collision cell is appropriate under standard conditions when simple fragmentation information is desired. However, the collision cell can contain other gases allowing the investigation of reactions in the gas phase. A reactive intermediate that has been generated in the cone can be introduced to a gas in the collision cell and the ensuing speciation can be monitored. For instance, we have shown that the generation of $RhCl(PPh_3)(Ph_2P(CH_2)_4PPh_2Bn^+)$ through phosphine dissociation at the cone and the introduction of propylene into the collision cell leads to production of $RhCl(PPh_3)(Ph_2P(CH_2)_4PPh_2Bn^+)$(propylene).[30] Further discussion on this system can be found in Chapter 3. Alternatively, a reactive gas can be introduced at the cone (Figure 1-3, C) and the products of the reaction then examined in the collision cell, as demonstrated in our group through the C-H activation of various hydrocarbons by anionic ruthenium carbonyl clusters.[31]

Comparison of CID data to data collected of a solution can provide information about what is actually present in solution and what species are generated from various conditions in the ESI process. (Even though ESI is a soft ionization technique, some molecules are inherently fragile and even the amount of energy required to obtain an acceptable spectrum is enough to cause fragmentation.) These types of details are important when working out the appropriate conditions for an experiment to ensure that the spectrum obtained is representative of actual solution phase speciation.

1.5.2 Energy Dependent ESI-MS/MS (EDESI-MS/MS)

For simple analytes a summation of the data collected at various voltages during a CID experiment will present an easily understood picture of sequential fragmentation. In other circumstances there can be several processes occurring at different times that complicate the spectrum after summation. The two dimensional presentation of a summation plot describes *m/z* and ion intensities only, and resembles a normal mass spectrum. The information about the energy at which a given fragmentation has occurred is not represented. The use of a contour map can provide clear presentation of peak intensities at all voltages. Together with a summation plot, the method of presenting EDESI data effectively shows three pieces of important data in two dimensions.[32] An example is shown in Figure 1-5.

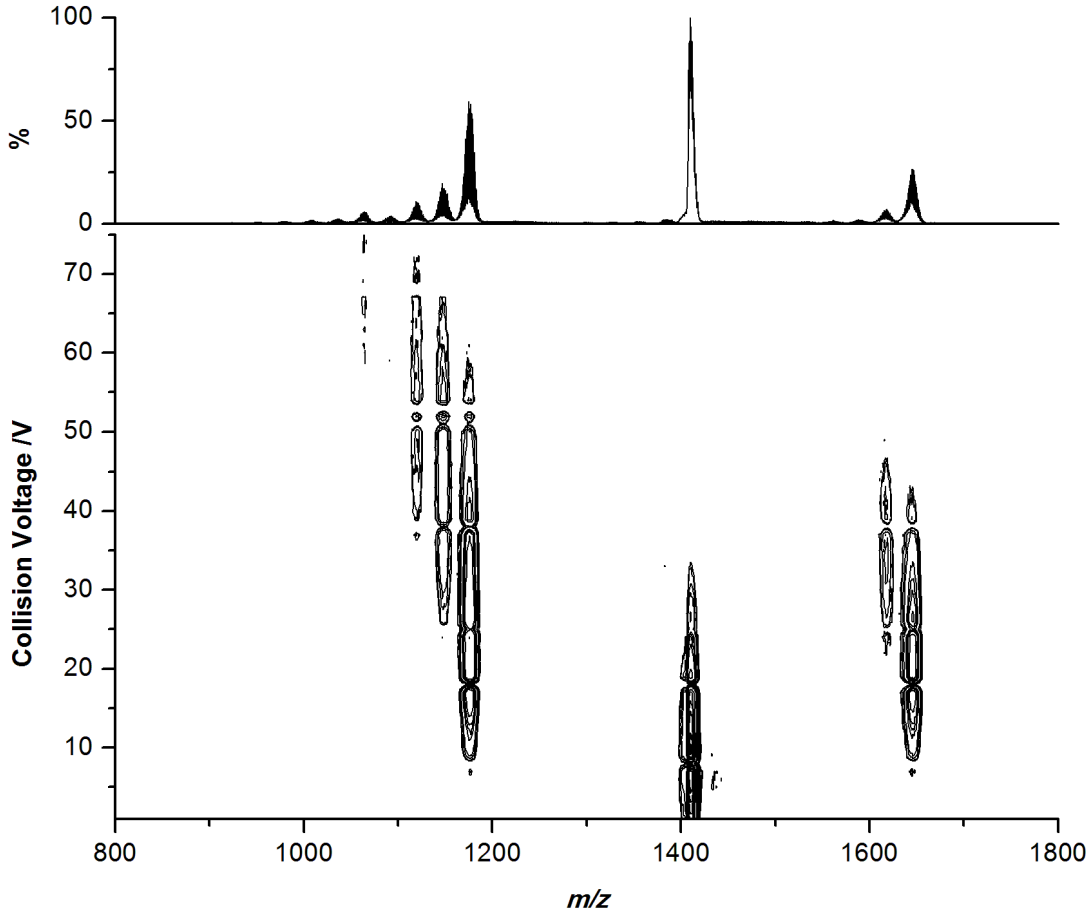

Figure 1-5. EDESI-MS/MS plot of the fragmentation of $[\{RuC(CO)_{16}Ag_2I\}_2]^{2-}$ at 1410 *m/z*. The dimeric anion is split into two monomers with different *m/z* values followed by sequential loss of carbonyl ligands.

1.6 ESI-MS in catalytic investigations

1.6.1 Charged metal complexes

The study of catalytic reactions by ESI-MS can be achieved in several ways. Relying on the dissociation of an ionic ligand to confer a charge on the metal center has been a popular means to examine the nature of the metal-containing species in a mixture. Several examples of this methodology follow. These examples are by no means meant to be a comprehensive list but serve as examples of the types of solution phase reactions that have been studied by ESI-MS in this way.

Vicent and co-workers[33] used ESI-MS to fully characterize the hydrosilylation of terminal alkynes via an iridium carbene complex (Scheme 1-1). The complexes under investigation had previously been shown to be poor catalysts for this transformation, and the study aimed to take advantage of the slow reactivity to identify intermediates. The system was monitored at regular intervals until the reaction was complete by performing a sample dilution directly out of the reaction vessel followed by introduction into the mass spectrometer. The metal complex became ESI-active through loss of the chloride ligand to give a positively charged metal center. Due to the fragile nature of the species the spectra were collected at a cone voltage of just 5 V and solvent coordinated species were observed. Studies of the hydrosilylation of phenylacetylene and 4-aminophenylacetylene under functional catalytic conditions allowed, for the first time, the detection and characterization of all reactive intermediates in this process.

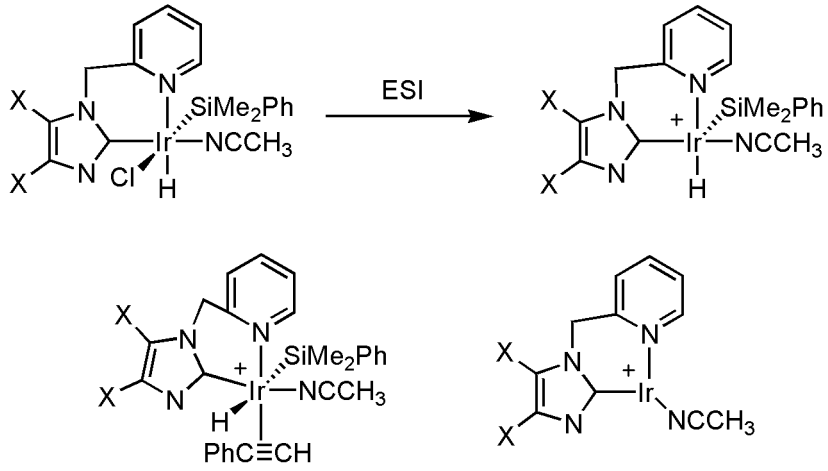

Scheme 1-1. This iridium complex investigated by Vicent *et al.* relies on the loss of Cl^- for it (top) and all related intermediates (examples shown, bottom) to be detectable by ESI-MS. X = H or Cl.

In 1994 Aliprantis and Canary[34] utilized ESI-MS for the direct observation of intermediates of the Suzuki coupling of bromopyridines and aryl boronic acids (Figure 1-6) by $Pd(PPh_3)_4$ under catalytic conditions. Intermediates were observed after oxidative addition of the bromopyridine

to the Pd(0) center, either by loss of bromine or protonation of pyridine, to give $[Pd(pyH)(PPh_3)_2Br]^+$ or $[Pd(py)(PPh_3)_2]^+$ respectively. The transmetalation intermediate $[Pd(pyH)(PPh_3)_2(Ar)]^+$ was observed (only as the pyridinium) after addition of the boronic acid to the reaction mixture. Signals for the pyridine starting material and coupled product were also readily observed due to the basic nature of the pyridine nitrogen. A series of acids was used and the reaction was monitored by sampling at regular time intervals.

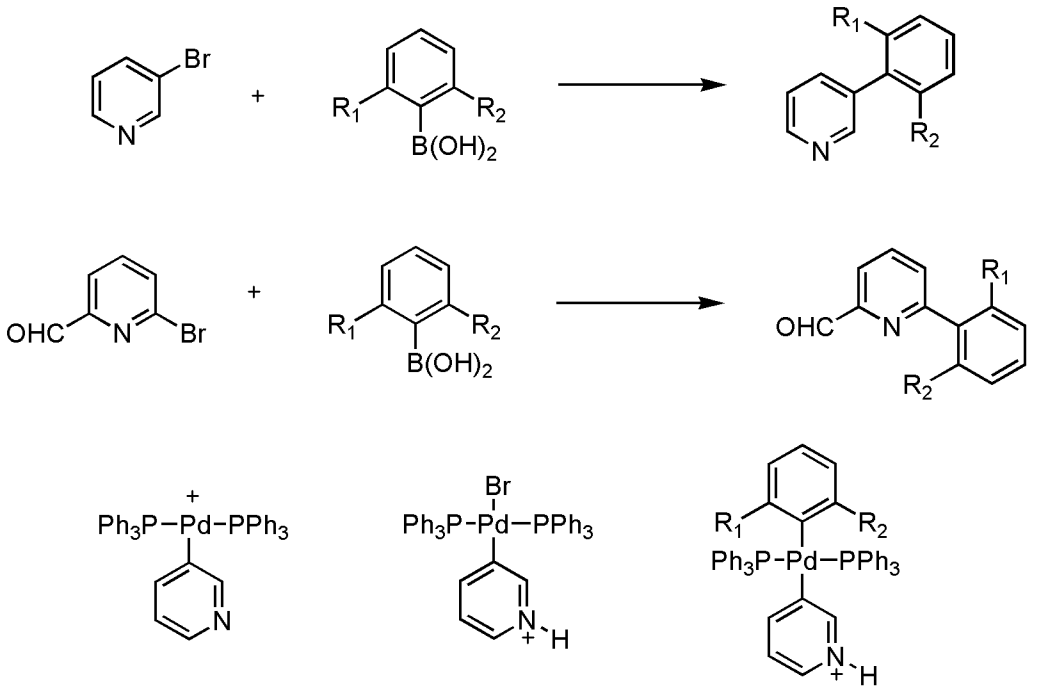

Figure 1-6. A summary of the pyridines and boronic acids used to study Suzuki cross-coupling reactions by Aliprantis and Canary. R_1, R_2 are either H,H; H,CH_3 or CH_3, CH_3. Also shown are the reactive intermediates observed by ESI-MS.

In 2004 Eberlin and co workers[35] used ESI to conduct structural characterization of intermediates of the coupling of arene diazonium salts with olefins in the Heck reaction. The product of oxidative addition for 4-$MeOPhN_2BF_4$ to $[Pd(dba)_3]\cdot dba$ was readily observed as several different species including $[Pd(MeOPh)(dba)_2]^+$, $[Pd(MeOPh)(dba)(CH_3CN)]^+$,

$[Pd(MeOPh)(CH_3CN)_2]^+$, and $[Pd(MeOPh)(CH_3CN)_3]^+$ due to ligand exchange between dba (dibenzylideneacetone) and the solvent, acetonitrile. The initial product of the addition, $[Pd(4\text{-}MeOPhN_2)(L)_2]^+$ where L = a neutral donor ligand, was proposed to be too short-lived to be observed. Sampling of the reaction showed that product distributions changed over time leading to the development of a proposed equilibrium between the above mentioned species. Further investigation with several different olefins showed that $[Pd(MeOPh)(dba)(MeCN)]^+$ was the most active to olefin insertion (Scheme 1-2). Using CID the authors were able to reproduce the proposed final step in the mechanism; transfer of a hydride from the olefin to the Pd was implied from a peak corresponding to $[Pd(H)(dba)]^+$. CID studies were used to confirm the identity of all intermediates.

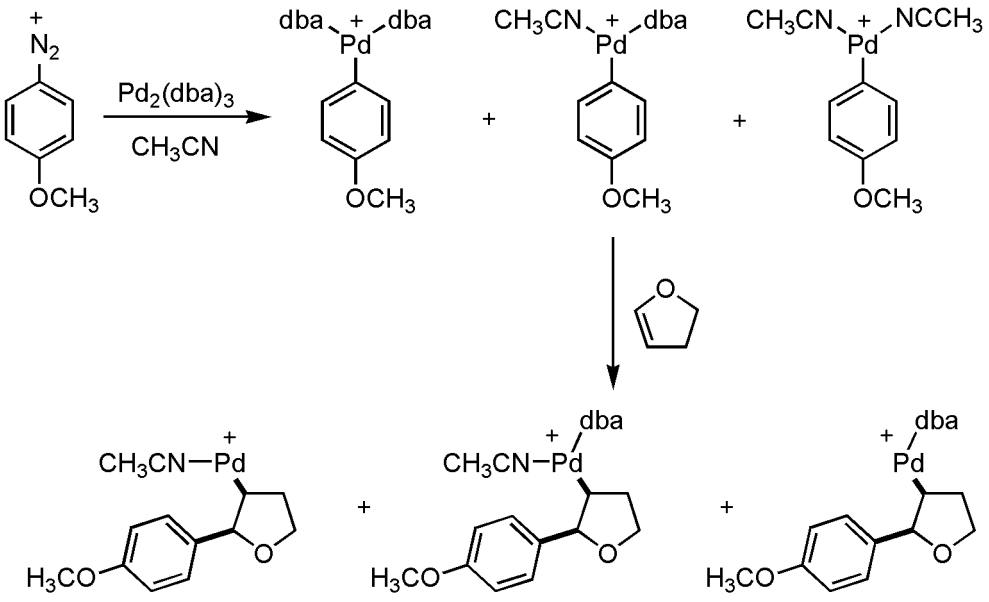

Scheme 1-2. Representative examples of the speciation observed by Eberlin *et al.* in their investigation of the Heck reaction by ESI-MS. Ionization was obtained through loss of a halide following oxidative addition of the aryl-halide substrate. dba = dibenzylideneacetone.

Santos, Eberlin and co workers[36] made use of ESI-MS to detect the major intermediates under real catalytic conditions (Figure 1-7) in a study of the Stille reaction. Because of the relatively short time scale required to collect data using this technique, transient, short-lived species are often observable. Radical cations of what is considered to be the active catalyst $[Pd(PPh_3)_2]^{\bullet+}$ were observed when both $Pd(PPh_3)_4$ or $Pd(OAc)_2/PPh_3$ were used as precatalysts. Solvated adducts containing water and acetonitrile were also readily observed due to the soft nature of ESI. They determined that the active catalyst is likely present in its neutral form, $Pd(PPh_3)_2$, in solution and that the radical cation is produced during the ionization process. Intermediates of oxidative addition of 3,4-dichloroiodobenzene were detectable through loss of iodide to generate a cationic palladium center. After addition of tributylvinyltin, an intermediate of transmetalation was also detected as a radical cation. The species formed after transmetalation was complete was neutral and was not observed in this case. However, the tributyltin cation was observed implying that tributyltin iodide was formed due to transmetalation. CID studies mirrored the reductive elimination of the newly coupled product as would be seen in solution.

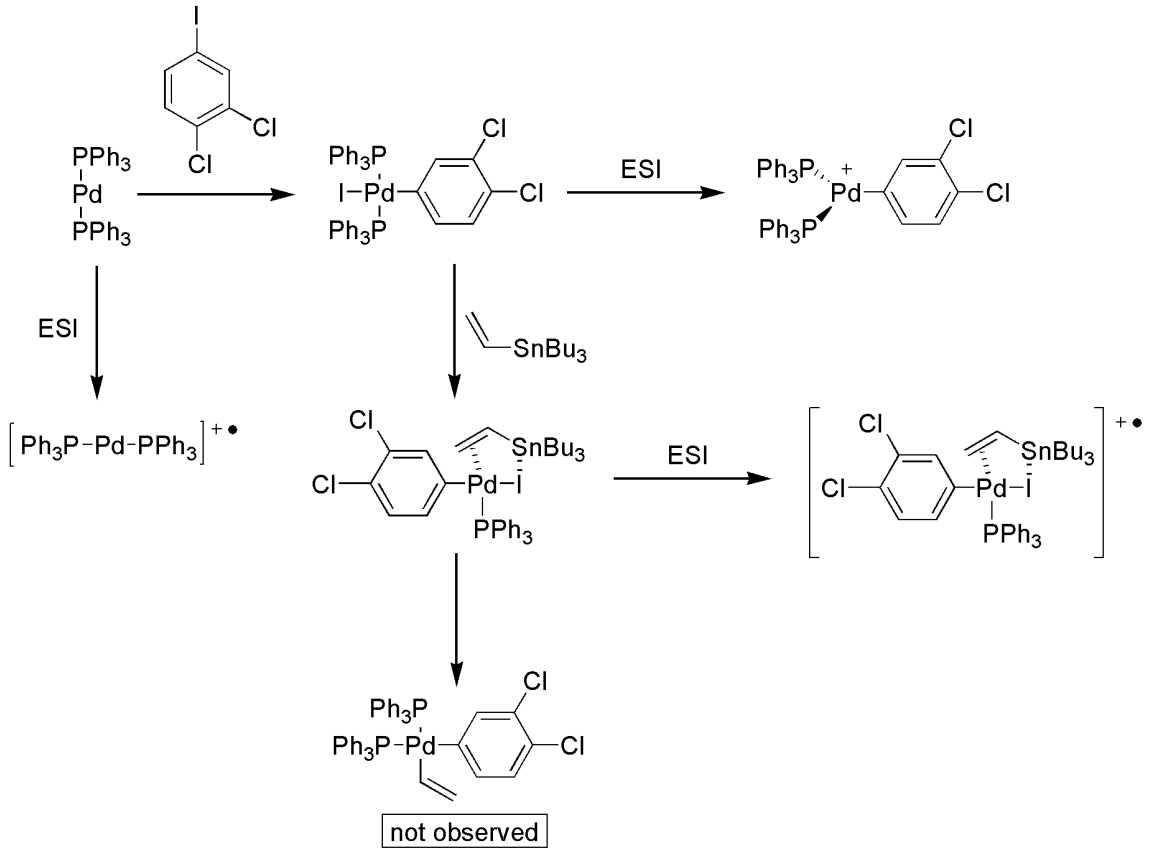

Figure 1-7. Examples of radical cations and cationic species observed by Santos *et al.* while investigating the Stille reaction by ESI-MS. The radical species are generated through electrochemical reduction of the palladium center during the ESI process.

Feichtinger and Plattner have studied the epoxidation of olefins by manganese compounds under catalytic conditions using ESI-MS.[37] They were able to prove the existence of the proposed active catalyst, a manganese(V)-oxo species, and probe the reactivity of this complex with various electron-rich olefins and sulfides. The epoxidation was monitored through appearance of the manganese(III) after addition of olefin and subsequent reductive elimination from the manganese(V)-oxo complex (Scheme 1-3). To ensure that the manganese(III) complex was a reliable ESI handle and not a product of fragmentation during the ESI process, CID experiments were conducted. Indeed no fragmentation was observed at energies comparable to those found in the source.

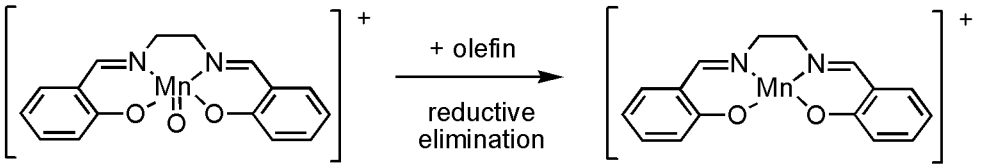

Scheme 1-3. Feichtinger and Plattner directly observed the active manganese(V)-oxo complex in the epoxidation of olefins.

1.6.2 Specialized ligands

The strength of a ligand-metal bond is often dependent on the other ligands that are present in that complex.[38] Relying on the dissociation of a halide (or other ionic ligand) supposes that all species throughout the cycle have the same tendency to undergo this process. It is likely that different species throughout the reaction are more or less likely to undergo this dissociation. Rather than depending on dissociation of an ionic ligand to infer charge on a complex, charged substrates can be incorporated into the reaction. In this way an ESI handle, a molecule that is charged and allows observation in ESI-MS, can be incorporated into the complex without placing a charge directly on the metal center and the dissociation of a ligand is not required. Similarly, ancillary ligands can be functionalized to render the complex detectable by ESI.

A molecule often becomes charged in solution through the basic or acidic sites it may contain. For example, species that contain functional groups such as $–NH_2$ or –OH are able to associate with a proton in acidic media or dissociate a proton in basic media to give $[M+H]^+$ or $[M-H]^–$ type species respectively. The major benefit of using electrospray as an ionization source is the detection of intact molecular species ideally leading to very simple spectra. However, molecules containing these functionalities are also prone to adduct formation with other ions; the most

commonly observed are Na^+ (positive mode) and Cl^- (negative mode). Multiple adducts can make the resulting spectrum quite complicated as one species is now represented by several different peaks (e.g. $[M + H]^+$, $[M + Na]^+$, $[M + K]^+$). The sensitivity can also be compromised as the intensity of one species is now divided among all of its representative peaks.

In an effort to ensure that any given species is represented only once in a spectrum, molecules that carry a permanent charge are employed. In our lab, these molecules are generally ligands or substrates that will be bound to a metal center. So long as the charged moiety is bound the entire complex is made ESI amenable. Ideally, the electronic and steric environment immediately surrounding the metal is altered as little as possible so that the chemistry involved may also remain unchanged. Therefore it is best to make substitutions which are as similar as possible to moieties normally found in the complex. Changes in solubility induced by the attachment of charge can be mitigated by modification of the counterion through salt metathesis.

A charge can be also affixed to the substrate that will be altered through the catalysis providing direct information on the transformations to the substrate. Information about the metal center can be obtained through functionalizing an ancillary ligand to incorporate a charge. Using a ligand that remains fixed to the metal throughout is the best way to ensure all transformations are accounted for. This approach implies that the ligand be covalently bound to the metal and would require synthesis of an entire catalyst which includes the charged ligand. A simpler method is to take advantage of the labile nature of certain metal-ligand interactions (e.g. the triphenylphosphine ligands of Wilkinson's catalyst or the cyclohexylphosphine ligands of Grubbs' catalyst). Adding just a small amount of charged ligand to a solution of the catalyst

allows the charged moiety to associate to the metal center in place of one neutral ligand. The preparation involved in this approach is considerably less time intensive and once the ligand is charged its use is not limited to a single system.

There is a plethora of charged ligands available for use in these types of studies. Rising interest in environmentally friendly chemistry has led to an interest in catalysis that can be conducted in ionic liquids or aqueous environments. Of particular interest are those that may be used in biphasic catalysis where the charged ligand can be altered to induce solubility in organic or aqueous media by, for example, a change in pH. Many of these ligands are well suited for use as ESI handles, but their potential in this capacity has not yet been fully realized.[39] One popular means for adapting traditional catalysts to aqueous chemistry is by modifying a ligand so that it becomes soluble in the appropriate medium and increases the likelihood that solubility will be imparted on the entire catalyst. Ideally, the synthesis of these ligands would involve a single step and produce high yields. Addition of sulfonate groups to aryl substituents using fuming sulfuric acid is commonly used to confer water-solubility on phosphines and, less commonly, bipyridine ligands. This approach was first used in 1958 to attach sulfonate groups to triphenylphosphine.[40] Depending on the conditions and stiochiometry of the reaction up to three substitutions are possible (Figure 1-8). Neutralization with sodium hydroxide gives the water-soluble sodium sulfonate salt ($L\text{-}SO_3^- Na^+$). Similar methodology was used to generate the other three phosphine ligands shown in Figure 1-8. The binaphthyl-bisphosphine was used in a rhodium complex for the hydroformylation of propene in water.[41] The chelating 1,2-bisdiphenylphosphine-ethane also required fuming sulfuric acid to give the sulfonated analogue, but the tris-(phenylpropyl)-phenylphoshine required only concentrated sulfuric acid to achieve sulfonation.[42]

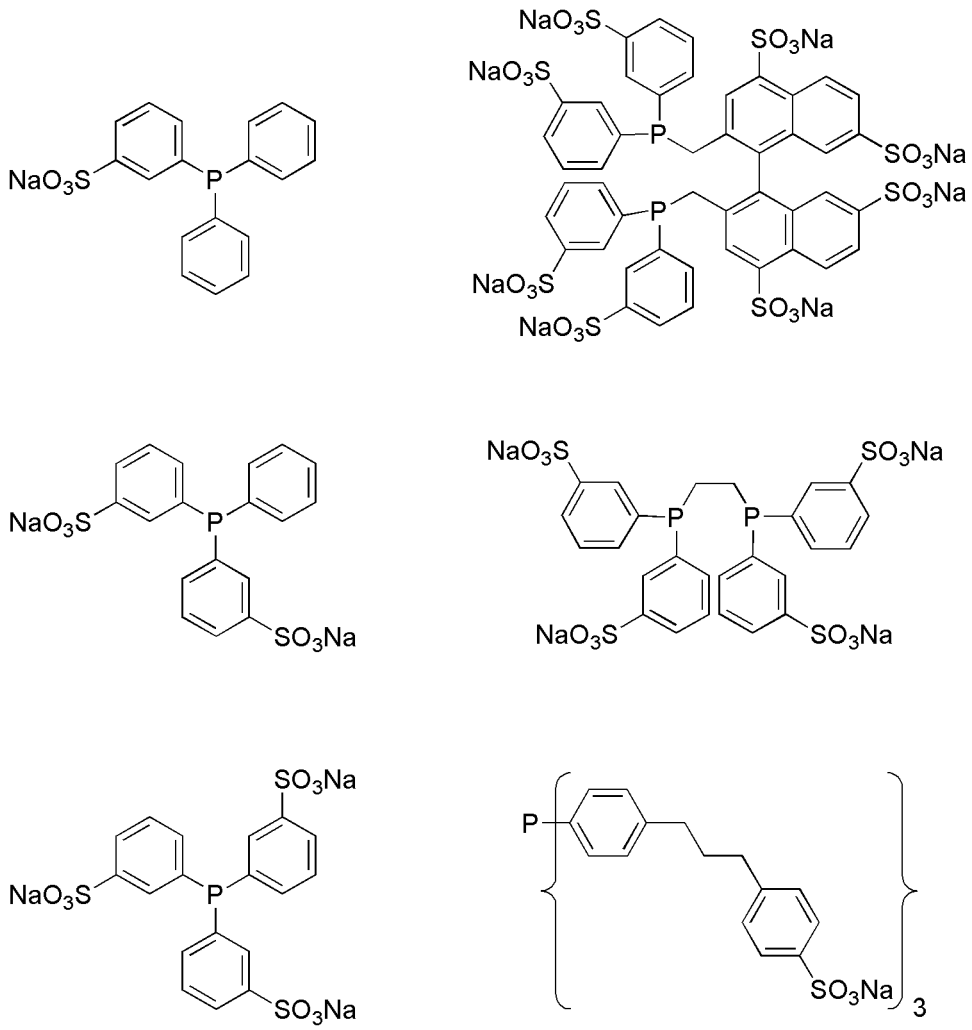

Figure 1-8. A selection of water-soluble sulfonated phosphine ligands.

Neutral ligands related to those in Figure 1-8 were synthesized by Nicholson and co-workers specifically for the study of otherwise neutral metal complexes by ESI-MS.[43] Starting from magnesium and a *p*-bromo substituted anisole or aniline, the desired aryl Grignard reagent was made and reacted with the appropriate chlorophosphine or chloroarsine (PPh_2Cl, PPhCl, PCl_3, $Cl_2P(CH_2)_2PCl_2$, or $AsCl_3$) to give the ligands shown in Figure 1-9. These specific ligands were chosen because of their similarities to the commonly used PPh_3 ligand, with substitution at the *para* position intended to leave the steric environment of the metal unperturbed. Several metal

complexes were made with each ligand. Molybdenum-carbonyl complexes of the ligands were prepared by reaction with $Mo(CO)_4(piperidine)_2$ in dichloromethane; iron-carbonyl complexes were prepared by reaction with $Fe(CO)_5$ in ethanol; ruthenium-carbonyl complexes were prepared by reaction with $Ru_3(CO)_{12}$ in toluene; platinum and palladium-chloride complexes were prepared by reaction with $PtCl_2(cod)$ or $PdCl_2(cod)$ in dichloromethane; gold-chloride complexes were prepared by reaction with $HAuCl_4$ in ethanol. They showed that carbonyl complexes of molybdenum, iron, and ruthenium were all ESI-active by association of a proton to a basic site on the ligand to give $[M + H]^+$ species. Halide complexes of platinum, palladium and gold ionized by loss of a halide, rather than association of a proton, to give $[M – Cl]^+$ species.

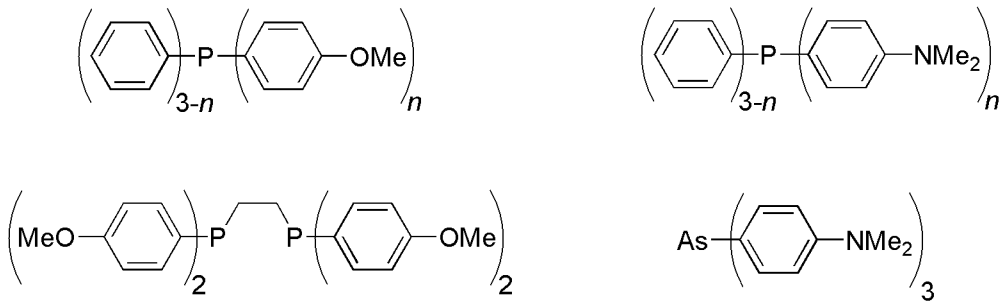

Figure 1-9. Phosphine ligands synthesized by Nicholson *et al.* from aryl Grignard, chlorophosphine and chloroarsine starting materials. n = 1, 2, 3.

Synthesis of ligands possessing a pendant ammonium or phosphonium group often requires protection and deprotection steps to avoid unwanted functionalization at the end of the molecule intended to bind to the metal. A phosphine ligand containing an ammonium functionality reported by Okano and co-workers required multiple steps including protection and deprotection of the phosphine.[44] The desired palladium complex was to be used as a catalyst in the phase transfer fluorocarbonylation of phenyl bromide. Starting from *m*-bromobenzoic acid, the amine was generated from the carboxylic acid through reaction with thionyl chloride and

dimethylamine followed by reduction with lithium aluminum hydride. Reaction with diphenylchlorophosphine installed the phosphine moiety. A protecting group was necessary to avoid alkylation at phosphorus, and H_2O_2 was used to generate phosphine oxide. Quaternization of the amine and deprotection of the phosphine gave the desired ligand that was then reacted with $PdBr_2$(cyclooctadiene) and sodium iodide in dichloromethane to give the palladium complex shown in Scheme 1-4. Alternatively, the amine was also quaternized after co-ordination to palladium.

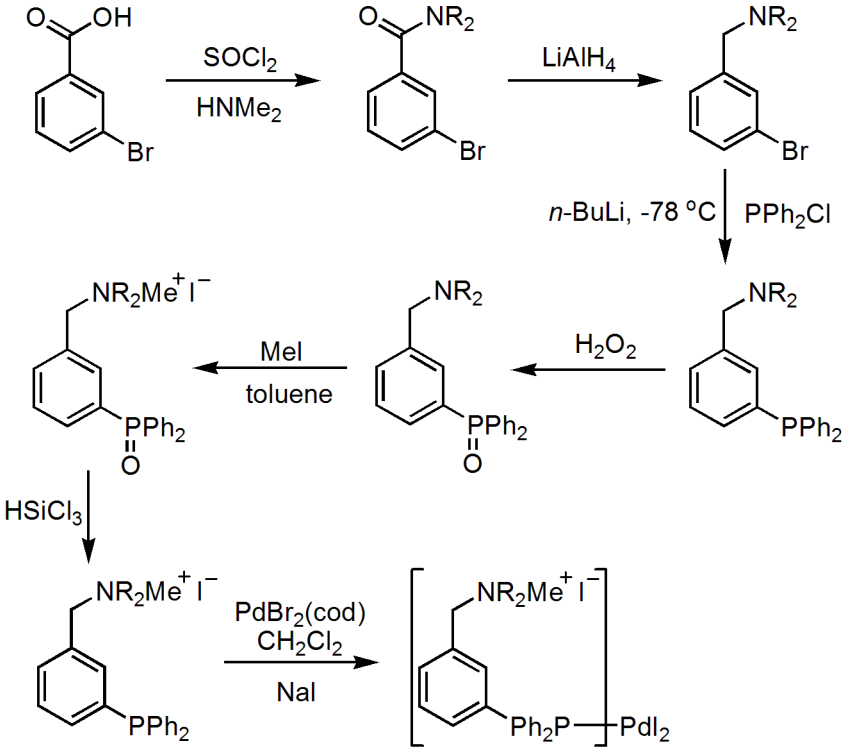

Scheme 1-4. The multi-step process used by Okano *et al*. to generate an efficient phase-transfer catalyst. R = CH_2 or *n*-butyl; cod = cyclooctadiene.

Grubbs and co-workers reported a modified alkylphosphine ligand in 1996[45] to enable them to perform olefin metathesis in water. Aliphatic phosphine ligands were of particular interest as their electron-donating nature is particularly beneficial in the study of olefin metathesis by the

ruthenium-carbene complex shown in (Scheme 1-5). Using borane as a protecting and activating group, alkyl phosphine ligands functionalized with ammonium tethers were synthesized. Quaternization of the amine proceeded without reaction at phosphorus or transfer of the borane protecting group to the amine. The equivalent iodide ligands were also made, although their solubility in water was limited. Deprotection and crystallization gave the ligands in greater than 95% yield.

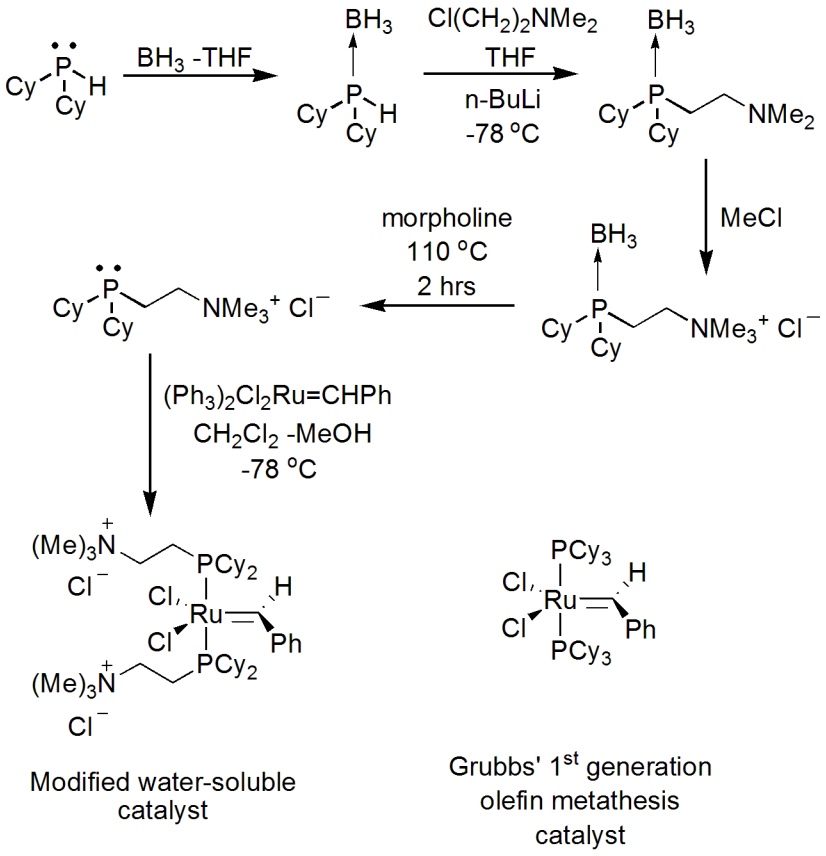

Scheme 1-5. Modifications to Grubbs' first generation catalyst (shown here) by Grubbs *et al*. for olefin metathesis to perform reactions in aqueous environments were later used by Chen and co-workers to study metathesis by ESI-MS.Cy = cyclohexyl, X = Cl or I.

The complex was later exploited by Chen and his group to study the system in the gas phase by ESI-MS using an octapole/quadrupole/octapole/quadrupole instrument (only the quadrupoles are

mass analyzers, the octapoles are ion guides that can cope with relatively high pressure and still contain the ions efficiently).[46,47] They were able to observe, for the first time, gas phase chemistry that parallels the chemistry observed in solution by the same catalyst. The catalyst was dissolved in dichloromethane and peaks for both the six- and five-coordinate ruthenium species (due to solution phase dissociation of one phosphine ligand) were observed (Scheme 1-6). Mass-selection of the five-coordinate species in the first quadrupole allowed for reaction with various olefins (butene, norbornene, cyclobutene and cyclopentene) in the collision cell. Conducting the same experiment with the six-coordinate species showed no addition of olefin, confirming that dissociation of a phosphine is a necessary step in the catalytic cycle. Addition of up to three olefin units was observed and data on the relative rates of reaction were obtained.

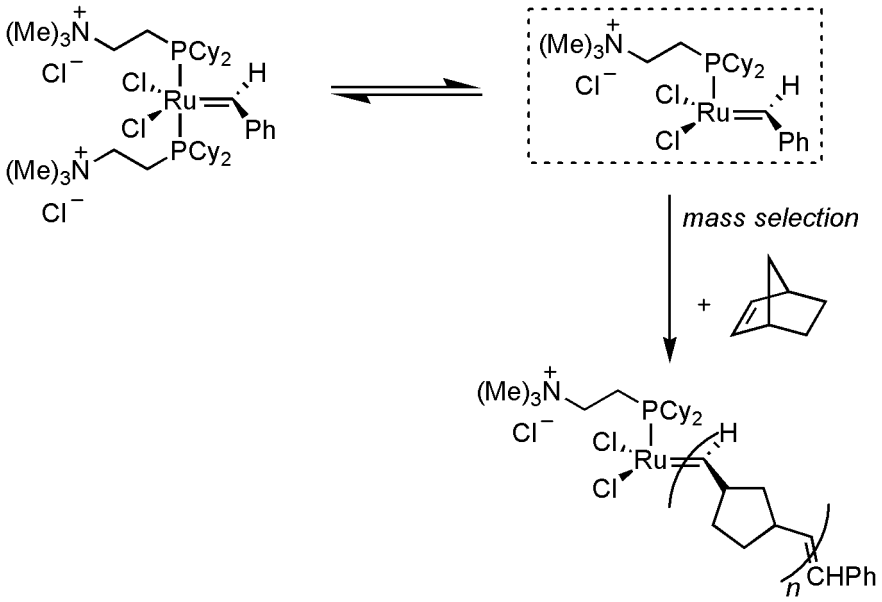

Scheme 1-6. Chen *et al.* were able to observe the active olefin metathesis catalyst, $[(Cy_2P(CH_2)_2NMe_3)Cl_2RuCHPh]^+$, in solution. Mass selection allowed subsequent reaction with olefins in the gas phase. n = 1-3.

Chen has also approached the study of olefin metathesis by ruthenium carbenes from a slightly different angle. The alkylidene was modified to include an alkyl ammonium group (Scheme 1-7) so that the growing polymer chain has a permanent charge.[48] The phosphine ligands in the complex are in equilibrium between free in solution and bound to the metal. The alkylidene does not dissociate from the complex at any point and serves as a reliable reference point for studying the fluctuation in these systems. The functionalized complexes were made *in situ* by reaction of the commercially available first and second generation catalysts, $(PCy_3)_2Cl_2Ru{=}CHPh$ and $(NHC)(PCy_3)Cl_2Ru{=}CHPh$, with 4-[(trimethylammonium)methyl]styrene in dichloromethane. In separate experiments for each catalyst, isolation of the active five-coordinate species in the first mass analyzer and reaction with norbornene in the collision cell allowed Chen to verify Grubbs' solution phase results showing that the second generation catalyst is much more reactive than its first generation counterpart.

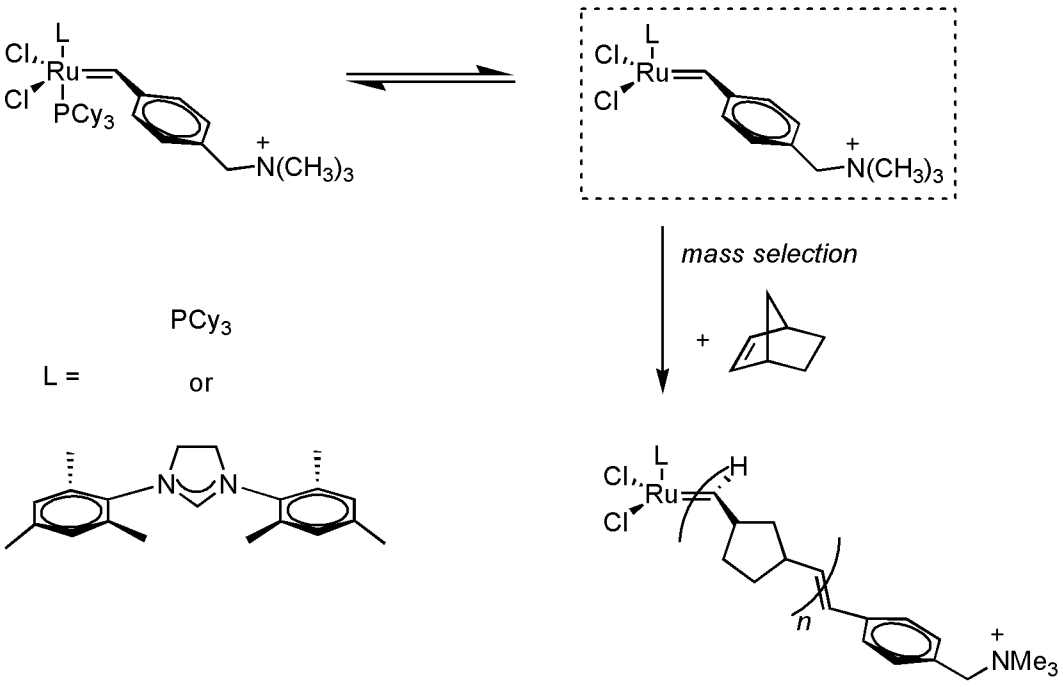

Scheme 1-7. The modification to the carbene ligand on Grubbs' first and second generation olefin metathesis catalysts used by Chen *et al.* to probe the reactivity of the catalysts in the gas phase.

In a separate study, the group used a similarly appended alkyl phosphonium carbene complex[49] made by stirring the catalysts, $(PCy_3)_2Cl_2Ru{=}CHPh$ and $(NHC)(PCy_3)Cl_2Ru{=}CHPh$, with tricyclohexyl(4-vinylbenzyl)-phosphonium chloride in dichloromethane followed by isolation of the material. CID experiments were employed to evaluate the activation energies for dissociation of the PCy_3 ligand in both the first and second generation catalysts. They were also able to calculate the activation energies for ring closing metathesis by both catalysts to generate norbornene using the same method.

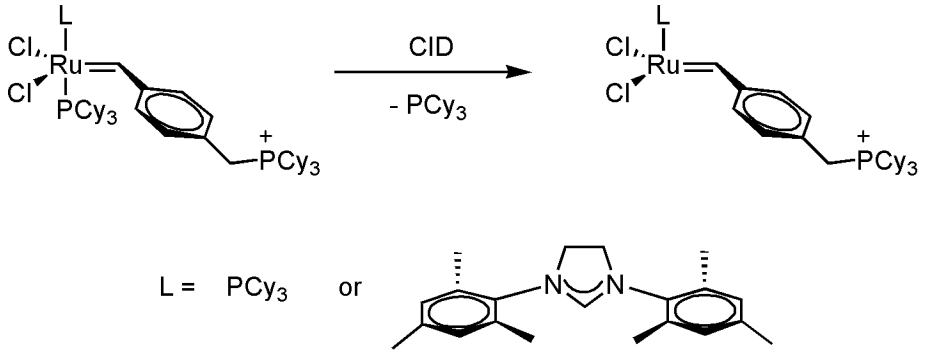

Scheme 1-8. Chen *et al.* used phosphonium-substituted carbene ligands in CID studies to probe the relative strengths of association in the ligand set of Grubbs' first and second generation olefin metathesis catalysts.

In our laboratory, we have shown the applicability of chargeable phosphine ligands to the study of metal complexes by ESI-MS. 1,8-bis(dimethylamino)naphthalene (Proton Sponge®) has a high basicity (its pK_a is approximately 12) such that it binds strongly and selectively to protons. Further discussion on the characteristics of this molecule can be found in Chapter 2. Triphenylphosphine was substituted with a proton sponge functionality by first brominating 1,8-bis(dimethylamino)naphthalene with *N*-bromosuccinimide followed by reaction with *n*-BuLi and diphenylchlorophosphine.[50] Due to the high basicity imparted by the proton sponge moiety, {1,8-Bis(dimethylamino)naphthalene-2-yl}diphenylphosphine was shown to give ESI-MS responses essentially equivalent to permanently charged phosphonium cations. Complexes of the ligand were obtained through reaction with various metals including $Fe_2(CO)_9$, $W(CO)_6$ and $(\eta^5\text{-}C_5H_5)Mn(CO)_3$ to give $Fe(CO)_4$(phosphine), $W(CO)_5$(phosphine) and $(\eta^5\text{-}C_5H_5)Mn(CO)_2$(phosphine).

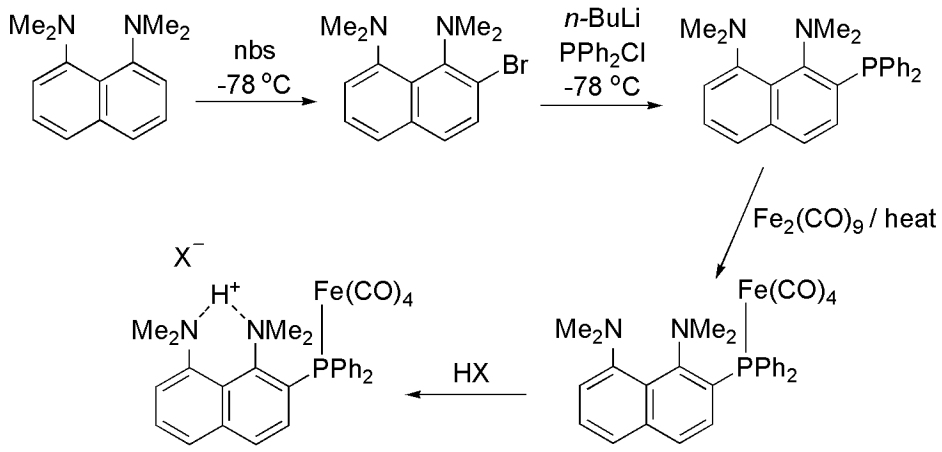

Scheme 1-9. Synthesis of {1,8-Bis(dimethylamino)naphthalene-2-yl}diphenylphosphine and generation of an ESI-active iron carbonyl complex. nbs = N-bromosuccinimide; X = Br^- or BF_4^-.

Bipyridine ligands can be altered to include charged groups as well. Bromination of the commercially available 4,4'-dimethyl-2,2'-bipyridine with *N*-bromosuccinimide and subsequent reaction with trimethlyamine gave the charged bipyridine shown in Scheme 1-10. The dication was reacted with $Pd(NH_3)_2Cl_2$ in water to give $PdCl_2$(2,2'-bipyridyl), an air and water stable, recyclable, and highly active catalyst for the Suzuki cross-coupling of a variety of aryl bromides (both activated and de-activated) with aryl boronic acids under aqueous, aerobic conditions.[51]

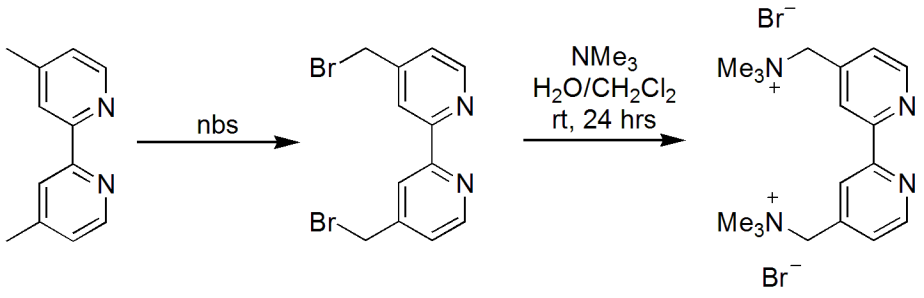

Scheme 1-10. 4,4'-Functionalized 2,2'-bipyridine ligands synthesized by Wu and co-workers. Nbs = *N*-bromosuccinimide.

A similar ligand was functionalized with imidazolium groups to promote solubility in ionic liquids.[52] Bromination of 6,6'-dimethyl-2,2'-bipyridine with *N*-bromosuccinimide followed by

reaction with methylimidazole and KPF_6 gives the dication in Scheme 1-11. The ligand was used to solubilise a copper catalyst in the ionic liquid [bmim][PF_6] for the oxidation of alcohols to aldehydes or ketones. Recycling of the catalyst was possible by washing the reaction mixture with diethyl ether, although a slight reduction in activity was observed with repeated cycling.

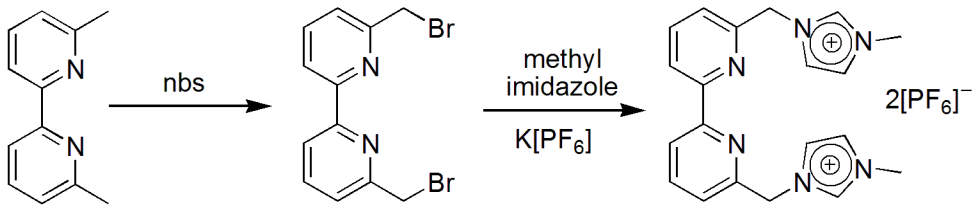

Scheme 1-11. 6,6'-Functionalized 2,2'-bipyridine ligands synthesized by Wu and co-workers. nbs = *N*-bromosuccinimide.

Kundu and co-workers aimed to make potentially chelating pyridine-imine ligands applicable to chemistry in aqueous environments.[53] Starting from the appropriately substituted aniline (at either the 3- or 4-position with a sulfonate or carboxylate group) reaction with 2-pyridinecarboxaldehyde gave the unsymmetrical ligand shown in Scheme 1-12. The ligand was made water-stable once co-ordinated to platinum with an electron rich olefin. The complexes were soluble in polar organic media, but not in non-polar solvents. Investigation of the use of this system in biphasic catalysis was under consideration and was dependant on the stability of the complex with varied pH. If ligands of this type were to be used in ESI-MS the charge would have to be generated in solution either through association of H^+ (for analysis in positive-ion mode) or dissociation of H^+ or Na^+ (for analysis in negative-ion mode).

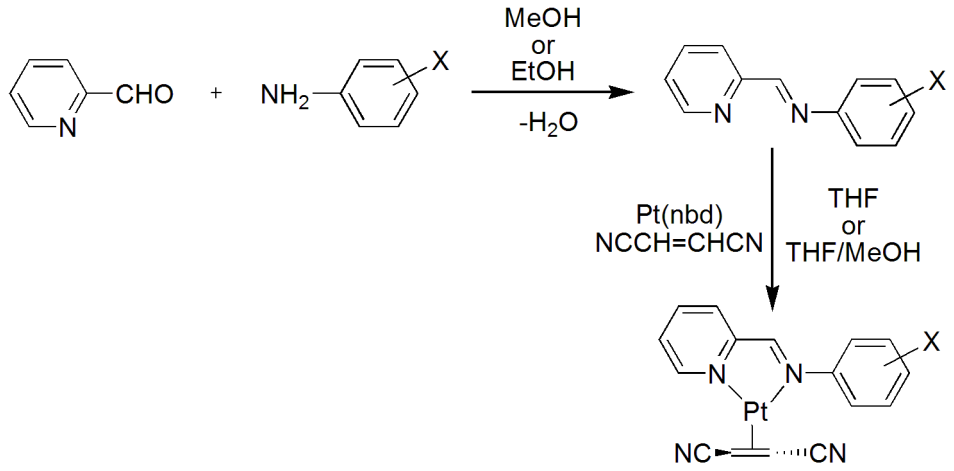

Scheme 1-12. Synthesis of pyridine-imine ligands by Kundu *et al*. with the aim to render the resulting platinum complex soluble in aqueous media. X = SO_3Na, COONa or COOH in the 3- or 4-positions; nbd = norbornene.

Like the sulfonate and carboxylic acid groups discussed above, crown ethers must rely on association of cations to become charged. Complexes of benzocrown ethers can be made in much the same way as the similar arene complexes. UV irradiation of benzocrown ethers with $Cr(CO)_6$ gave complexes of the type $Cr(CO)_3(\eta^6$-beznocrownether), shown in Figure 1-10. The benzo-18-crown-6 ligands were efficient IR sensors (*via* the CO ligands on chromium) for alkali-metal and 2-phenylethyl ammonium ions while the dibenzo-18-crown-6 analogues did not display the same sensitivity.[54-56] In a different vein, reaction of $[RuCl(\eta^6$-ethyl benzoate)$]_2$ in a melt of dibenzo-15-crown-5 afforded the dimeric species[57] $[RuCl(\eta^6$-dibenzo-15-crown-5$)]_2$ also shown in Figure 1-10. The complexes were further derivatized to arrive at mononuclear catalysts and were used in the study of enantioselective transfer-hydrogenation of acetophenone. Solubility properties were found to be adjustable by variation of the associated cation. The ESI studies of these complexes revealed that the molecules ionize through loss of Cl^- rather than through association of an alkali-metal cation to the ether. With a five-fold excess of NaCl, KCl or CsCl peaks for the cation-associated species were also observed.

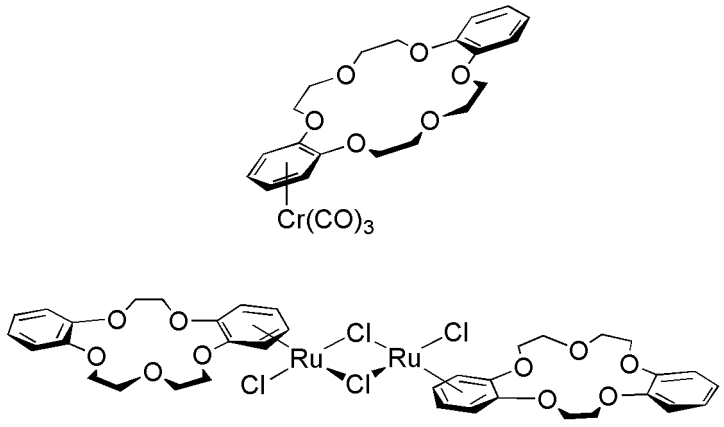

Figure 1-10. Substituted crown ethers used as IR sensors and precursors to catalysts for the transfer-hydrogenation of acetophenone.

1.7 Summary

There are numerous ionization methods available for mass spectrometric purposes, including electrospray ionization mass spectrometry (ESI-MS). Ions that exist in solution, either through acidic or basic sites or a permanent charge are introduced into the source of the mass spectrometer as a fine mist and desolvation produces gas phase ions. Traditionally used for large, robust organic molecules, the use of ESI to study fragile inorganic and organometallic systems was not quick to develop. Special considerations to make ESI applicable to inorganic systems make the implementation of ESI in this area increasingly prevalent. *In-situ* monitoring of reactions allows the progress of a reaction to be observed in real-time, while short introduction times allow for the examination of fast reactions. CID experiments lend both structural information as well as insight into reaction mechanisms through reaction in the gas phase.

Examination of catalytic systems can be achieved if the species of interest possess a charge. Metal complexes that ionize by loss of a halide ion are popular targets as they require no special ligand preparation. Synthesis of charged or chargeable ligands opens the potential applicability

of ESI-MS to a much wider range of systems. While ligands containing basic or acidic sites can offer synthetic simplicity, permanently charged ligands present a more controlled way to investigate catalytic systems as multiple charge pathways are minimized. The use of charged ligands with similar structures to those of the neutral ligands found in the catalyst allows the charge to be placed remotely from the metal center, such that the steric and electronic environment is perturbed as little as possible. There are many ligands available for use as ESI probes although they have not yet necessarily been used for this application.

Chapter 2. Metal-containing Proton Sponge® derivatives

2.1 Motivation

1,8-bis(dimethylamino)naphthalene (Proton Sponge®, Figure 2-1, D), was first reported by Brown in 1941.[58] It wasn't until the late 1960s that Alder drew attention to the fact that this particular substitution of naphthalene introduced a unique degree of basicity to the molecule.[59] Alder's work demonstrated how the sequential addition of methyl groups to 1,8-bis(amino)naphthalene increased the pK_a in an unsurprising fashion until the fourth substitution. The structures of the investigated molecules are given in Figure 2-1 and the pK_a's of their conjugate acids in water are 4.61, 5.61, 6.43, and 12.34 for 1,8-bis(amino)naphthalene, 1,8-bis(methylamino)naphthalene, 1-dimethylamino-8-methylaminonaphthalene and 1,8-bis(dimethylamino)naphthalene respectively. In comparison, the aromatic amines aniline and *N,N'*-dimethylaniline have pK_a's around 5.[60] The addition of four as compared to three methyl groups decreases the K_a by a factor of nearly 10^6. The large increase in basicity is due to a number of factors. The bulky nature of the dimethylamino groups and their close proximity to one another induces steric repulsion between the lone pairs of electrons on the two nitrogen centers. In order to relieve some of the repulsion the naphthalene system twists out of plane by about 30°.[59] The steric strain is easily relieved through association of a proton. The lone pairs on each nitrogen center can become equally involved in hydrogen bonding with the proton[61,62] and so are no longer repelled by one another allowing the naphthalene π system to move back to a near planar orientation.[63] The spatial arrangement of the dimethylamino groups allows access to only a proton; anything larger will not fit comfortably (a notable exception being a highly reactive palladium fragment[64]).

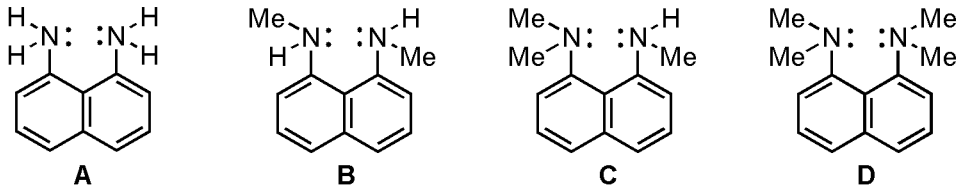

Figure 2-1. 1,8-naphthalene species used to demonstrate the extreme basicity of Proton Sponge®.
A: 1,8-bis(amino)naphthalene; **B**: 1,8-bis(methylamino)naphthalene;
C: 1-dimethylamino-8-methylaminonaphthalene; **D**: 1,8-bis(dimethylamino)naphthalene (Proton Sponge®).

Many variations of the proton sponge theme have been carried out in the last thirty years, largely led by Alder and Staab in the 1980s.[60,65] Some interesting examples are given in Figure 2-2. In the early 1980s, Alder announced his intention to investigate the effects of linking the nitrogen centers with alkyl chains of varying lengths (Figure 2-2, A) on the lone pair orientation.[66] Results on the characteristics of these molecules were to be discussed in a future publication but the work does not appear to have been reported.

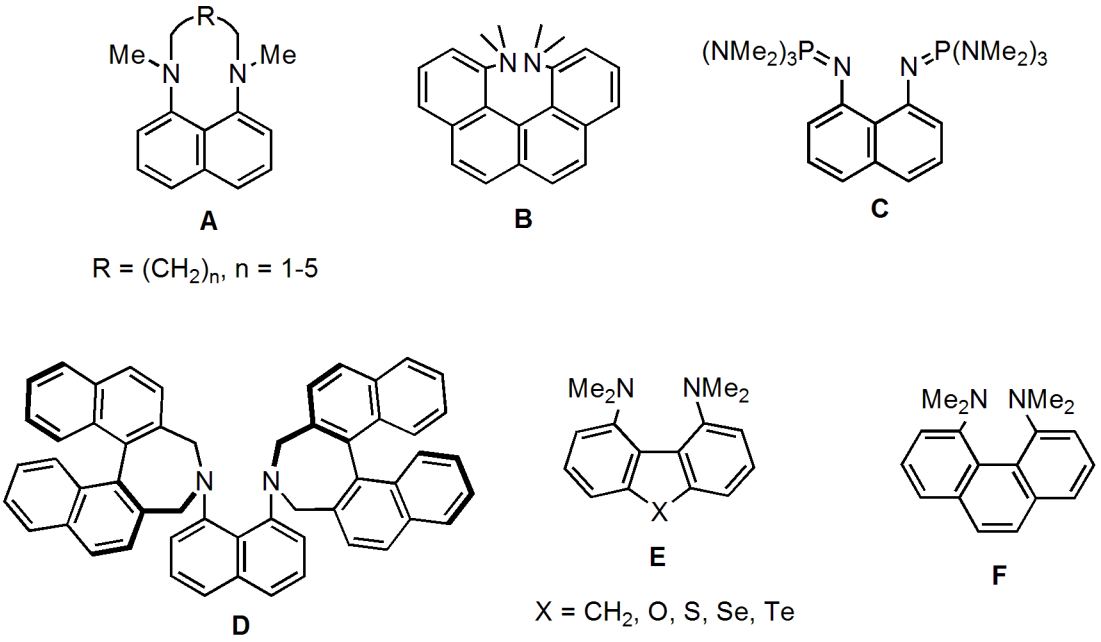

Figure 2-2. Variations on the proton sponge functionality. A) Fluorene-based derivatives;
B: 1,8-bis(hexamethyltriaminophosphazenyl)naphthalene; C: alkyl bridged 1,8-bis(methylamino)naphthalene;
D: 1,12-bis(dimethylamino)benzo[*c*]phenanthrene; E: chiral binaphthyl substituted naphthalene;
F: 4,5-bis(dimethylamino)phenanthrene.

A series of investigations by Staab showed that it was not just the proximity of the nitrogen centers that determined the strength of basicity but also the linearity of the resulting hydrogen bonds. The distance between the nitrogen centers in 1,16-diaza[6]helicene is approximately equal to the distance found in 1,8-bis(dimethylamino)naphthalene but the helicene does not display the same selective mono-protonation behaviour.[67] The fixed position of the nitrogen centers and the fact that they are on opposite sides of the central plane of the molecule means the N-H-N bond is not linear and so is not as strong. As a result Staab saw the bisprotonated species rather than the monoprotonated, and the molecule exhibited a basicity comparable to pyridine. To address this, Staab synthesized 1,12-bis(dimethylamino)benzo[*c*]phenanthrene (Figure 2-2, B) where the dimethylamino groups are capable of rotation about the nitrogen-aromatic ring bond. The flexibility in directionality of the lone pairs to facilitate formation of a linear N-H-N bond and the proximity of the nitrogen centers gave rise to monoprotonation. Even so, the basicity was similar to that of *N*,*N*-dimethylaniline. In contrast to 1,8-bis(dimethylamino)naphthalene, protonation of the phenanthrene does not provide significant relief of steric strain and the marked increase in basicity is not observed.[68]

In 2005, the superbase 1,8-bis(hexamethyltriaminophosphazenyl)naphthalene[69] (Figure 2-2, C) was synthesized, combining the high basicity of phosphazanes and proton sponges. A superbase is defined as a combination of two or more basic functionalities in one molecule generating new characteristics.[70] The measured p*K*a of the new molecule was 29.9 in acetonitrile, almost 10^{12} more basic than 1,8-bis(dimethylamino)naphthalene. The N-H-N bonds were unsymmetrical.

The example shown in Figure 2-2, D is an excellent example of imparting chiral functionality to the parent naphthalene.[71] This particular molecule was to be used in circular dichroism experiments as a probe to determine the absolute configuration of amino acids.

In an effort to further investigate the nature of the N-H-N bond, Staab proposed that a fluorene-based system would orient the nitrogen lone pairs in a more linear fashion to create a stronger hydrogen bond. To this end he synthesized 4,5-bis(dimethylamino)fluorene (Figure 2-2, E).[60] He found a pK_a of 12.8 (in 35% dimethylsulfoxide in water), slightly higher than that for 1,8-bis(dimethylamino)naphthalene, and the relief of steric strain upon protonation was similar to that for the parent naphthalene. A series of fluorene-like molecules were made by varying the atom in the "X" position. The increasing larger atoms sequentially push the dimethylamino groups closer in proximity and it was found that the variations caused a decrease in the basicity of these molecules compared to the fluorene derivative. In the same investigation, 4,5-bis(dimethylamino)phenanthrene (Figure 2-2, F) was introduced. The phenanthrene backbone is twisted so the two nitrogen centers lie above and below the plane of the molecule. Still, the amino groups are too close together to form a perfectly linear hydrogen bond, and not a great deal of steric relief is found after association of a proton. The pK_a was determined to be only 11.5 (35% DMSO in H_2O).

The exclusive and strong association of a proton to these types of molecules makes them potentially perfect probes for ESI-MS investigations. As discussed in Chapter 1, eliminating the possibility for multiple charge pathways greatly simplifies the resulting spectrum, making this particular type of molecule very attractive. The only obstacle is functionalizing this convenient

probe to make it applicable to catalytic investigations. This end has been achieved previously in our group through an analogue of triphenylphosphine, a common ligand in catalytic systems, that contains the proton sponge functionality. {1,8-Bis(dimethylamino)naphthalene-2-yl}diphenylphosphine was synthesized (Section 1.6.2) and used to show that ESI-MS investigations of neutral metal complexes were possible when a chargeable ligand was employed.[50]

2.2 Results and Discussion

The direction we had envisioned for this work was toward molecules that would possess a similarly highly basic site once bound to a metal center. We were particularly drawn to the scaffold of the fluorene sponges introduced by Staab and the similarity it bore to the orientation of 2,2'-bipyridine ("bipy") chelating to a metal. In our case the metal center would take the place of the atom in the X position in Figure 2-2, E. To this end, we investigated the functionalization of 2,2'-bipyridine. Bipy ligands are common in coordination chemistry [72-74] so their incorporation into our investigations seemed like an appropriate choice. The idea was to substitute bipyridine at the 3 and 3' positions to arrive at 3,3'-*N,N'*-bis(dimethylamino)-2,2'-bipyridine (**2.1**) and to rely on coordination to a metal center to properly orient the two groups toward each other (Scheme 2-1).

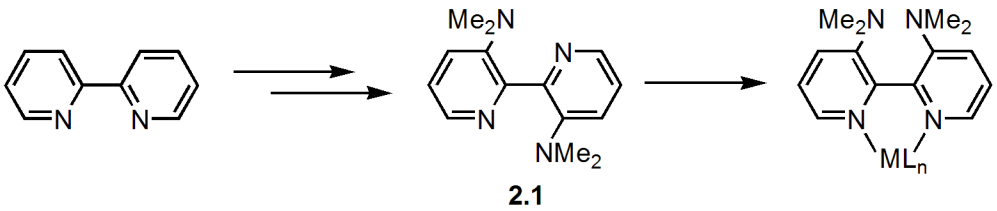

2.1

Scheme 2-1. General route to metal-containing proton sponge derivatives.

Once the functionalized bipyridine has coordinated to the metal and the dimethylamino groups adopted the expected orientation, addition of a proton source should render the entire complex amenable to ESI-MS analysis, and provide considerable structural interest in being the first metal-containing proton sponge. The effect of the relatively flexible coordination environment of the metal was also of structural interest – it is possible, of course, that the metal coordinates to one pyridine nitrogen and one dimethylamino nitrogen. In this case, an identical site would be available on the other side of the ligand, which itself could bind another metal centre or H^+.

Synthesis of the known 3,3'-bis(amino)-2,2'-bipyridine (**2.2**) was achieved through reported procedures.[75] An Ullmann coupling was used to generate 3,3'-dinitro-2,2'-bipyridine from two equivalents of 2-chloro-3-nitropyridine and $SnCl_2 \cdot 2H_2O$ in HCl was used to reduce the nitro groups to amines (Scheme 2-2).

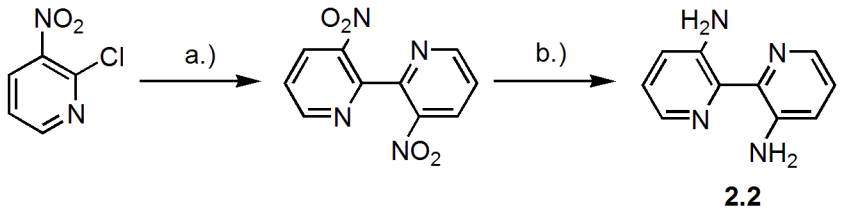

2.2

Scheme 2-2. Synthesis of **2.2**. a.) $Cu_{(s)}$,1,4-dioxane, reflux, 16 hrs; b.) $SnCl_2 \bullet H_2O$/HCl, reflux, 1 hr.

It was presumed that methylation of the two amino groups would proceed fairly easily. However, many different approaches were taken to methylate **2.2** to give **2.1** with limited success. Giam and Hauck had methylated 3-aminopyridine to give 3-dimethlyaminopyridine using formic acid and formaldehyde.[76] When this procedure was applied to **2.2** the ESI-MS analysis of the resulting material showed no product formation and a strong signal corresponding to the diamino starting material. Several other methylation procedures were investigated with varying sources of

base and the methyl group. Staab's synthesis of a fluorene-based proton sponge used sodium hydride and dimethyl sulfate.[60] ESI-MS analysis of the product of the reaction of **2.2**, four equivalents of dimethyl sulfate and excess sodium hydride showed no evidence of starting material or any methylated products.

Table 2-1. Selected literature procedures attempted for the methylation of **2.2** to give **2.1**. Substrates given are those used in the original procedures.

Substrate	Methyl Source	Base	Reference
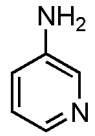	Formic acid/formaldehyde		**76**
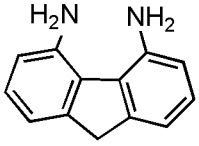	Me_2SO_4	NaH	**60**
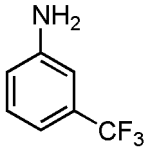	Me_3PO_4	NaOH	**77**
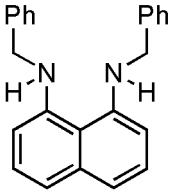	MeI	NaH	**78**
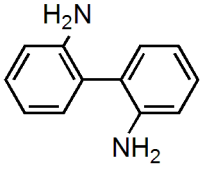	Me_2SO_4	NaOH	**79**

Further approaches focused on amine-substituted aromatic systems. Sheppard achieved methylation of *m*-trifluoromethylaniline to *m*-trifluoromethyl-*N*,*N*-dimethylaniline using trimethylphosphate.[77] Reaction of **2.2** with a slight excess of neat trimethylphosphate and treatment with aqueous sodium hydroxide gave an indistinguishable product distribution by

NMR spectroscopy. Charmant and co-workers used methyl iodide to methylate a benzylamine-substituted naphthalene proton sponge derivative.[78] The addition of excess sodium hydride and four equivalents of methyl iodide to **2.2** in tetrahydrofuran lead to a mixture of products that had incorporated one to five methyl groups as could be seen in the ESI-MS spectrum in dichloromethane.

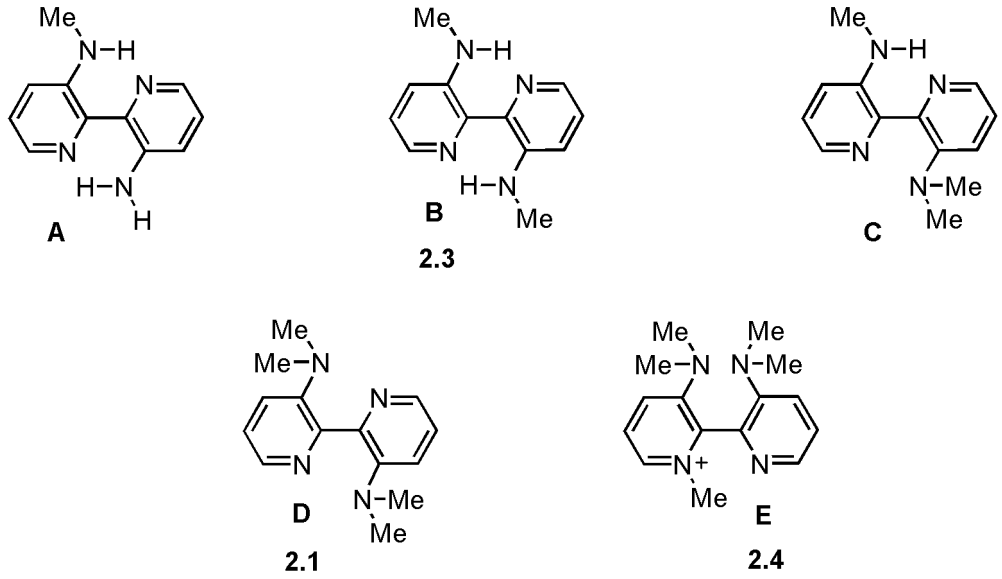

Figure 2-3. Possible products from methylation of **2.2**. A: 3-methylamino-3'-amino-2,2'-bipyridine; B: 3,3'-bis(methylamino)-2,2'-bipyridine (**2.3**); C: 3-methylamino-3'-dimethylamino-2,2'-bipyridine; D: 3,3'-*N,N'*-bis(dimethylamino)-2,2'-bipyridine (**2.1**); E: 3,3'-*N,N'*-bis(dimethylamino)-2,2'-pyridine-methylpyridinium iodide (**2.4**).

2,2'-diaminobiphenyl is structurally very similar to **2.2**. Shaw and Turner were able to methylate the biphenyl to 2,2'-bis(dimethylamino)biphenyl using dimethyl sulfate and sodium hydroxide.[79] Using the same conditions on **2.2** gave a range of methylated products (Figure 2-3) from one to five which were easily observed by ESI-MS (Figure 2-4).

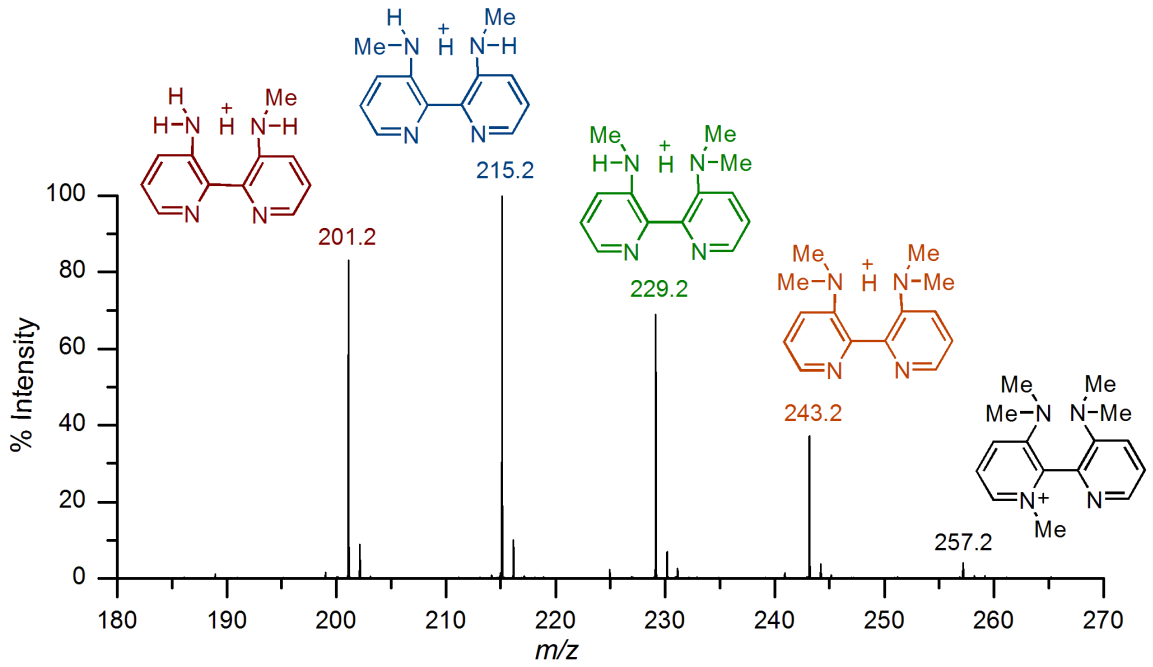

Figure 2-4. Typical product distribution resulting from methylation of **2.2**. ESI-MS run in positive mode in CH_2Cl_2. $[M + H]^+$ = 201.2, 215.2, 229.2, 243.2 *m/z*, and $[M]^+$ = 257.2 *m/z*.

2.2 contains two sites where intramolecular hydrogen bond might form between an amine hydrogen and the nitrogen in the opposite pyridine ring. Per-methylation of these amine groups eliminates the possibility for these hydrogen bonds to form. If the amine nitrogens are only partially methylated the possibility of hydrogen bonds remains. The formation and retention of these hydrogen bonds is clearly favourable. As can be seen from Figure 2-4 the most intense species is 3,3'-bis(methylamino)-2,2'-bipyridine (**2.3**) which has been methylated once on each of the two amino groups. This mono-methylation allows for two separate hydrogen bonds between the amine hydrogen and the pyridine nitrogen in opposite rings. Crystals of **2.3** were obtained from the reaction of **2.2** with sodium hydride and methyl iodide as described above and were isolated by slow evaporation of diethyl ether (Figure 2-5, Appendix 1).

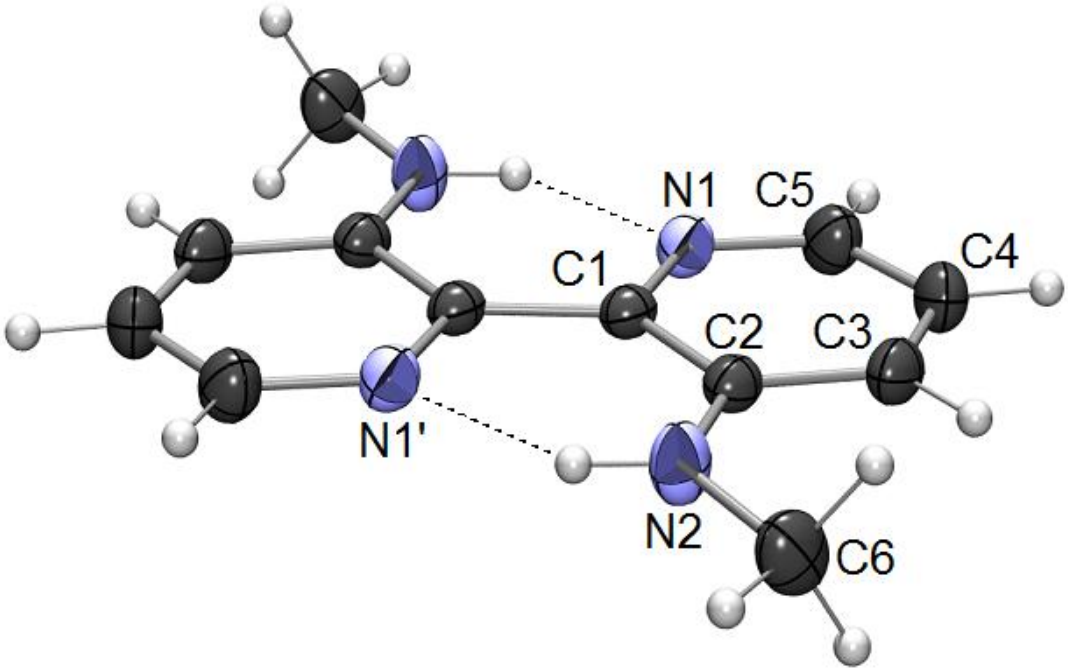

Figure 2-5. X-ray crystal structure of **2.3**. Non-hydrogen atoms are represented by Gaussian ellipsoids at the 70% probability level. Hydrogen atoms are shown with arbitrarily small thermal parameters. Primed atoms are related to unprimed ones vi the crystallographic inversion center (1/2, 0, 1/2) at the midpoint of the C1–C1' bond. Dotted lines indicate hydrogen-bonded N–H…N interactions. Selected interatomic distances (Å): C1-C1' = 1.487(2); N1-N2' = 2.6448(15); N1-C1 = 1.3463(16); N1-C5 = 1.3323(17); N2-C2 = 1.3537(17); N2-C6 = 1.4422(17). Selected bond angles (°): N2-C2-C1 = 122.85(11); C1-N1-C5 = 121.30(11). Selected torsion angle (°): N1-C1-C2-N2: 178.58(12).

The bipyridine core of **2.3** is essentially identical to unsubstituted 2,2'-bipyridine with respect to bond lengths and angles. The C-N1 and C-C bond lengths in the two equivalent pyridine rings average 1.34 and 1.40 Å respectively while the average bond angle is 119.99°. The comparative numbers for 2,2'-bipyridine are 1.36 Å, 1.39Å and 119.79° respectively.[80] As with 2,2'-bipyridine, N1 and N1' are arranged *trans* to one another but while 2,2'-bipyridine is co-planar the two equivalent pyridine rings of **2.3** lie in parallel planes separated by 0.064 Å. The presence of a hydrogen bond is evident from the structure. A hydrogen bond can be classified as strong, moderate or weak by evaluating factors such as bond length, bond angles and comparison of the lengths of the hydrogen bond and the covalent bond between the hydrogen and the atom to which it is bonded.[81] By several measures the interaction in **2.3** can be characterized as moderate

in strength (Table 2-2). The strength of this interaction agrees with the theory that retention of hydrogen bonding opportunities is a complicating factor in the methylation of the amines.

Table 2-2. Relative trends to determine the strength of H-bonds.

H-bond Parameters	**2.3**	Strong	Moderate	Weak
Interaction Type		Strongly covalent	Mostly electrostatic	Electrostatic or dispersed
Bond Length (N2H-N1' [Å])	**1.96**	1.2 – 1.5	1.5 – 2.2	> 2.2
N2-H vs. N2H-N1' [Å]	**0.88 vs. 1.96**	N2-H ≈ N2H-N1'	N2-H < N2H-N1'	N2-H << N2H-N1'
H-bond Angle (N2-H-N1' [°])	**133.3**	170 - 180	> 130	> 90

Attempts were made to inhibit the formation of these hydrogen bonds to facilitate the desired methylation. Coordination of **2.2** to a metal center engages the lone pairs of the pyridine nitrogen so they are no longer available to form hydrogen bonds with an amine hydrogen. $Mo(CO)_4$(nbd) was selected for this task.[82,83] Displacement of the norbornadiene[84] with **2.2** to give $Mo(CO)_4$(**2.2**) effectively removed the possibility of the formation of intramolecular hydrogen bonds within the bipyridine molecule (Scheme 2-3). Confirmation that coordination had occurred through both pyridine nitrogen centers was obtained through comparison to the IR stretching frequencies of $Mo(CO)_4$(2,2'-bipyridine).[85,86] Sodium hydride and dimethyl sulfate as described above were used to methylate $Mo(CO)_4$(**2.2**). Upon completion the infrared spectrum contained no CO stretching frequencies and the ESI-MS spectrum showed products containing one to four methyl groups as well as starting material. The procedure involving sodium hydride and methyl iodide also described above gave a mixture of methylated products as before.

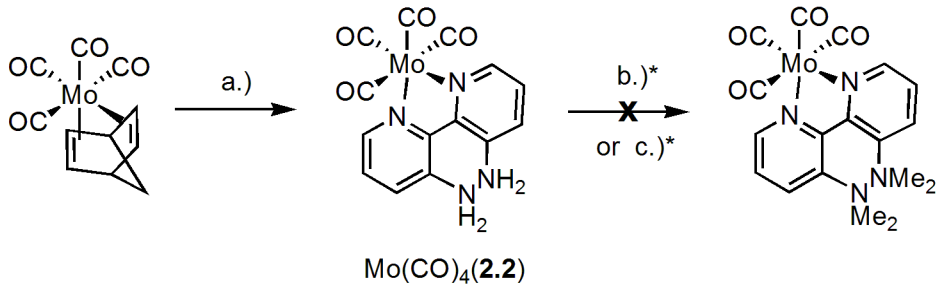

Mo(CO)$_4$(**2.2**)

Scheme 2-3. Attempted methylation of Mo-coordinated **2.2**. a.) **2.2**, benzene, 80 °C, 3hrs; b.) NaH, Me_2SO_4, THF, 66 °C, 4 hrs; c.) NaH, MeI, THF, 66 °C, 2 hrs. *Procedures did not give desired result.

As an alternate approach we tried cross-coupling variations of 3-dimethylaminopyridine (Scheme 2-4). 3-dimethylaminopyridine and 2-chloro-3-dimethylaminopyridine were made using procedures described above although other preparations have been reported.[87,88] The nitropyridine species was reduced using $SnCl_2 \cdot 2H_2O$ in HCl and the subsequent aminopyridine was methylated using formic acid and formaldehyde to give 3-dimethylaminopyridine and 2-chloro-3-dimethylaminopyridine. The copper catalyzed Ullmann coupling of two equivalents of 2-chloro-3-dimethylaminopyridine to give **2.1** was shown by NMR to have yielded no product. The iron catalyzed cross-coupling[89] of 2-chloro-3-dimethylaminopyridine and 3-dimethylamino-2-lithiopyridine (easily generated *in-situ* using ^{n}BuLi in THF and formation verified through independent quenching experiments) also generated no product. ESI-MS of the product showed peaks for both starting materials but no bipyridine.

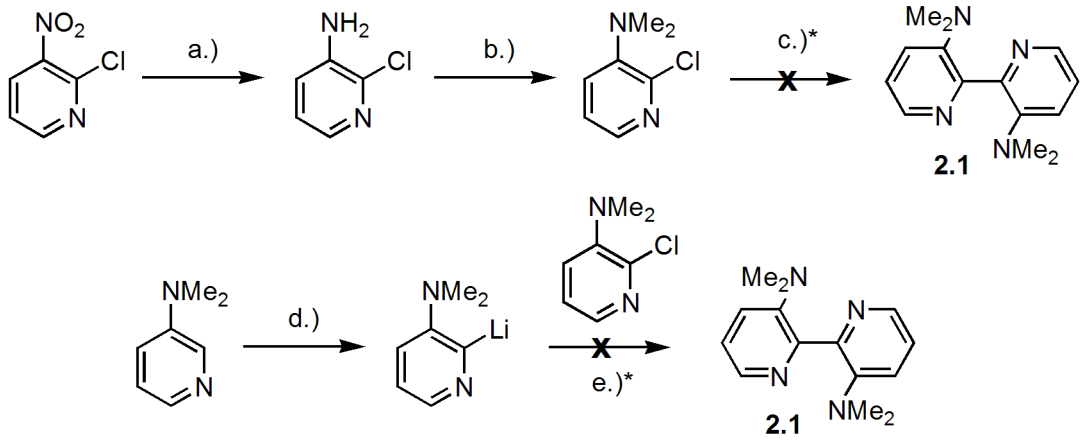

Scheme 2-4. Experimental conditions for attempted coupling of dimethylamino pyridine derivatives. a.) $SnCl_2 \bullet H_2O$/HCl, reflux, 1 hr; b.) formic acid, formaldehyde, 105 °C, 8 hrs; c.) $Cu_{(s)}$/1,4-dioxane, reflux, 16 hrs; d.) ^{n}BuLi/TMEDA, –78 °C, 3 hrs; e.) $Fe(acac)_3$, NMP, –78 °C, 1 hr/rt, 2 hrs. *Procedures did not result in coupled product.

Since the above methylation attempts produced a mixture of products including the pyridinium salt, another strategy which presented itself was to push the reaction all the way to the pyridinium salt followed by removal of one methyl group (Scheme 2-5). This goal was achieved through reaction of **2.2** and neat methyl iodide to give exclusively 3,3'-*N,N'*-bis(dimethylamino)-2,2'-pyridine-methylpyridinium iodide (**2.4**) by ESI-MS. After removal of the excess methyl iodide (under high vacuum on Schlenk line) **2.4** was heated with pyridinium chloride[90] for ten minutes. Even at this short reaction time the demethylation procedure gave 3-methylamino-3'-amino-2,2'-bipyridine and 3,3'-bis(methylamino)-2,2'-bipyridine.

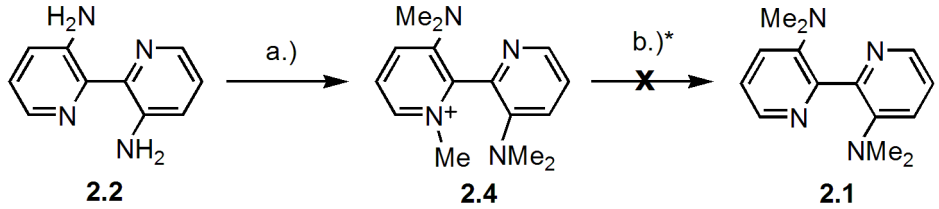

Scheme 2-5. Experimental conditions for demethylation of **2.4**. a.) neat MeI, rt, 3 days; b.) pyridinium chloride, reflux, 10 min. *Procedure gave 3-methylamino-3'-amino-2,2'-bipyridine and 3,3'-bis(methylamino)-2,2'-bipyridine and not **2.1**.

In the course of investigating routes to **2.1** two 3,3'-bis(X)-2,2'-bipyridine (X = Cl or Br) molecules were made from **2.2** through a bis(azide) intermediate[91,92] as shown in Scheme 2-6. An alternate synthesis of 3,3'-bis(chloro)-2,2'-bipyridine has recently been reported through a nickel catalyzed cross-coupling.[93] The intention was to perform substitution chemistry on these molecules to arrive at **2.1**. A lithium-amino-borane reagent (LAB) was made from ^{n}BuLi and $BH_4{\cdot}NMe_2$ in tetrahydrofuran.[94] However, upon addition of the LAB to the bis(halogen) species no aminated product was observed.

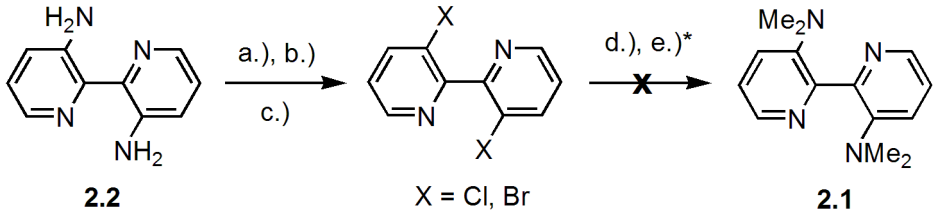

Scheme 2-6. Synthesis of 3,3'-bis(X)-2,2'-bipyridine (X = Cl or Br) and experimental conditions for reaction to give **2.1**. a.) $NaNO_2$, H_2SO_4, CH_3COOH, 0 °C, 30 min; b.) CuX_2, HCl, 0 °C, 30 min, 70 °C, 30 min; c.) NaOH, NaCN; d.) LiH_3BNMe_2, THF, 0 °C, 15 min/rt, 90 min; e.) HCl, MeOH, reflux, 16 hrs. *Substitution products not observed.

2.3 Conclusions

It seems that the biggest factor working against the successful synthesis of **2.1** was the possibility of hydrogen bond formation between the amino groups on one pyridine ring with the nitrogen in the opposite pyridine ring. Offering support to this theory is the crystal structure of **2.3** (Figure 2-5) where the hydrogen bond is clearly illustrated. In order to assess this hypothesis several control experiments were completed (as described in Section 2.2). First, synthesis of the analogous biphenyl molecule has been reported by Shaw and Turner and was easily reproduced. The synthesis of 3-dimethylaminopyridine as reported by Giam and Hauck can also be repeated without difficulty. These two molecules both share a resemblance to the desired end product but

both eliminate the possibility of formation of this specific hydrogen bond. 1,8-bis(amino)naphthalene also does not have this competing hydrogen bond to deal with during methylation to give 1,8-bis(dimethylamino)naphthalene.

It also cannot be steric factors alone as most of the examples given in Figure 2-2 have far more steric bulk imposed by the amine substituents than the bipyridine molecules we were attempting to synthesize. Bipyridine has the advantage of rotation about the 2-2' bond that the examples given above do not have. Any bulk added by methylation of the amine groups in the bipyridine molecule can be accommodated by rotation of this bond.

Steric factors may come into play however, when attempting to methylate the bipyridine ligand when coordinated to Mo in the complex [$Mo(CO)_4$(**2.2**)]. In this case the two amino groups would be forced considerably closer together making substitution at these positions more difficult. The increased interaction could have caused dissociation from the molybdenum center (as evidenced by ESI results discussed above) creating similar conditions; and therefore product distributions; as had been previously observed.

Several competing factors are thought to have limited the success of the Ullmann coupling of 2-chloro-3-dimethylaminopyridine. While electron-withdrawing groups (e.g. NO_2) located *ortho* to the halogen activate the molecule, electron-donating groups (e.g. NMe_2) would have the opposite effect. Particularly bulky substituents in this position will also hinder the formation of coupled products.[95] Similar complications seem plausible for the attempted iron catalyzed coupling.

2.4 Experimental

2-chloro-3-dimethylamino pyridine,[75,76] 3,3'-diamino-2,2'-bipyridine,[75] and $Mo(CO)_4$(norbornadiene)[82] were made by literature methods. All other chemicals were used as obtained (Aldrich, Oakville, Canada). All other chemicals were used as obtained (Aldrich, Oakville, Canada). Solvents were HPLC grade and purified on an MBraun solvent purification system (SPS). Gases were obtained from Airgas (Calgary, Canada). NMR spectra were collected on either an AV-300 or AV-500 Bruker spectrometer. Internal reference was made to $CHCl_3$ (1H d = 7.26 ppm). All mass spectra were obtained on a Micromass Q-ToF *micro* hybrid quadrupole/time-of-flight mass spectrometer in positive ion mode using pneumatically-assisted electrospray ionization with a capillary voltage of 2900 V, source temperature of 80 ℃ and desolvation temperature of 100 °C. Solutions were run in dichloromethane and introduced to the mass spectrometer by a syringe pump at a rate of 10 μL min^{-1}. Internal calibrants for accurate mass experiments were protonated triphenylphosphine oxide ($[C_{15}H_{18}PO + H]^+$ = 278.0939 *m/z*), tetrapropylammonium bromide ($[C_{12}H_{28}N]^+$ = 186.2222 *m/z*), and tetrabutylammonium bromide ($[C_{16}H_{36}N^+]^+$ = 242.2848 *m/z*) as indicated where applicable. Higher mass accuracy is provided in these instances.

3,3'-bis(methylamino)-2,2'-bipyridine (3). Sodium hydride (0.052 g, 2.2 mmol) was added to (3,3'-diamino-2,2'-bipyridine (0.104 g, 0.55 mmol) in THF (15 ml) and stirred for thirty minutes resulting in bubbling and giving a yellow solution. Methyl iodide (0.31 g, 0.14 ml, 2.2 mmol) was added and the solution was refluxed for 90 minutes. Sodium hydroxide was added (3 M, 1 ml) and the mixture extracted with diethyl ether (4 × 10 ml) until no colour remained in the aqueous phase. The organic phase was dried over magnesium sulfate and reduced in volume *via*

rotary evaporator. The yellow solid was re-dissolved with a minimal amount of diethyl ether and cooled to –5 °C to give yellow crystalline material (30 mg, 25%). M.p. = 148-150 °C. ESI-MS (+ve, CH_2Cl_2 + formic acid): *m/z* = experimental: 215.1298 $[C_{12}H_{14}N_4 + H]^+$, calculated: 215.1297; calibrated against $[C_{12}H_{28}N]^+$. ^{1}H NMR (300 MHz, $CDCl_3$): δ(ppm) = 2.92 (s, 6H); 7.06 (dd, $^3J_{HH}$ = 1.53, 8.37 Hz, 2H); 7.15 (dd, $^3J_{HH}$ = 4.55, 8.42 Hz, 2H); 7.91 (dd, $^3J_{HH}$ = 1.62, 4.47 Hz, 2H); 9.43 (s, 2H). ^{13}C (500 MHz, $CDCl_3$): δ (ppm) = 29.80; 117.69; 123.30; 133.13; 140.25; 145.81.

3,3'-dichloro-2,2'-bipyridine.[91,92] To a cold solution (0 °C) of sodium nitrite (370.2 mg, 5.4 mmol) in concentrated sulfuric acid (4 ml) was slowly added a solution of 3,3'-diamino-2,2'-bipyridine (453.2 mg, 2.4 mmol) in glacial acetic acid (4 ml) and stirred for 30 minutes. The ice bath was removed and the reaction stirred at room temperature for 30 minutes and then cooled to 0 °C. A cold solution of copper (I) chloride (2.09 g, 210 mmol) in concentrated hydrochloric acid (5 ml) was then added. The reaction was kept at low temperature so to keep the evolution of gas at a slow rate. After 25 minutes the reaction was heated to 70 °C until effervescence stops, water was added (14 ml) and the reaction stirred overnight. The green-blue, cloudy reaction mixture was filtered and the blue crystals retrieved dissolved in water (15 ml), made alkaline using saturated aqueous sodium hydroxide and sodium cyanide (0.5 g, 10 mmol) added. *CAUTION: solution must be alkaline before addition of sodium cyanide to prevent the formation of toxic hydrogen cyanide (HCN).* The aqueous mixture was extracted with dichloromethane (2 × 25 ml) which was washed once with water (50 ml), dried over magnesium sulfate, taken to near dryness on the rotary evaporator and dried under high vacuum to give a shiny yellow solid (111.1 mg, 20% yield). M.p. = 125-128 °C. ESI-MS (+ve, CH_2Cl_2 + formic

acid): *m/z* = experimental: 224.9848 $[C_{10}H_6Cl_2N_2 + H]^+$, calculated: 224.9986; calibrated against $[C_{16}H_{36}N]^+$. ^{1}H NMR (300 MHz, $CDCl_3$): δ(ppm) = 7.36 (dd, $^3J_{HH}$ = 4.55, 8 Hz, 2H); 7.84 (dd, $^3J_{HH}$ = 1.41, 8 Hz, 2H); 8.64 (dd, $^3J_{HH}$ = 1.41, 4.55 Hz, 2H). ^{13}C (300 MHz, $CDCl_3$): δ(ppm) = 124.5; 131.0; 137.4; 147.5; 155.7.

3,3'-dibromo-2,2'-bipyridine.[91,92] As for 3,3'-dichloro-2,2'-bipyridine but with CuBr in place of CuCl. 3,3'-diamino-2,2'-bipyridine (505.7 mg, 2.72 mmol). White solid retrieved (83.6 mg, 10% yield). M.p. = 148-150 °C. ESI-MS (+ve, CH_2Cl_2 + formic acid): *m/z* = experimental: 314.8899 $[C_{10}H_6Br_2N_2 + H]^+$, calculated: 314.8956; calibrated against $[C_{18}H_{15}PO + H]^+$. ^{1}H NMR (300 MHz, $CDCl_3$): δ(ppm) = 7.28 (dd, $^3J_{HH}$ = 4.45, 8 Hz, 2H); 8.02 (dd, $^3J_{HH}$ = 1.4, 8 Hz, 2H); 7.1 (dd, $^3J_{HH}$ = 1.4, 4.45 Hz, 2H). ^{13}C (300MHz, $CDCl_3$): δ(ppm) = 120.4; 124.9; 140.7; 148.1; 157.1.

$Mo(CO)_4$(3,3'-diamino-2,2'-bipyridine).[82,84] $Mo(CO)_4$(nbd) (164.1 mg, 0.548 mmol) is added to a solution of 3,3'-diamino-2,2'-bipyridine (100.1 mg, 0.538 mmol) in benzene (5 ml) and the reaction was refluxed for three hours covered in aluminum foil. The benzene was removed under high vacuum and the brown solid taken up in dichloromethane to give a red solution. Layering of hexanes over the red dichloromethane solution produces a yellow precipitate. IR (CH_2Cl_2): ν (cm^{-1}) 2013, 1901, 1871, 1824.

3,3'-N,N'-bis(dimethylamino)-2,2'-bipyridine (2.1), attempted syntheses:

Route A: Methylation of 3,3'-diamino-2,2'-bipyridine to 3,3'-N,N'-bis(dimethylamino)-2,2'-bipyridine.[76] 3,3'-diamino-2,2'-bipyridine (100 mg, 5.37×10^{-4} mol) was refluxed in formic acid

(8 ml) and formaldehyde (8 ml) for eight hours to give a bright yellow solution. 4 M hydrochloric acid (20 ml) was added and the solution was taken to near dryness on high vacuum. The yellow-orange solid is taken up in distilled water (15 ml) and 18 M sodium hydroxide (10 ml) was added to give a murky brown mixture. The slurry was extracted with benzene (5 × 15 ml), the organic layer dried with magnesium sulfate and taken to near dryness. ESI-MS (+ve, CH_2Cl_2 + formic acid): *m/z* = 187.1 $[C_{10}H_{10}N_4 + H]^+$.

Route B: Methylation of 3,3'-diamino-2,2'-bipyridine to 3,3'-*N,N'*-bis(dimethylamino)-2,2'-bipyridine.[77] 3,3'-diamino-2,2'-bipyridine (0.500 g, 2.69 mmol) was added to trimethylphosphate (0.785 g, 5.60 mmol) and the yellow solution heated at 200 °C for two hours to give a black sticky substance. Sodium hydroxide (15% aq, 10 ml) and water (15 ml) was added and the mixture stirred for two hours. The black mixture was extracted with diethyl ether (3 × 20 ml), the organic layer dried with magnesium sulfate and sodium hydroxide pellets and then dried under high vacuum. NMR of the resulting orange-brown oil shows an indistinguishable mixture of products.

Route C: Methylation of 3,3'-diamino-2,2'-bipyridine to 3,3'-*N,N'*-bis(dimethylamino)-2,2'-bipyridine.[60] Sodium hydride (320 mg, 13.33 mmol) was added to a solution of 3,3'-diamino 2,2'-bipyridine (0.392 g, 2.11 mmol) in tetrahydrofuran in four equal portions to give a cloudy yellow suspension. Dimethyl sulfate (2.4 ml, 1.80 g, 14.3 mmol) was slowly added and the mixture was refluxed for three hours to give a brown slurry. Methanol (300 ml) was added to the room temperature reaction and the entire mixture poured over sodium hydroxide (saturated aq, 15 ml). The volume was reduced *via* rotary evaporator, water (200 ml) was added

and extracted with ether (200 ml, 4 × 100ml). The volume of bright orange, organic solution was brought to about 50 ml on the rotary evaporator and then under high vacuum. The organic layer was then washed with dilute hydrochloric acid (3 × 30 ml), dried over magnesium sulfate and taken to dryness on the rotary evaporator to give an orange solid. ESI-MS analysis showed no starting material or any methylated products.

Route D: Methylation of 3,3'-diamino-2,2'-bipyridine to 3,3'-*N,N'*-bis(dimethylamino)-2,2'-bipyridine.[79] Dimethyl sulfate (0.70 ml, 0.526 g, 4.17 mmol) was added to a suspension of 3,3'-diamino-2,2'-bipyridine (174.2 mg, 0.935 mmol) in water (5 ml) in portions (0.21, 0.21 and 0.28 ml), and after each addition was shaken for ten minutes and made alkaline with sodium hydroxide (10% aq). The yellow solution was then heated at 100 °C for 15 minutes. ESI-MS (+ve, CH_2Cl_2 + formic acid): *m/z* = 201.2 $[C_{11}H_{12}N_4 + H]^+$; 215.3 $[C_{12}H_{14}N_4 + H]^+$; 229.2 $[C_{13}H_{16}N_4 + H]^+$; 243.2 $[C_{14}H_{18}N_4 + H]^+$; 257.2 $[C_{14}H_{21}N_4]^+$.

Route E: Methylation of 3,3'-diamino-2,2'-bipyridine to 3,3'-*N,N'*-bis(dimethylamino)-2,2'-bipyridine.[78] Sodium hydride (0.633 g, 26.4 mmol) was added to a solution of 3,3'-diamino-2,2'-bipyridine (0.123 g, 0.659 mmol) in THF and stirred for 90 minutes. Methyl iodide (0.375 g, 0.16 ml, 2.64 mmol) was then added and the mixture refluxed for one hour. After cooling to room temperature the mixture was poured over sodium hydroxide (3M, 15 ml) and stirred for 30 minutes. The aqueous layer is extracted with diethyl ether (2 × 50 ml), the organic layer passed through an alumina plug to give a clear yellow solution. The ether was removed via rotary evaporator to give an orange-yellow oil. ESI-MS (+ ve, CH_2Cl_2 + formic

acid): *m/z* = 201.2 $[C_{11}H_{12}N_4 + H]^+$; 215.2 $[C_{12}H_{14}N_4 + H]^+$; 229.2 $[C_{13}H_{16}N_4 + H]^+$; 243.2 $[C_{14}H_{18}N_4 + H]^+$; 257.2 $[C_{14}H_{21}N_4]^+$.

Route F: Homo-coupling of 2-chloro-3-dimethylamino pyridine. 2-chloro-3-dimethylamino pyridine (1.42 g, 9.14 mmol) was added to a slurry of activated copper (1.45 g, 22.79 mmol) in dry DMF (35 ml) and refluxed overnight. The hot reaction mixture was poured over H_2O (400 ml) and isolated via suction filtration and extracted with dioxane *via* Soxhlet apparatus. The dioxane was removed on a rotary evaporator, the solid taken up in CH_2Cl_2, washed with aqueous ammonia followed by H_2O and dried over $MgSO_4$. NMR (300 MHz, $CDCl_3$) showed no coupled product.

Route G: Coupling of 2-chloro-3-dimethylamino pyridine and 3-dimethylamino pyridine.[89] A 1:1 solution of ^{n}BuLi:TMEDA (^{n}BuLi 1.6M in hexanes, 4.09 ml, 6.54 mmol) was added *via* cannula to a solution of 3-diemthylamino pyridine (0.799 g, 6.54 mmol) in THF at –78 °C and stirred for three hours to give a bright orange solution. In a separate Schlenk flask 2-chloro-3-dimethylamino pyridine (0.872 g, 5.56 mmol) was added to a solution of $Fe(acac)_3$ (96.9 mg, 2.74×10^{-4} mol) and NMP (3.19 g, 3.1 ml, 32.15 mmol) in dry THF (30 ml) to give a deep red-orange solution that was cooled to –78 °C. The 3-dimethylamino pyridine solution was then transferred *via* cannula to the 2-chloro-3-dimethlyamino pyridine solution to give a deep red-purple colour and stirred at –78 °C for one hour before being allowed to warm to room temperature. Concentrated HCl (10 ml) was then added and stirred for one hour. The solution was made alkaline with sodium hydroxide (1M, 10 ml), extracted with diethyl ether (4 × 50ml),

dried with $MgSO_4$ and taken to dryness on a rotary evaporator to give a yellow-orange solid. ESI-MS (+ve, CH_2Cl_2 + formic acid): *m/z* = 157.1 $[C_6H_9ClN_2 + H]^+$; 123.1 $[C_6H_{10}N_2 + H]^+$.

Route H: Methylation of $Mo(CO)_4$(3,3'-diamino-2,2'-bipyridine) to $Mo(CO)_4$(3,3'-*N,N'*-bis(dimethylamino)-2,2'-bipyridine). Reduction procedures were followed as above for sodium hydride/dimethyl sulfate[60,78] and sodium hydride/methyl iodide[78] using the metal complex in place of free 3,3'-dimaino-2,2'-bipyridine. For NaH/Me_2SO_4: ESI-MS (+ve, CH_2Cl_2 + formic acid): *m/z* = 201.2 $[C_{11}H_{12}N_4 + H]^+$; 215.2 $[C_{12}H_{14}N_4 + H]^+$; 229.2 $[C_{13}H_{16}N_4 + H]^+$; 243.2 $[C_{14}H_{18}N_4 + H]^+$). For NaH/MeI: ESI-MS (+ve, CH_2Cl_2 + formic acid): *m/z* = 201.2 $[C_{11}H_{12}N_4 + H]^+$; 215.2 $[C_{12}H_{14}N_4 + H]^+$; 229.2 $[C_{13}H_{16}N_4 + H]^+$; 243.2 $[C_{14}H_{18}N_4 + H]^+$; 257.2 $[C_{14}H_{21}N_4]^+$.

Route I: Demethylation of 3,3'-*N,N'*-bis(dimethylamino)2,2'-pyridine-pyridinium iodide. Pyridinium chloride (6.58 g, 56.9 mmol) was added to 3,3'-*N,N'*-bis(dimethylamino)-2,2'-pyridine-pyridinium iodide (0.170 g, 0.066 mmol) and heated at 225 °C for 10 minutes. ESI-MS (+ve, CH_2Cl_2 + formic acid): *m/z* = 201.2 $[C_{11}H_{12}N_4 + H]^+$; 215.2 $[C_{12}H_{14}N_4 + H]^+$.

Route J: Halogen substitution of 3,3'-bis(chloro)-2,2'-bipyridine. $LiH_3BN(Me)_2$ was made according to literature procedures.[94] LiH_3BNMe_2 (0.95 M, 0.27 ml, 0.25 mmol) was added to 3,3'-dichloro-2,2'-bipyridine (50.8 mg, 0.22 mmol) in THF (1 ml) at 0 °C to give a deep red solution. The reaction was stirred at 0 °C for 15 minutes and then at room temperature for 90 minutes. HCl (3M, 3.3 ml) and methanol (3.3 ml) were then added at 0 °C and stirred for 15 minutes. The reaction was refluxed overnight, the volume reduced to approximately 5 ml, made

alkaline with saturated sodium hydroxide and extracted with CH_2Cl_2 (3 × 10 ml). The peach-coloured organic layer was dried with $MgSO_4$ and reduced to dryness. ESI-MS (+ve, CH_2Cl_2): *m/z* = 230.3 $[C_{10}H_6Cl_2N_2 + Li]^+$.

Chapter 3. Hydrogenation of olefins by $RhCl(PPh_3)_3$

3.1 Introduction: Elucidating the mechanism

In 1965 the synthesis of $RhCl(PPh_3)_3$ was independently reported by the groups of Coffey, Bennett and Wilkinson (Figure 3-1, **A**).[96-98] Wilkinson and co-workers showed the complex was capable of hydrogenating olefins and acetylenes through a rhodium-hydride intermediate. Investigation of $RhCl(PPh_3)_3$ (widely known as "Wilkinson's catalyst") has continued to the present day and its mediation of the hydrogenation of olefins is one of the most well-understood catalytic mechanisms, and is a textbook classic.[38,99,100] The generally accepted cycle is shown in Figure 3-1. Discussion of the cycle will refer to the structures by their representative letter (**A** through **J**).

The hydride species $RhCl(PPh_3)_nH_2$ (n = 1 or 2) was produced by bubbling hydrogen gas through a solution of **A** in benzene. The dissociation of a triphenylphosphine (PPh_3) ligand from $RhCl(PPh_3)_3H_2$ (**F**) was reported to be facile, yielding $RhCl(PPh_3)_2H_2$ (**C**) so that a vacant site for an incoming unsaturated species was established (the vacant site being occupied by a solvent molecule in the interim). The issue of PPh_3 dissociation became a hot topic in the years following as several publications investigated the amount of "free" PPh_3 found in solution due to the dissociation from **A**.[101-103] It was established that there is indeed dissociation of PPh_3 to give the active $RhCl(PPh_3)_2$ (**B**) but that it exists in an equilibrium heavily weighted to the right (Figure 3-1, $K = 1.4 \times 10^{-4}$ M for the dissociation of PPh_3 from **A**) so that the concentration of free PPh_3 is not appreciable.

Extensive NMR investigations by Tolman and co-workers in 1972[104] showed that addition of H_2 to **A** is nearly quantitative to give **F** and the process is indeed reversible as reported by Wilkinson.[97] Using stopped-flow spectroscopy, Halpern and co-workers[105] were able to show that the majority of species **F** was generated through addition of H_2 to **B** followed by rapid association of PPh_3. The reactivity of **B** with respect to addition of H_2 is 10^4 times faster than addition to **A**, so that the rate of H_2 addition to form **F** actually becomes dependent on the rate of dissociation of PPh_3 from **A**.

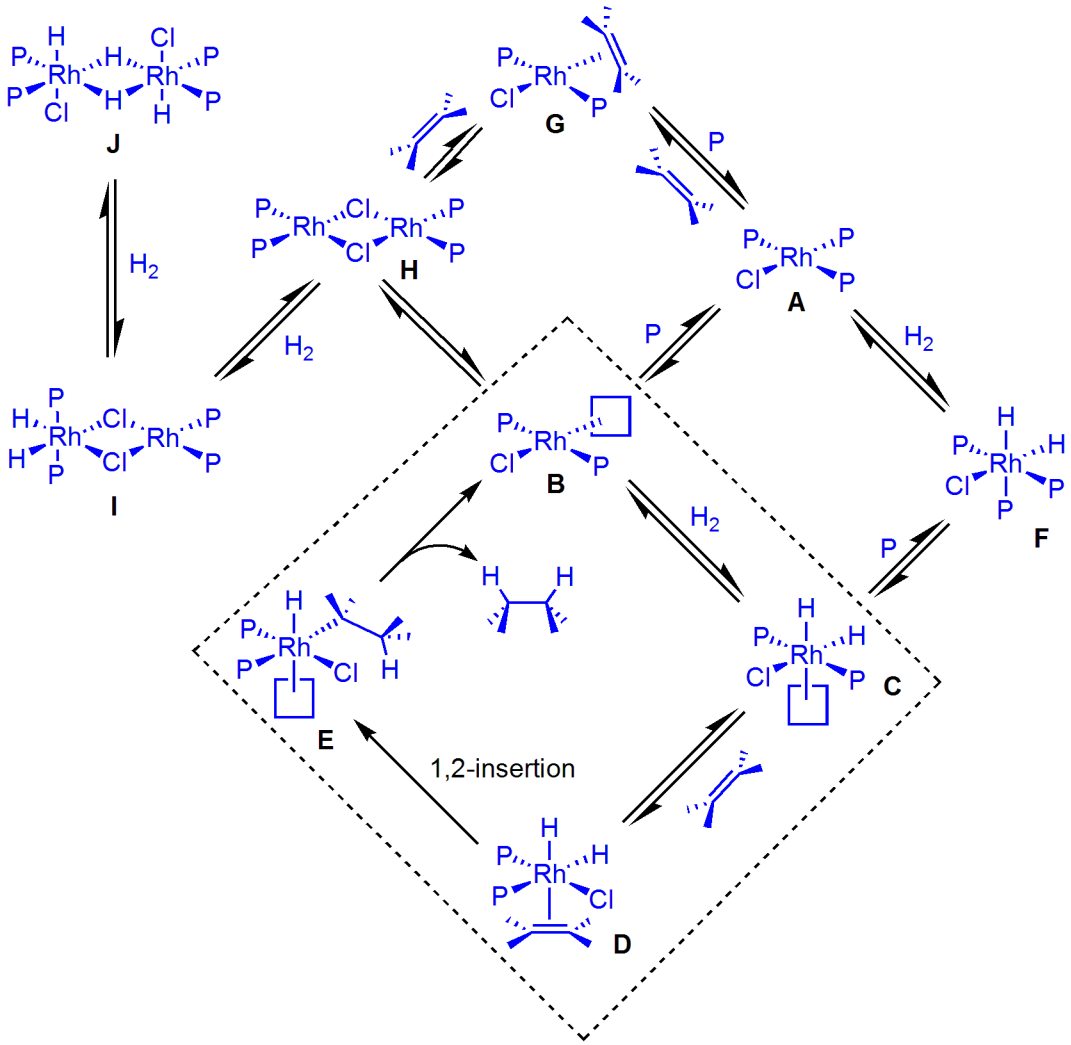

Figure 3-1. The catalytic cycle for the hydrogenation of olefins using Wilkinson's catalyst. The dashed lines enclose the productive part of the cycle. P = PPh_3.

The productive part of the mechanism can be accessed at several points. Dissociation of PPh_3 from **F** to give **C** was shown to occur *trans* to a hydride with the equilibrium lying towards **F**. The resulting vacant coordination site is likely to be the location for the incoming olefin to give $RhCl(PPh_3)_2H_2$(olefin) (**D**).[104] With an excess of PPh_3 to suppress formation of **B**, **C**, and **H,** Halpern was able to focus exclusively on characterization of, and direct reaction with, species **A** and **F**.[106,107] The investigation showed that dissociation of H_2 from **F** to give **A** is much slower than addition of olefin to **C**. Therefore, the dissociation of a PPh_3 ligand from **F** to give **C** could be trapped by an incoming olefin to give **D**. In this way, the cycle moves forward as formation of **D** is favoured over reductive elimination of H_2 to move back to **A**. Support for the dissociation of PPh_3 *trans* to a hydride from **F** to give **C** was provided by Brown. Through magnetization-transfer experiments and molecular modelling they were able to show that the dissociated phosphine always returns *trans* to a hydride.[108] Their data show that the PPh_3 dissociation leads to a molecule with two equivalent hydrides and Brown introduced the possibility that the PPh_3 ligands in **C** were arranged *cis* to one another and not *trans* as originally proposed by Wilkinson.[109] In 1994 Duckett showed that the PPh_3 ligands in **D** are indeed oriented *cis* with respect to one another, as are the hydrides which are equivalent on the NMR timescale.[110] Therefore, upon dissociation of a PPh_3 ligand from **F**, isomerization of the coordination sphere must occur before arriving at **D** (Scheme 3-1).

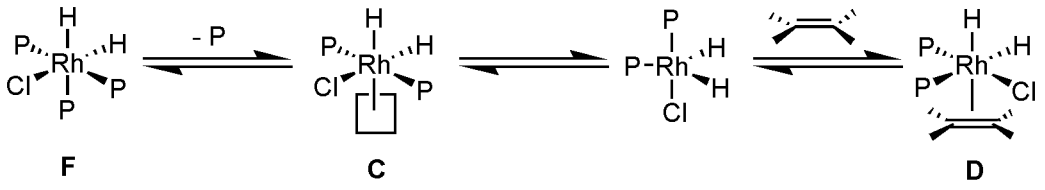

Scheme 3-1. The isomerization of the ligand sphere of $RhCl(PPh_3)_2H_2$ to arrive at a complex containing *cis* PPh_3 ligands was suggested by Brown and confirmed by Duckett.

The 1,2-insertion of the olefin into the Rh-H bond has been identified as the rate-determining step. Wilkinson proposed that this step, based on a kinetic isotope effect of 0.9, involved simultaneous breaking of the Rh-H bonds and formation of C-H bonds as would be seen in a concerted mechanism.[109] In 1967, they further reported that steric bulk and decreased ring strain of the olefin slows the reaction, lending credence to their initial statement.[111] In 1977, Halpern postulated that the rate-determining step was likely migratory insertion of the olefin, and he determined that it principally involved Rh-H bond breaking, measuring a kinetic isotope effect of 1.15. The same study concluded that insertion of the olefin resulted in a coordinatively unsaturated species (**E**) as the rate of insertion was independent of the concentration of PPh_3.[106]

Wilkinson reported in 1965 that PPh_3 dissociation from **A** gives the coordinatively unsaturated complex **B**, which then undergoes dimerization to give the chloride-bridged $Rh_2(\mu\text{-}Cl)_2(PPh_3)_4$ (**H**). He later reported that the dimer takes up two moles of H_2 (one per rhodium center) to give $Rh_2(\mu\text{-}Cl)_2(PPh_3)_2(\mu\text{-}H)_2H_2$ (**J**) with bridging chloride ligands.[109] Several years later Tolman and co-workers[112] reported details about the stereochemistry of addition of H_2 to the dimer indicating that H_2 addition occurred on only one of the two Rh centers to give the mixed Rh(I)/Rh(III) species **I**. They argued that addition of H_2 occurred directly to **H** and was not the result of dimerisation of **A** and **C**. Halpern added that the rate of addition of H_2 to **H** was comparable to the rate of addition to **A** and that **I** is not catalytically active.[105] It wasn't until the mid-1990s that Duckett and Eisenberg reported the interesting geometry[110] of the tetrahydride species **J** elucidated from advanced NMR techniques involving the use of spin-doped molecular hydrogen (parahydrogen).[113] Duckett went on to conclude that **I** and **J** are not directly involved in the active cycle and their formation is responsible for reduced activity of the system.[110] Addition of

excess PPh_3 or olefin to the dimer will break the halide bridges to give $RhCl(PPh_3)_3$(olefin) (**G**) and **A**. However, Duckett also observed a $Rh_2Cl_2(PPh_3)_3H_2$(olefin) dimer with bridging chlorides, a mixed Rh(I)/Rh(III) complex, where H_2 had added to one rhodium and the olefin had added to the other. Investigations on this system have continued with Duckett and co-workers providing extensive ^{31}P, ^{1}H, and ^{103}Rh NMR data for the speciation of this system.[114,115]

3.2 Investigations with ESI-MS

It is the goal of our group to establish the utility of charged ligands for the investigation of catalytic systems. In order to take on systems that are less well studied it is necessary to validate our approach using a system that is well understood. The hydrogenation of olefins by Wilkinson's catalyst is just such a system. Showing that it is possible to observe the same species by ESI-MS that have been reported for this system for the last fifty years through more conventional techniques would provide such a validation.

As discussed in Chapter 1, many reports rely on the dissociation of an ionic ligand to impart a charge to the metal center, and therefore the complex. Our group prefers to make use of the spectator ligands of the complex by introducing small modifications that change the steric and electronic environment of the complex as little as possible. Phosphine ligands are of particular interest as they are easily modified and are applicable to many different systems. In our group, Nicola Farrer previously reported the application of bisphosphine monoxides, $Ph_2P(O)(o\text{-}C_6H_4)PR_2$ (R = aryl or alkyl)[116] and a triphenylphosphine derivative that incorporates a proton sponge functionality in place of one phenyl group, {1,8-bis(dimethylamino)naphthalene-2-yl}diphenylphosphine[50] to the study of neutral metal

complexes. While these ligands were effective, they rely on the basicity of their functional groups to produce $[M + Na]^+$ and $[M + H]^+$ ions. We became interested in phosphine ligands that incorporated a permanent charge as a more facile route to a similar end. While numerous syntheses to such compounds are known, the number of steps required is often substantial, especially in the preparation of phosphine/ammonium ligands. In mixed P/N ligands, the phosphorus must first be protected, the nitrogen alkylated and the phosphorus deprotected (Section 1.6.2). Such high synthetic overhead needs to be avoided in order for ESI-MS analysis to become routine, and the ideal reaction is of course one step in high yield. Accordingly, we looked at P/P ligands, as bis- and trisphosphines are commercially available. It turned out that monoalkylation of bisphosphines was first reported in 1969.[117] Ercolani and co-workers benzylated 1,1-diphenylphosphinomethane and 1,2-diphenylphosphinoethane to give ligands of the type $[Ph_2P(CH_2)_nPPh_2(CH_2Ph)]^+ X^-$ (n = 1 or 2, X = Cl, Br or I). The authors used the ligands to study their electronic effects on tetrahedral, zwitterionic Co and Ni complexes of the form $MX_3[Ph_2P(CH_2)_nPPh_2(CH_2Ph)]$. In 1974, Taylor and co-workers employed similar synthetic methodology to arrive at $[W(CO)_5\{PPh_2(R)PPh_2(Me)\}]^+$ complexes (R = ethylene and acetylene).[118] It appears as though these types of ligands have not been utilized since that time.

It was our intention to synthesize ligands of this type and add them to solutions of $RhCl(PPh_3)_3$ to substitute one of the PPh_3 ligands for the charged phosphine (Equation 3-1). Such a substitution would make the complex ESI-active and the catalytic system amenable to study by ESI-MS.[30] This approach requires the phosphine ligands to be labile, but fortunately this is often a prerequisite for catalytic activity.

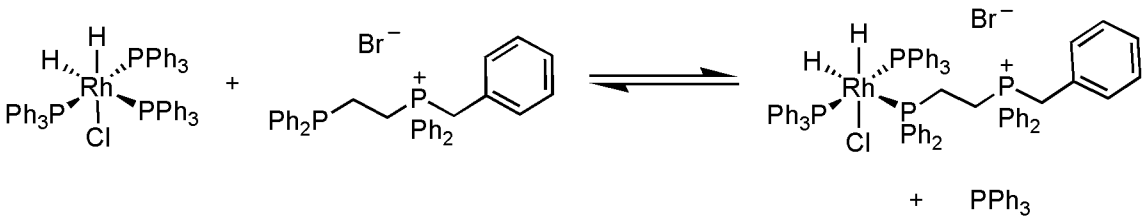

Equation 3-1

3.3 Results and Discussion

3.3.1 Ligand synthesis and solid-state structure

The general preparation of the phosphine ligands of interest is shown in Equation 3-2. The phosphine starting materials were all commercially available and the addition of benzyl bromide in tetrahydrofuran gave the desired product in one step. Minimal work-up was required and a variety of salts were easily accessed upon metathesis of the bromide salt obtained from the benzylation.

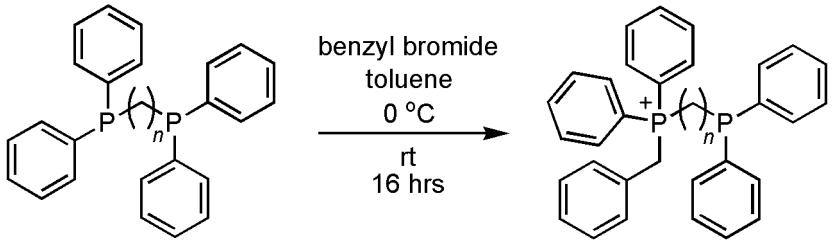

Equation 3-2

Shown in Figure 3-2 are the ligands obtained by this method, including one chelating bisphosphine/phosphonium ligand; 1-diphenylphosphino-1-benzyldiphenylphosphonium-methane [**3.1**]$^{+}$ Br^{-}, 2-diphenylphosphino-1-benzyldiphenylphosphonium-ethane [**3.2**]$^{+}$ Br^{-} and BPh_4^{-}, 1,1-bis(diphenylphosphino-methyl)-1-benzyldiphenylphosphonium-methyl-ethane

[**3.3**]$^{+}$ Br^{-}, 4-diphenylphosphino-1-benzyldiphenylphosphonium-butane [**3.4**]$^{+}$ Br^{-}, BF_4^{-} and PF_6^{-} and 6-diphenylphosphino-1-benzyldiphenylphosphonium-hexane [**3.5**]$^{+}$ Br^{-}.

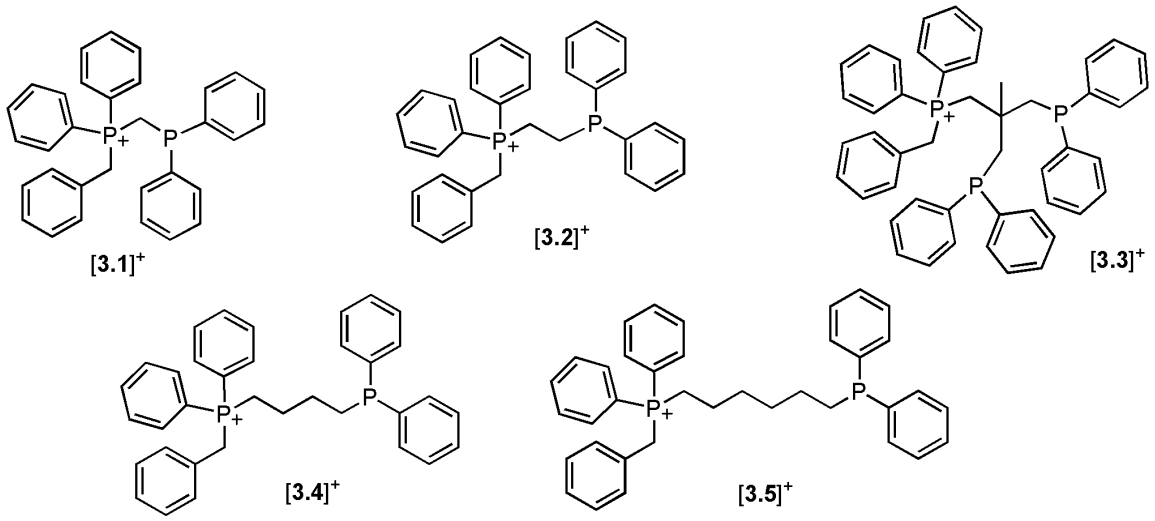

Figure 3-2. The set of ligands synthesized in this study. Counterions were either Br^{-}, BF_4^{-} or PF_6^{-}.

None of the bromide salts generated single crystals and neither did the tetraphenylborate (BPh_4^{-}) or tetrafluoroborate (BF_4^{-}) salts. The hexafluorophosphate salt [**3.4**]$^{+}$ PF_6^{-} provided single crystals (from layering of hexanes over a solution in dichloromethane) and the X-ray crystal structure was obtained as shown in Figure 3-3. Further characterization is given in Appendix 2. The structure shows that functionalization of one end of the molecule leaves the other end essentially unchanged. The phosphine moiety (P2) in [**3.4**]$^{+}$ PF_6^{-} is extremely similar to the starting material 1,4-bis(diphenylphosphino)butane[119] and the related 1-diphenylphosphino-11-bromoundecane[120] in both bond lengths and angles. The P-C bond lengths were all within 0.1 Å and the sum of the C-P-C angles is 303.78°, 304.05° and 308.78° for [**3.4**]$^{+}$ PF_6^{-}, 1,4-bis(diphenylphosphino)butane and 1-diphenylphosphino-11-bromoundecane respectively. The ^{31}P NMR shifts of the starting material and the uncharged phosphine in

[**3.4**]$^{+}$ Br^{-} are –15.6 and –16.7 ppm respectively, demonstrating how similar their magnetic environments are.

The environment surrounding the phosphonium moiety (P1) is as expected. The C-P-C bond angles are close to an ideal tetrahedral arrangement with values ranging from 107.47(13) to 111.57(13)° while the angles in P2 are more constrained due to the presence of the lone pair and are in the range of 99.43(13) to 103.58(13)°.

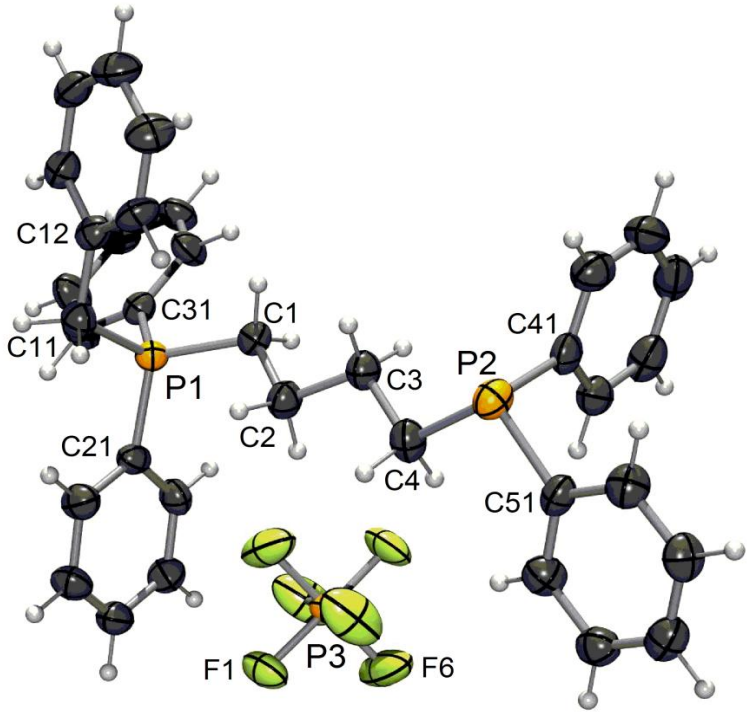

Figure 3-3. Single crystal X-ray structure of [**3.4**]$^{+}$ [PF_6]$^{-}$. Selected bond distances(Å): P(1)-C(31) 1.792(3); P(1)-C(21) 1.794(3); P(1)-C(1) 1.803(3); P(1)-C(11) 1.813(3); P(2)-C(41) 1.834(3); P(2)-C(4) 1.838(3); P(2)-C(51) 1.840(3). Selected bond angles (°): C(31)-P(1)-C(21) 109.80(12); C(31)-P(1)-C(1) 108.86(13); C(21)-P(1)-C(1) 110.62(12); C(31)-P(1)-C(11) 111.57(13); C(21)-P(1)-C(11) 107.47(13); C(1)-P(1)-C(11) 108.53(13); C(41)-P(2)-C(4) 100.77(13); C(41)-P(2)-C(51) 99.43(13); C(4)-P(2)-C(51) 103.58(13). Image drawn with ellipsoids at 70% probability using ORTEP-3.[121]

3.3.2 Method development

The approach we took for this investigation was to add a small amount of ligand to a solution of **A** so that the equilibrium between species **A** and **B** would allow incorporation of the charged ligand into the complex. The first iteration involved the addition of [**3.2**]$^{+}$ Br^{-} to the catalyst in solution. One complication arose instantly. The chloride anion of the catalyst was undergoing exchange with the [**3.2**]$^{+}$ bromide counter-ion as described in Equation 3-3 and shown in Figure 3-4.

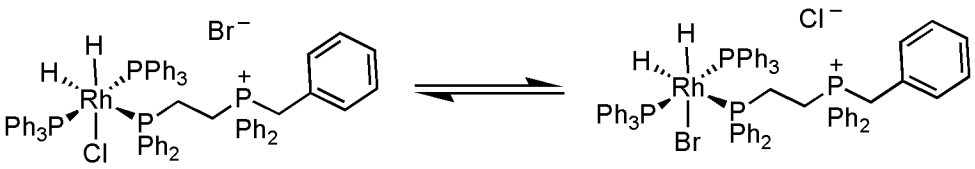

Equation 3-3

While the peaks were readily assigned the incorporation of a bromide ion created at least one extra peak per halide containing species. In a spectrum collected of **A** and [**3.2**]$^{+}$ Br^{-} the presence of the bromide ion already generated several additional peaks (Figure 3-4). As the investigations continued, the speciation would only become more complicated even before consideration of the additional bromide containing species. Also, the reactivity of $RhBr(PPh_3)_3$ may not have been comparable to $RhCl(PPh_3)_3$. For these reasons the bromide counter-ion was metathesized for the non-coordinating BF_4^- anion. This alleviated the issue of halide exchange and an unnecessarily complicated spectrum.

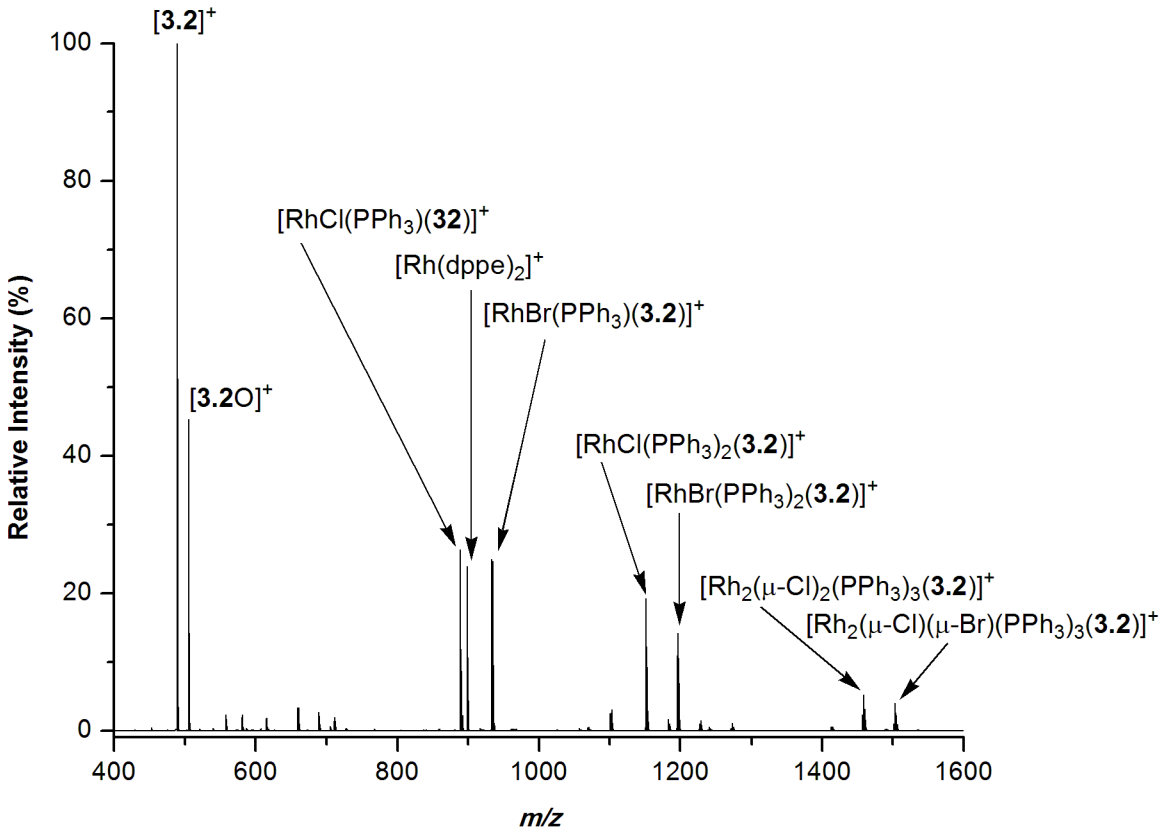

Figure 3-4. Positive-ion ESI-MS resulting from the addition of [**3.2**]$^{+}$ Br^{-} in 1:1 EtOH:benzene.

During the course of the experiments with **A** and [**3.2**]$^{+}$ BF_4^{-} the two main degradation products visible by ESI-MS were formation of [**3.2**O]$^{+}$ and $[Rh(dppe)_2]^{+}$ (dppe = 1,2-bis(diphenylphosphino)ethane). It is believed that the $[Rh(dppe)_2]^{+}$ species arose due to the length of the $(CH_2)_2$ alkyl chain of [**3.2**]$^{+}$. We suspect that de-alkylation (to give $[P(Ph)_2Bn]^{+}$ at 353.1 *m/z* and $[Bn(Ph)_2P(CH_2)_2P(Ph)_2Bn]^{2+}$ at 290.1 *m/z*) of [**3.2**]$^{+}$ generates dppe which binds to the rhodium center to give the known complex $RhCl(dppe)_2$.[122] Dppe is commonly used as a chelating ligand due to the energetically stable five-membered ring formed by the metal and the ligand. This species then ionizes by loss of the chloride ligand to give the observed $[Rh(dppe)_2]^{+}$ (Figure 3-4). Upon switching to the [**3.4**]$^{+}$ BF_4^{-} ligand this de-alkylation reaction was avoided, presumably because the interaction of the phosphonium moiety with the

rhodium center is no longer favourable due to the seven-membered ring that would be formed with the $(CH_2)_4$ alkyl chain.

It was during the course of these experiments that the large effect of cone voltage on the speciation in the spectra was fully realized. The voltage applied across the skimmer cones changes the number of ions registered by the detector. As the cone voltage is increased the number of ions that are successfully drawn towards the cone and into the instrument increases, thus increasing the number of ions that successfully reach the detector. As can be seen from Figure 3-5 this relationship is essentially linear, meaning that by increasing the applied cone voltage the sensitivity of the analysis can be improved. Accordingly, samples of robust organic molecules are typically run at high voltages (e.g. 40 V or higher). The situation is different when considering organometallic and metal-containing molecules. These species are often much more fragile than their organic counterparts and the high voltages used to achieve high sensitivity often result in fragmentation of the species of interest. Because of this, the analysis of catalytic mixtures must be done at substantially lower cone voltages (e.g. 5 – 10 V) to avoid losing valuable information due to low energy processes such as ligand dissociation. The investigation of these systems is therefore an effort to obtain data that is representative of intact solution speciation in reasonable time frames. Perfectly acceptable signal to noise ratios can nevertheless be achieved through longer acquisitions, even at these low voltages. The good data obtained under these conditions is partly a function of the ligand design: operating at low cone voltage, and therefore low total ion current, is more than made up for by the fact that greasy, surface-active ions have a particularly high response in ESI-MS.

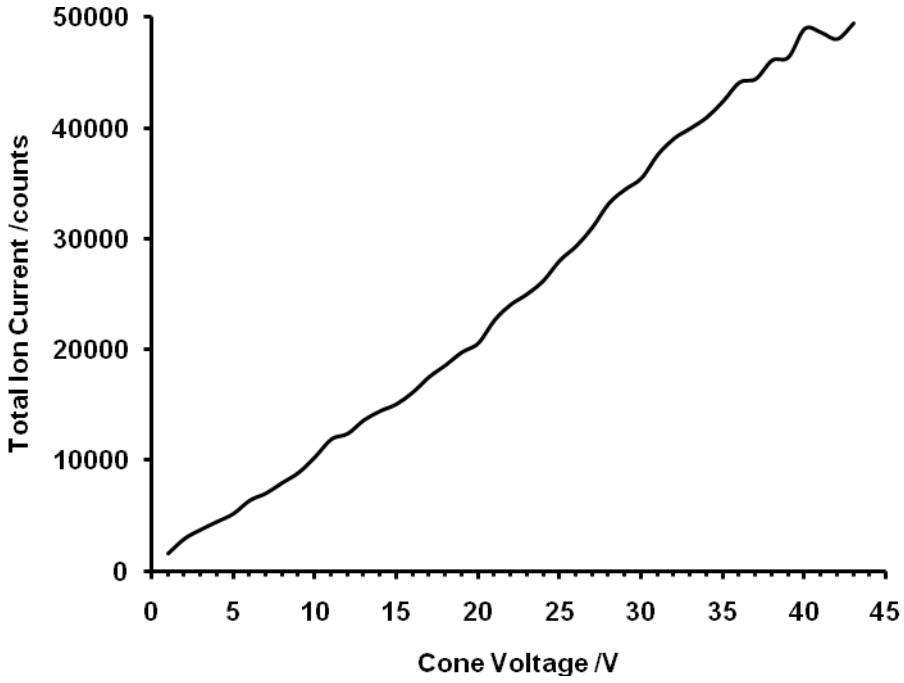

Figure 3-5. The relationship between cone voltage and total ion current registered at the detector is close to linear.

The changes in intensity of any species can be investigated by plotting the ion count for a given mass range (encompassing the entire isotope pattern) and plotting *versus* cone voltage. An example is shown Figure 3-6. A spectrum was collected at each cone voltage and the intensity of $[RhCl(PPh_3)_2(\mathbf{3.4})]^+$ was selected so that a profile of the intensity of an ion over a voltage range was produced (Figure 3-6, A). The intensity initially increased with cone voltage due the effect described in Figure 3-5. However, at a given voltage the ion began to fragment and a decline in intensity was observed as a result. The data was then normalized by the total ion count to account for variations in signal (caused by the effects described in Figure 3-5 as well as fluctuations in the spray emerging from the capillary) so that the behaviour of the species of interest is clearly presented (Figure 3-6, B).

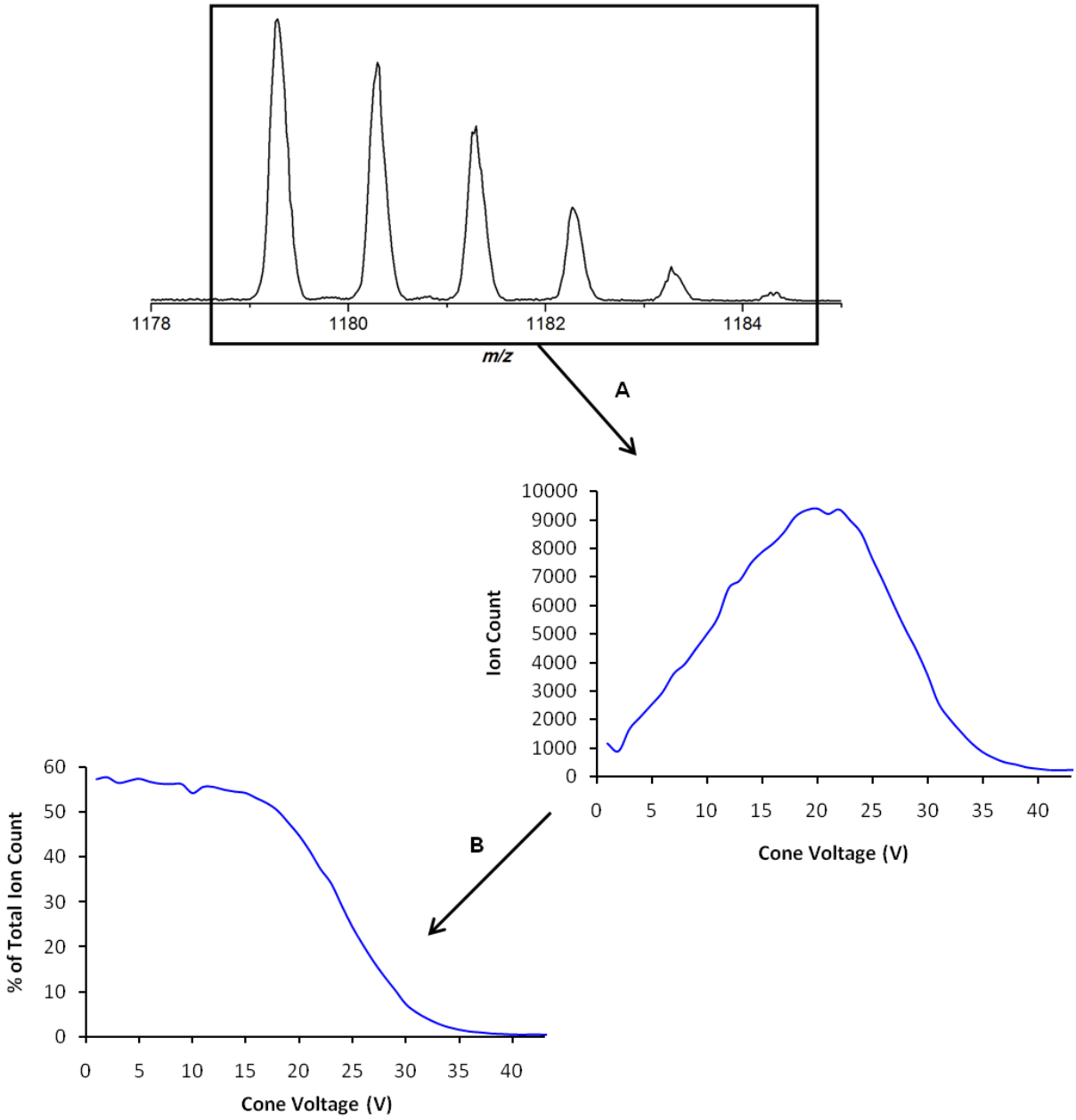

Figure 3-6. The intensity of an ion with changing cone voltage can be monitored by compensating for the total ion count of the spectrum. A) The intensity of a species is plotted as a function of the cone voltage. B) Each individual intensity reading is normalized to the total ion current for each individual cone voltage.

Figure 3-7 is a plot of the intensity of the two related **A** and **B**-type species $[RhCl(PPh_3)_2(\mathbf{3.4})]^+$ and $[RhCl(PPh_3)(\mathbf{3.4})]^+$. While at low voltages (i.e. below 10 V) $[RhCl(PPh_3)(\mathbf{3.4})]^+$ has an intensity of only a few percent of the total ion current, at high voltages the relative intensities of **A** and **B** are reversed (an example of a spectrum collected at 10 V is shown in Figure 3-8 and at

20 V in Appendix Figure 1). The plot shows that even at moderate cone voltages the mass spectra of these labile rhodium complexes contained large amounts of fragments produced during the ionization process, thus the solution phase speciation is inaccurately represented at high voltages.

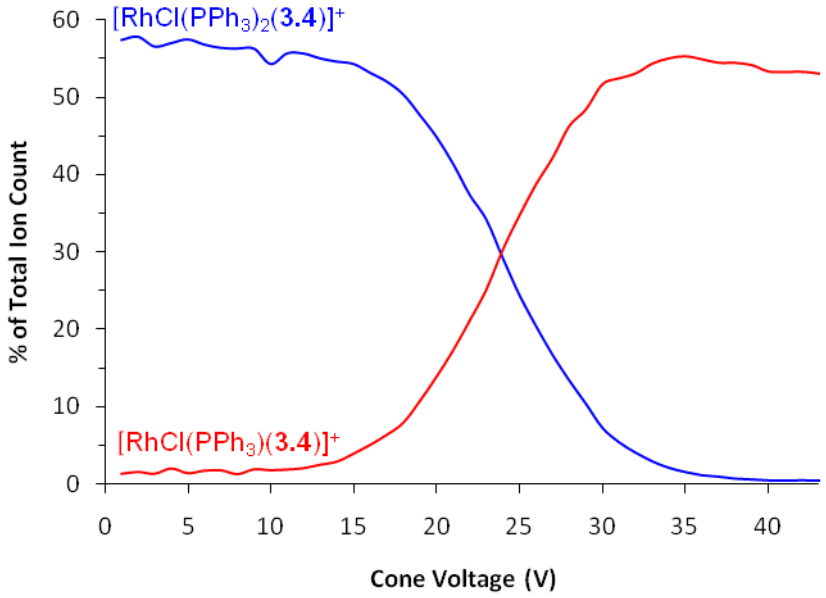

Figure 3-7. The relative intensities of $[RhCl(PPh_3)_2(\mathbf{3.4})]^+$ and $[RhCl(PPh_3)(\mathbf{3.4})]^+$ with increasing cone voltage (V).

Several solvent systems were used (dichloromethane, ethanol and 1:1 ethanol:benzene) before settling on chlorobenzene as the most appropriate solvent. Chlorobenzene provides the best balance of the following criteria: solvent suitability for ESI, low extent of oxide formation, clean spectra and high signal-to-noise ratio.

3.3.3 A solution of $[3.4]^+$ BF_4^- and $RhCl(PPh_3)_3$ in chlorobenzene

Approximately 0.015 mmol of **A** and 0.003 mmol of $[\mathbf{3.4}]^+$ BF_4^- (20 mol%) were dissolved in 12 ml of chlorobenzene and stirred until all the solid had dissolved to give an orange solution.

The small amount of ligand was intentional for several reasons. Adding such a small amount would perturb the equilibrium of the system the least. The formation of multiply charged species due to association of more than one charged ligand was minimized (i.e. formation of fewer $[RhL_x(\mathbf{3.4})_n]^{n+}$ ions, where $n > 1$). Doping in the ligand in this fashion has a further key advantage: regardless of the concentration of the catalyst, the amount of charged ligand can be selected to match the appropriate concentration range for ESI-MS analysis. These two values are often quite different: catalyst concentrations are typically millimolar, whereas ESI-MS can cope with much lower values. This advantage becomes especially notable when high catalyst loadings are required and the stoichiometric amount of ligand would result in an inappropriately high concentration.

A typical spectrum is shown in Figure 3-8. As soon as all solid material was dissolved and a spectrum could be acquired, incorporation of $[\mathbf{3.4}]^+$ into the coordination sphere of **A** to give $[RhCl(PPh_3)_2(\mathbf{3.4})]^+$ was observed as the base peak (1179.2 *m/z*). The **B**-type species $[RhCl(PPh_3)(\mathbf{3.4})]^+$ was also readily observed (917.2 *m/z*), though principally as a fragment from the base peak (*vide supra*). Dimeric species were observed at higher *m/z* values including **H**-type species $[Rh_2(\mu\text{-}Cl)_2(PPh_3)_3(\mathbf{3.4})]^+$ (1581.2 *m/z*). Free $[\mathbf{3.4}]^+$ appeared at 517.2 *m/z* as well as $[\mathbf{3.4}O]^+$ at 533.2 *m/z*. The dissociation of chloride from **A** to give $[Rh(PPh_3)_3]^+$ was observed at 889.2 *m/z*. In spite of the small amount of $[\mathbf{3.4}]^+$, some multiply charged species were observed such as $[RhCl(\mathbf{3.4})_2]^{2+}$ and $[RhCl(PPh_3)(\mathbf{3.4})_2]^{2+}$ (586.2 and 717.2 *m/z*). Due to the soft nature of the technique, some ion aggregates were also observed, including $[RhCl(PPh_3)(\mathbf{3.4})_2\ BF_4]^+$ (1521.4 *m/z*). In the discussion of this system, reference will be made, for instance, to "**A**-type species." Grouping of the ions observed is necessary as a single species was commonly

represented by several peaks. For example, $RhCl(PPh_3)_3$ was observed as the **A**-type ions $[RhCl(PPh_3)_2(\mathbf{3.4})]^+$, $[RhCl(PPh_3)(\mathbf{3.4})_2]^{2+}$, and $[RhCl(PPh_3)(\mathbf{3.4})_2\ BF_4]^+$.

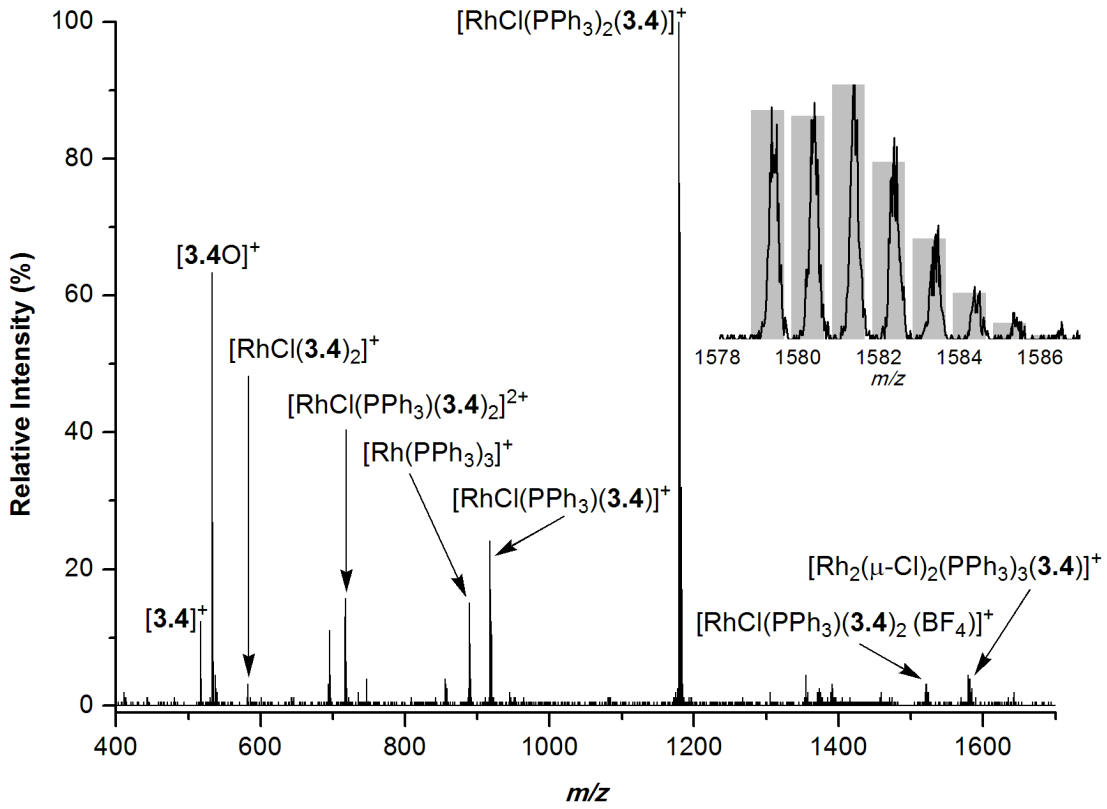

Figure 3-8. Positive-ion ESI-MS of $[\mathbf{3.4}]^+\ BF_4^-$ and $RhCl(PPh_3)_3$ in chlorobenzene. Cone voltage = 10 V. Inset: isotope pattern for $[Rh_2(\mu\text{-}Cl)_2(PPh_3)_3(\mathbf{3.4})]^+$ with calculated pattern (grey bars).

CID studies of **A**-type species $[RhCl(PPh_3)_2(\mathbf{3.4})]^+$ and $[RhCl(PPh_3)(\mathbf{3.4})_2]^{2+}$ were carried out. The CID data in Figure 3-7 shows that $[RhCl(PPh_3)_2(\mathbf{3.4})]^+$ preferentially lost a PPh_3 ligand, as indicated by the match of disappearance and appearance rates of the two species, indicating that $[\mathbf{3.4}]^+$ is bound more strongly to the rhodium center than PPh_3. Figure 3-9 shows the MS/MS analysis of $[RhCl(PPh_3)(\mathbf{3.4})_2]^{2+}$ which also fragmented *via* loss of phosphine ligands. This particular situation was complicated by the two charged ligands resulting in an increase in charge density. The Coulombic repulsion between the two positive charges was enough to make loss of

[**3.4**]$^+$ competitive with loss of PPh_3. Because [RhCl(PPh_3)(**3.4**)$_2$]$^{2+}$ has a charge of +2, loss of one [**3.4**]$^+$ ligand produced a fragment with a charge of +1 at *higher m/z* than the parent ion. The high intensity of [**3.4**]$^+$ in Figure 3-9 is due to further fragmentation of the [RhCl(PPh_3)(**3.4**)]$^+$ product ion generated from the loss of [**3.4**]$^+$ from [RhCl(PPh_3)(**3.4**)$_2$]$^{2+}$.The fragile nature of these **A**-type species is in keeping with is what is known about the facile dissociation of PPh_3 in solution.

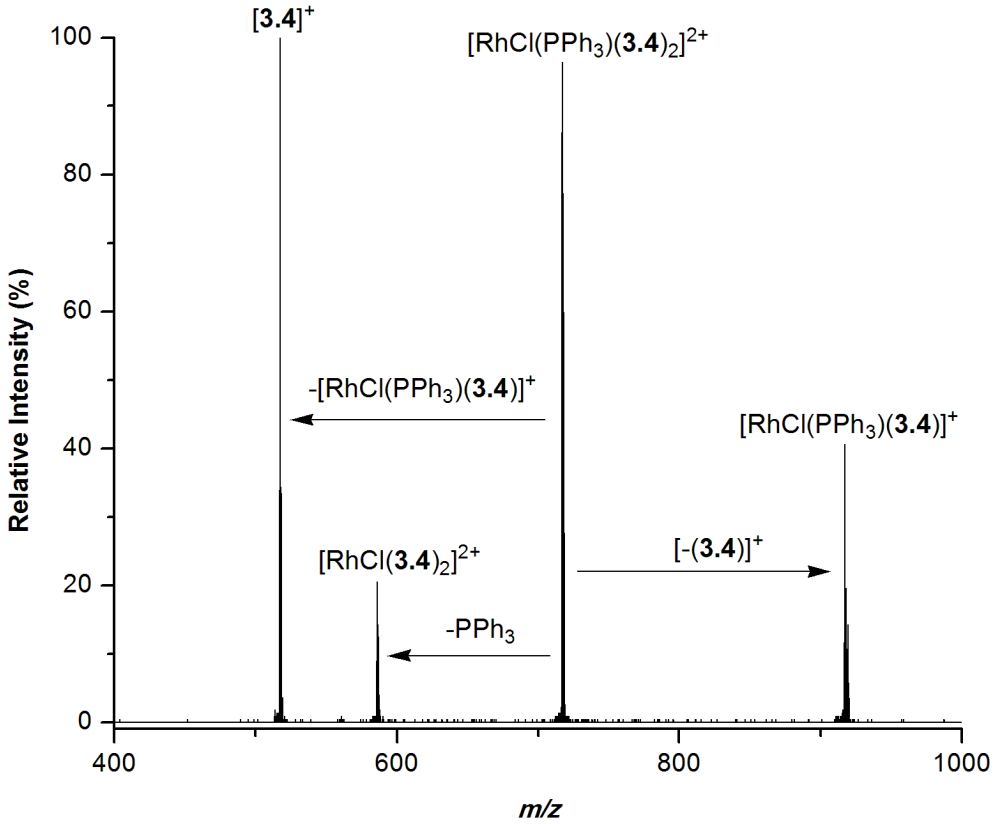

Figure 3-9. Positive-ion ESI-MS/MS of [RhCl(PPh_3)(**3.4**)$_2$]$^{2+}$. Cone voltage = 10 V.

Analysis of **H**-type species [Rh_2(μ-Cl)$_2$(PPh_3)$_3$(**3.4**)]$^+$ through MS/MS showed that loss of PPh_3 ligands did not occur at all (Figure 3-10). Instead, symmetric splitting into the two **B**-type species [RhCl(PPh_3)(**3.4**)]$^+$ and [RhCl(PPh_3)$_2$] (neutral fragments are not observed). Note the absence of [Rh_2(μ-Cl)$_2$(PPh_3)$_2$(**3.4**)]$^+$ at 1319.0 *m/z* or [**3.4**]$^+$ at 517.2 *m/z* that would have

resulted from loss of a phosphine ligand. This behaviour is again in keeping with known solution phase behaviour as the process observed in the gas phase is the reverse of the dimerisation of two equivalents of **B** that is believed to generate **H**.

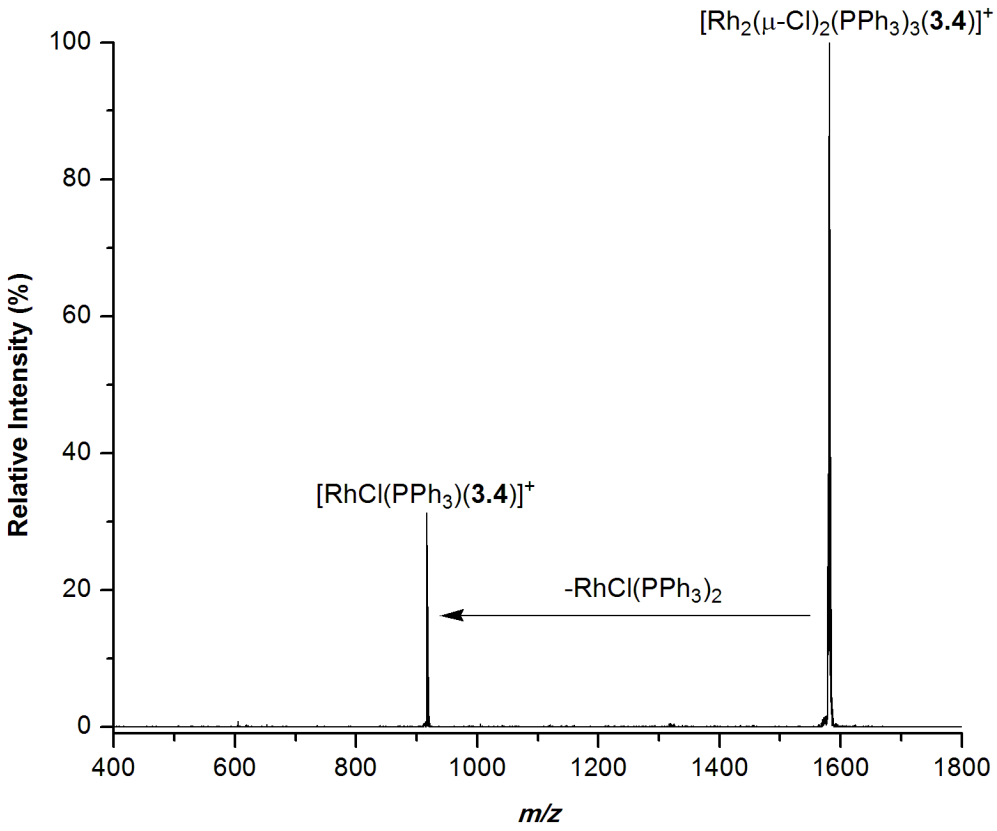

Figure 3-10. Positive-ion ESI-MS/MS of $[Rh_2(\mu\text{-}Cl)_2(PPh_3)_3(\mathbf{3.4})]^+$ shows symmetric fragmentation of the dimer to give $[RhCl(PPh_3)(\mathbf{3.4})]^+$ and the neutral $RhCl(PPh_3)_2$. Cone voltage = 10 V and the collision voltage was increased from 0 to 50 V.

The degree of incorporation of $[\mathbf{3.4}]^+$ into **A** was determined in an NMR experiment. Adding equivalent amounts of **A** and $[\mathbf{3.4}]^+ Br^-$ showed complete disappearance of the signal due to free $[\mathbf{3.4}]^+$ (Appendix Figure 2) indicating 100% incorporation into the complex, while an appropriate amount of PPh_3 was generated. The spectrum is quite complicated due to the possibilities of *cis* and *trans* isomers as well as multiple $[\mathbf{3.4}]^+$ ligands being associated with one rhodium center.

Therefore, the NMR results agreed with the MS/MS experiments that qualitatively indicated that [**3.4**]$^+$ is more strongly bound to rhodium than PPh_3.

3.3.4 Addition of H_2 to [3.4]$^+$ BF_4^- and $RhCl(PPh_3)_3$ in chlorobenzene

The addition of H_2 to the system was accomplished by the simple expedient of bubbling it through a solution of **A** and [**3.4**]$^+$ BF_4^-. The colour of the solution changed from orange to yellow within about fifteen seconds. Samples were removed from the reaction vessel for ESI-MS analysis *via* gas-tight syringe. The spectrum obtained from this solution is shown in Figure 3-11. At first glance, little seems to have changed, but upon closer examination, it was clear that addition of H_2 had occurred to [$RhCl(PPh_3)_2$(**3.4**)]$^+$ to give **F**-type species [$RhCl(PPh_3)_2H_2$(**3.4**)]$^+$ (1181.2 *m/z*) at two *m/z* higher. An expansion of this peak is given in Figure 3-12. Analysis of the composition of this species shows that 87% of the [$RhCl(PPh_3)_2$(**3.4**)]$^+$ was hydrogenated. These results are in keeping with the nearly quantitative addition of H_2 reported by Tolman in 1972.[104]

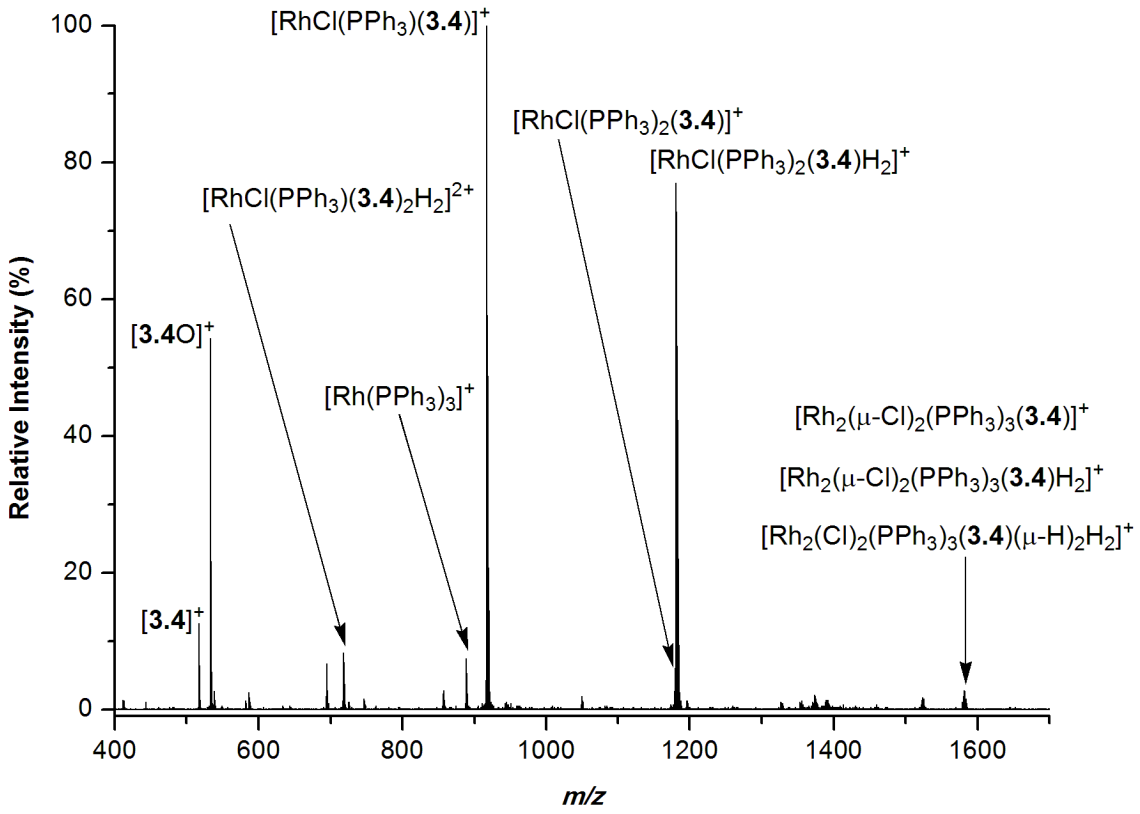

Figure 3-11. Positive-ion ESI-MS of [**3.4**]$^+$ BF_4^- and $RhCl(PPh_3)_3$ in chlorobenzene with H_2 bubbling. Cone voltage = 10 V.

The evaluation of H_2 addition to any species in the reaction must take into account the overlapping signals of the hydrogenated and non-hydrogenated species. Isotope patterns for the two overlapping species were calculated separately using a molecular weight and isotope pattern calculator. The intensities of each peak in the two patterns were separately copied into the same Microsoft Excel spreadsheet. Combining different relative proportions of the two overlapping patterns in the signal generated a calculated percentage of hydrogen addition that best matched the observed patterns. Changing the relative proportions by two or three percent produced a noticeable change in the quality of the agreement between calculated and experimental values. Addition of H_2 to the **A**-type species $[RhCl(PPh_3)(\mathbf{3.4})_2]^{2+}$ to give $[RhCl(PPh_3)(\mathbf{3.4})_2H_2]^{2+}$ was also observed, as well as addition of H_2 to the dimeric **H**-type species to give **I**- and **J**-type

species $[Rh_2(\mu\text{-}Cl)_2(PPh_3)_3(\mathbf{3.4})H_2]^+$ and $[Rh_2(Cl)_2(PPh_3)_2(\mathbf{3.4})_2H_2(\mu\text{-}H)_2]^+$. Figure 3-12 shows the degree of hydrogen addition for six representative species as well as an example of a poor calculated match for the relative proportions of **A** and **F**-type species $[RhCl(PPh_3)_2(\mathbf{3.4})]^{2+}$ and $[RhCl(PPh_3)_2(\mathbf{3.4})H_2]^{2+}$.

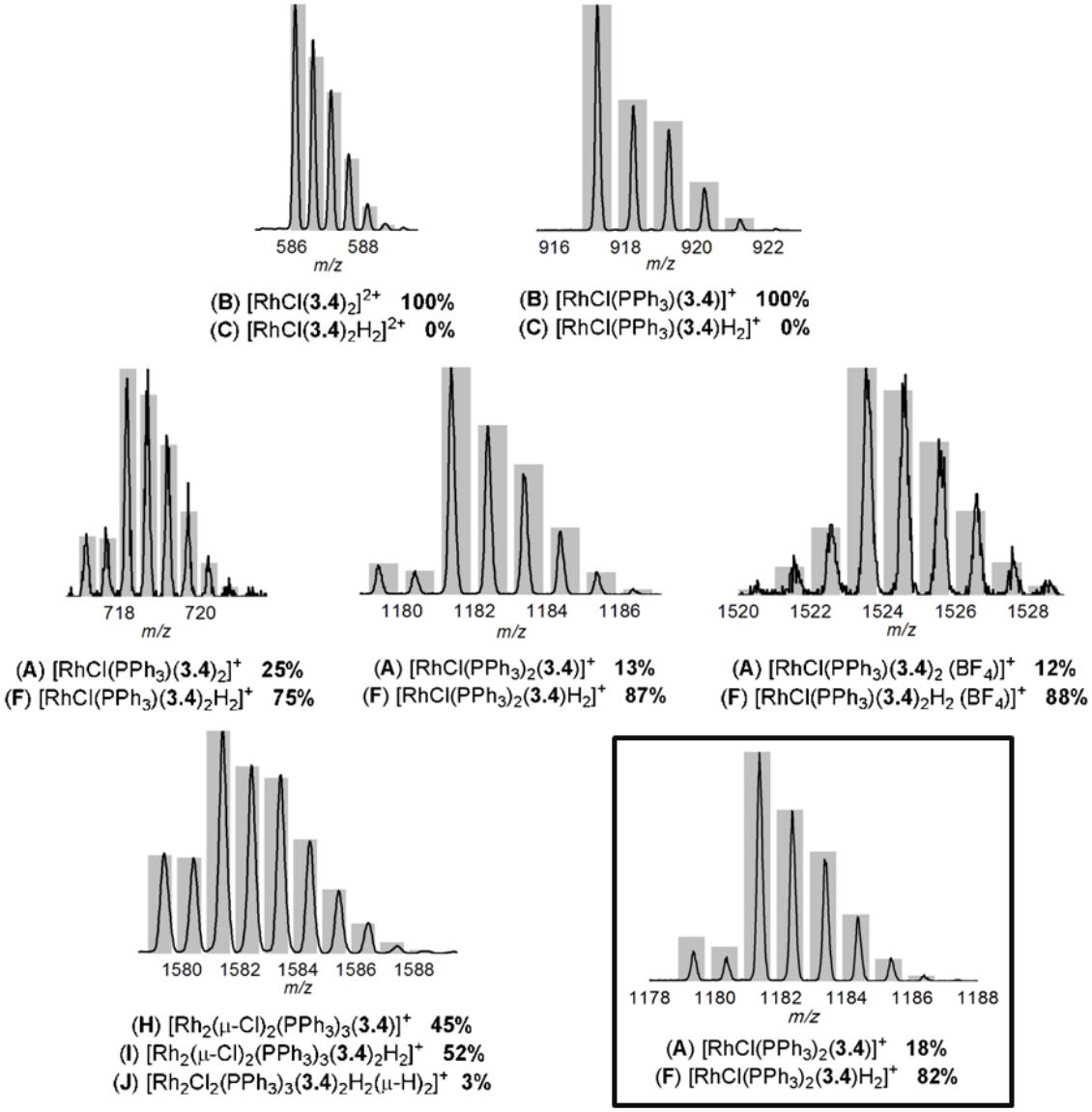

Figure 3-12. Isotope patterns for key species; the calculated values (grey bars) combine the isotope patterns for the two listed species in the proportions given, which provide the best possible fit for the data. Inset: an example of a poor match for the relative proportions of **A** and **F**.

Immediately obvious from Figure 3-12 is the 0% hydrogen addition to **B**-type species $[RhCl(\mathbf{3.4})_2]^+$ and $[RhCl(PPh_3)(\mathbf{3.4})]^+$. It would appear that **C**-type species are not readily observed in the ESI-MS of the solution. However, **C**-type species $[RhCl(PPh_3)(\mathbf{3.4})H_2]^+$ *were* generated in the gas phase by a careful MS/MS experiment of **F**-type species $[RhCl(PPh_3)_2(\mathbf{3.4})H_2]^+$. Upon CID with Ar in the collision cell, $[RhCl(PPh_3)(\mathbf{3.4})H_2]^+$ first lost PPh_3 followed immediately by loss of a hydrogen molecule as evidenced by the equal intensity of $[RhCl(PPh_3)(\mathbf{3.4})H_2]^+$ and $[RhCl(PPh_3)(\mathbf{3.4})]^+$ in Figure 3-13. We never observed that that loss of H_2 occurred before loss of PPh_3. It was necessary to carefully monitor the energy provided to the system as at 6 V the two product ions are of equal intensity. At 5 V no appreciable fragmentation was observed and at 7 V only the three-coordinate $[RhCl(PPh_3)(\mathbf{3.4})]^+$ was observed.

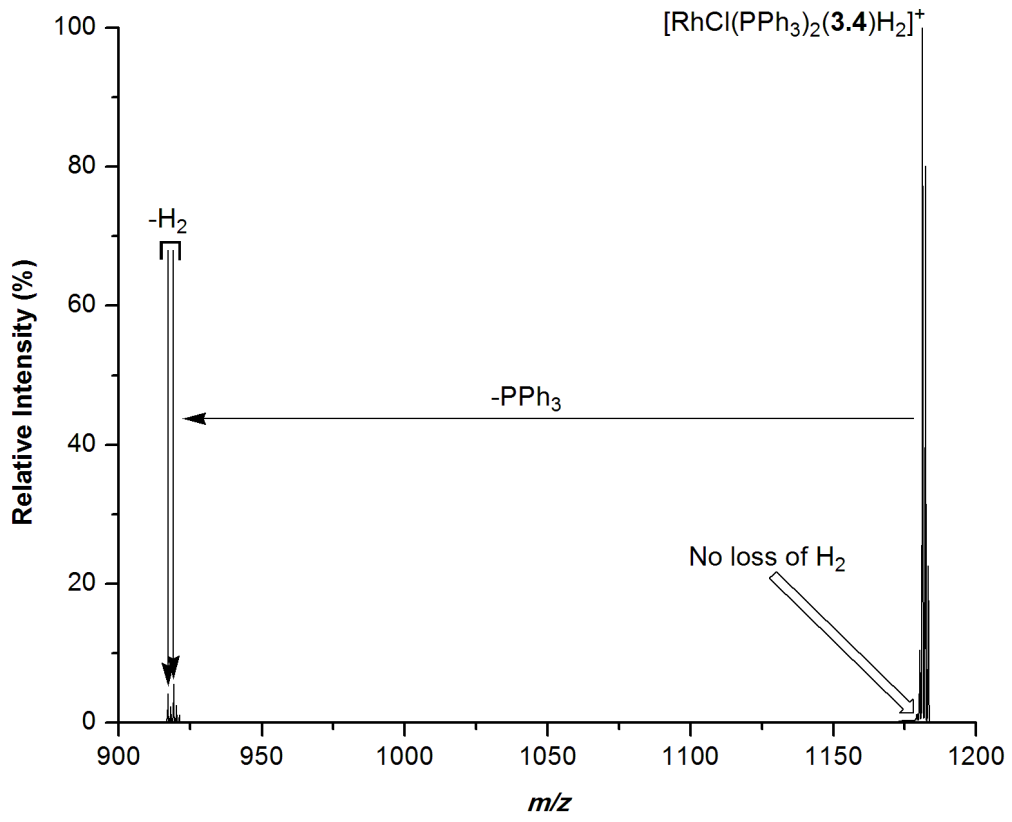

Figure 3-13. Positive-ion ESI-MS/MS of $[RhCl(PPh_3)_2(\mathbf{3.4})H_2]^+$. Cone voltage = 10 V and collision energy was held at 6 V.

An interesting mirror to the gas phase results was the appearance of the spectrum after addition of H_2 (Figure 3-11). In comparison to Figure 3-8 the relative concentration of $[RhCl(PPh_3)(\mathbf{3.4})]^+$ had greatly increased following H_2 addition. This behaviour is similar to the gas phase results in that dissociation of PPh_3 from $[RhCl(PPh_3)_3(\mathbf{3.4})H_2]^+$ (**F**-type species) to give $[RhCl(PPh_3)(\mathbf{3.4})H_2]^+$ (**C**-type species) caused the H_2 to be more labile and generate $[RhCl(PPh_3)(\mathbf{3.4})]^+$ (**B**-type species) as a direct consequence of the dissociation of PPh_3 (evidenced by the equivalent energies at which these processes occurred). Examination of the relative concentrations of $[RhCl(PPh_3)_2(\mathbf{3.4})H_2]^+$ and $[RhCl(PPh_3)(\mathbf{3.4})]^+$ with increasing cone voltage supports this assumption (Figure 3-14). It can be seen that even at very low energies the concentration of $[RhCl(PPh_3)(\mathbf{3.4})]^+$ is approximately 15% higher than the solution that does not

contain hydrogen (Figure 3-7 above). The increased intensity generated at higher voltages were a direct result of the fragmentation of $[RhCl(PPh_3)_2(\mathbf{3.4})H_2]^+$ losing PPh_3 and H_2 essentially simultaneously. Both CID at the cone (Figure 3-14) and MS/MS experiments in the collision cell (Figure 3-13) show that the dissociation of PPh_3 from $[RhCl(PPh_3)_2(\mathbf{3.4})H_2]^+$ makes the H_2 fragment much more labile. Also notable is the voltage at which PPh_3 was lost from $[RhCl(PPh_3)_2(\mathbf{3.4})H_2]^+$ and $[RhCl(PPh_3)_2(\mathbf{3.4})]^+$. The hydrogen-containing species loses PPh_3 at approximately 5 V while loss from $[RhCl(PPh_3)_2(\mathbf{3.4})]^+$ did not start until 10 V. The data seen in these plots is consistent with NMR data that shows that the dissociation of PPh_3 from **F** is three orders of magnitude faster than dissociation from **A**.[108]

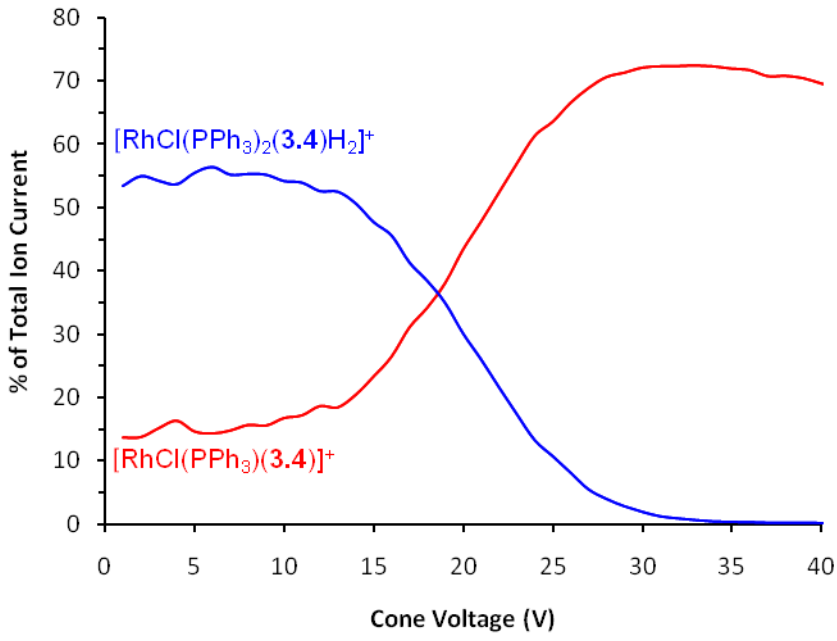

Figure 3-14. The relative intensities of $[RhCl(PPh_3)_2(\mathbf{3.4})H_2]^+$ and $[RhCl(PPh_3)(\mathbf{3.4})]^+$ with increasing cone voltage (V). Note that while these ions are related, fragmentation of **A** is not entirely responsible for the abundance of **B**.

Efforts were made to produce enough $[RhCl(PPh_3)(\mathbf{3.4})H_2]^+$ at the cone to enable further reaction in the collision cell, however insufficient amounts were isolated in the quadrupole to allow further gas phase reactivity.

3.3.5 Addition of cyclohexene to $[3.4]^+ BF_4^-$ and $RhCl(PPh_3)_3$ in chlorobenzene

Addition of cyclohexene to a hydrogen saturated solution of $[\mathbf{3.4}]^+ BF_4^-$ and **A** in chlorobenzene caused the solution to turn yellow in colour (from orange) and did not result in observation of the expected alkene-containing **D**-type species $[RhCl(PPh_3)(\mathbf{3.4})(C_6H_{10})]^+$. The new species observed were 2 *m/z* less than the expected species, corresponding to $[Rh(PPh_3)_2(C_6H_8)]^+$, $[RhCl(\mathbf{3.4})(C_6H_8)]^+$ and $[RhCl(PPh_3)(\mathbf{3.4})(C_6H_8)]^+$ at 707.2, 735.2 and 997.2 *m/z* respectively (Appendix Figure 4). MS/MS of $[RhCl(PPh_3)(\mathbf{3.4})(C_6H_8)]^+$ showed that the C_6H_8 fragment was strongly bound to the metal center relative to the other ligands as the major fragments observed were $[RhCl(\mathbf{3.4})(C_6H_8)]^+$ (loss of PPh_3), free $[\mathbf{3.4}]^+$ (loss of $\mathbf{3.4}]^+$), and only a small amount of $[RhCl(PPh_3)(\mathbf{3.4})]^+$ (due to loss of C_6H_8) was seen (Figure 3-15).

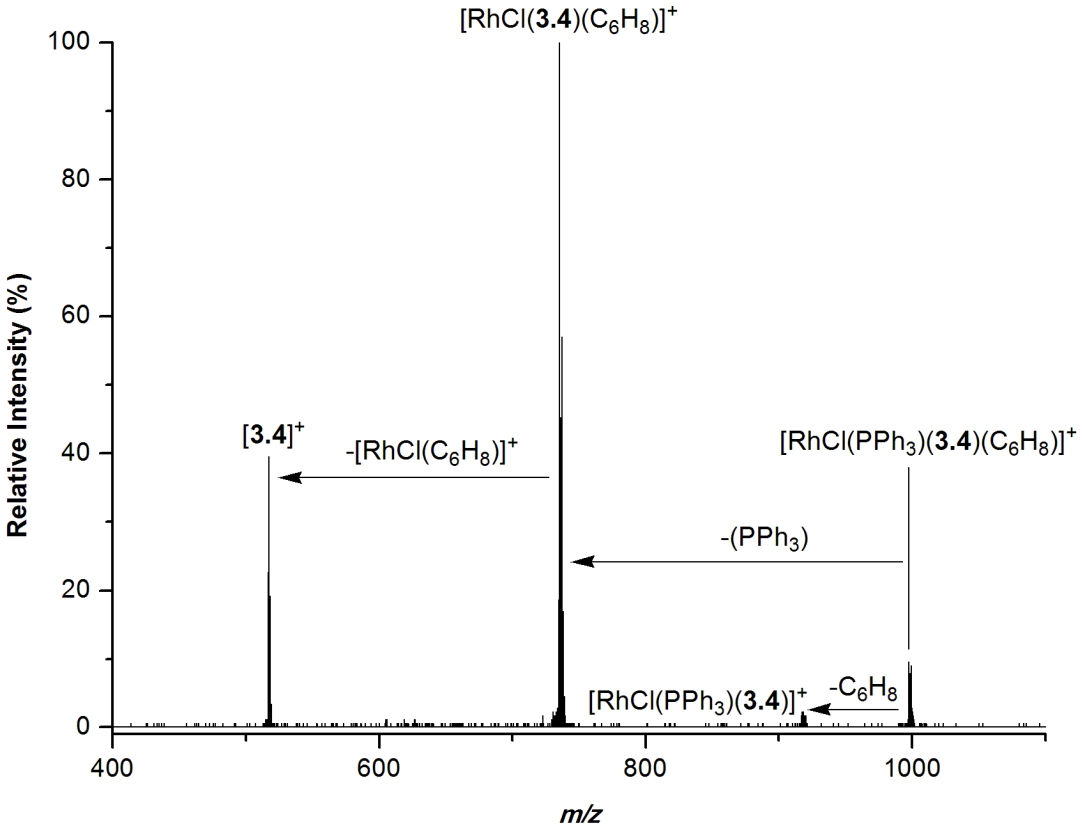

Figure 3-15. Positive-ion ESI-MS/MS of $[RhCl(PPh_3)(\mathbf{3.4})(C_6H_8)]^+$. Cone voltage = 10 V and collision voltage was increased from 0 to 50 V.

The source of the C_6H_8 ligand is possibly an impurity (undetectable by NMR) in the cyclohexene and is thought to be 1,4-cyclohexadiene rather than 1,3-cyclohexadiene, as the cyclohexene is purified by distillation over maleic anhydride prior to use which removes conjugated dienes. This theory was tested by adding pure 1,3- and 1,4-cyclohexadiene directly to solutions of $[\mathbf{3.4}]^+ BF_4^-$ with **A.** Both dienes formed both $[Rh(PPh_3)_2(C_6H_8)]^+$ and $[RhCl(\mathbf{3.4})(C_6H_8)]^+$ (Appendix Figure 5 and Appendix Figure 6). The MS/MS spectra were collected and show the same fragmentation pattern as the peaks observed in the original spectrum (Appendix Figure 7 to Appendix Figure 12). It was observed however, that addition of 1,3-cyclohexadiene to the solution resulted in immediate colour change of the solution and formation of these two species. In contrast, addition of 1,4-cyclohexadiene resulted in a slower colour change and the growth of these peaks over a

few minutes. Figure 3-16 and Figure 3-17 show the combined intensities of $[Rh(PPh_3)_2(C_6H_8)]^+$ and $[RhCl(\mathbf{3.4})(C_6H_8)]^+$ over time for the addition of 1,4- and 1,3-cyclohexadiene and cyclohexene, to $RhCl(PPh_3)_3$ and $[\mathbf{3.4}]^+ BF_4^-$ in chlorobenzene. Formation of these species with 1,3-cyclohexadiene was nearly instantaneous, with the diene species dominating the spectrum (represented by high percentage of total ion current). Addition of 1,4-cyclohexadiene, however, causes a slow increase in the intensity of these two peaks. It is believed that the slow growth was due to the isomerization of 1,4- to 1,3-cyclohexadiene and that 1,3-cyclohexadiene acts as a catalyst poison by binding strongly to rhodium. It is known that conjugated dienes are difficult to reduce at 1 atm of H_2 although it is possible at elevated pressures (60 atm).[111]

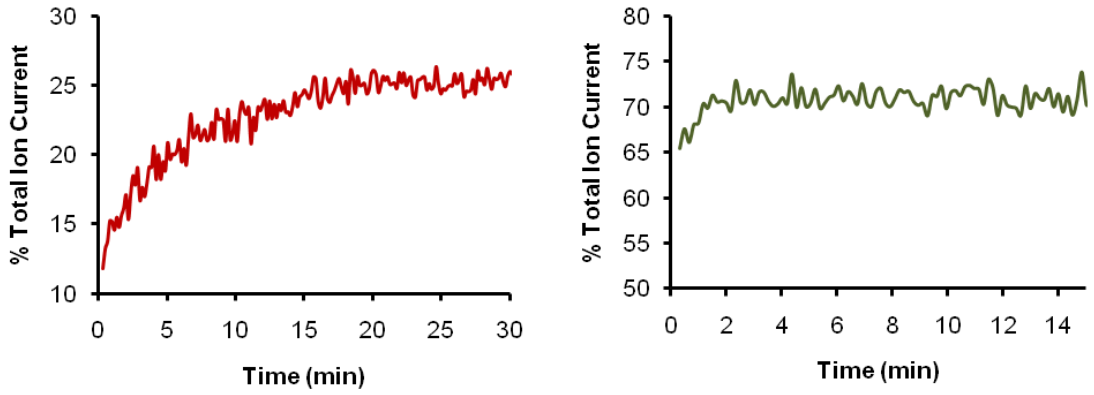

Figure 3-16. Combined intensities of $[Rh(PPh_3)_2(C_6H_8)]^+$ (707.2 *m/z*) and $[RhCl(\mathbf{3.4})(C_6H_8)]^+$ (735.2 *m/z*) over time after addition of 1,4-cyclohexadiene (left) and 1,3-cyclohexadiene (right) to a solution of $RhCl(PPh_3)_3$ and $[\mathbf{3.4}]^+ BF_4^-$ in chlorobenzene. Cone voltage = 10 V.

Tracking the appearance of these species with the original cyclohexene reveals a trace that has features of both the 1,3- (rapid appearance) and 1,4-cyclohexadiene (low abundance). Finding out exactly what is going on in this reaction will require a substantially more detailed analysis than obtained in this preliminary examination.

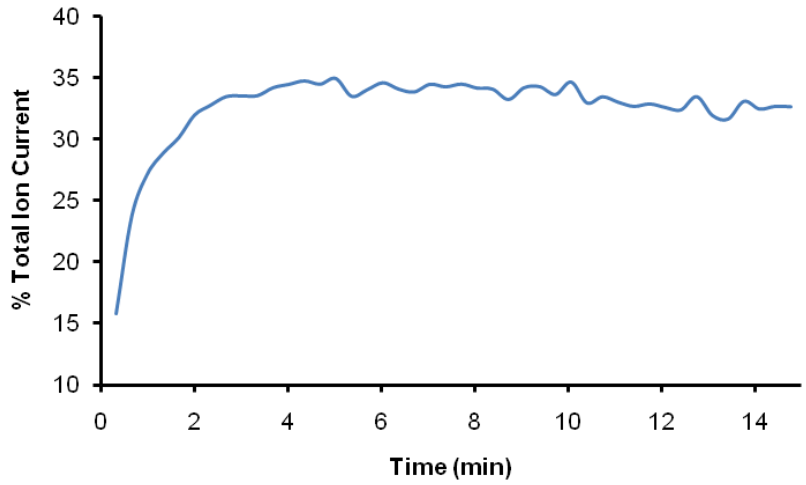

Figure 3-17. Combined intensities of $[Rh(PPh_3)_2(C_6H_8)]^+$ (707.2 *m/z*) and $[RhCl(\mathbf{3.4})(C_6H_8)]^+$ (735.2 *m/z*) over time after addition of cyclohexene to a solution of $RhCl(PPh_3)_3$ and $[\mathbf{3.4}]^+ BF_4^-$ in chlorobenzene. Cone voltage = 10 V.

3.3.6 Addition of cyclohexene to $[3.4]^+ BF_4^-$, $RhCl(PPh_3)_3$ and H_2 in chlorobenzene

No olefin-containing species (**D**) were observed from the addition of cyclohexene to a continuously hydrogen-saturated solution of $[\mathbf{3.4}]^+ BF_4^-$ and **A** although the same peaks were observed as above. The disappearance of all **F**-type species, such as $[RhCl(PPh_3)_2(\mathbf{3.4})H_2]^+$, is an important change to note. This was yet another result in agreement with the known solution phase behaviour of this system. The alkene present in the system will trap any **C**-type species to form **D**-type species therefore driving the equilibrium away from **F** species.

Bubbling ethylene through a hydrogen-saturated solution of $[\mathbf{3.4}]^+ BF_4^-$ produced a very small amount (about 2%) of the **D**-type species $[RhCl(PPh_3)(\mathbf{3.4})(H_2C{=}C_2H)]^+$ but the disappearance of **F**-type species was not observed (Appendix Figure 13) as in the addition of cyclohexene. However, it is known that ethylene is not reduced by this catalyst at 1 atm H_2, so this result is consistent with prior work.[111]

A summary of the solution phase speciation observed after addition of H_2 and after addition of cyclohexene is given in Table 3-1. The table is organized according to the number of phosphine ligands in the complex and reflects the various changes observed with addition of the two substrates.

Table 3-1. Solution speciation by positive-ion ESI-MS (10 V) at various stages in the catalytic hydrogenation of cyclohexene using Wilkinson's catalyst and $[\mathbf{3.4}]^+ BF_4^-$ in chlorobenzene.

Species	Assignment Within Cycle	Identity	*m/z*	Intensity before H_2 addition	Intensity after H_2 addition	Intensity after cyclohexene addition
Free ligand		$[\mathbf{3.4}]^+$	517.2	13%	13%	4%
Oxidised ligand		$[\mathbf{3.4}O]^+$	533.2	63%	55%	34%
$RhClP_2$	B	$[RhCl(\mathbf{3.4})_2]^{2+}$	586.2	11%	3%	<1%
	B	$[RhCl(PPh_3)(\mathbf{3.4})]^+$	917.2	24%	100%	6%
RhP_3^+		$[Rh(PPh_3)_3]^+$	889.2	15%	8%	30%
$RhClP_3$	A	$[RhCl(PPh_3)(\mathbf{3.4})_2]^{2+}$	717.2	16%	9%	<1%
	F	$[RhCl(PPh_3)(\mathbf{3.4})_2H_2]^{2+}$	718.2	-	3%	<1%
	A	$[RhCl(PPh_3)_2(\mathbf{3.4})]^+$	1179.3	100%	10%	100%
	F	$[RhCl(PPh_3)_2(\mathbf{3.4})H_2]^+$	1181.3	-	77%	<1%
	A	$[RhCl(PPh_3)(\mathbf{3.4})_2(BF_4)]^+$	1521.4	4%	<1%	2%
	F	$[RhCl(PPh_3)(\mathbf{3.4})_2H_2(BF_4)]^+$	1523.4	-	2%	<1%
$Rh_2Cl_2P_4$	H	$[Rh_2Cl_2(PPh_3)_3(\mathbf{3.4})]^+$	1581.2	6%	2%	3%
	I	$[Rh_2Cl_2(PPh_3)_3(\mathbf{3.4})H_2]^+$	1583.2	-	2%	<1%
	J	$[Rh_2Cl_2(PPh_3)_3(\mathbf{3.4})H_2]^+$	1585.2	-	<1%	<1%

3.3.7 Reaction of $[RhCl(PPh_3)(3.4)]^+$ with H_2 and propylene in the gas phase

Gas phase reactivity at the cone has been employed in our group in the past.[31] We thought that it might be possible to generate the **C**-type species $[RhCl(PPh_3)(\mathbf{3.4})H_2]^+$ by gas phase reaction

with H_2 in the collision cell (Figure 1-4). Both the four coordinate $[RhCl(PPh_3)_2(\mathbf{3.4})]^+$ (**F**) and three coordinate $[RhCl(PPh_3)(\mathbf{3.4})]^+$ (**B**) were examined. The species of interest was isolated in the quadrupole mass analyzer and introduced to H_2 in the collision cell. The result of addition of H_2 would be an increase in *m/z* of two mass units, but no addition was evident for either species. H_2 is a very light molecule and gas phase reactions with H_2 are known to be inefficient, perhaps accounting for the lack of reactivity.[123] (It is possible to increase the number of gas phase collisions by increasing the pressure in the collision cell. Chen and co-workers have described the use of octapole and 24-pole ion guides to increase the efficiency of reactions of organometallic species in the gas phase, but even this system has not been used to study the addition of H_2 in the gas phase.)[124-127]

The same reaction was attempted for the addition of propylene to $[RhCl(PPh_3)_2(\mathbf{3.4})]^+$ and $[RhCl(PPh_3)(\mathbf{3.4})]^+$ in the gas phase. First, $[RhCl(PPh_3)_2(\mathbf{3.4})]^+$ was isolated in the quadrupole and allowed to come into contact with propylene in the collision cell. No addition of propylene was observed. In a separate experiment, $[RhCl(PPh_3)(\mathbf{3.4})]^+$ was isolated (having been generated by CID in the cone region) and reacted with propylene in the collision cell. Figure 3-18 shows the addition of propylene to $[RhCl(PPh_3)(\mathbf{3.4})]^+$ to give $[RhCl(PPh_3)(\mathbf{3.4})(C_3H_6)]^+$ at 959.2 *m/z* (42 mass units higher). The product was formed at only 0.6% the intensity of the parent ion but the signal-to-noise ratio and isotope match are excellent, confirming the identity of the peak. Furthermore, this signal is absent when the collision gas is simply Ar. This gas-phase reaction essentially duplicates the transformation of **A** to **G**, and the lack of reactivity of olefin with **A** suggests the reaction is probably dissociative, i.e. dissociation of PPh_3 from **A** to give **B** followed by coordination of olefin to give **G**.

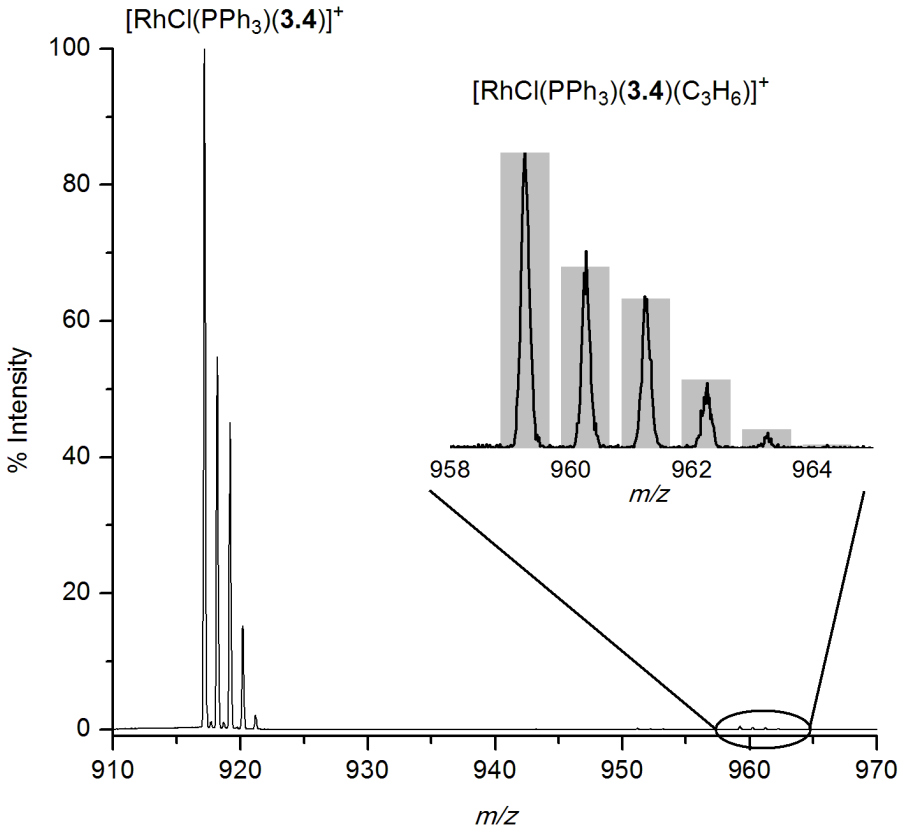

Figure 3-18. Positive-ion ESI-MS of reaction of $[RhCl(PPh_3)(\mathbf{3.4})]^+$ with propylene in the collision cell. Cone voltage = 10 V and collision energy was held at 2 V.

3.4 Conclusions

The simple, one-step syntheses of the phosphine/phosphonium ligands from commercially available materials makes them a particularly attractive ligand for applications of the sort described above. They provide an effective way to impart a charge to the otherwise neutral $RhCl(PPh_3)_3$, thereby making the catalyst detectable by ESI-MS. Due to the labile nature of the PPh_3 ligands, incorporation of the charged ligand into the complex is facile and only small amounts of custom ligand are necessary. With careful attention paid to the conditions of the analysis (such as low cone voltage to minimize fragmentation) an accurate description of the

solution phase speciation can be provided by ESI-MS. The results described above agree with all reports on the behaviour of this system obtained by standard spectroscopic techniques. All previously reported off-cycle species (**A**, **F, H-J**) were readily observed and characterized based on their *m/z* value, isotope pattern, MS/MS fragmentation patterns, and reactivity under different conditions. The "active species" **B** and **C** could be generated in the gas phase by CID and MS/MS experiments and off-cycle species **G** was observed by reaction of C in the gas phase with propylene. The significance of diene impurities as potential catalyst poisons is revealed explicitly for the first time, and provides a strong hint to the synthetic chemist that dienes should be avoided, and if possible, eliminated from hydrogenation reactions if maximal activity is desired. Collectively, these experiments are an illustrative example of how useful ESI-MS can be in probing speciation during catalytic reactions, and give confidence in the ability of the technique to probe new and less well studied reactions.

3.5 Experimental

All syntheses were performed under an inert atmosphere of N_2 using standard glovebox or Schlenk procedures. Solvents were HPLC grade and purified on an MBraun solvent purification system (SPS). Chlorobenzene was distilled over CaH_2 under N_2. Benzyl bromide was distilled and stored over molecular sieves at 3 °C. Cyclohexene was refluxed and distilled over maleic anhydride under N_2. All other chemicals were used as obtained from Aldrich (Oakville, Canada). Gases were obtained from Airgas (Calgary, Canada). NMR spectra were collected on either an AV-300 or AV-360 Bruker spectrometer. Internal references to $CHCl_3$ (^1H δ = 7.26 ppm), C_6D_5H (^1H δ = 1.16 ppm) and external reference to 85% aqueous H_3PO_4 (^{31}P) were used as appropriate. The ligand exchange reaction was examined using ^{31}P NMR by dissolving

$RhCl(PPh_3)_3$ (16 mg, 0.017 mmol) and $[\mathbf{3.4}]^+ BF_4^-$ (103 mg, 0.017 mmol) in 1 mL of chlorobenzene : C_6D_6 (4:1).

Mass spectrometry

All mass spectra and gas phase experiments were performed on a Micromass Q-ToF *micro* hybrid quadrupole/time-of-flight mass spectrometer in positive ion mode using pneumatically-assisted electrospray ionization with a capillary voltage of 2900 V, source temperature of 100 °C and desolvation temperature of 180 °C. Solutions were run in chlorobenzene and introduced to the mass spectrometer by a syringe pump at a rate of 2 mL h^{-1}. Accurate mass data were obtained (after careful calibration) by locking to an internal standard, either $[C_{32}H_{68}N]^+ Br^-$ (466.5352 *m/z*) or $[C_{48}H_{100}N]^+ Br^-$ (690.7856 *m/z*), whichever was closer to the target mass. MS/MS experiments were conducted with argon in the collision cell. The appropriate peak was mass selected (usually with a broad enough window to accommodate the full isotope pattern, i.e. ~8 *m/z*) and the selected ion fragmented at the stated voltage(s) in the argon-filled collision cell. Gas phase reactivity studies were conducted with the appropriate reactive gas in place of argon in the collision cell after allowing the cell to purge with the reactive gas for 2 hours. All mass spectra were collected for a sufficiently long period to obtain a signal-to-noise ratio of at least 20:1; this ranged from a few seconds for ordinary mass spectra to 10 minutes for gas phase reactions. ESI-MS spectra of the catalyst mixture were obtained by adding to 12 mL of chlorobenzene $RhCl(PPh_3)_3$ (14 mg, 1.25 mmol L^{-1}) and $\mathbf{3.4}^+ BF_4^-$ (2 mg, 0.28 mmol L^{-1}) to give a bright orange solution. Hydrogen (99.995%) passed through the catalyst solution resulted in a peach-coloured solution in less than 30 seconds.

1-diphenylphosphino-1-benzyldiphenylphosphonium-methane bromide ([3.1]$^+$ Br$^-$). To a solution of 1,1-bisdiphenylphosphinomethane (510 mg, 1.33 mmol) in 15 mL dry, N_2-purged toluene at 0 ºC was slowly added a dilute solution of benzyl bromide (227 mg, 157 μL, 1.33 mmol) in 1 mL dry, N_2-purged toluene. The clear, colourless solution was left to warm to room temperature overnight under N_2. The resulting white microcrystalline powder (330 mg, 45% yield) was retrieved via suction filtration, washed with cold toluene, and dried under high vacuum for 12 h. M.p.: 207-208 °C. ESI-MS (+ve, CH_2Cl_2): *m/z* = experimental: 475.1745 $[P_2C_{32}H_{29}]^+$, calculated: 475.1744; calibrated against $[C_{32}H_{68}N]^+$. ^{1}H NMR (300MHz, $CDCl_3$): δ(ppm) = 4.28 (d, $^1J_{HP}$ = 14, 2H), 4.96 (d, $^1J_{HP}$=14, 2H), 7.09-7.79 (mm, 25H). ^{31}P NMR (360 MHz, $CDCl_3$): δ(ppm) = 26.07 (d, $^2J_{PP}$ = 58, P$^+$), –27.63 (d, $^2J_{PP}$ = 58, P).

1-diphenylphosphino-2-benzyldiphenylphosphonium-ethane bromide ([3.2]$^+$ Br$^-$). As for [**3.2**]$^+$ Br$^-$; 1,2-bisdiphenylphosphinoethane (501 mg, 1.26 mmol) to benzyl bromide (215 mg, 150 μL, 1.26 mmol) to give a white powder (319 mg, 45% yield). M.p.: 218-220 °C. ESI-MS (+ve, CH_2Cl_2): *m/z* = experimental: 489.1900 $[P_2C_{33}H_{31}]^+$, calculated: 489.1901; calibrated against $[C_{32}H_{68}N]^+$. ^{1}H NMR (300MHz, $CDCl_3$): δ(ppm) = 2.17 (m, 2H), 3.04 (m, 2H), 5.06 (d, $^1J_{HP}$ = 14, 2H), 6.93-7.77 (mm, 25H). ^{31}P NMR (360 MHz, $CDCl_3$): δ(ppm) = 28.24 (d, $^3J_{PP}$ = 42, P$^+$), –12.14 (d, $^3J_{PP}$ = 42, P).

1-diphenylphosphino-2-benzyldiphenylphosphonium-ethane tetraphenylborate ([3.2]$^+$ BPh$_4^-$). The tetraphenylborate salt of [**3.2**]$^+$ was obtained by adding one equivalent of sodium tetraphenylborate (962 mg, 2.81 mmol) in 150 mL N_2-purged methanol to **2**$^+$ Br$^-$ (1.599 g, 2.81 mmol) in 250 mL N_2-purged anhydrous ethanol. The resulting white precipitate (1.503 g,

66% yield) was isolated by suction filtration and dried under high vacuum. ^{31}P NMR and positive-ion ESI-MS were identical to the bromide equivalent; the negative ion ESI-MS showed *no* Br^-, only BPh_4^- (318.2 *m/z*).

1,1-bis(diphenylphosphino-methyl)-1-benzyldiphenylphosphonium-ethane bromide ([3.3]$^+$ Br$^-$). To a solution of 1,1,1-tris(diphenylphosphino-methyl)ethane (220 mg, 0.35 mmol) in 5 mL dry, N_2-purged toluene at 0ºC was slowly added a dilute solution of benzyl bromide (60 mg, 41 μL, 0.35 mmol) in 1 mL dry, N_2-purged toluene. The clear, colourless solution was left to warm to room temperature overnight under N_2. The clear, colourless solution was reduced to half its volume under high vacuum and 2 mL N_2-purged hexane was added. The resulting white powder (7 mg, 3% yield) was retrieved via suction filtration, washed with cold toluene, and dried under high vacuum for 12 h. M.p.: 106-109 °C. ESI-MS (+ve, CH_2Cl_2): *m/z* = experimental: 715.2814 $[P_3C_{48}H_{46}]^+$, calculated: 715.2813; calibrated against $[C_{48}H_{100}N]^+$. ^{1}H NMR (300MHz, $CDCl_3$): δ(ppm) = 1.00 (s, 3H), 2.03 (d, $^1J_{HP}$ = 15, 2H), 2.69 (d, $^1J_{HP}$ = 13 ,2H), 3.97 (d, $^1J_{HP}$ = 14, 2H), 4.84 (d, $^1J_{HP}$ = 14, 2H), 6.81-8.26 (mm, 46H). ^{31}P{^{1}H} NMR (360 MHz, $CDCl_3$): δ(ppm) = 23.76 (P^+), –26.04 (P).

1-diphenylphosphino-4-benzyldiphenylphosphonium-butane bromide ([3.4]$^+$ Br$^-$). As for [**3.1**]$^+$ Br^-; 1,4-bisdiphenylphosphinobutane (500 mg, 1.17 mmol) to benzyl bromide (200 mg, 140 μL, 1.17 mmol) to give a white powder (181 mg, 26% yield). M.p.: 156-158 °C. ESI-MS (+ve, CH_2Cl_2): *m/z* = experimental: 517.2209 $[P_2C_{35}H_{35}]^+$, calculated: 517.2214; calibrated against $[C_{32}H_{68}N]^+$. ^{1}H NMR (300MHz, $CDCl_3$): δ(ppm) = 1.50 (m, 4H), 1.92 (d, $^3J_{HH}$ = 7, 2H),

3.12 (m, 2H), 4.90 (d, $^{1}J_{HP}$ = 12, 2H), 6.97-7.76 (mm, 25H). $^{31}P\{^{1}H\}$ NMR (360 MHz, $CDCl_3$): δ(ppm) = 27.86 (P^+), –16.72 (P).

1-diphenylphosphino-4-benzyldiphenylphosphonium-butane tetrafluoroborate ([3.4]$^+$ BF_4^-) and hexafluorophosphate ([3.4]$^+$ PF_6^-). The tetrafluoroborate salt of [**3.4**]$^+$ was obtained by stirring 2.5 equivalents of sodium tetrafluoroborate (108 mg, 0.98 mmol) with [**3.4**]$^+$ Br^- (235 mg, 0.39 mmol) in 20 mL N_2-purged methanol. The methanol was removed by evaporation under high vacuum and N_2-purged H_2O was added to the resulting solid to dissolve the excess sodium tetrafluoroborate and the sodium bromide by-product. 1-diphenylphosphino-4-benzyldiphenylphosphonium-butane tetrafluoroborate was isolated from the resulting white slurry by suction filtration and dried under high vacuum (213 mg, 89% yield). The hexafluorophosphate salt was made in identical fashion in 73% yield. The ^{31}P NMR and positive-ion ESI-MS of both were identical to the bromide equivalent; the negative ion ESI-MS showed *no* Br^- and only BF_4^- (87.0 *m/z*) or PF_6^- (144.9 *m/z*), respectively. Colourless, block-like single crystals of [**3.4**]$^+$ PF_6^- suitable for X-ray structural analysis were obtained by layering first a thin layer of cold 1-butanol followed by hexane over a concentrated dichloromethane solution of [**3.4**]$^+$ PF_6^- in a crystallisation tube in the glovebox, then storing at –33 °C.

1-diphenylphosphino-6-benzyldiphenylphosphonium-hexane bromide ([3.5]$^+$ Br^-). As for [**3.1**]$^+$ Br^-; 1,6-bisdiphenylphosphinohexane (100 mg, 0.22 mmol) to benzyl bromide (40 mg, 26 μL, 0.22 mmol) to give a white powder (28 mg, 20% yield). M.p.: 132-134 °C. ESI-MS (+ve, CH_2Cl_2): *m/z* = experimental: 545.2527 $[P_2C_{37}H_{39}]^+$, calculated: 545.2527; calibrated against $[C_{32}H_{68}N]^+$. ^{1}H NMR (300MHz, $CDCl_3$): δ(ppm) = 1.26 (m, 8H), 1.85 (m, 2H), 3.11 (m, 2H),

4.85 (d, $^{2}J_{HP}$ = 15, 2H), 6.95-7.73 (mm, 25H). $^{31}P\{^{1}H\}$ NMR (360 MHz, $CDCl_3$): δ = 27.93 (P^{+}), –15.92 (P).

Chapter 4. Dehydrocoupling of silanes by $RhCl(PPh_3)_3$

4.1 Introduction

In 1969, not long after Wilkinson and coworkers reported on the hydrogenation of olefins by $RhCl(PPh_3)_3$,[97] they reported on the stoichiometric activation of Si-H bonds of tertiary silanes by the same catalyst.[128] Si-H bonds are of similar strength to H-H bonds, and frequently undergo related reactions, so this reaction is analogous to the oxidative addition of dihydrogen to $RhCl(PPh_3)_3$. In 1973, Ojima and co workers reported the activity of $RhCl(PPh_3)_3$ in the dehydrogenative coupling of silanes to give dimers as well as polysilanes.[129] Several groups reported the tendency of the catalyst towards disproportionation of the substituents on silicon and that redistribution was more likely for aryl than alkyl silanes.[130-135] The exact mechanism of Si-Si bond formation is still a matter of debate. Many authors have suggested the involvement of a rhodium-silylene intermediate, first proposed by Ojima and co workers (Figure 4-1), although no direct evidence has been provided.[129,136-139]

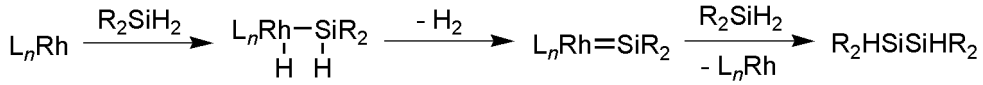

Figure 4-1. Ojima *et al*. proposed a rhodium-silylene species may be involved in the dehydrocoupling of silanes by $RhCl(PPh_3)_3$.

Goikhman and Milstein, for example, postulated the formation of a silylene based on the generation of $Rh(i\text{Pr}_3P)_2(OTf)(H)_2$ from addition of Ph_2SiH_2 to $Rh(i\text{Pr}_3P)_2(OTf)$ (Figure 4-2).[131] Trapping of the silylene with another equivalent of $Rh(i\text{Pr}_3P)_2(OTf)$ gave the rhodium-silylene $Rh(i\text{Pr}_3P)_2(SiPh_2)(OTf)$.

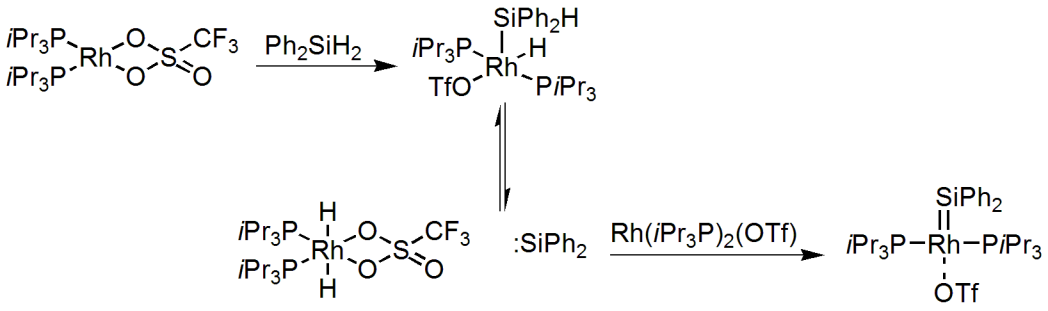

Figure 4-2. Generation of silylene intermediate as proposed by Goikhman and Milstein.

Curtis and Epstein proposed a mechanism for the dehydrocoupling of silanes by $RhCl(PPh_3)_3$ that does not involve a silylene intermediate.[140] Oxidative addition of one Si-H bond to the rhodium-hydride species, reductive elimination of H_2 and addition of a second silane sets the complex ready for reductive elimination of the coupled product (Figure 4-3).

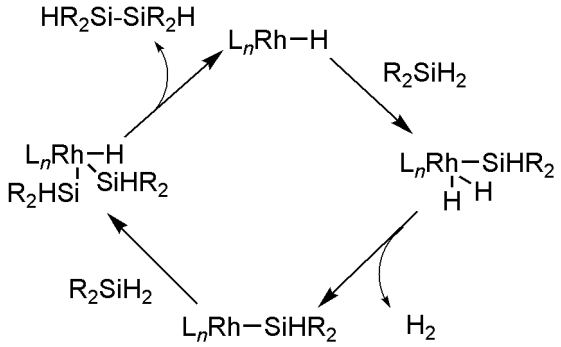

Figure 4-3. Possible mechanism for the dehydrocoupling of silanes proposed by Curtis and Epstein.[137,140]

The Rosenberg group at UVic has had a long-standing interest in this reaction, exemplified by their report of a high-yielding route to $(Ph_2SiH)_2$[141] through dehydrocoupling of Ph_2SiH_2. Several Rosenberg students have since studied the reaction to identify the Rh-containing products resulting from the addition of secondary silanes to Wilkinson's catalyst, to gain insight into the mechanism of silane dehydrocoupling, and made the following observations based primarily on evidence from ^{31}P NMR.[142]

A 1:1 reaction of di(*n*-hexyl)silane and $RhCl(PPh_3)_3$ in d_6-benzene in an NMR tube was monitored by ^{31}P NMR. The oxidative addition product $RhCl(PPh_3)_2(H)(SiHhex_2)$ is observed (it is nearly always seen in investigations with this substrate)[143] and diminished over a one hour period. At the same time, a broad peak consistent with species involved in phosphine exchange develops, accompanied by multiple signals corresponding to hydride-containing species in the ^1H NMR. Further stoichiometric reaction in toluene allowed the group to precipitate and isolate some rhodium-containing products. The bright yellow solid obtained from this approach contained peaks in the room temperature ^{31}P NMR due to $RhCl(PPh_3)_3$, $RhCl(PPh_3)_2(H)(SiHhex_2)$, $Rh(PPh_3)_3(H)$ and $RhCl(PPh_3)_3(H)_2$, verified by previously reported chemical shifts.[143-147] Several other unidentified species generated a large broad signal consistent with species involved in phosphine exchange. Cooling to 210 K allowed identification of $Rh(PPh_3)_4(H)$[147] and better resolution of the inequivalent phosphines in $Rh(PPh_3)_3(H)$ and $RhCl(PPh_3)_3(H)_2$.

In these results, $Rh(PPh_3)_n(H)$, where n = 3 or 4, were the major rhodium-containing species in the reaction. $Rh(PPh_3)_3(H)$ was the predominant species and it seems reasonable that this species was in equilibrium with PPh_3 generated during the oxidative addition of hex_2SiH_2 so that $Rh(PPh_3)_4(H)$ is formed. The source of the hydride is suspected to be reductive elimination of hex_2SiHCl from $RhCl(PPh_3)_2(H)(SiHhex_2)$ with re-association of another PPh_3.[145,146,148] The stoichiometric reaction has been revisited several times in an effort to detect the chlorosilane by ^{29}Si NMR. A small amount was observed only once, although signals due to $(hex_2SiH)_2O$ were consistently observed (a condensation product related to the hydrolysis of the Si-Cl bond in the chlorosilane). Absent from any of the ^{31}P spectra were peaks due to complexes containing more

than one silane group. There were also other peaks that contained rhodium but were not identifiable.

The applicability of ESI-MS to the study of catalytic systems was validated through the investigation of hydrogenation of olefins by Wilkinson's catalyst, $RhCl(PPh_3)_3$. Results obtained for analysis of that system by ESI-MS were in agreement with results that had been reported over the past 40 years by conventional means. In a system where the mechanism is not well understood, ESI-MS is well-suited to lend new insights into the speciation and progression of the reaction and the identification of potential intermediates, particularly for those species present before the rate determining step.

4.1.1 Method Development

In a standard ESI experiment the sample that is introduced into the source is essentially open to the atmosphere. The phosphine ligands in this particular system are prone to oxidation and the reactive intermediates formed in the reactions are sensitive to both water and oxygen. A bench-top glove box was machined with a small hole in one side to allow a section of PEEK tubing to pass from the inside of the box directly into the source of the mass spectrometer (Figure 4-4).[149] With this technology is it possible to carry out entire reactions and any relevant ESI-MS analysis under inert atmosphere. The olefin hydrogenation reactions were carried out outside of the glove box for the simple reason that the integrated ESI-MS/glovebox system was not fully functional until January 2010. In the following discussion, all solutions and additions were done in the glove box. Samples were removed from the reaction vessel and introduced into the mass spectrometer without ever being directly exposed to the atmosphere.

Figure 4-4. The analysis of air-sensitive systems can be achieved by coupling a glove box directly to the mass spectrometer. A length of PEEK tubing is run from the syringe pump inside the box directly into the source.

4.1.2 Complications arising with chlorobenzene

Investigations carried out in the Rosenberg group were conducted in either benzene or toluene. Chlorobenzene has been used successfully in previous experiments with this catalyst. Due to the similarity to benzene and its acceptable ESI-efficiency we chose to utilize this solvent once again. However, upon addition of $Rh(PPh_3)_n(H)$ and $[\mathbf{3.4}]^+$ BF_4^- in chlorobenzene the growth of rhodium-chloride species was observed. The only source of chloride in this experiment was the solvent. We concluded that activation of the chlorobenzene had led to the change in speciation by replacement of the hydride ligand with a chloride (rhodium hydrides were implicated as intermediates in a similar process involving $RhCl(PPh_3)_3$ in the activation of chlorinated ethylenes).[146] When the solvent was changed to fluorobenzene the corresponding

fluorine-containing species were not observed. Further discussion is given in Section 4.2.5 . The equivalent reaction was not noticed in the spectra of $RhCl(PPh_3)_3$ in the investigations of olefin hydrogenation and the intensities of $[RhCl(PPh_3)_2(\mathbf{3.4})]^+$ and $[RhCl(PPh_3)_2(\mathbf{3.4})H_2]^+$ (once formed) did not appear to increase over time.

4.2 Results and Discussion

4-diphenylphosphino-1-benzyldiphenylphosphonium-butane tetrafluoroborate, $[\mathbf{3.4}]^+ BF_4^-$, was chosen as the ESI-active ligand due to the success of its implementation with previous study of Wilkinson's catalyst. $[\mathbf{3.4}]^+ BF_4^-$ (0.28 mmol L^{-1}) was added to a solution of $RhCl(PPh_3)_3$ (0.96 mmol L^{-1}) in fluorobenzene and the dynamics of the reaction were examined by monitoring the reaction following silane addition. The gross features of the reaction were consistent from one trial to another. The experiment that is discussed in detail below involved injecting the reaction solution continuously for 48 minutes and collecting one ESI-MS every 20 seconds for 144 complete compositional analyses.

4.2.1 Addition of hex_2SiH_2 to $[3.4]^+ BF_4^-$ and $RhCl(PPh_3)_3$ in fluorobenzene

Addition of di(*n*-hexyl)silane to a solution of $[\mathbf{3.4}]^+ BF_4^-$ and $RhCl(PPh_3)_3$ caused the solution to turn yellow (from orange) immediately. A sample was withdrawn from the flask into a gas-tight syringe and infused into the mass spectrometer within 15 seconds from addition of the silane (so these first 15 seconds are not represented in the following data). The data was obtained as one spectrum every 20 seconds. Over a period of 48 minutes, this amounted to 144 individual snapshots of the reaction progress. Any part of this data may be combined to provide a picture of the reaction profile over any given period of time. A summation of the spectra collected in the

first two minutes (6 individual spectra) is shown in Figure 4-5. Peak assignments for identifiable species can be found in Table 4-1 and the full spectrum can be found in Appendix Figure 14.

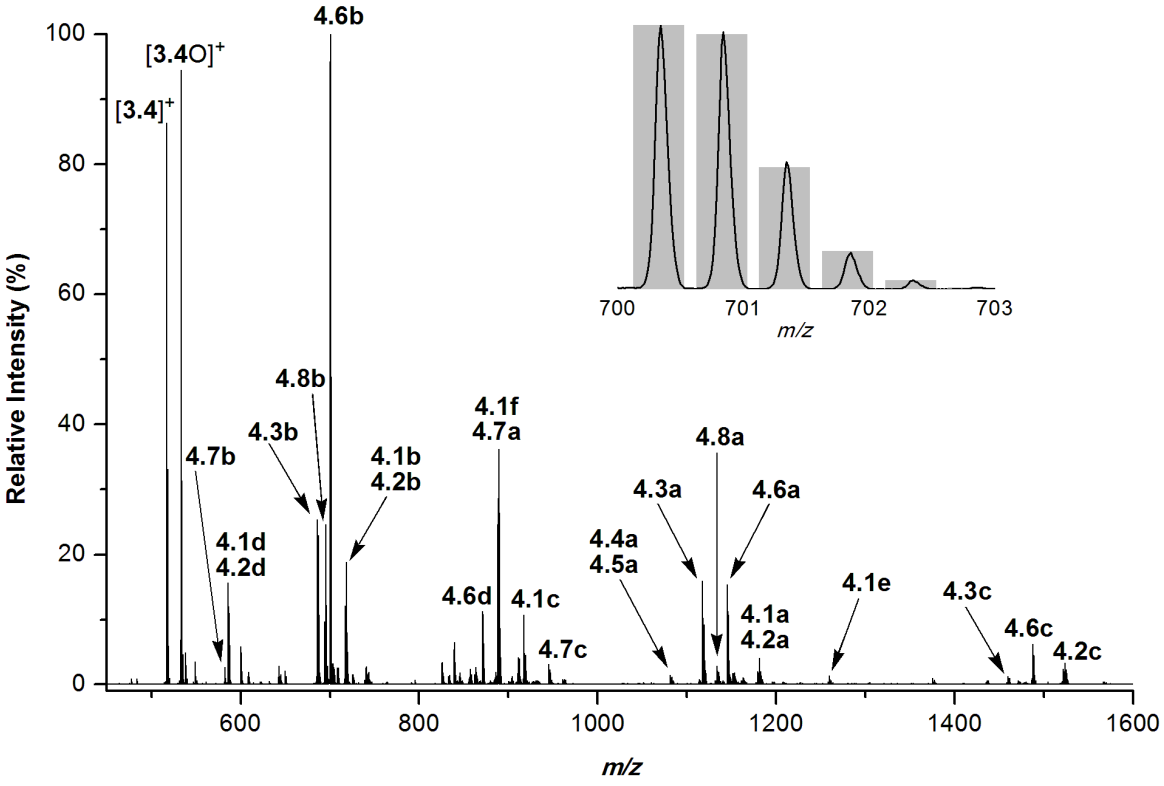

Figure 4-5. Positive-ion ESI-MS obtained from a summation of the first five minutes after addition of hex_2SiH_2 to a solution of [**3.4**]$^+$ BF_4^- and $RhCl(PPh_3)_3$. Peak assignments are given in Table 4-1. **4.4b** is visible in the summation of all 144 spectra collected. **4.1g** is observed at 1865.6 *m/z*. Cone voltage = 10 V. Inset: isotope pattern for $[Rh(PPh_3)(\mathbf{3.4})_2H]^{2+}$ and calculated pattern (grey bars).

Table 4-1. Peak assignments for the addition of hex_2SiH_2 to a solution of $[\mathbf{3.4}]^+ BF_4^-$ and $RhCl(PPh_3)_3$ in fluorobenzene.

Species	Group	Number Assignment	m/z
$[\mathbf{3.4}]^+$			517.2
$[\mathbf{3.4}O]^+$			533.2
$RhCl(PR_3)_3$	**4.1**		
$[RhCl(PPh_3)_2(\mathbf{3.4})]^+$		4.1a	1179.2
$[RhCl(PPh_3)(\mathbf{3.4})_2]^{2+}$		4.1b	717.2
$[RhCl\ (PPh_3)(\mathbf{3.4})]^+$		4.1c	917.2
$[RhCl(\mathbf{3.4})_2]^{2+}$		4.1d	586.2
$[RhCl(\mathbf{3.4})_2\ BF_4]^+$		4.1e	1260.3
$[RhCl(\mathbf{3.4})_3\ BF_4]^{2+}$		4.1f	888.8
$[RhCl(\mathbf{3.4})_3(BF_4)_2]^+$		4.1g	1865.6
$RhCl(PR_3)_3(H)_2$	**4.2**		
$[Rh(PPh_3)_2(\mathbf{3.4})Cl(H)_2]^+$		4.2a	1181.3
$[Rh(PPh_3)(\mathbf{3.4})_2Cl(H)_2]^{2+}$		4.2b	718.2
$[Rh(PPh_3)(\mathbf{3.4})_2Cl(H)_2\ BF_4]^+$		4.2c	1524.4
$[Rh(\mathbf{3.4})_2Cl(H)_2]^{2+}$		4.2d	587.2
$RhCl(PR_3)_2(H)(SiHhex_2)$	**4.3**		
$[RhCl(PPh_3)(\mathbf{3.4})(H)(SiHhex_2)]^+$		4.3a	1117.2
$[RhCl(\mathbf{3.4})_2(H)(SiHhex_2)]^{2+}$		4.3b	686.3
$[RhCl(\mathbf{3.4})_2(H)(SiHhex_2)\ BF_4)]^+$		4.3c	1460.5
$Rh(PR_3)_3(SiHhex_2)$	**4.4**		
$[Rh(PPh_3)(\mathbf{3.4})(SiHhex_2)]^+$		4.4a	1081.4
$[Rh(\mathbf{3.4})_2(SiHhex_2)]^{2+}$		4.4b	668.3
$Rh(PR_3)_3(SiHhex_2)(H)_2$	**4.5**		
$[Rh(PPh_3)(\mathbf{3.4})(SiHhex_2)(H)_2]^+$		4.5a	1083.6
$Rh(PR_3)_3(H)$	**4.6**		
$[Rh(PPh_3)_2(\mathbf{3.4})(H)]^+$		4.6a	1145.3
$[Rh(PPh_3)(\mathbf{3.4})_2(H)]^{2+}$		4.6b	700.2
$[Rh(PPh_3)(\mathbf{3.4})_2(H)\ BF_4]^+$		4.6c	1488.5
$[Rh(\mathbf{3.4})_3(H)\ BF_4]^{2+}$		4.6d	872.1
$Rh(PR_3)_3^+$	**4.7**		
$[Rh(PPh_3)_3]^+$		4.7a	889.2
$[Rh(PPh_3)_2(\mathbf{3.4})]^{2+}$		4.7b	572.2
$[Rh(PPh_3)(\mathbf{3.4})_2\ BF_4]^{2+}$		4.7c	742.8
$RhCl(PR_3)_2(H)(Si\{OH\}hex_2)$	**4.8**		
$[RhCl(PPh_3)(\mathbf{3.4})(H)(Si\{OH\}hex_2)]^+$		4.8a	1133.7
$[RhCl(\mathbf{3.4})_2(H)(Si\{OH\}hex_2)]^{2+}$		4.8b	694.3

Immediately upon addition the spectrum is dominated by the ligand, ligand oxide and rhodium-hydride species, [**3.4**]$^+$, [**3.4**O]$^+$ and [Rh(PPh_3)(**3.4**)$_2$(H)]$^+$ at 517.2, 533.2, and 700.2 *m/z* respectively. However, the appearance of the spectrum changed rapidly from the initial moments to the end of the experiment. The intensity of each species in Table 4-1 was examined over time (as described in Section 3.3.2) generating the plot shown in (Figure 4-6) containing some 28 different sets of data. It was evident from the spectrum itself that there are many different species present, particularly at relatively low intensities. Arranging the data as in Figure 4-6 shows how complicated the analysis of a fluxional and changing system can be.

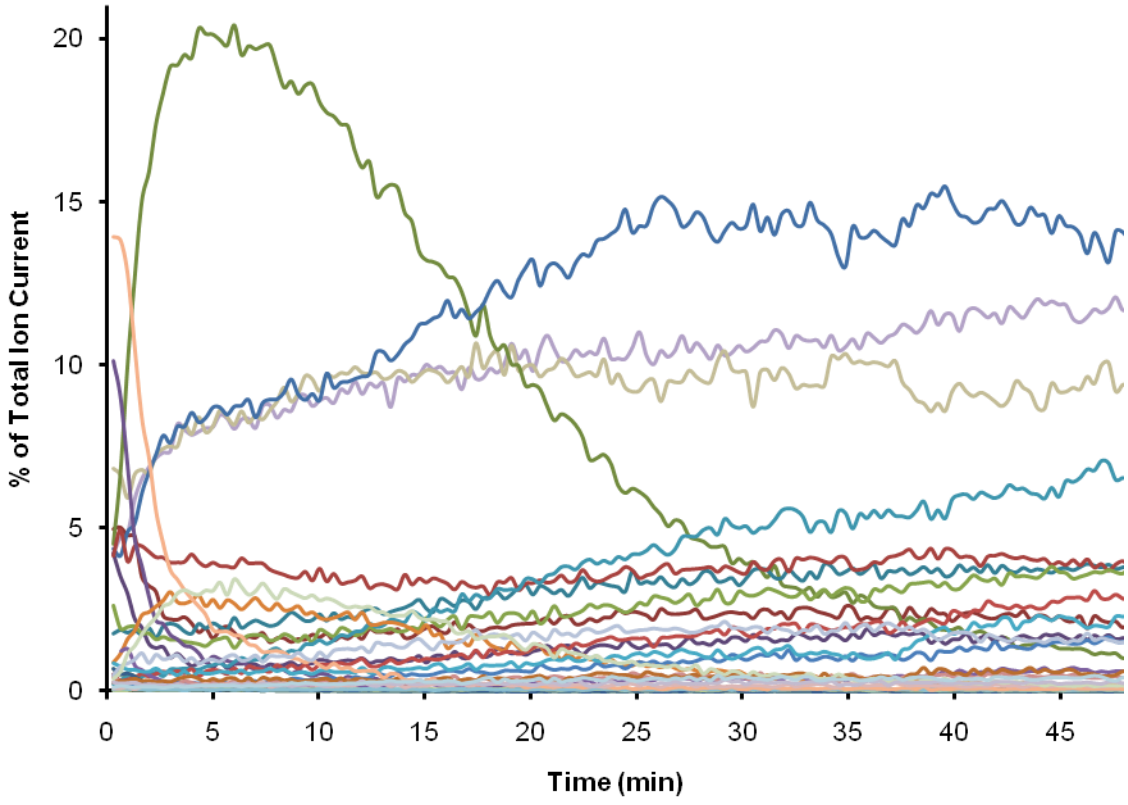

Figure 4-6. Individual intensity over time plots for each identifiable peak in the spectrum of [**3.4**]$^+$ BF_4^-, $RhClPPh_3$, and hex_2SiH_2 in fluorobenzene. Cone voltage = 10 V.

It was determined in the analysis of olefin hydrogenation that one species is effectively represented by several peaks. For example, Wilkinson's catalyst itself, $RhCl(PPh_3)_3$, is represented by the ions $[RhCl(PPh_3)_2(\mathbf{3.4})]^+$ (1179.2 *m/z*), $[RhCl(PPh_3)(\mathbf{3.4})_2]^{2+}$ (717.2 *m/z*), $[RhCl(PPh_3)(\mathbf{3.4})_2\ BF_4]^+$ (1260.3 *m/z*) and even $[RhCl(\mathbf{3.4})_3\ BF_4]^{2+}$ (888.8 *m/z*) and $[RhCl(\mathbf{3.4})_3(BF_4)_2]^+$ (1865.6 *m/z*). All of these peaks followed the same trace over time and they are all related (differing only by dissociation of PPh_3, nature of the phosphine ligands and ion aggregation) so that they all represented $RhCl(PR_3)_3$ (**4.1**) in the spectrum (where $PR_3 = PPh_3$ or $[\mathbf{3.4}]^+$). The behaviour of each peak was examined individually and in relation to the other traces of the same species (Figure 4-7). If the species followed the same trend over time and were chemically related their relative intensities were combined.

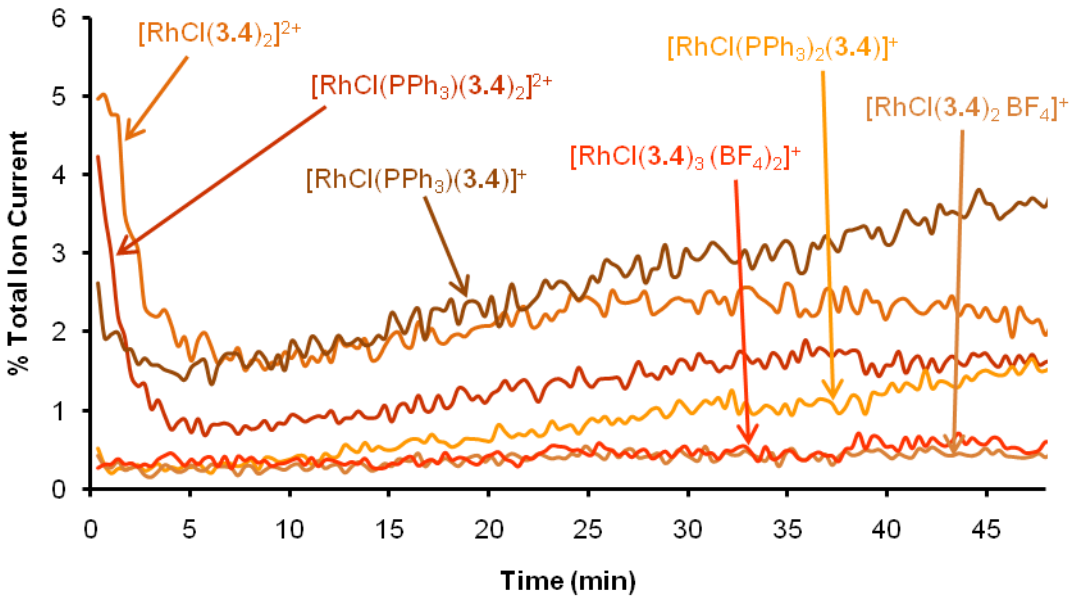

Figure 4-7. Changes in intensity for **4.1**-related species over time. Cone voltage = 10 V.

$[RhCl(\mathbf{3.4})_2]^{2+}$, $[RhCl(PPh_3)(\mathbf{3.4})_2]^{2+}$ and $[RhCl(PPh_3)(\mathbf{3.4})]^+$ are the most intense of the six peaks presented in Figure 4-7 and clearly followed the same trend of initially decreasing to less than

half of their initial intensity around five minutes into the reaction. At this point the intensities of these species began to increase to varying degrees. $[RhCl(\mathbf{3.4})_2]^+$ and $[RhCl(PPh_3)(\mathbf{3.4})_2]^{2+}$, which showed the largest decline initially, increased only slightly from their lowest points to 2% and about 1.5% respectively. $[RhCl(PPh_3)(\mathbf{3.4})]^+$ which showed the least initial decline in intensity showed the highest subsequent increase to 3.5%, even surpassing the initial intensity of just over 2.5%. $[RhCl(PPh_3)_2(\mathbf{3.4})]^+$ was less intense but followed the same trend as $[RhCl(PPh_3)(\mathbf{3.4})]^+$. The peaks could not be further organized by the number of PR_3 ligands they contained as species containing two PR_3 groups followed similar trends to species containing three PR_3 groups. It was already established that dissociation of PPh_3 from $[RhCl(PPh_3)_2(\mathbf{3.4})]^+$ occurred even at the low cone voltages (Section 3.3.2), so the inclusion of these peaks seemed justifiable. $[RhCl(PPh_3)(\mathbf{3.4})_2\ BF_4]^+$ and $[RhCl(PPh_3)(\mathbf{3.4})_3\ (BF_4)_2]^+$, both containing BF_4^- counterions, are more constant throughout the analysis. However, only differing by association to a counterion meant that these traces were included in the summation of $RhCl(PR_3)$. A comment on behaviour could be made based on the overall charge of the complex, as the species that exhibit the sharpest decline in intensity within the first five minutes are both doubly-charged. An explanation for this could be the dissociation of one $[\mathbf{3.4}]^+$ ligand, from $[RhCl(PPh_3)(\mathbf{3.4})_2]^{2+}$ and $[RhCl(\mathbf{3.4})_2]^{2+}$, in order to relieve repulsion from the two charged ligands. The increase in intensity of $[RhCl(PPh_3)(\mathbf{3.4})]^+$ may also be indirectly associated with the dissociation of one $[\mathbf{3.4}]^+$ from $[RhCl(PPh_3)(\mathbf{3.4})_2]^{2+}$.

The behaviour of $RhCl(PR_3)_3(H)_2$-related species (**4.2**) are shown in Figure 4-8. $[RhCl(PPh_3)(\mathbf{3.4})_2(H)_2]^{2+}$ was the most intense of the peaks in the group and showed a steady increase starting from an intensity of just under 2%. The intensity began to level off at about

3.5% at 35 minutes. The singly-charged $[RhCl(PPh_3)(\mathbf{3.4})(H)_2]^+$ showed the same tend of steadily increasing starting at 0.5% and finishing at nearly 3% intensity but differed from $[RhCl(PPh_3)(\mathbf{3.4})_2(H)_2]^{2+}$ in that there was no indication of a plateau. The ion aggregate $[RhCl(PPh_3)(\mathbf{3.4})_2(H)_2\ BF_4]^{2+}$ decreased slightly from its initial intensity of just under 1% to about 0.5% and began to increase in intensity again at 10 minutes. All peaks in this group were of the **4.2** variety. This is comparable to the results obtained in the investigation of the hydrogenation of olefins by the same catalyst. The five-coordinate $RhCl(PR_3)_2(H)_2$ was generated only under carefully controlled conditions in the collision cell (Section 3.3.4).

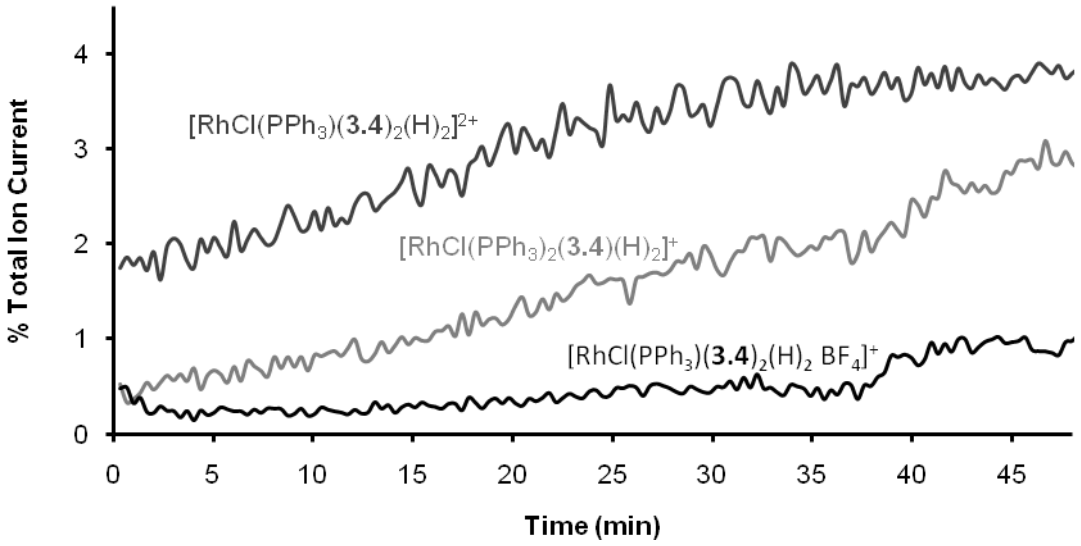

Figure 4-8. Changes in intensity for **4.2**-related species over time. Cone voltage = 10 V.

The oxidative addition of hex_2SiH_2 to $RhCl(PR_3)_2$ was evident by species containing both the silane and rhodium center. $[RhCl(PPh_3)(\mathbf{3.4})(H)(SiHhex_2)]^+$ and the doubly-charged $[RhCl(\mathbf{3.4})_2(H)(SiHhex_2)]^{2+}$ were present at the beginning of the analysis at 10% and 14% intensity respectively (Figure 4-9). Both species quickly decreased in intensity to 1% and 2% by the time five minutes had passed. A continued decrease in intensity brought the two species to

baseline levels within 25 minutes. The less intense [RhCl(**3.4**)$_2$(H)(SiHhex$_2$) BF$_4$]$^+$ also rapidly decreased in intensity from less than 1% to reach baseline level by five minutes due to the relatively low starting intensity. All peaks in this group were due to variations of the five coordinate RhCl(PR$_3$)$_2$(H)(SiHhex$_2$) as no RhCl(PR$_3$)$_3$(H)(SiHhex$_2$) (**4.3**) or RhCl(PR$_3$)(H)(SiHhex$_2$) species were observed.

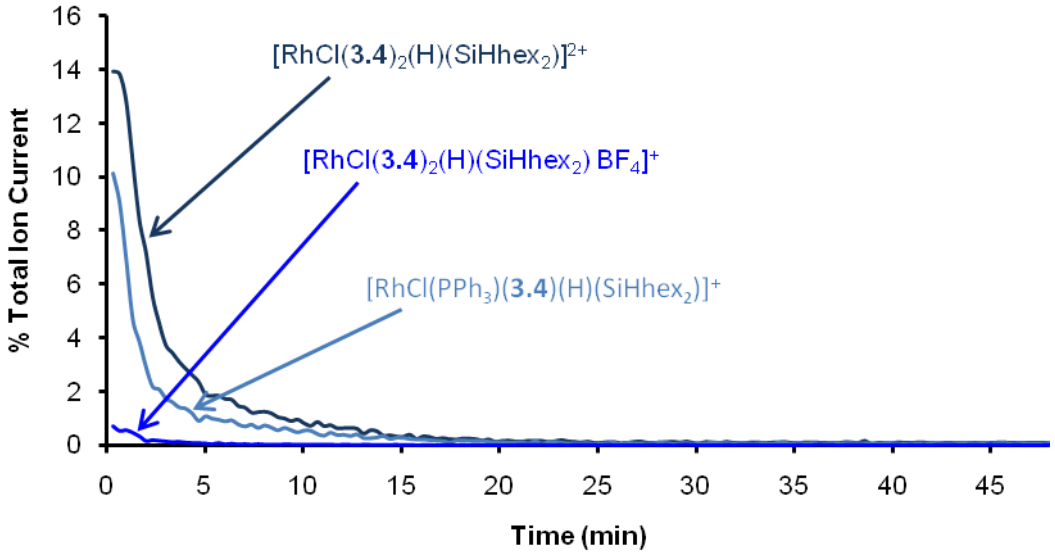

Figure 4-9. Changes in intensity for **4.3**-related species over time. Cone voltage = 10 V.

Because [RhCl(PPh$_3$)(**3.4**)(H)(SiHhex$_2$)]$^+$ (1117.2 *m/z*) is the product of oxidative addition of hex$_2$SiH$_2$ to RhCl(PPh$_3$)$_3$, it was of particular interest. Further investigation of this peak by ESI-MS/MS could provide insight into its potential reactivity. The ESI-MS/MS spectrum of [RhCl(PPh$_3$)(**3.4**)(H)(SiHhex$_2$)]$^+$ is shown in Figure 4-10. Loss of hex$_2$SiH$_2$ to give [RhCl(PPh$_3$)(**3.4**)]$^+$ (the exact opposite process to the oxidative addition) was present even at a collision voltage of zero, indicating that this process is quite facile. However, at voltages spanning 10 to 17 V, loss of H$_2$ from the parent ion was also observed.

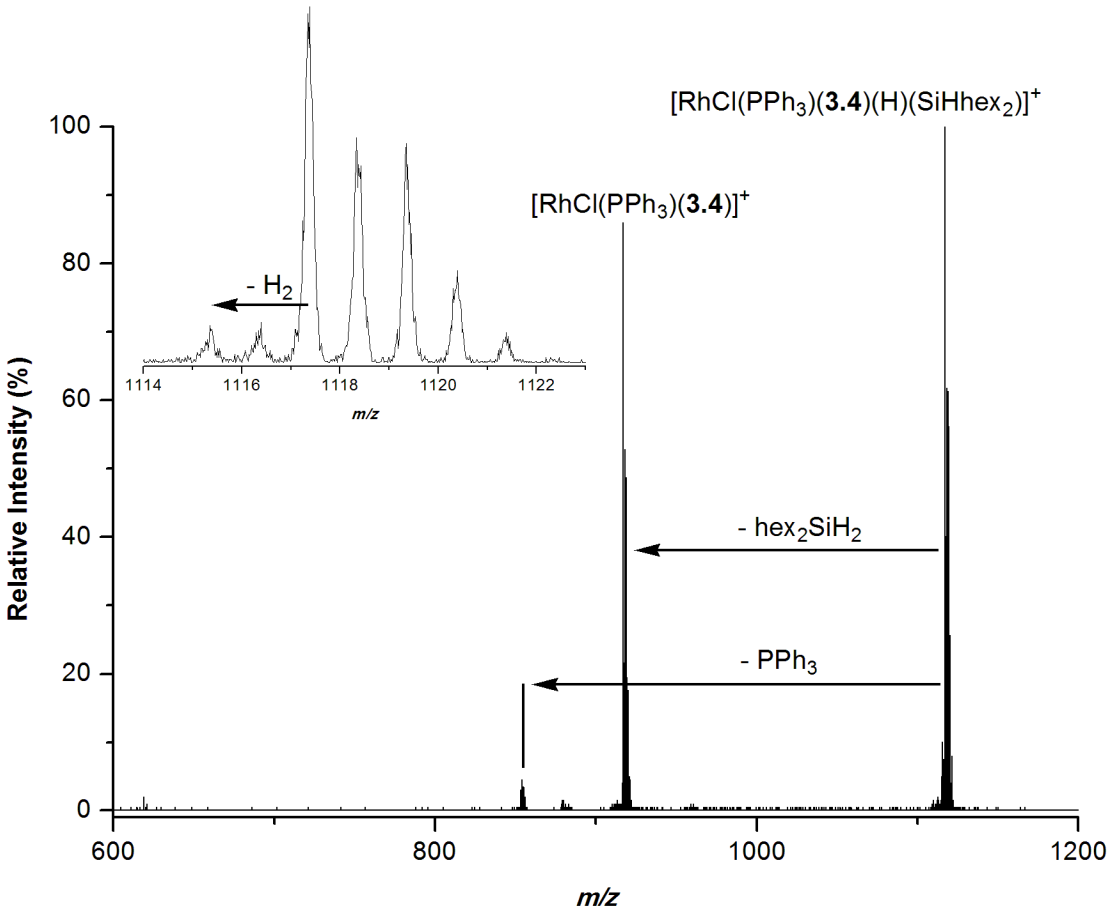

Figure 4-10. Positive-ion ESI-MS/MS of $[RhCl(PPh_3)(\mathbf{3.4})(H)(SiHhex_2)]^+$. Cone voltage = 0 V; collision voltage was increased from 0 to 15 V. Inset: expansion showing loss of H_2 from the parent ion.

Two peaks attributed to $Rh(PR_3)_2(SiHhex_2)$ (**4.4**) were identified, albeit at very low relative intensities (Figure 4-11). The intensities of both $[Rh(PPh_3)(\mathbf{3.4})(SiHhex_2)]^+$ and $[Rh(\mathbf{3.4})_2(SiHhex_2)]^{2+}$ were relatively constant. The signal-to-noise of the less intense species is inherently worse due to the low overall intensity of the peak in the spectrum. No $(PR_3)_3$ variations were observed for this group.

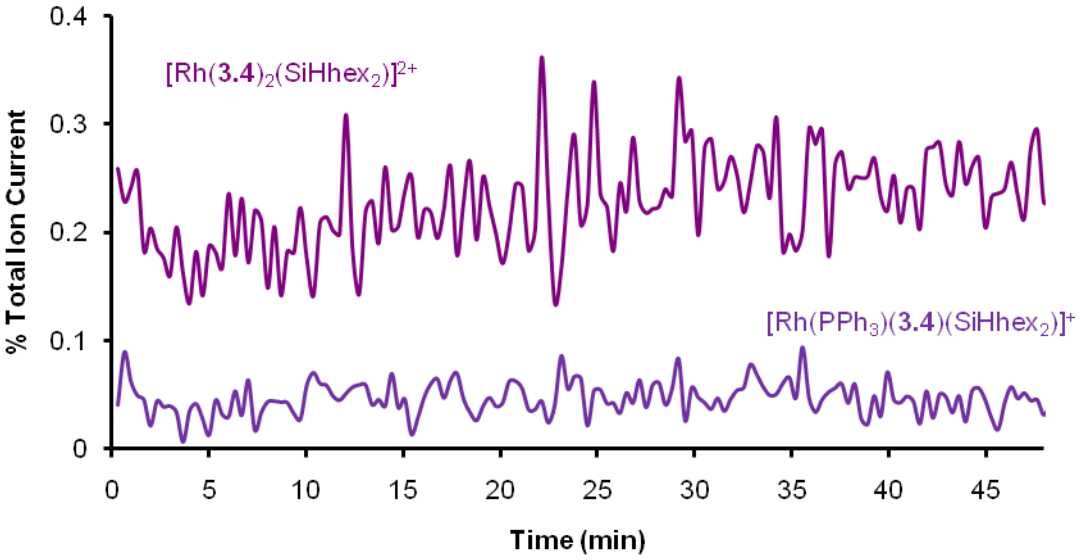

Figure 4-11. Changes in intensity for **4.4**-related species over time. Cone voltage = 10 V.

Only one peak attributed to $Rh(PR_3)_2(SiHhex_2)(H)_2$-related species (**4.5**) was identified, albeit at very low relative intensity (Figure 4-12). $[Rh(PPh_3)(\mathbf{3.4})(SiHhex_2)(H)_2]^+$ remained relatively constant throughout the experiment at an average value of between 0.2 and 0.3%. No $(PR_3)_3$ variations were observed for this group.

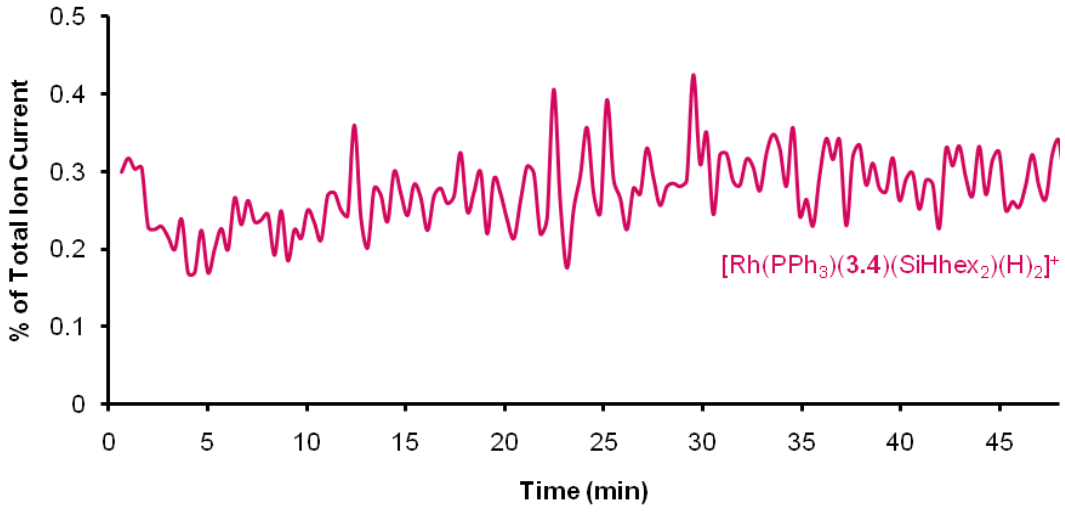

Figure 4-12. Changes in intensity for **4.5**-related species over time. $Rh(PPh_3)(\mathbf{3.4})(SiHhex_2)(H)_2$ was the only peak to fall into this group. Cone voltage = 10 V.

Traces for the peaks related to generation of the rhodium-hydride species $Rh(PR_3)_3(H)$ (**4.6**) are shown in Figure 4-13. Within the first five minutes the doubly-charged $[Rh(PPh_3)(\mathbf{3.4})_2(H)]^{2+}$ had reached its maximum intensity of 25%, increasing from an initial intensity of only 4%. After this point, the intensity began to drop off and was approaching an intensity of 2% by 45 minutes. This species was by far the most intense of this group and went through the most dramatic changes in intensity over time. However, $[Rh(PPh_3)_2(\mathbf{3.4})(H)]^{+}$ and $[Rh(\mathbf{3.4})_3(H)\ BF_4]^{2+}$ follow the same trend of increasing to three to four times their original intensity in the first five minutes and then gradually decreasing in intensity. $[Rh(PPh_3)(\mathbf{3.4})_2(H)\ BF_4]^{+}$ showed less exaggerated changes but followed the same general trend. The three less intense peaks returned essentially to baseline levels by 45 minutes due to their relatively low intensities. Interestingly, all of the species in Figure 4-13 contained three PR_3 ligands. No species of this type containing only two phosphine ligands, i.e. $Rh(PR_3)_2(H)$, were observed.

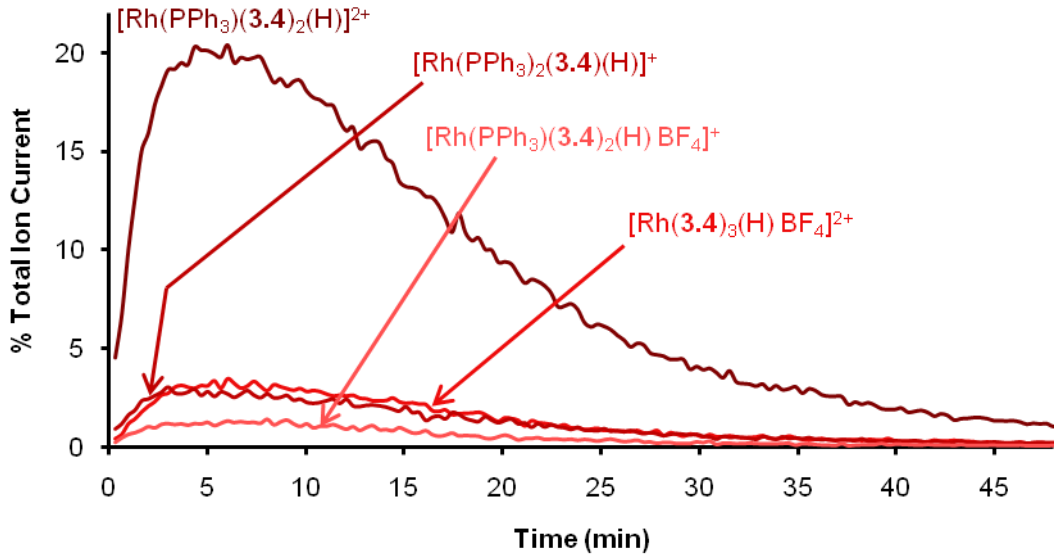

Figure 4-13. Changes in intensity for **4.6**-related species over time. Cone voltage = 10 V.

$[Rh(PR_3)_3]^+$-related species (**4.7**) were represented by three different peaks (Figure 4-14). The intensity of $[Rh(PPh_3)_3]^+$ decreased from 5% to 3% within the first 17 minutes of reaction and then climbed back up to about 4% towards the end of the experiment. $[Rh(PPh_3)(\mathbf{3.4})_2\ BF_4]^+$ and $[Rh(PPh_3)_2(\mathbf{3.4})]^{2+}$ were present in 0.2% and less than 0.1% relative intensity respectively. Both ions increased slightly within the first five minutes of data collection and then remained at a constant intensity throughout the reaction.

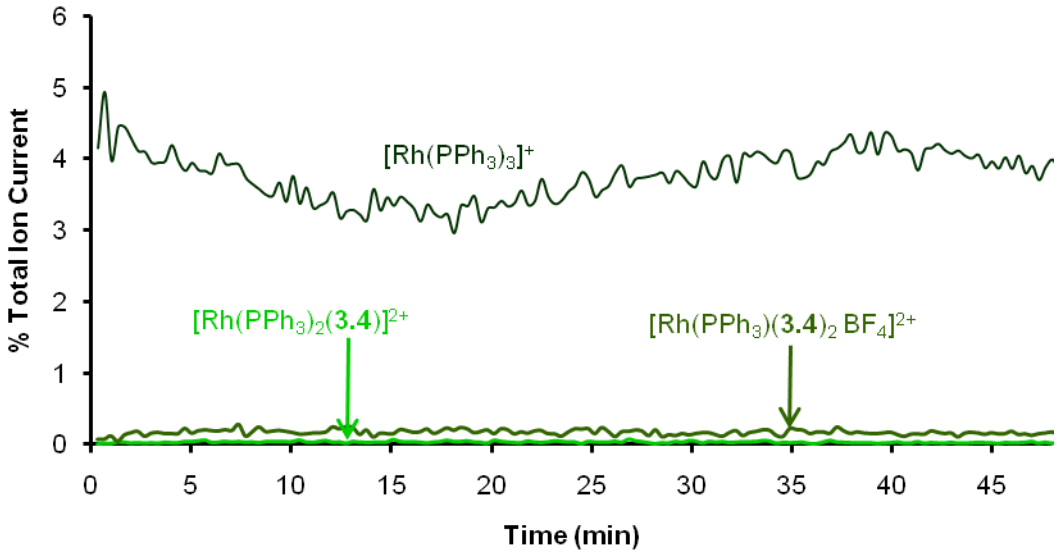

Figure 4-14. Changes in intensity for **4.7**-related species over time. Cone voltage = 10 V.

Species related to a presumed decomposition product, $RhCl(PR_3)_3(H)(Si\{OH\}hex_2)$ (**4.8**), were observed and their intensities over time are presented in Figure 4-15. $[RhCl(PR_3)(\mathbf{3.4})_2(H)(Si\{OH\}hex_2)]^+$ was present at nearly 0% relative intensity at the beginning of the reaction and steadily increased in intensity throughout the experiment to reach 7% by 48 minutes. $[RhCl(\mathbf{3.4})_2(H)(Si\{OH\}hex_2)]^{2+}$ also increased, but only from 1% at the beginning to 2% by the end of the experiment.

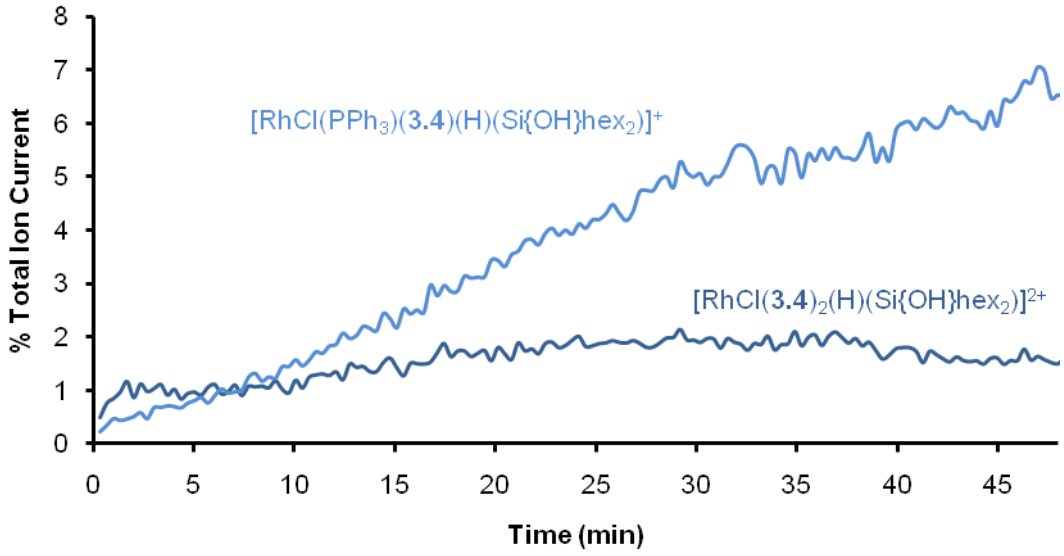

Figure 4-15. Changes in intensity for **4.8**-related species over time. Cone voltage = 10 V.

4.2.2 Inferences from ESI-MS data

The addition of one equivalent of hex_2SiH_2 to $RhCl(PPh_3)_3$ and monitoring the reaction by ESI-MS for 48 minutes generated a great deal of data. The first 15 seconds or so of the reaction were not captured due to the amount of time it took to obtain a sample and begin injection into the mass spectrometer. Following the examination of the Figures in Section 4.2.1 , the intensities of peaks within each group were combined to give one trend for each group. Summation of the peaks in each group exaggerated the general trends seen in each individual trace. Combining related peaks made the analysis of this system much less daunting, as a total of 28 different signals were reduced to just 10 different species (Figure 4-16 and Table 4-1). **4.4** and **4.5** are shown in a separate figure to allow expansion of the *y*-axis as these species were present in low concentration throughout the experiment (Figure 4-17). Organizing the summed traces next to one another on the same graph allowed for facile comparison of the different trends. It was obvious that the system changed quite rapidly within the first five minutes.

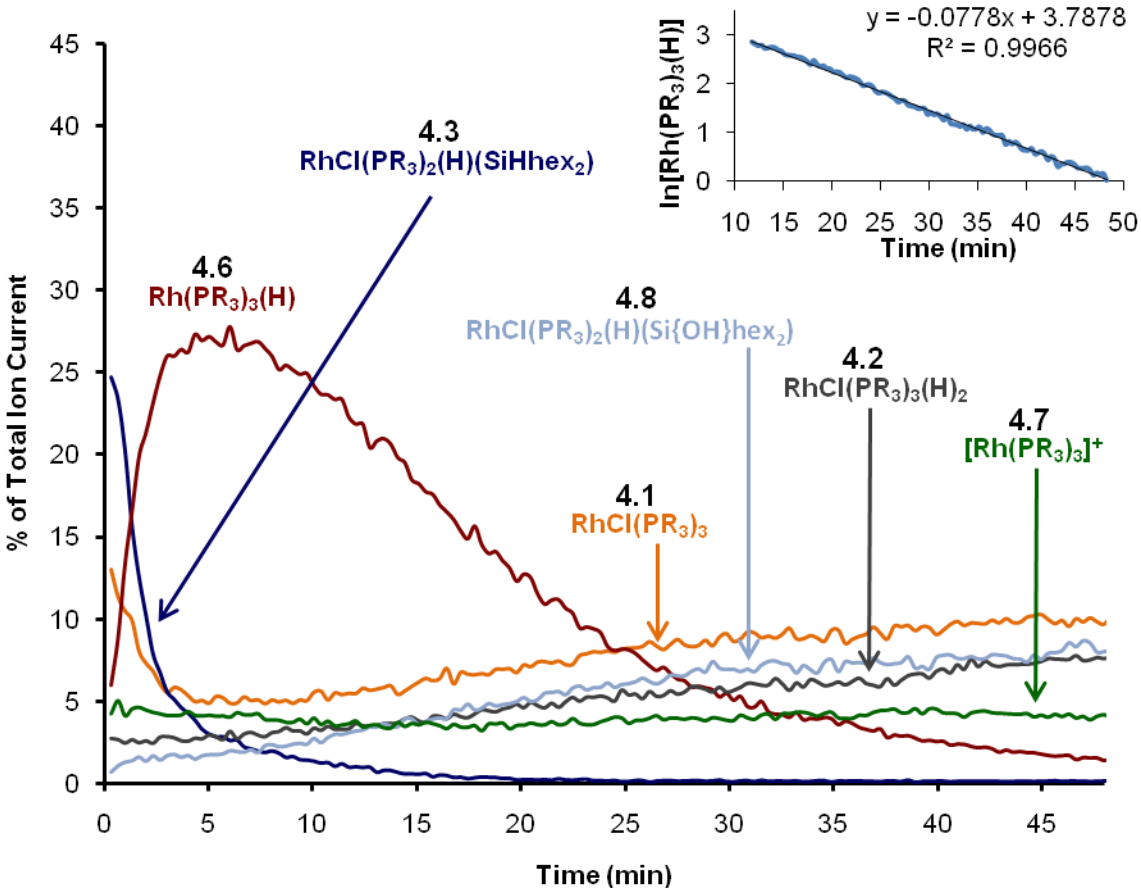

Figure 4-16. Combined intensities for species groups **4.1** to **4.8** (excluding **4.4** and **4.5**) in the spectrum of [**3.4**]$^+$ BF_4^-, $RhClPPh_3$, and one equivalent of hex_2SiH_2 in fluorobenzene. Cone voltage = 10 V. The traces for [**3.4**]$^+$ and [**3.4**O]$^+$ have been removed for clarity. Inset: decay for **4.6**; $t_{1/2}$ = 8.9 min.

Examination of Figure 4-16 showed that **4.7** remained constant between 4.5 and 5% for the duration of the experiment. In relation to the other species presented in this graph, its intensity was constant throughout. The amount of **4.7** found in solution is dependent on the amount of **4.1** present. This is further discussed in Sections 4.2.3 and 4.2.4 . It is therefore safe to conclude that **4.7**-related species are not involved in the dehydrocoupling of silanes to any great extent.

The summation of all species related to Wilkinson's catalyst, **4.1**, decreased in intensity from 13 to 5% in the first five minutes of the reaction and grew back to about 9% intensity within the 48 minutes the system was monitored. A slight change in the slope of the line can be seen at about

30 minutes. $RhCl(PPh_3)_3(H)_2$ was formed nearly instantaneously as its initial concentration was already 3% relative intensity. The steady re-growth of $RhCl(PPh_3)_3$ was mirrored in the trace for $RhCl(PPh_3)_3(H)_2$ which reached 7% intensity by the end of the experiment, although the slight change in slope is not apparent in the latter species. Variance in their final intensities (9% and 7%) was due to their varying intensities at the beginning of the experiment and the changes in behaviour of **4.1** at the five and 30 minute point so that the rate of increase in intensity decreases. There is only one source of hydride in the system. Therefore, the generation of **4.2** could only have come about by reaction of some species with hex_2SiH_2. And due to the similarity in the changes in intensity of **4.1** and **4.2**, the processes by which they are generated are closely related.

There were two species that underwent very dramatic changes within the first five minutes. **4.3** declined very sharply from 25% to just 2.5% within the first five minutes followed by a continued decline to approach to 0% by 20 minutes. Also within those first five minutes, **4.6** increased in intensity from 6 to 26% relative intensity. The strength of this signal then began to decrease and reached its original intensity at about 25 minutes, approaching 2% by the end of the experiment. From inspection of the lines for **4.3** and **4.6** it appears as though the two species are closely related as **4.3** decreases in intensity at a comparable rate to the appearance of **4.6**. A plausible explanation is that the formation of **4.6** ultimately resulted from the oxidative addition of hex_2SiH_2 to **4.1** to give **4.3**. Subsequent reductive elimination of hex_2SiHCl would have then produced $Rh(PR_3)_2(H)$ and re-association of a PPh_3 ligand would have given **4.6**.

4.6 follows a first order decay ($t_{1/2}$ = 8.9 minutes, inset Figure 4-16). Reaction of hex_2SiH_2 with **4.1** is fast and so is the reductive elimination to give **4.6**. **4.6** will now react with other species in

the reaction (for example, HCl to give **4.2**). If these reactions are slow the decay will be slow. In order to obtain pseudo-first order behaviour, the reactants must be present in excess to **4.6**, and so this explanation is weak given that the reaction being studied is stoichiometric. A second, and perhaps a more likely, explanation is the decay actually represents the dissociation of one PR_3 from **4.6** to give $Rh(PR_3)_2H$ which quickly reacts with other species in the reaction. As $Rh(PR_3)_2(H)$ gets consumed and the equilibrium shifts, the signal for **4.6** gradually decreases.

The decomposition product **4.8** was not present at the outset of data collection but did steady increase in intensity as the reaction continued to a final intensity of 8%. The rate of increase is comparable to that seen for **4.1** and **4.2**. A similar change in slope can be observed as was seen for **4.1** at around 30 minutes so that the rate of increase in intensity decreases after this point. Again, the difference in final intensity of **4.8** to **4.2** and **4.1** can be attributed to the differences in initial intensity.

It is believed that **4.8**-related species were formed from reaction of H_2O with hex_2SiHCl to give $hex_2Si(OH)Cl$ followed by oxidative addition to **4.6**. Silyl chlorides are water-sensitive, rapidly hydrolyzing to form silanols (which condense to form siloxanes)[150] and even though great care was taken to ensure all chemicals were handled and prepared properly just a small amount of water in the system would have led to formation of $hex_2Si(OH)Cl$. A trace amount of H_2O (perhaps in the form of a small, slow leak) would lead to the observed trend of slowly increasing intensity throughout the experiment. As discussed above, it is possible that reductive elimination of hex_2SiHCl from **4.3** would generate the free chlorosilane. Even though this process was not

observed in the ESI-MS/MS of this peak, the reductive elimination would also generate $Rh(PR_3)_2(H)$ which *was* indirectly observed as **4.6**.

4.5 and **4.4** were present at relatively low intensities throughout the analysis, but are nonetheless important species (Figure 4-17). A sample of baseline intensity is also shown to verify that these species are more than simply noise. The species were detected and are genuine, even if changes in intensity during the experiment were not especially dramatic.

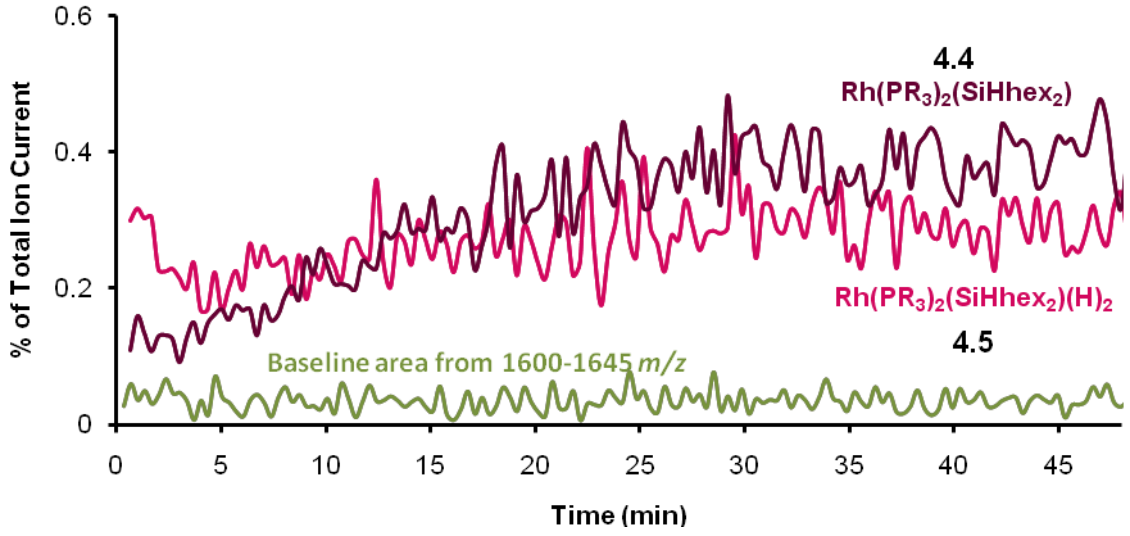

Figure 4-17. Combined intensities for species groups **4.4** and **4.5** in the spectrum of $[\mathbf{3.4}]^+ BF_4^-$, $RhClPPh_3$, and hex_2SiH_2 in fluorobenzene. Cone voltage = 10 V. An example of fluctuation in baseline intensity is shown for comparison.

4.5 could have been generated as a result of oxidative addition of hex_2SiH_2 to rhodium hydride $Rh(PR_3)_2(H)$ (or to **4.6** with displacement of PPh_3). Reductive elimination of H_2 from this species would have given **4.4** (which could also have conceivably been generated from reductive elimination of HCl from **4.3**).

At this stage, **4.4** would be ready for oxidative addition of another equivalent of hex_2SiH_2 to give $Rh(PR_3)_2(SiHhex_2)_2(H)$ as shown in Scheme 4-1. Reductive elimination from this species would result in the coupled product, $hex_2HSi\text{-}SiHhex_2$ and $Rh(PR_3)_2(H)$. However, no sign of $Rh(PR_3)_2(SiHhex_2)_2(H)$-type species were ever seen.

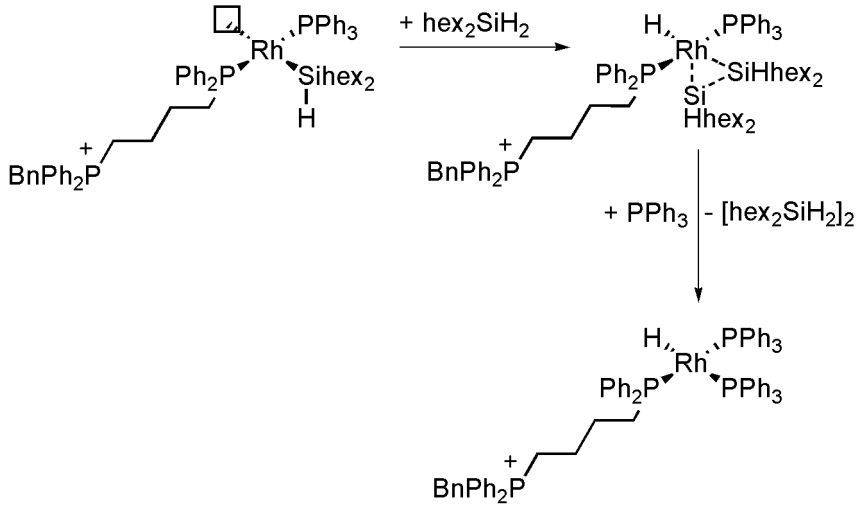

Scheme 4-1. Addition of two equivalents of hex_2SiH_2 to $Rh(PR_3)_2(H)$ would provide the conditions necessary to generate the coupled $hex_2HSi\text{-}SiHhex_2$ product.

Even though ESI-MS provides molecular weight information only, further structural data concerning molecular connectivity can be obtained from ESI-MS/MS data. The structural arrangement of **4.4** may just as well be $Rh(PR_3)_2(H)(:Sihex_2)$.

Loss of hex_2SiH_2 from **4.3** at very low voltages (even at 0 V, Figure 4-10) indicates that reductive elimination of hex_2SiH_2 is very easy. However, generation of H_2 implies that some degree of oxidative addition has in fact taken place. α-hydride elimination of the hydride bound to the silane would give a rhodium center with two hydride ligands, ready for reductive elimination of H_2 (Scheme 4-2) to give the observed $[RhCl(PR_3)_2(Sihex_2)]^+$. A comparable

process of α-elimination is possible for the **4.4** to give the silylene intermediate $Rh(PR_3)_2(H)(:Sihex_2)$.

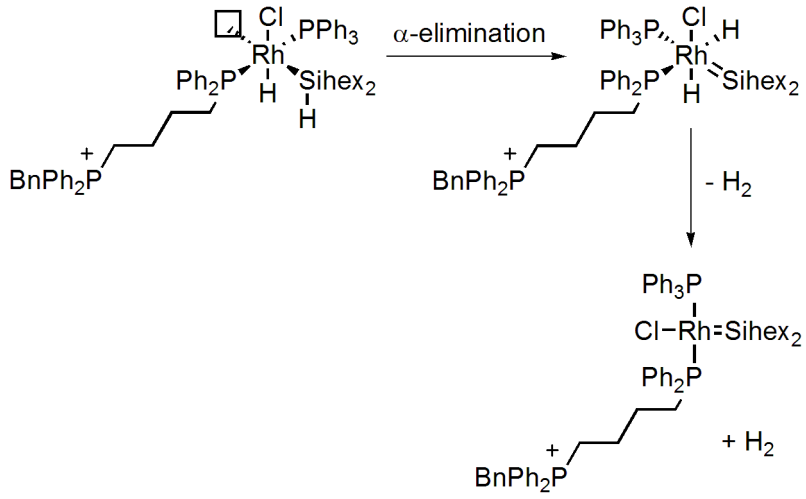

Scheme 4-2. α-hydride elimination may lead to a rhodium-silylene intermediate species.

4.2.3 Application of data to a potential cycle

The changes in intensity of the species discussed above, their apparent related behaviour and the inferences concluded from these two pieces of information lead us to speculate upon a potential mechanism that accounts for our observations.

Starting from **4.1**, loss of one PR_3 ligand generates a vacant site for an incoming hex_2SiH_2 substrate. Oxidative addition gives **4.3** which can then undergo reductive elimination of either hex_2SiHCl or HCl to give $Rh(PR_3)_2(H)$ or **4.4**. From $Rh(PR_3)_2(H)$, oxidative addition of another equivalent of hex_2SiH_2 will give **4.5**. Reductive elimination of H_2 from this species will generate **4.4** which could also be generated from the reductive elimination of HCl from **4.3**. The structure of **4.4** is not known for certain. There are two factors that contribute to the proposed existence of

a silylene intermediate. At no point in the progress of the reaction was any rhodium species containing more than one silane moiety observed and comparison of the ESI-MS/MS of $RhCl(PR_3)_2(H)(SiHhex_2)$ shows that the generation of a silylene intermediate through α-elimination is conceivable for these types of complexes. Silylenes are known to be very reactive[151] and contact with hex_2SiH_2 in solution would generate the coupled $hex_2HSi\text{-}SiHhex_2$ (effectively, insertion of $:Sihex_2$ into an Si-H bond).

The role of even trace amounts of H_2O was found to be detrimental to the reaction progress. If the hex_2SiHCl, generated from **4.3**, were to have come into contact with H_2O, $hex_2Si(OH)H$ and HCl would be generated. Oxidative addition of HCl to **4.6** would give **4.2** which is in equilibrium with $RhCl(PR_3)_3$ as determined by previous investigations of this catalyst (Chapter 3 and references therein). **4.1** can then continue on to the productive cycle. Oxidative addition of $hex_2Si(OH)H$ to **4.1** (and displacement of one PR_3 ligand) would generate the observed $RhCl(PR_3)_2(H)(Si\{OH\}hex_2)$ which appears to be a dead end in the reaction given its steady increase in intensity throughout the examination. **4.7** is generated in the ESI process by dissociation of a chloride ligand and does not seem to be involved in the productive cycle.

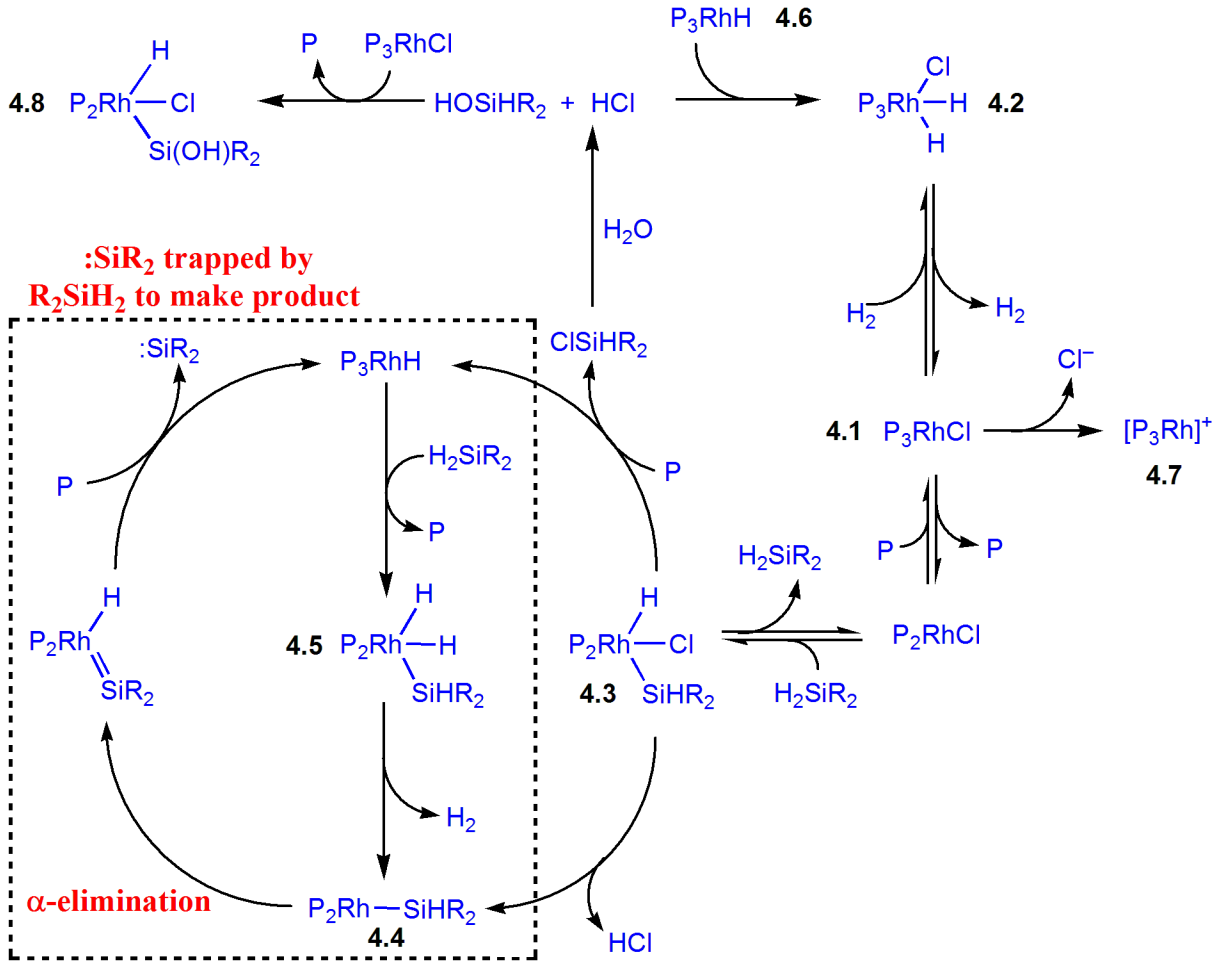

Figure 4-18. Potential mechanism of dehydrocoupling of silanes by $RhCl(PPh_3)_3$ based on the ESI-MS and ESI-MS/MS data obtained for the process with hex_2SiH_2 in fluorobenzene. The dashed lines enclose the productive part of the cycle. P = PPh_3.

4.2.4 Reproducibility and the consequence of water

The governing factor in the reproducibility of the results presented in Figure 4-16 is the presence of water in the system. No water was intentionally added and as mentioned above, it is suspected that there was trace amounts present that led to the observed data. The low concentration required in ESI-MS studies makes small amounts of water disproportionately significant. Repeating the experiment on different days shows a variation in the behaviour of some species more than others. Shown in Figure 4-19 are two additional duplicate experiments for the addition

of one equivalent of hex_2SiH_2 to a solution of $RhCl(PPh_3)_3$ and $[\mathbf{3.4}]^+$ $[BF_4]^-$ in fluorobenzene. When the amount of water in the system (exhibited by species **4.8**) was low, the amount of **4.6** observed was generally higher than when there was little water present. As more **4.8** formed, a greater amount of HCl was generated as a consequence thereby consuming **4.6**. When the amount of **4.8** was high to begin with, **4.6** was not present long enough for its signal to accumulate. When the amount of **4.8** was low in the beginning, **4.6** was present in larger quantity and decreased in intensity as **4.8** was generated.

Notable in both Figure 4-16 and Figure 4-19 is high initial abundance of **4.3** followed by a sharp decline. The high initial intensity, due to fast oxidative addition of the silane to the catalyst, is independent of the amount of water in the system. The consumption of **4.3** is not solely dependent on the elimination of hex_2SiHCl (the elimination of HCl would also cause a decrease in intensity) so the intensity would be expected to decrease with or without water present. However, with a greater amount of **4.8** present, implying more water in the system, the decrease in intensity of **4.3** was more rapid (Figure 4-19 top and bottom) as the elimination of hex_2SiHCl from **4.3** was driven by the consumption of the silylchloride by water.

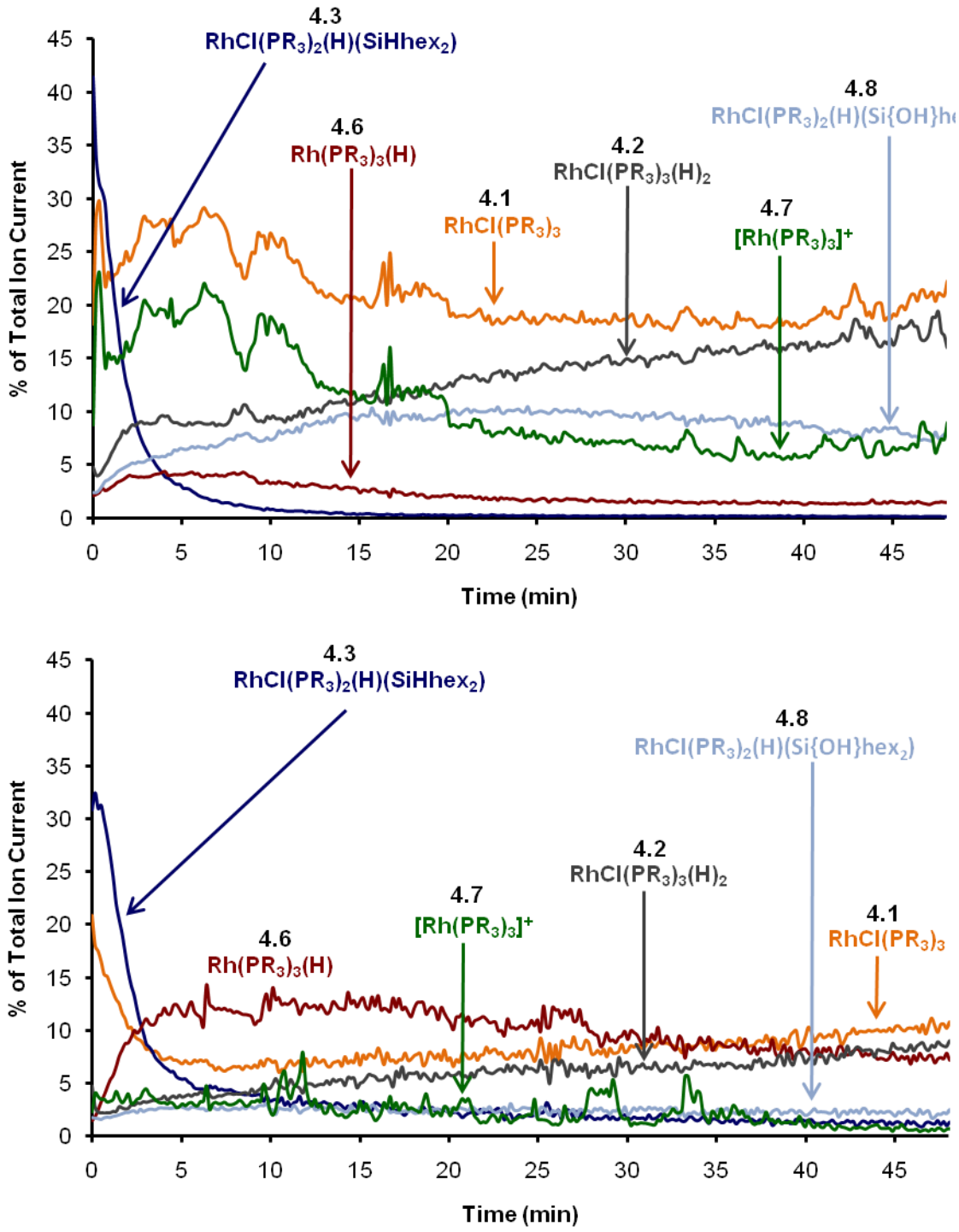

Figure 4-19. Results for two additional solutions of [**3.4**]$^{+}$ BF_4^-, $RhClPPh_3$, and one equivalent of hex_2SiH_2 in fluorobenzene. Combined intensities for species groups **4.1** to **4.8** (excluding **4.4** and **4.5**) with respect to time are presented. Cone voltage = 10 V.

Figure 4-16 seems to show that the behaviour of **4.7** was constant throughout the experiment. Figure 4-19, however, shows that this was not always the case. It might be expected that the behaviour of **4.7** would correlate more closely to **4.1** but this does not seem to be a consistent trend either, possibly because **4.7** is related to **4.1** through two equilibria (chloride association and phosphine substitution) and so changes in **4.1** are only slowly reflected in the intensity of **4.7**. In the instance where the initial intensity of **4.7** was high (Figure 4-19, bottom), the intensity of **4.6** was relatively low.

The behaviour of **4.8** itself was not consistent between the three experiments. In Figure 4-16, the intensity consistently rises and in Figure 4-19 the intensity increases only at the beginning of the run and even eventually decreases in the bottom plot. **4.8**-related species are prone to reductive elimination in the same manner that **4.3**-related species are. In fact, $hex_2SiH(OH)$ was lost from $[RhCl(PPh_3)(\mathbf{3.4})(H)(Si\{OH\}hex_2)]^+$ in MS/MS experiments (Appendix Figure 15) in the same way hex_2SiH_2 is lost from $[RhCl(PPh_3)(\mathbf{3.4})(H)(SiHhex_2)]^+$ (Figure 4-10). **4.1**-related species $[RhCl(PPh_3)(\mathbf{3.4})]^+$ would be generated from reductive elimination of $hex_2Si\{OH\}H$ and indeed as **4.8** decreases in Figure 4-19, the intensity of **4.1** begins to increase.

The relationship between water contamination and the speciation observed over time requires further investigation, including the deliberate addition of water. Use of isotopic labelling in the form of D_2O will also be informative, e.g. to distinguish the relative importance of the two possible reductive eliminations from **4.3**.

4.2.5 Addition of $[\mathbf{3.4}]^+$ BF_4^- to $Rh(PPh_3)_3(H)$ and $Rh(PPh_3)_4(H)$ in fluorobenzene

We have proposed a rhodium-hydride intermediate as an entry point into the catalytic cycle for the dehydrocoupling of silanes (Figure 4-18). To investigate this further, solutions of $Rh(PPh_3)_3(H)$ and $Rh(PPh_3)_4(H)$ were examined. Once dissolved in chlorobenzene $Rh(PPh_3)_3(H)$ and $Rh(PPh_3)_4(H)$ both gave yellow solutions. Addition of $[\mathbf{3.4}]^+$ BF_4^- did not change the appearance of the solution. Incorporation of the charged ligand into the complex was observed immediately. Strong peaks for $[Rh(PPh_3)(\mathbf{3.4})_2(H)]^{2+}$ (700.2 *m/z*), $[Rh(\mathbf{3.4})_3(H)\ BF_4]^{2+}$ (872.1 *m/z*), $[Rh(PPh_3)_2(\mathbf{3.4})(H)]^+$ (1145.3 *m/z*) and $[Rh(PPh_3)(\mathbf{3.4})_2(H)\ BF_4]^+$ (1488.5 *m/z*) as well as $[Rh(PPh_3)_3]^+$ (formed by loss of H^-, 889.2 *m/z*) were present as soon as the spectrum was collected (ca. 1 minute after mixing). After just 15 minutes, peaks for $[RhCl(PPh_3)_2(\mathbf{3.4})]^+$ and other chloride-containing species were seen 34 *m/z* units higher than the species present in the initial moments (Figure 4-20). The same changes in the spectra were obtained when $Rh(PPh_3)_3(H)$ was used in place of $Rh(PPh_3)_4(H)$ (Appendix Figure 16). When the solvent was changed to fluorobenzene the corresponding fluorine-containing species were not observed.

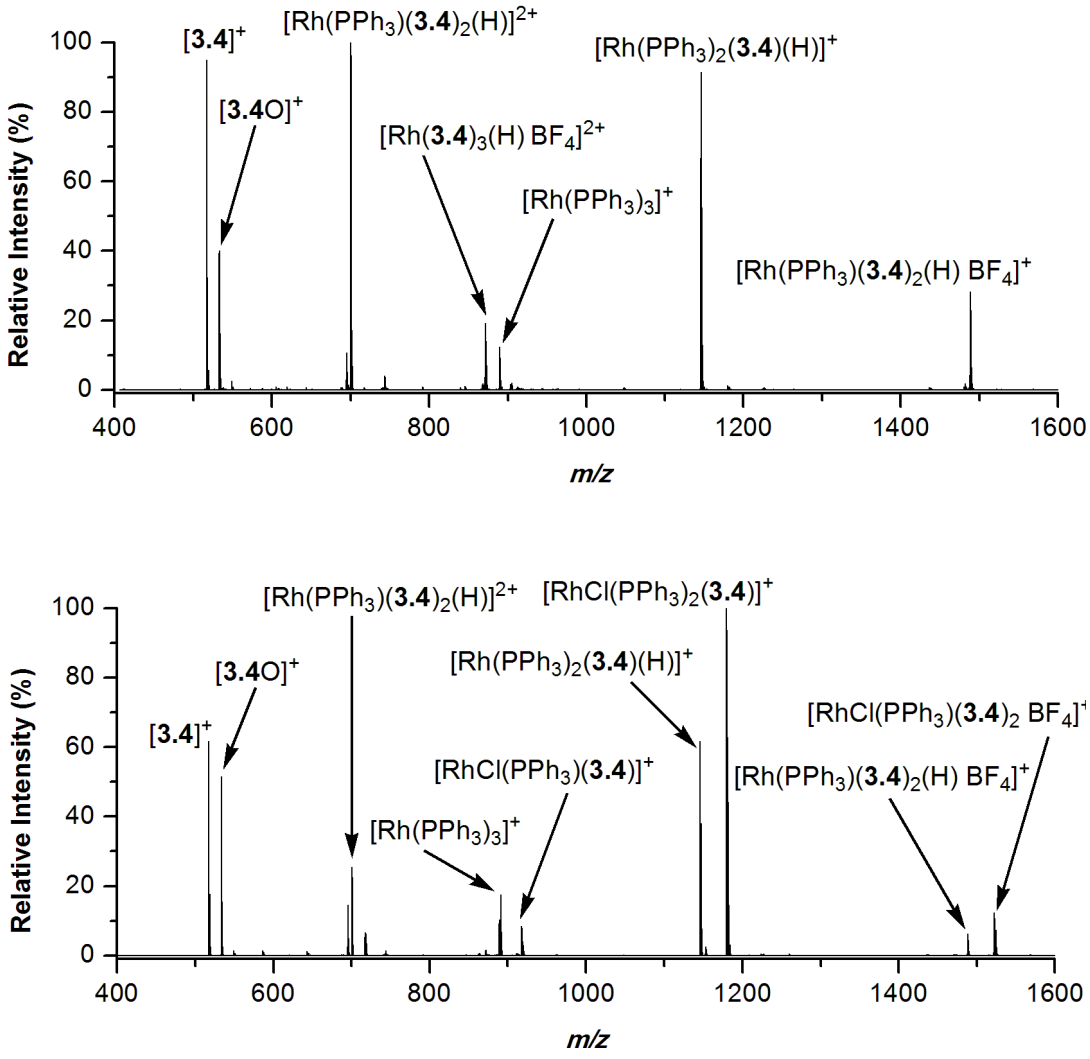

Figure 4-20. Positive-ion ESI-MS of a solution of $Rh(PPh_3)_4(H)$ and $[\mathbf{3.4}]^+ BF_4^-$ in chlorobenzene. Cone voltage = 10 V. Top: t = 0; bottom: t = 15 min.

Once dissolved in fluorobenzene, $Rh(PPh_3)_3(H)$ and $Rh(PPh_3)_4(H)$ both gave yellow solutions. Again, addition of $[\mathbf{3.4}]^+ BF_4^-$ did not change the appearance of the solution. Incorporation of the charged ligand into the complex was observed immediately, and relatively simple spectra were obtained (Figure 4-21, Appendix Figure 17). All peaks were the same as in the initial spectrum collected in chlorobenzene without the additional formation of chloride-containing species: $[Rh(PPh_3)(\mathbf{3.4})_2(H)]^{2+}$ at 700.2 *m/z*, $[Rh(PPh_3)_3]^+$ (formed through loss of H^-) at 889.2 *m/z*, $[Rh(PPh_3)_2(\mathbf{3.4})(H)]^+$ at 1145.3 *m/z* and $[Rh(PPh_3)(\mathbf{3.4})_2(H)\,BF_4]^+$ at 1488.5 *m/z*. Both

$Rh(PPh_3)_3(H)$ and $Rh(PPh_3)_4(H)$ gave similar spectra as no peak for $[Rh(PPh_3)_3(\mathbf{3.4})(H)]^+$ or other $Rh(PR_3)_4(H)$ species were observed (where $PR_3 = PPh_3$ or $[\mathbf{3.4}]^+$).

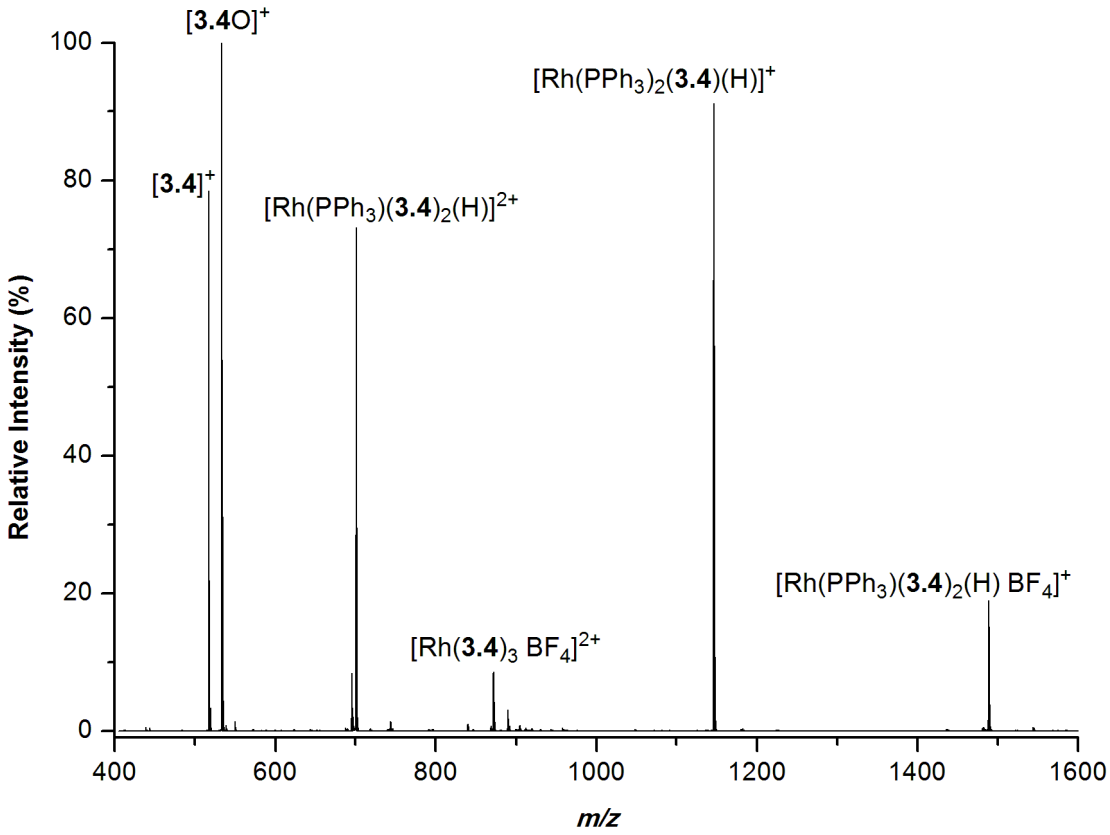

Figure 4-21. Positive-ion ESI-MS of a solution of $Rh(PPh_3)_4(H)$ and $[\mathbf{3.4}]^+$ BF_4^- in fluorobenzene. Cone voltage = 10 V.

4.2.6 Addition of hex_2SiH_2 to solutions of $[3.4]^+$ BF_4^- and $Rh(PPh_3)_3(H)$ or $Rh(PPh_3)_4(H)$ in fluorobenzene

Addition of di(*n*-hexyl)silane to a solution of $[\mathbf{3.4}]^+$ BF_4^- and $Rh(PPh_3)_4(H)$ did not cause a change in the appearance of the solution. One equivalent of silane was added and a sample was immediately removed from the reaction vessel *via* a gas-tight syringe. As can be seen from Figure 4-22, the major peaks in the spectrum did not change, although a change in their relative

intensities was observed. Comparison of Figure 4-22 and Figure 4-21 shows that the relative amount of rhodium-containing species was much lower compared to the free phosphine (oxide) after addition of hex_2SiH_2. Similar results were obtained from the addition of di(*n*-hexyl)silane to $Rh(PPh_3)_3(H)$ (Appendix Figure 18).

A peak for the **4.4** species, $[Rh(PPh_3)(\mathbf{3.4})(SiHhex_2)]^+$, was observed at 1081.4 *m/z* as well as the **4.5** species $[Rh(PPh_3)(\mathbf{3.4})(SiHhex_2)(H)_2]^+$ at 1083.6 *m/z*. The presence of these species supported that hex_2SiH_2 could add directly to the hydride species and was followed by reductive elimination of one equivalent of H_2. Again, no evidence of $Rh(PR_3)_n(SiHhex_2)_2$ species was observed.

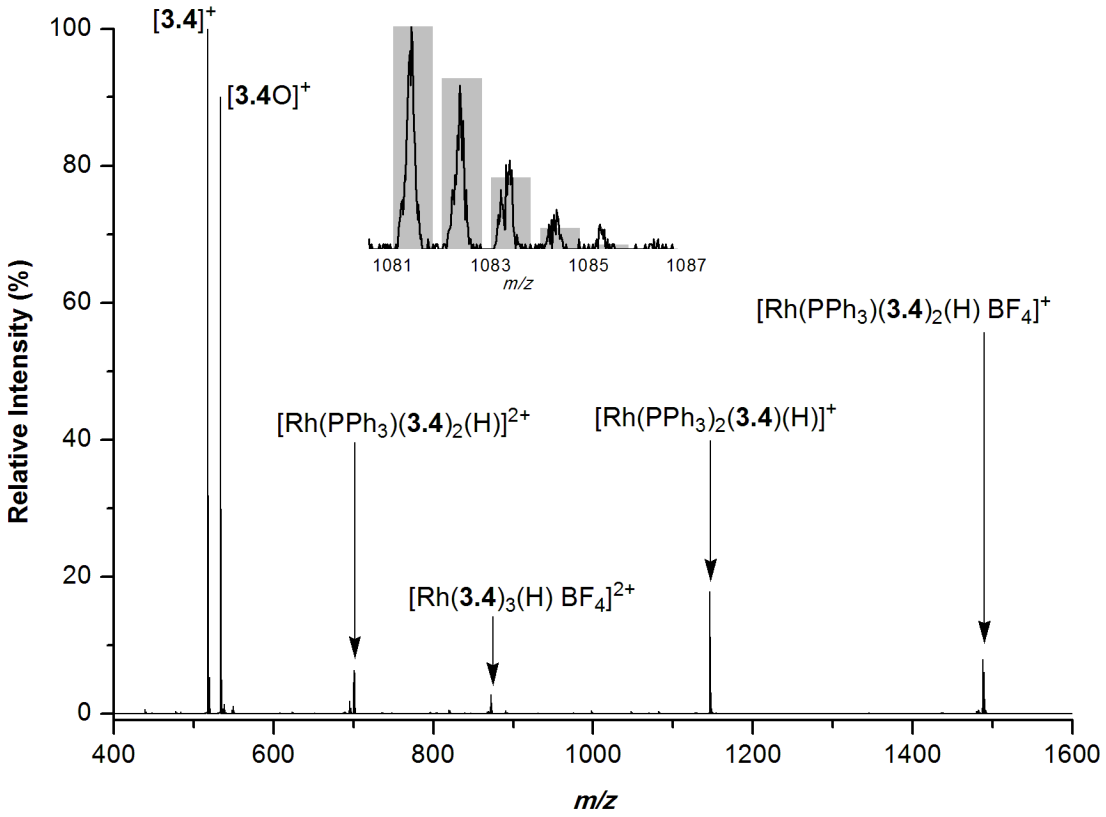

Figure 4-22. Positive-ion ESI-MS of the addition of hex_2SiH_2 to a solution of [**3.4**]$^+$ BF_4^- and $Rh(PPh_3)_4(H)$ in fluorobenzene. Cone voltage = 10 V. Inset: isotope pattern for [$Rh(PPh_3)$(**3.4**)$(SiHhex_2)$]$^+$ and calculated values (grey bars).

4.2.7 Comparison to known speciation

The results obtained in this study are in good agreement with NMR data of 1:1 addition of di(*n*-hexyl)silane to $RhCl(PPh_3)_3$ in d_6-benzene. The presence and disappearance of **4.3** in the NMR was mirrored in the ESI-MS by an immediate strong signal followed by rapid decline in intensity. The high intensity of **4.6** species toward the beginning of the reaction also agrees with the dominant amount of hydride containing species reported by the Rosenberg group. $Rh(PR_3)_4(H)$ species were not observed, but given that they were also not observed in a solution of $Rh(PPh_3)_4(H)$, this was not surprising. **4.1** and **4.2** were also observed in both experiments.

Absent from any of the ESI-MS, as well as the ^{31}P NMR, were peaks due to complexes containing more than one silane group.

Reductive elimination of hex_2SiHCl was *not* observed in the ESI-MS/MS of **4.3**, even though it is implicated in the mechanism proposed above. Other than the silanol, no evidence of hex_2SiHCl has been readily observed in the NMR of these solutions either.

4.3 Conclusions

The investigation of dehydrocoupling of di(*n*-hexyl)silane using Wilkinson's catalyst, $RhCl(PPh_3)_3$, by ESI-MS was undertaken. Relying on the labile nature of the PPh_3 ligands, a charged phosphine, 4-diphenylphosphino-1-benzyldiphenylphosphonium-butane tetrafluoroborate, was doped into catalyst solution and incorporated into the coordination sphere of the complex. Not only were 28 individual species readily indentified, but their intensities were easily isolated and monitored over time to give a reaction profile for each species. Despite attempts to generate a system in which each species has only one representative peak, multiple ligand exchange, counterion aggregation and the fragile nature of the complex meant that one species was often represented by several peaks. Combination of the contributions due to similar species greatly simplified the picture of the reaction.

Less than one hour of data collection time leads to a detailed summary of the behaviour of 10 different species. Inspection of their intensities over time allowed inferences to be made about the formation of various species, and their relation to other elements of the ESI-MS/MS data provided insight into the structure of a potential reactive intermediate in the process. A plausible scheme that connects all of the information obtained is shown in Figure 4-18. The data appears

to support the possibility of a silylene reactive species based on the absence of any $Rh(PR_3)_n(SiHhex_2)_2(H)$ species and the loss of H_2 in the ESI-MS/MS of $[RhCl(PPh_3)_3(\mathbf{3.4})(H)(SiHhex_2)]^+$. However, given that these investigations were carried out in a 1:1 $RhCl(PPh_3)_3$:hex_2SiH_2 ratio, the absence of $Rh(PR_3)_n(SiHhex_2)_2(H)$ species is not surprising.

While perhaps no absolute conclusions can be drawn on the exact mechanism by which the coupling of silanes with $RhCl(PPh_3)_3$ proceeds, new insight into the early time regime has been made possible. Data on the first minutes of the process is easily attainable by fast sampling and rapid data collection. Data obtained by traditional means such as NMR would necessarily miss the very early time regime due to the time required for sample preparation. ESI-MS has the ability to detect species present at concentrations far below that of NMR. Also, data obtained by NMR would be averaged over minutes, where ESI-MS has the capability to provide snapshots in the time frame of seconds. In this instance, providing time-resolved data on 10 different species related to the dehydrocoupling of silanes by Wilkinson's catalyst.

4.4 Experimental

All mass spectra were performed on a Micromass Q-ToF *micro* hybrid quadrupole/time-of-flight mass spectrometer in positive ion mode using pneumatically-assisted electrospray ionization with a cone voltage of 10 V, capillary voltage of 3100 V, source temperature of 120 °C and desolvation temperature of 150 °C. Solutions were run in fluorobenzene and introduced to the mass spectrometer by a syringe pump at a rate of 10 μl min^{-1}. ESI-MS spectra of the catalyst mixture were obtained by adding to 12 ml of fluorobenzene $RhCl(PPh_3)_3$ (11 mg, 0.012 mmol, 0.96 mmol L^{-1}) and $[\mathbf{3.4}]^+$ BF_4^- (2 mg, 0.003 mmol, 0.28 mmol L^{-1}) to give a bright orange

solution. To this solution was added hex_2SiH_2 (2 mg, 0.012 mmol) to give a bright yellow solution within seconds. Fluorobenzene was distilled over CaH_2. Ph_3SiH, Ph_2SiH_2, $(n\text{-}C_6H_{12})_2SiH_2$, $Rh(PPh_3)_3H$ and $Rh(PPh_3)_4H$ were obtained from the Rosenberg group at the University of Victoria.

Chapter 5. Collaborative studies

As discussed above, ESI-MS is suited for the identification of solution phase speciation, given that those species are charged. Follow-up analyses may include MS/MS and CID experiments that can provide further characterization of species of interest. The McIndoe group has a long-standing collaboration with Professor Paul Dyson of the École Polytechnique Fédérale de Lausanne (EPFL) in Switzerland. These have typically involved the use of ESI-MS methodology developed in our laboratory for difficult characterization problems faced by the Dyson group. I have been involved in three such collaborations, which are outlined below. The first has been published[152] and our contributions are complete for the second and third; both manuscripts are close to submission.

5.1 Ruthenium-silver metal clusters; $[PPN]_2[\{Ru_6C(CO)_{16}Ag_2X\}_2]$ (X = Cl or I)

5.1.1 Introduction

Mixed-metal transition metal clusters are of interest as they provide the opportunity for synergistic behaviour between the two (or more) metal atoms. Many heterogeneous catalysts, for example, contain two or more metals – the three-way catalytic converters used in cars that remove CO, nitrogen oxides and residual hydrocarbons typically contain cerium, platinum and other precious metals. Efforts to make molecular mimics of such catalysts have included synthesis of mixed-metal clusters and decomposing them on mesoporous silica.[153-155] However, characterization of such systems has been very much limited to X-ray crystallographic analysis, which looks only at solid-state structure. Solution techniques are limited: IR spectra provide a

simple fingerprint only and NMR is uninformative. ESI-MS promised to provide a more detailed picture of solution speciation for complicated multinuclear, mixed-metal clusters.

The synthesis of the ruthenium-silver heterometallic cluster $[\{Ru_6C(CO)_{16}Ag_2I\}_2]^{2-}$ from two monomeric units of a $[Ru_6C(CO)_{16}Ag_2I]^-$ was achieved through addition of AgI to $[Ru_6C(CO)_{16}]^{2-}$ ($[\mathbf{5.1}]^{2-}$) in THF with an 80% yield (Equation 5-1).

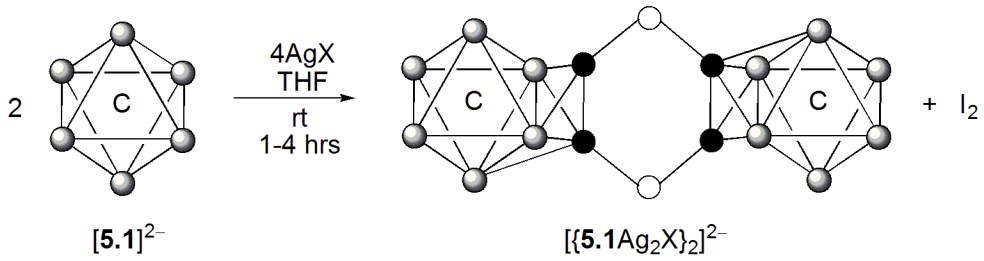

Equation 5-1

There is a silver-silver bond in each monomer and a weak association between the silver atoms of neighbouring monomers. The two cores are made up of six ruthenium atoms arranged in an octahedral geometry, each with four bonds to neighbouring ruthenium atoms, and a carbide atom situated in the center. The outside of each ruthenium octahedron is decorated with 16, symmetrically arranged, carbonyl atoms. Two silver atoms cap one face and one edge of the octahedron through silver-rhodium bonds. The two monomers are connected together by two silver-iodide-silver (Ag-I-Ag) bridges. The crystal structure of $[\{Ru_6C(CO)_{16}Ag_2I\}_2]^{2-}$, denoted as $[\{\mathbf{5.1}Ag_2I\}_2]^{2-}$, is given in Figure 5-1.

To add insight into the formation of these clusters, our lab was asked to conduct ESI investigations on the solution phase speciation as the reaction progressed. Further, MS/MS and

EDESI analysis of various species was to be conducted in an effort to lend information on the connectivity and relative bond strengths within the molecule. Through regular sampling of the reaction mixture (in 30 minute intervals), the formation of $[\{\mathbf{5.1}Ag_2I\}_2]^{2-}$ was monitored over time by ESI-MS in the negative ion mode. Selected species were further examined by ESI-MS/MS.

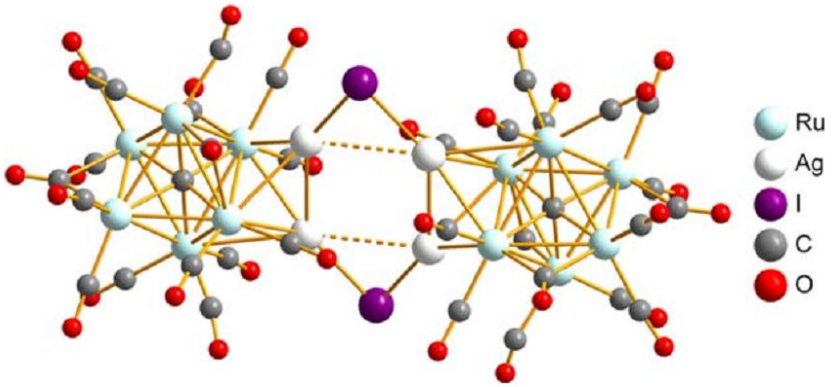

Figure 5-1. X-ray crystal structure of $[N(C_4H_9)_4]_2[\{Ru_6C(CO)_{16}Ag_2I\}_2]$ obtained by the Dyson group from THF/hexanes at 4 °C.

5.1.2 Results and Discussion

The synthesis of the cluster was first completed by Dyson and co-workers and the $[N(C_4H_9)_4]^+$ cation was used. When the reaction was repeated in our lab for the purposes of monitoring the reaction by ESI-MS, the $[PPN]^+$ cation (PPN = $[Ph_3PNPPh_3]^+$) was used instead. Because of the high yield (80%) of the reaction it would not be unreasonable to expect a mass spectrum dominated by the product cluster. Interestingly, this was not observed. Before addition of AgI, the two main peaks in the mass spectrum were 533.6 and 1605.6 *m/z* which were attributed to $[\mathbf{5.1}]^{2-}$ and $[\mathbf{5.1}\ PPN]^-$ respectively (Table 5-1). This was expected as the starting material was

the only species present in solution and ion aggregation is commonly seen for multiply charged species due to the soft nature of the technique.

Upon addition of AgI the mass spectrum changed almost immediately (Figure 5-2, A). An aliquot of the reaction mixture was diluted in dichloromethane and introduced into the mass spectrometer at 30 minute intervals from the time of addition up to and including two hours. The base peak remained as [**5.1**]$^{2-}$ but the ion paired species [**5.1** PPN]$^{-}$ was greatly diminished. Several new species began to grow in, particularly the peak attributed to [**5.1**AgI]$^{2-}$. It was this species that became the base peak in the spectrum after 30 minutes (Figure 5-2, B) and remained the dominant species through the two hour time period (Figure 5-2, D) as other species changed in intensity. Even 24 hours later, [**5.1**AgI]$^{2-}$ was still the base peak and the next most intense species reached just 20% relative intensity (Figure 5-2, E).

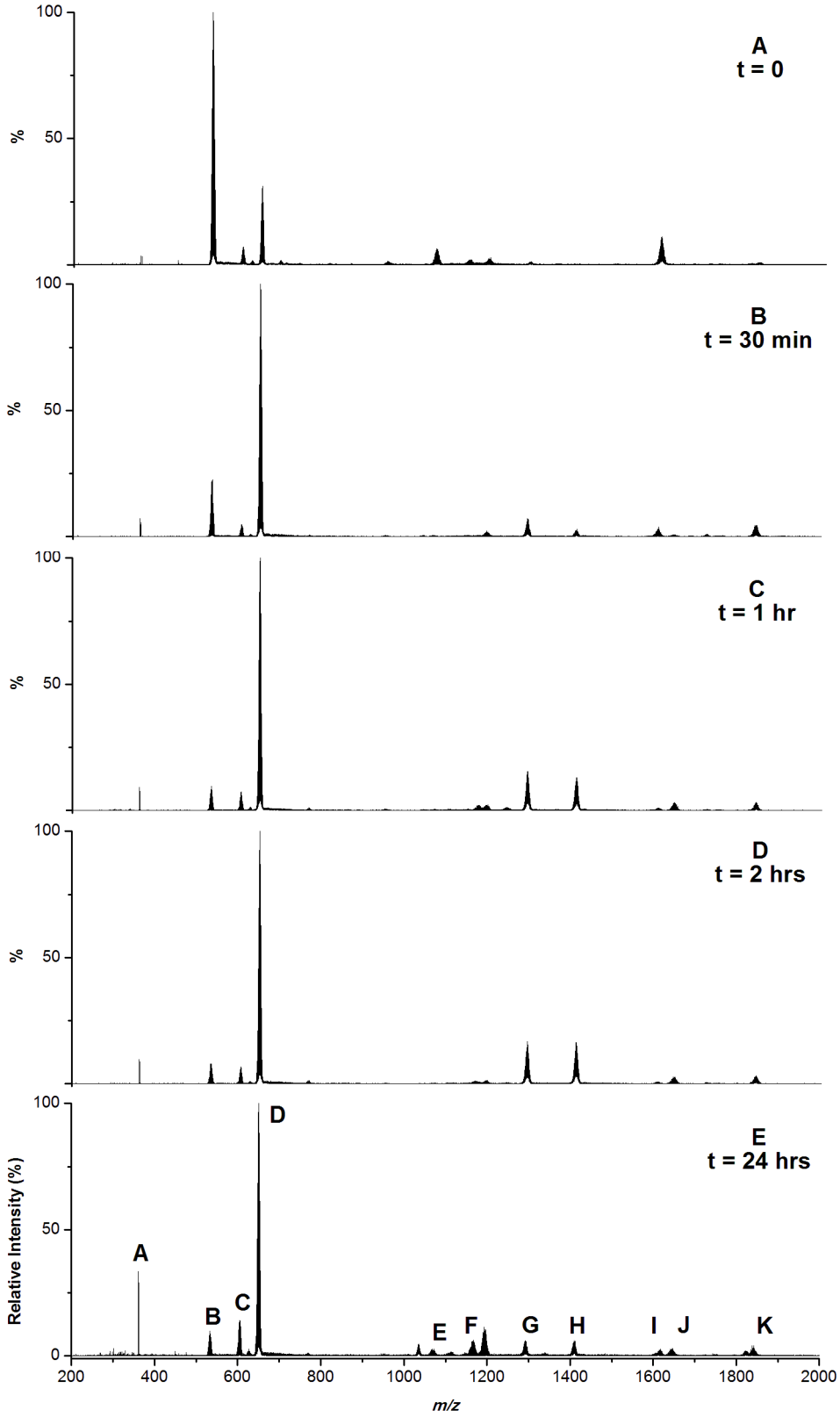

Figure 5-2. Reaction profile of [**5.1**]$^{2-}$ and AgI in THF. ESI-MS spectra were run in CH_2Cl_2. A: t = 0; B: t = 30 min; C: t = 1 hr; D: t = 2 hrs; E: t = 24 hrs. Peak assignments are given in Table 5-1.

The changes in speciation that occur as a reaction progresses can easily be observed with ESI-MS provided that no overlapping peaks are present. If two species are expected to occur at similar *m/z* values, attention to should be paid to the resulting isotope pattern. In this particular case, special attention should be paid to the formation of multiply charged species from the corresponding singly charged species. A monomer and dimer can occur at the same mass to charge ratio; even though the species is twice as heavy it carries twice the charge placing it at the same *m/z*. By looking closely at the isotope pattern of a given species it is possible to determine the charge that the species carries. For example, isotope patterns due to a species carrying a single charge are spaced one *m/z* unit apart while a species that carries two charges has a pattern separated by 0.5 of an *m/z* unit. This property means the transition of $[\mathbf{5.1}Ag_2I]^-$ into the product ion $[\{\mathbf{5.1}Ag_2I\}_2]^{2-}$ can be monitored without difficulty by examining the peak separation. The two species will carry the same *m/z* but careful examination of the isotope pattern at different time intervals shows the formation of the dimer at the expense of the monomer (Figure 5-3). The uneven peak intensities in the bottom spectrum are due to incomplete dimerisation and after 24 hours of stirring in solution all peak heights are nearly equivalent.

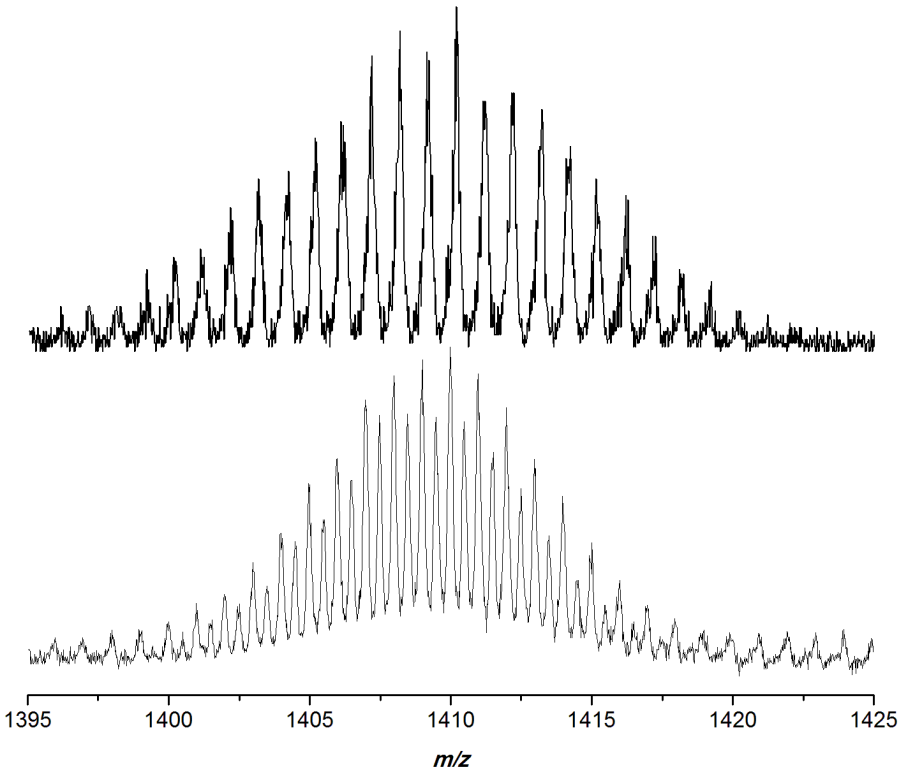

Figure 5-3. Expansion of the peak due to [**5.1**Ag_2I]$^-$ (top, t = 1 hr) and [{**5.1**Ag_2I}$_2$]$^{2-}$ (bottom, t = 2 hrs).

Selected MS/MS fragmentation studies were performed on several species of particular interest. The ion [{**5.1**Ag_2I}$_2$]$^{2-}$ was mass selected and accelerated into the collision cell where contact with neutral, inert argon molecules results in fragmentation of the ion. As can be seen from Figure 5-4, the fragmentation of [{**5.1**Ag_2I}$_2$]$^{2-}$was not symmetrical. Fragmentation occurred to give two ruthenium-containing clusters, each carrying a single charge, and one of these clusters was of greater *m/z* than the other. As the ions were increasingly accelerated, sequential loss of CO molecules from the monomers was observed. The two main fragments were not equal in intensity due to further fragmentation of [**5.1**Ag_3I_2]$^-$ through loss of $(AgI)_2$ to give [**5.1**Ag]$^-$. The cleavage of the dimer is the primary event at low energies as it can be seen that loss of smaller fragments from the [{**5.1**Ag_2I}$_2$]$^{2-}$ core is minimal.

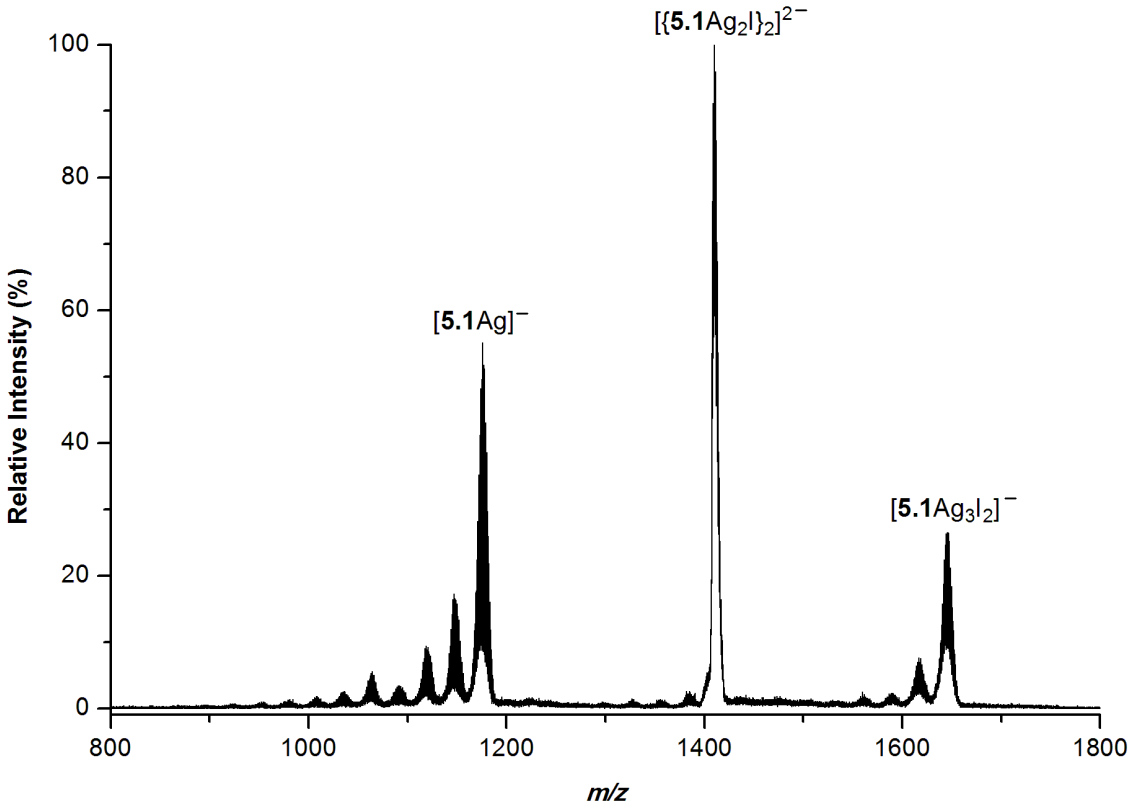

Figure 5-4. Negative-ion ESI-MS/MS of $[\{\mathbf{5.1}Ag_2I\}_2]^{2-}$. Collision voltage was increased from 0 to 80 V and the resulting spectra were summed.

The comparison of MS/MS spectra with spectra collected from solution can provide information about what was actually present in solution and what species were generated through fragmentation during the ionization process (Section 3.3.2). The solution phase spectra of the reaction mixture show that $[\mathbf{5.1}Ag]^-$ was present in the initial moments and then in relatively negligible amounts as the reaction proceeded. However, $[\mathbf{5.1}Ag_3I_2]^-$ was not present at the outset and was present in larger quantities only in the later stages of the reaction. The two species were not present in comparable quantities at the same time at any stage, as would be expected if they were fragmentation products of $[\{\mathbf{5.1}Ag_2I\}_2]^{2-}$.

Table 5-1. Peak assignments for spectra collected during the formation reaction of $[\{Ru_6C(CO)_{16}Ag_2I\}_2]^{2-}$ and select MS/MS data.

Species:	Mass to charge ratio: (*m/z*)	Peak Assignment:	MS/MS Fragments (*m/z*):
A	360.8		
B	533.6	$[\mathbf{5.1}]^{2-}$	
D	605.3	$[\mathbf{5.1}AgCl]^{2-}$	
E	650.7	$[\mathbf{5.1}AgI]^{2-}$	126.9 (I^-), 1175.3
F	1068.6	$[\mathbf{5.1}\ H]^-$	
G	1175.4	$[\mathbf{5.1}Ag]^-$	
H	1292.6	$[\{\mathbf{5.1}Ag\}_2AgI]^{2-}$	
I	1410.6	$[\{\mathbf{5.1}Ag_2I\}_2]^{2-}$	1175.3, 1646.8
J	1605.5	$[\mathbf{5.1}\ PPN]^-$	
K	1646.8	$[\mathbf{5.1}Ag_3I_2]^-$	
L	1840.6	$[\mathbf{5.1}AgI\ PPN]^-$	126.9 (I^-), 1175.3

While MS/MS data can provide valuable information on the identity and characteristics of any given species, the two–dimensional summation of the resulting spectra means that data on the energies at which fragmentation occurred is lost (Section 1.5.2). The EDESI-MS/MS contour map of $[\mathbf{5.1}AgI]^{2-}$ is shown in Figure 5-5. Several processes were evident and occurred at slightly different fragmentation energies. The first series (Figure 5-5, A), which began at the lowest collision voltage, was due to $[Ru_6C(CO)_nAgI]^{2-}$ where n = 7 - 16. All other peaks were assigned to similar series with the exception that fragmentation of the parent ion $[\mathbf{5.1}AgI]^{2-}$ to give a singly–charged cluster occurred before loss of CO ligands. The generation of free I^- from $[Ru_6C(CO)_{16}AgI]^{2-}$ can be seen at the same relatively low collision voltage as the beginning of the $[Ru_6C(CO)_nAg]^-$ (n = 0 - 16) series (Figure 5-5, D). Slightly overlapped with this series was a separate series, that started at higher collision voltages, arising from the loss of AgI from

$[Ru_6C(CO)_{16}AgI]^-$ to give $[Ru_6C(CO)_n]^{2-}$ (n = 9 - 16) (Figure 5-5, B). The two series overlap due to the similarity in mass of Ag (106.9 Da) and 4 × CO (112.0 Da) and the width of the isotope patterns in the resulting peaks. $[Ru_6C(CO)_nAgI]^-$ (n = 0 - 8) and $[Ru_6C(CO)_n]^-$ (n = 0 - 10) are generated from electron autodetachment, a process known for gas phase dianions,[156,157] from $[Ru_6C(CO)_8AgI]^{2-}$ and $[Ru_6C(CO)_{10}]^{2-}$ respectively (Figure 5-5, F and E).

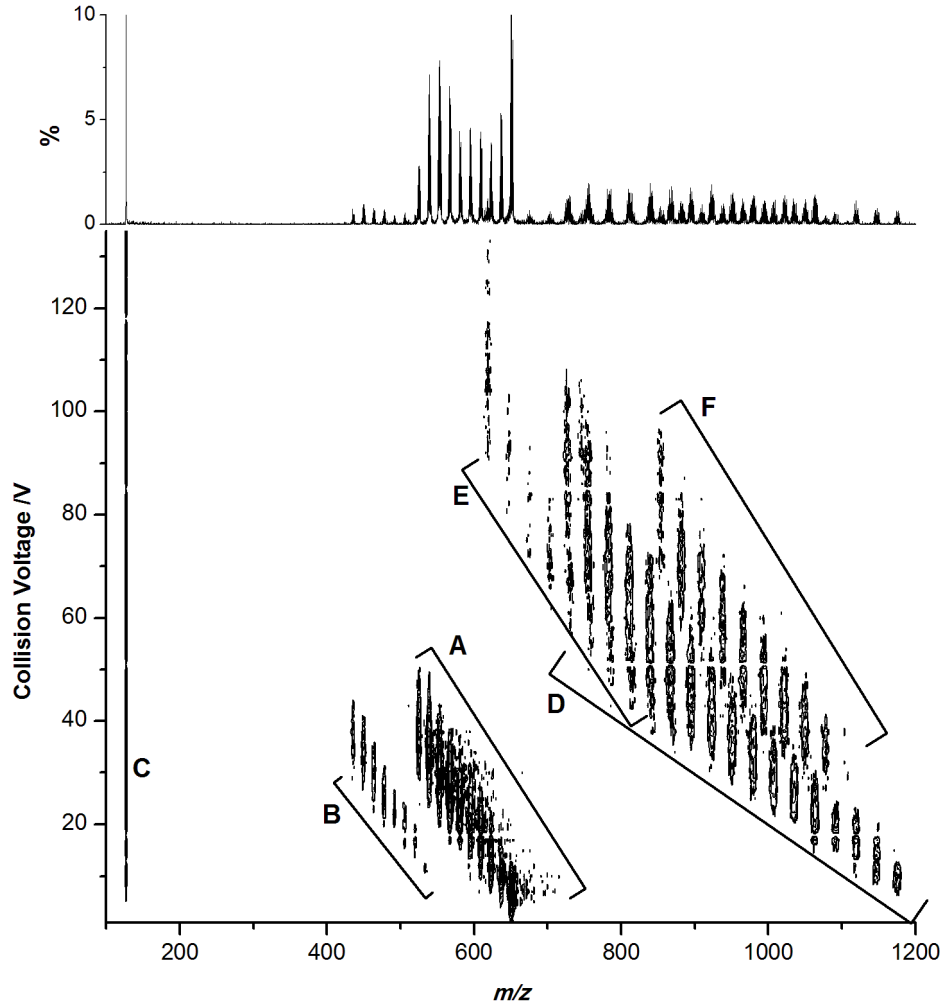

Figure 5-5. Summation plot and EDESI-MS/MS of $[\mathbf{5.1}AgI]^{2-}$. A = $[Ru_6C(CO)_nAgI]^{2-}$ (n = 7 - 16); B = $[Ru_6C(CO)_n]^{2-}$ (n = 9 - 16); C = I^-; D = $[Ru_6C(CO)_nAg]^-$ (n = 0 - 16); E = $[Ru_6C(CO)_n]^-$ (n = 0 – 10); F = $[Ru_6C(CO)_nAgI]^-$ (n = 0 - 8).

Similar results to those obtained above were seen when $[\mathbf{5.1}]^{2-}$ and AgCl were dissolved in THF (Appendix Figure 19). The relative intensities of some species varied between the two solutions

but the base peak, [**5.1**AgCl]$^{2-}$, and the ion, [{**5.1**Ag_2Cl}$_2$]$^{2-}$, were present in the same relative amounts as compared to the AgI system.

The relative abundance of [**5.1**AgX]$^{2-}$ (X = I or Cl) appears to make perfect sense given the ratio of starting material to halide present in solution (approximately 5:1 in X:[**5.1**]$^{2-}$). Even though the spectrum showed the [{**5.1**Ag_2I}$_2$]$^{2-}$ ion was present in relatively small amounts, the Dyson group established that the reaction was complete within four hours with an 80% yield. It seems reasonable to propose that solution phase equilibria may be responsible for this apparent disagreement in results (Scheme 5-1). This hypothesis was investigated through addition of a second halide source.

$$[\mathbf{5.1}Ag_3X_2]^- + [\mathbf{5.1}Ag]^- \rightleftharpoons 2[\mathbf{5.1}Ag_2X]^{1-} \rightleftharpoons [\{\mathbf{5.1}Ag_2X\}_2]^{2-}$$

Scheme 5-1. Possible solution-phase equilibrium leading to the high yield of [{**5.1**Ag_2I}$_2$]$^{2-}$.

It was already known from solid state characterisation that the mixed halide [{**5.1**Ag_2}$_2$ClBr]$^{2-}$ species was obtainable. The degree to which halide exchange can occur within the system was examined by ESI-MS by adding NMe_4Br to a THF solution of $(PPN)_2$(**5.1**) and excess AgCl. The spectrum (Figure 5-6) changed dramatically from what was seen without the excess halide and all peaks were readily assigned. Most apparent was the absence of any dimeric species. The only species present were of the type [**5.1**Ag_nX_n]$^{2-}$ (n = 1 or 2; X = Cl or Br) and those that paired with a counterion to give [**5.1**Ag_nX_n NMe_4]$^-$ or [**5.1**Ag_nX_n PPN]$^-$. The excess bromide removed all halide bridges and supplied an equal amount of halide to silver atoms in each cluster. The ease with which bromide could be incorporated into the clusters was evidenced by the almost equal distribution of chloride and bromide species. Not only can the bromide ion break the

chloride bridge in any given cluster but redistribution of the halides occured readily to give the distribution seen in Figure 5-6.

If the reaction was not in equilibrium the excess halide would not be incorporated into the dimeric species to form the halide-saturated silver species seen in the resulting ESI spectrum.

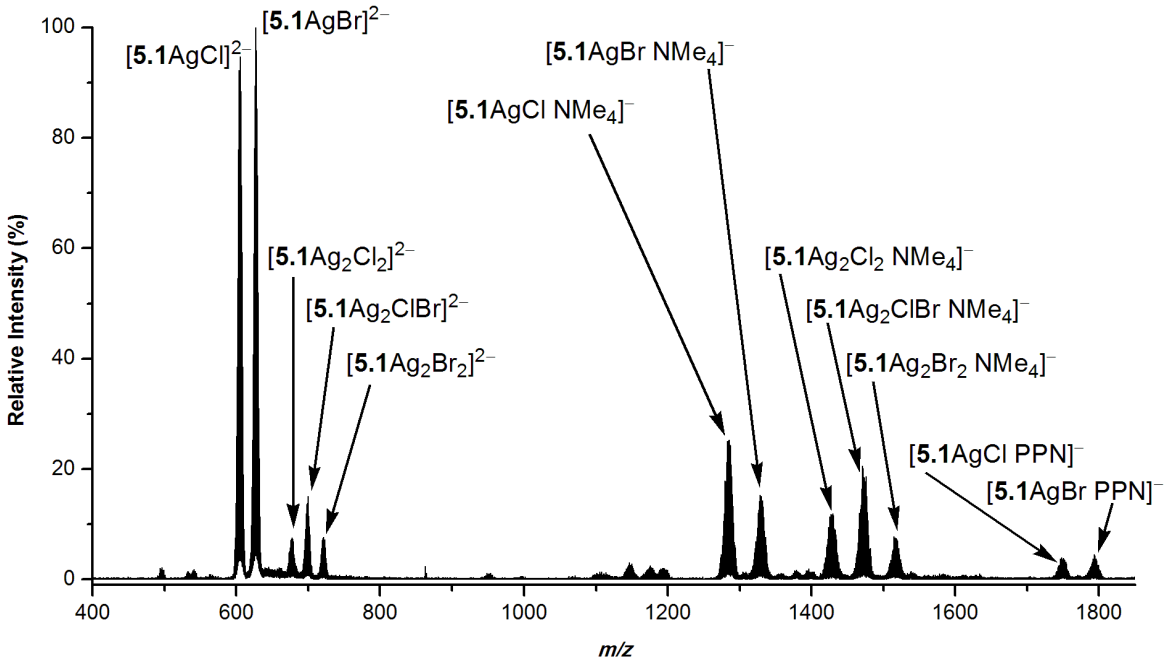

Figure 5-6. Negative-ion ESI-MS resulting from the addition of NMe_4Br to a solution of $[\mathbf{5.1}]^{2-}$ and AgCl in THF. The spectrum was acquired 2 hours after addition of the ammonium salt.

5.1.3 Conclusions

Monitoring reaction progress by ESI-MS established how product distributions change over time. Clearly evident are species whose detection would be complicated in NMR or UV-Vis due to structural similarities. ESI-MS provides a very clear picture of the entire reaction system. MS/MS investigations confirm that the spectra observed during monitoring of the reaction are

most likely due to solution phase speciation and not a result of fragmentation from the ionization process.

The ESI mass spectra collected for the addition of AgX to a solution of $[\mathbf{5.1}]^{2-}$ in THF (Equation 5-1) were initially more complex than expected from the high yield of a single product reported by the Dyson group. All peaks were due to some derivative of the $[\mathbf{5.1}Ag]^{-}$ core with various numbers of Ag^{+} and X^{-} units to give both monomeric and dimeric species. One might expect to see a spectrum dominated by a peak at 1410.6 *m/z* due to the product dimer. Instead, a series of other easily identified species were observed and the base peak was due to $[\mathbf{5.1}AgI]^{2-}$ at 650.7 *m/z*. It is therefore reasonable to conclude that there exists an equilibrium in solution (Scheme 5-1) and that selective crystallization of $[\{\mathbf{5.1}Ag_2I\}_2]^{2-}$ was responsible for the high yield. This conclusion was further supported by the ease of incorporation of a second halide into nearly all species in solution. The ESI-MS studies provide suggestions for future work: isolation of the previously unknown $[\mathbf{5.1}Ag_2X_2]^{2-}$ cluster via addition of X^{-} to $[\{\mathbf{5.1}Ag_2I\}_2]^{2-}$:

$$[\{\mathbf{5.1}Ag_2X\}_2]^{2-} + 2X^{-} \rightleftharpoons 2[\mathbf{5.1}Ag_2X_2]^{2-}$$

Equation 5-2

5.2 Ion pairing in a mixed anion salt

5.2.1 Introduction

It is known that the ESI-MS peak intensities for two species in a single spectrum are not necessarily a reliable measure of their relative concentrations. One molecule may not ionize as efficiently as another even within one spectrum and the trends observed are not always readily predictable. As mentioned in Chapter 1, many different factors are involved that ultimately determine the surface activity of an ion.

During the ESI process, the droplets which emerge from the Taylor cone (Section 1.2) will continue to become smaller in size as desolvation continues. Once a critical size is reached there will either be ion evaporation or Coulomb explosion to generate gas phase ions. The ions that are most efficiently transferred to the gas phase are those that are found on the surface of the droplet, rather than those at the center. The propensity of a molecule to exist near the surface of a droplet will therefore affect the likelihood that it will be drawn into the gas phase (Figure 1-2), and this propensity is dependent upon several different factors.[17,18]

One such factor is the tendency of an ion to pair with a counterion. If an ion is strongly attracted to its counterion and exists as a paired, neutral species it will reside in the center of a droplet undergoing desolvation and will eventually be removed by the vacuum. Solvation effects also play an important role in the location of a species in a droplet. The more readily an ion is solvated the more likely it is to be found in the interior of the droplet where the largest amount of solvent is available. This phenomenon has been well studied and many have demonstrated the efficiency with which hydrophobic species are transferred to the gas phase in water and

water-miscible solvents. Tang and Kebarle have demonstrated the ESI-MS over-representation of alkylammonium versus alkali metal salts from equimolar solutions in methanol.[25] Milman and Alfassi have shown the efficiency of transfer to the gas phase from a solution in water increases with increasing hydrophobicity of the ion.[158]

Most studies that address this issue of ion pairing use ionic liquids as aggregate species (of the type $[cation_1\text{-}anion\text{-}cation_2]^+$ or $[anion_1\text{-}cation\text{-}anion_2]^-$) are readily observed.[159,160] CID studies have been reported on the strengths of association in mixed ion aggregates for various different cations and anions.[161]

An alternative way to look at the effects of ion pairing is to employ a multiply charged ion and two different counterions. The synthesis and characterization of a dicationic species having two different counterions was completed by the Dyson group. The imidazolium-sulfonium cation ($[\mathbf{5.2}]^{2+}$) with iodide (I^-) and bistriflimide (Tf_2N^-) counterions (Figure 5-7) was examined in several different solvents. The two counterions are quite different from each other in both size and lipophilicity.

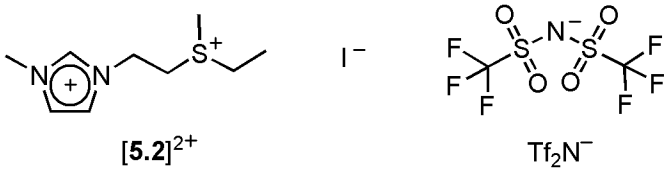

Figure 5-7. Imidazolium sulfonium cation ($[\mathbf{5.2}]^{2+}$) with iodide (I^-) and bistriflimde (Tf_2N^-) counterions.

The premise was to investigate which ion pair, $[\mathbf{5.2}Tf_2N]^+$ or $[\mathbf{5.2}I]^+$, would be most abundant in the gas phase in various solvents. In computations performed by the Dyson group it was found that the strength of association with $[\mathbf{5.2}]^{2+}$ followed the trend $I^- > Tf_2N^- > PF_6^-$; data supported

by recent studies with similar ions by Tsuzuki and co workers.[162,163] Our investigation aimed to assess the degree to which the strength of the [**5.2**I]$^+$ ion pair would lead to preferential dissociation of Tf_2N^- and disproportionally high intensities of [**5.2**I]$^+$ in the gas phase by simple ESI analyses of [**5.2**Tf_2NI] in various solvents.

5.2.2 Results and Discussion

The solvents chosen for this analysis were water, acetonitrile, methanol and acetone. Other solvents were tried including hexanes, chlorobenzene, chloroform, dichloromethane and ethanol but the compound was not soluble. In all cases the signal for the [**5.2**Tf_2N]$^+$ ion was more intense than that for [**5.2**I]$^+$ (Figure 5-8). When [**5.2**ITf_2N] was dissolved in acetonitrile the signals were close to equal with [**5.2**I]$^+$ having 95% the intensity of [**5.2**Tf_2N]$^+$. The response of [**5.2**I^-] with respect to [**5.2**Tf_2N^-] in acetone, methanol and water was approximately 50%, 9% and less than 1% respectively. These results are in direct opposition to what was expected with respect to the calculations described above and led us to consider the very different hydrophobicities of the two anions. As described by Milman and Alfassi, increasing the hydrophobic nature of an ion will increase its surface activity. Therefore, the role of solvent polarity should be considered because as the hydrophobicity of the solvent increases, the relative surface activity of the hydrophobic ion will decrease. The two solvents with the most different responses were water and acetonitrile. The polarity of these two solvents fits the expected trend with the more polar solvent giving the highest relative response for [**5.2**Tf_2N]$^+$. As the polarity of the solvent decreases it would be expected that the difference in response would also decrease. This was indeed observed with the relative responses for [**5.2**I]$^+$ and [**5.2**Tf_2N]$^+$ in acetonitrile at just 5% different from one another. If the dielectric constants (ε, a relative measure of the molecule's dipole moment) are taken into

consideration (acetonitrile 36.64, acetone 21.01, methanol 33.00 and water 80.10)[164] it becomes apparent that the polarity of the solvent alone does not determine the intensity of the response. If this were the case, the response for [**5.2**Tf_2N]$^+$ relative to [**5.2**I]$^+$ should be the greatest in acetone.

Another factor to consider is the ability of the solvent to effectively solvate the ions, which also depends on its ability to form hydrogen bonds. The solvation of an ion by water involves the formation of a cage-like structure connected by these hydrogen bonds. The large hydrophobic anion Tf_2N^- would be less effectively solvated by water and so its "free" concentration would be less favourable. The I^- would be more effectively solvated in water leading to preferential dissociation of I^-. This will draw the iodide to the interior of the droplet where it can be effectively solvated. This effect would get progressively less pronounced as the ability of the solvent to form regular structures around the anion decreases. That is to say, as the hydrogen bonding ability of the solvent decreases the amount of free (unpaired) I^- will also decrease and the relative concentrations of [**5.2**Tf_2N]$^+$ and [**5.2**I]$^+$ would become more comparable. The hydrogen bonding nature of the solvent would have little effect on the solvation of the Tf_2N^- due to its hydrophobic nature. By this measure the results appear to follow more of a trend.

Not only is water the most polar, so the surface activity of [**5.2**Tf_2N]$^+$ would be the highest, but it is also the best at hydrogen bonding, so the solvation of I^- would be most efficient. As a result, the relative concentrations of [**5.2**Tf_2N]$^+$ and [**5.2**I]$^+$ are exaggerated. Even though acetonitrile is *not* the least polar it *is* the least effective at forming hydrogen bonds and this factor outweighs the moderate polarity.

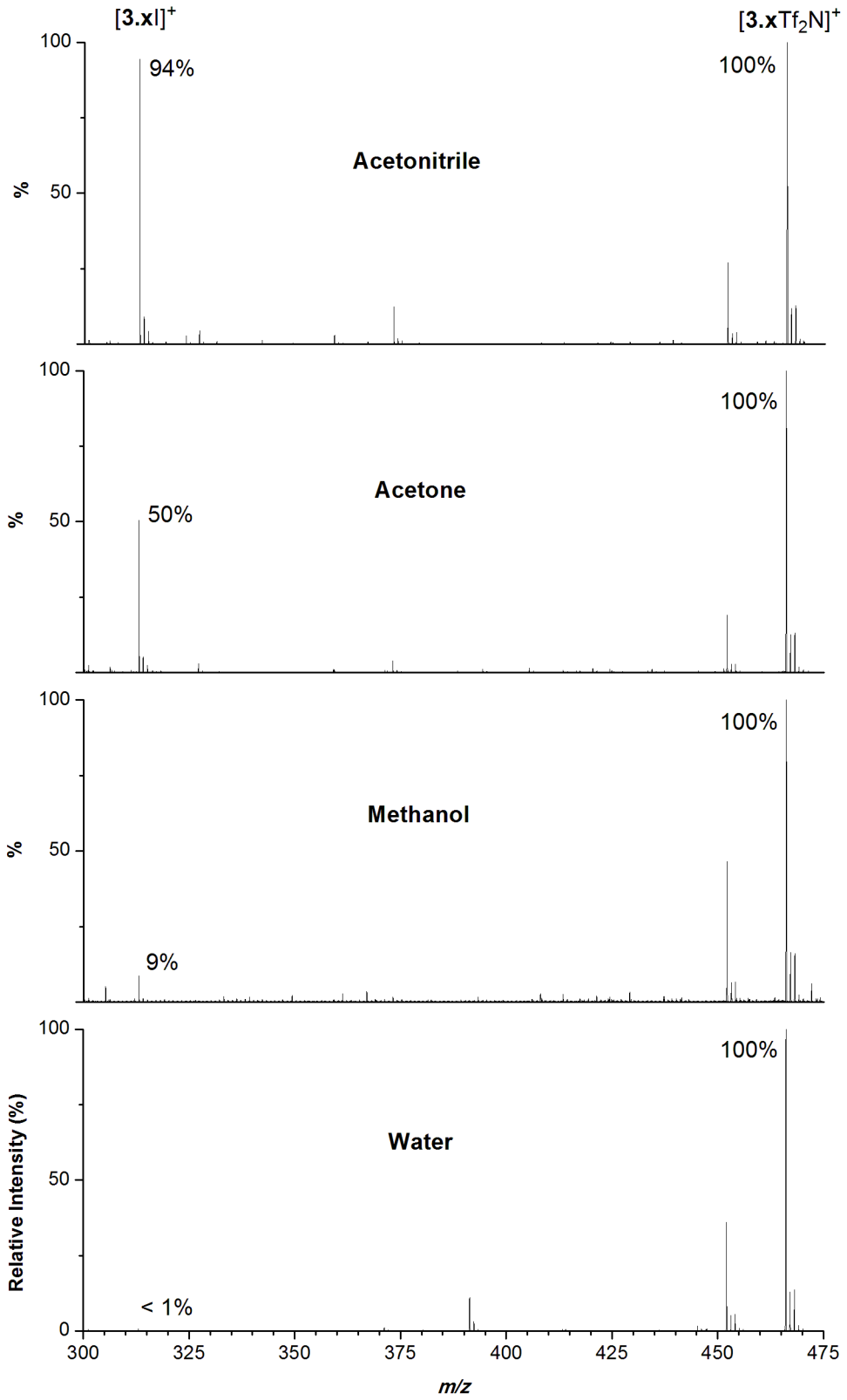

Figure 5-8. ESI mass spectra obtained from dissolving [**5.2**$IN(SO_2CF_3)_2$] in various solvents. [**5.2**(I)]$^+$ = 313.1 *m/z* and [**5.2**$\{N(SO_2CF_3)_2\}$]$^+$ = 466.2 *m/z*.

5.2.3 Conclusions

It is accepted that the surface activity of an ion determines the intensity of its ESI-MS response. The factors that contribute to the surface activity of an ion are sometimes not predictable, and so determining with certainty the relative responses of two ions can be complicated. In an effort to assess these factors, a dicationic species with two very different counterions was used.

The effect of polarity of the solvent was not as prominent as may have been expected from comparison of the lipophilicity of the ions. The ability of the solvent to engage in hydrogen-bonding outweighed the effects of absolute polarity. The relative intensities of [**5.2**I]$^+$ and [**5.2**Tf_2N]$^+$ observed were a result of the more favourable solvation of the iodide counterion (by solvents capable of hydrogen bonding) which promoted preferential dissociation of iodide from [**5.2**ITf_2N].

These types of relationships are being studied further in our group through comparison of a series of solutions containing two different salts. As a means of studying the effects of ion pairing, both salts consist of the same cation but different anions. Several different solvents were used in order to examine the effects of polarity.

5.3 Ruthenium-carbonyl compounds for cell growth inhibition

5.3.1 Introduction

Though a toxic gas, carbon monoxide (CO) has growing application in pharmaceutical chemistry.[165] It has been shown to affect the cardiovascular system in terms of reduced graft rejection, regulation of blood pressure in stressful conditions, and as an anti-inflammatory.[166] Metal carbonyls containing organic functionality have been shown to exhibit some anti-cancer activity. Derivatives of acetylenehexacarbonyldicobalt were shown to slow the growth of cancer cells.[167,168] Due to their potential wide application in medicine, the term CORMs (CO-releasing molecules) was coined in 2002 in a report on the activity of molecules such as $Fe(CO)_5$, $Mn_2(CO)_{10}$, and $\{RuCl_2(CO)_3\}_2$ as CO-delivery agents.[169]

The ruthenium trimers shown in Figure 5-9 contain phosphine ligands modified with a glucose moiety to enhance their solubility in biological systems,[170] and were expected to act as CORMs. In tests with myoglobin acting as a CO receptor, $Ru_3(CO)_{10}(PC_9O_6H_{13})_2$ (**5.3**) was found to release six out of a possible ten equivalents of CO where and $Ru_3(CO)_9(PC_9O_6H_{13})_3$ (**5.4**) released five of the possible nine equivalents.[171]

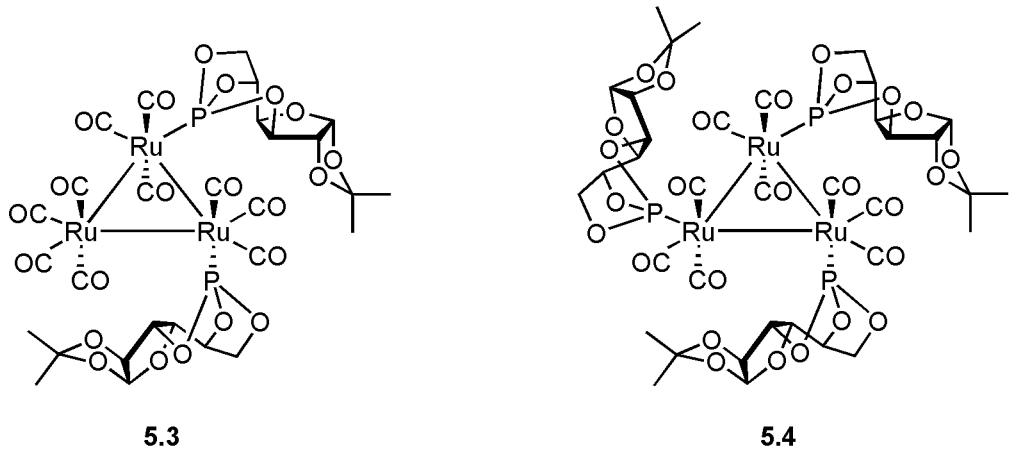

5.3 **5.4**

Figure 5-9. Structures of $Ru_3(CO)_{10}(PC_9O_6H_{13})_2$ (**5.3**) and $Ru_3(CO)_9(PC_9O_6H_{13})_3$ (**5.4**).

We were asked to conduct MS/MS studies on these two molecules to determine the facility with which they released CO. In particular, evidence that phosphine ligands of this sort facilitate the loss of CO was sought. Carefully conducted ESI-MS/MS experiments can provide information on the relative bond strengths within a molecule, and in particular on the relative strengths of metal-ligand bonds within a complex (Section 1.5.1).

5.3.2 Results and Discussion

On their own, the molecules are not ESI active. Dissolving either **5.3** or **5.4** in methanol and introducing them into the instrument does not give any signal. Addition of sodium iodide provides a route for the molecule to become charged through association of a sodium, presumably with an oxygen atom in one of the phosphate ligands, to give $[M + Na]^+$ peaks. As discussed in Section 1.5.2 , EDESI-MS/MS is an information-rich way to present ESI-MS/MS data. EDESI-MS/MS spectra are shown for $[\mathbf{5.3} + Na]^+$ (1103.8 *m/z*, Figure 5-10) and $[\mathbf{5.4} + Na]^+$ (1323.9 *m/z*, Figure 5-11).

Sequential loss of CO molecules with increasing collision energy occurred for each of the two molecules. For [**5.3** + Na]$^+$ there was loss of one CO ligand even at 1 V. The energy required to remove successive ligands increased in a more or less step-wise fashion with two exceptions (Table 5-2). The cross-peak for **5.3** with eight CO ligands (loss of two) is smaller than that for nine CO ligands, meaning that this fragment does not require as much energy to lose the next equivalent of CO. The opposite is true for **5.3** with five CO ligands (loss of five) as the cross-peak for this species is larger than its neighbours, meaning these CO ligands are more tightly held to the ruthenium center. The gradual increase in the energy required for further fragmentation continues until two CO ligands remained. Removal of the next CO ligand became more difficult as successive ligands were removed, as evidenced by the increase in the size of the cross-peak for each successive fragment. This indicates that as each CO ligand was removed from the complex the remaining CO ligands were held more tightly.

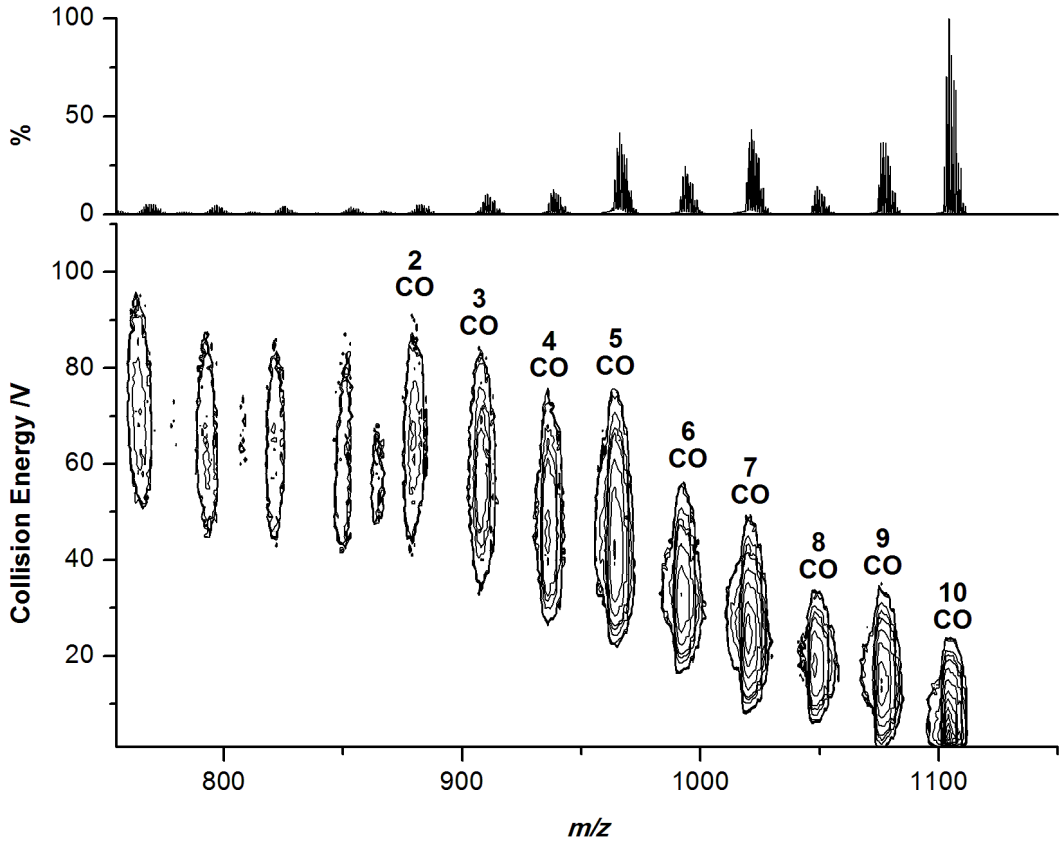

Figure 5-10. EDESI-MS/MS for [**5.3** + Na]$^+$ (1103.8 *m/z*) in methanol. Cone voltage = 20 V. (Full spectra are shown in Appendix Figure 20)

For [**5.4** + Na]$^+$ there was loss of one and even two CO ligands even at 1 V. The energy required to remove successive ligands increased in a more or less step-wise fashion with two exceptions (Table 5-2). The cross-peak for **5.4** with seven CO ligands (loss of two) is smaller than that for nine CO ligands, meaning that this fragment does not require as much energy to lose the next equivalent of CO. The opposite is true for **5.4** with four CO ligands (loss of five) as the cross peak for this species is larger than its neighbours meaning these CO ligands are more tightly held to the ruthenium center. The gradual increase in the energy required for further fragmentation continues until two CO ligands remained. The same trend in increasing size of cross-peaks was seen for **5.4** as for **5.3**.

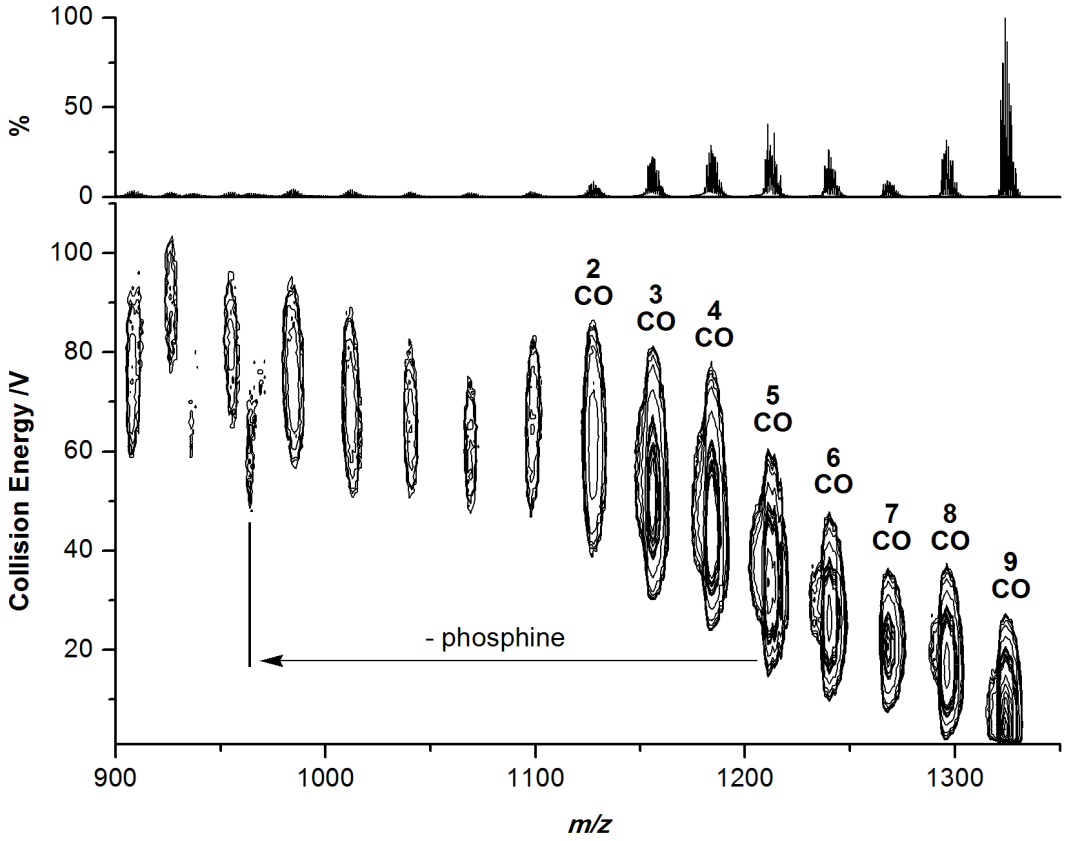

Figure 5-11. EDESI-MS/MS for [**5.4** + Na]$^+$ (1323.9 *m/z*) in methanol. Cone voltage = 20 V. (Full spectra are shown in Appendix Figure 21)

The energy required for loss of CO moieties is comparable between the two molecules. The first CO ligand is lost from both **5.3** and **5.4** occurs between 1 to 23 and 1 to 27 V respectively. The anomalies described above for each of the two molecules were observed for the same number of CO ligands lost for each molecule even though the absolute number of CO ligands was different. The peak for both **5.3** and **5.4** with two CO ligands was prevalent over approximately the same energy range, 42 – 88 and 40 – 85 V respectively.

Table 5-2. Energy related to the dissociation of carbonyl ligands from **5.3** and **5.4**.

5.3 Number of CO ligands	Energy Range (V)	**5.4** Number of CO ligands	Energy Range (V)
10	1 – 23		
9	1 – 35	9	1 – 27
8	6 – 34	8	2 – 37
7	8 – 49	7	7 – 36
6	16 – 56	6	9 – 47
5	22 – 76	5	14 – 60
4	26 – 75	4	25 – 77
3	33 – 84	3	31 – 80
2	42 – 88	2	40 – 85

One notable difference between the two MS/MS spectra was the loss of one phosphine ligand from **5.4** once the molecule reached five CO ligands (loss of four CO ligands). Loss of phosphine from **5.3** was not observed. However, only a fraction of the molecules lose the phosphine ligand as the series of loss of CO from the molecule containing all three phosphine ligands continues down to two carbonyls.

Although the sequential loss of carbonyl ligands is perhaps not surprising, loss of carbonyl over phosphine ligands was unexpected. In ESI-MS/MS of other metal-carbonyl clusters containing a non-chelating phosphine ligand, such as $Ru_6C(CO)_{16}(PPh_3)$, increasing the collision energy results in the dissociation of the phosphine *first* followed by sequential loss of CO ligands.[172] It is suspected that loss of carbonyl ligands, generating increasingly more coordinative unsaturation about each ruthenium, provided a site for coordination of the phosphine oxygen atoms on neighbouring ruthenium atoms. Therefore, the phosphine ligands were held more tightly due to bridging between multiple metal centers.

5.3.3 Conclusions

Both molecules behaved similarly with the exception that **5.4** lost one equivalent of phosphine from **5.4** with five CO ligands. The loss of one extra equivalent of CO from **5.3** in tests by the Dyson group appears to be simply a function of possessing one more CO ligand from the start. The number around each ruthenium center at the end of the ESI-MS/MS experiment is the same in either case. The phosphine ligands are more tenaciously bound as compared to monodentate phosphine ligands due to the ability of the sugar ligands to fold back onto the vacant coordination sites of neighbouring ruthenium atoms as CO ligands are successively removed.

5.4 Experimental

Solvents were HPLC grade and purified on an MBraun solvent purification system (SPS). Gases were obtained from Airgas (Calgary, Canada). $[C_9H_{18}N_2S][I][N(SO_2CF_3)_2]$ was obtained from the Dyson group, Lausanne, Switzerland. All mass spectra were obtained on a Micromass Q-ToF *micro* hybrid quadrupole/time-of-flight mass spectrometer in positive ion mode using pneumatically-assisted electrospray ionization.

$[PPN]_2[\{Ru_6C(CO)_{16}Ag_2X\}_2]$ (X = Cl or I). All manipulations were performed under an inert atmosphere of dry nitrogen using standard Schlenk techniques. The silver halides were prepared from $AgNO_3$ by reaction with the potassium or sodium halides. $[Ru_6C(CO)_{16}][PPN]_2$ was made from previously established methods.[173] For $[\{Ru_6C(CO)_{16}Ag_2I\}_2][PPN]_2$: AgI (27.4 mg, 1.17×10^{-4} mol) was added to a solution of $[Ru_6C(CO)_{16}][PPN]_2$ (50.1 mg, 2.33×10^{-5} mol) in THF (5 ml).[152] Capillary voltage was set at 2900 V, source and desolvation gas temperatures were at 40 and 100 °C, respectively. Cone voltage was set at 5 V. Samples were diluted in

dichloromethane and infused via syringe pump at 5–10 μL min^{-1}. All spectra were collected in negative ion mode.

$[C_9H_{18}N_2S][IN(SO_2CF_3)_2]$. The wet, yellow-brown solid was washed with chlorobenzene and dried under a stream of $N_{2(g)}$ to give a white solid. The white solid was then dissolved in the appropriate solvent (2 mg in 10 ml) for ESI-MS analysis. Source and desolvation gas temperatures were at 100 and 120 °C respectively for methanol, acetonitrile, and acetone and 120 and 150 °C for water. Capillary voltage was set at 2700 V. Cone voltage was set at 10 V. Samples were infused via syringe pump at 10 μL min^{-1}. All spectra were collected in positive mode.

$Ru_3(CO)_{10}(PC_9O_6H_{13})_2$ and $Ru_3(CO)_9(PC_9O_6H_{13})_3$ were obtained from the Dyson group, Lausanne, Switzerland. Capillary voltage was set at 2700 V, source and desolvation gas temperatures were at 80 and 100 °C, respectively. Cone voltage was set at 20 V. Samples were diluted in methanol (2 mg in 10 ml) and infused via syringe pump at 10 μL min^{-1}. All spectra were collected in positive ion mode.

Chapter 6. Conclusions and Future Work

The work presented here describes the development of the methodology required to enhance the usefulness of ESI-MS as a tool in the study of catalytic systems. As a soft ionization technique that operates on dilute solutions, ESI is well suited to this task. Of particular interest were charged ligands that would provide a convenient ESI handle. The incorporation of a charged ligand into the coordination sphere of the catalyst itself would render the entire complex ESI active, so long as the charged ligand remained coordinated to the metal.

The first obstacle that had to be overcome was the synthesis of suitable ligands for this application. The initial target was a bipyridine derivative, modeled on the highly basic Proton Sponge® molecule (Figure 2-1). The parent molecule is extremely selective to association of a proton over any other small ions due to the steric environment surrounding the coordination site. It was thought that a properly functionalized 2,2'-bipyridine derivative (Scheme 2-1) had the potential to show the same selectivity, thereby inferring a charge on the metal once the ligand was bound. Arriving at the 3,3'-diamino-2,2'-bipyridine through literature procedures was straight forward. While the methylation of the diamine was assumed to be a simple undertaking, it proved to be non-trivial and mostly led to inseparable product mixtures resulting from addition of one to five methyl groups. Due to chronic difficulties with the purification of this ligand, the project was abandoned.

Once it was established that the bipyridine work was not fruitful, reconsideration of our objectives was necessary. In order to move forward with the use of ESI-MS as a tool in catalyst investigation its reliability had to be assessed. Rather than relying on the ligand becoming

charged in solution as in the bipyridine approach, the next ligand was to include a permanently charged functionality. Traditionally chelating bisphosphine ligands were easily monosubstituted using an alkyl halide to generate a monodentate phosphine/phosphonium. The procedure was significantly shorter and less complicated than most procedures involving the functionalization of phosphine moieties in the presence of other functional groups. The labile phosphine ligands of Wilkinson's catalyst offered the possibility to incorporate a charged functionality into the coordination sphere of the metal simply by addition of a charged ligand of similar structure to a solution of the catalyst. In this way, the independent synthesis of a charged complex was avoided. Due to the established wealth of information about the hydrogenation of olefins by $RhClPPh_3$ (Wilkinson's catalyst), this process was chosen as a means to provide proof of principle for the methodology. Comparing the data available in the literature to the data obtained by ESI-MS investigations had the potential to validate the technique.

A series of these ligands were made with varying numbers of carbon atoms between the two phosphine centers. ESI-MS analysis of a solution of Wilkinson's catalyst and approximately 0.1 equivalents of charged phosphine/phosphonium ligand showed that incorporation of the charged ligand into the coordination sphere had indeed occurred. Optimization of the system involved variation of the charged ligand, ligand counterions, solvent composition and instrumental settings to arrive at standard operating conditions that best suited the system at hand. 1-diphenylphosphino-4-benzyldiphenylphosphonium-butane bromide ($[\mathbf{3.4}]^+ [BF_4]^-$, Figure 3-3) was found to be an appropriate ligand and was used for all further investigations involving this catalyst. All off cycle species were readily identified, as well as the active catalyst and the product of hydrogen addition to the catalyst. MS/MS was used to confirm the composition of

various species and CID was used to assess the gas phase reactivity of selected components. Even though no species containing both an olefin and hydride ligands were ever observed, all species observed were in agreement with literature reports. With the confidence that catalytically relevant species are observable using the methodology at hand, a less well understood system could be examined.

Wilkinson's catalyst is also used in the dehydrocoupling of silanes to form di- and tri-silanes and the mechanism involved in this transformation has not been elucidated. Interest in this system was peaked through discussions with the Rosenberg group who are interested in this particular mechanistic determination. It was thought that data obtained through ESI-MS analysis may lend insight into NMR results previously collected in the Rosenberg group. Using the same method of doping a solution of the catalyst with a small amount of [**3.4**]$^{+}$ [BF_4]$^{-}$ followed by addition of one equivalent of silane, observation of key species already implicated by NMR data was achieved. Not only were these species readily identified but changes in their intensities were monitored over time (Figure 4-16) and were examined in relation to one another. The new data presented potential relationships between the different species over time and allowed the construction of a plausible reaction scheme (Figure 4-18). Although there is still some ambiguity as to the role of a silylene in the mechanism the data presented here provide a time dimension that was not previously available.

The QToF instrument used in the McIndoe group is capable of MS/MS and CID experiments, techniques that can lend detailed information on a species of interest. Within a long-standing collaboration with the Dyson group, MS/MS experiments were used to characterize ruthenium

clusters (Equation 5-1) and to assess the activity of two CORMs (Figure 5-9). Further, interest in the varying surface activity of ions in ESI instigated examination of a dication possessing two different counterions (Figure 5-7). Analysis of the relative intensities of the two possible ion pairs determined that the solvation of the iodide counterion was a better predictor of the activity of each ion pair over the polarity of the solvent.

Future work in the areas discussed in this thesis will likely focus on the dehydrocoupling of silanes by Wilkinson's catalyst. Synthesis of various charged silane molecules will allow for direct observation of the transformations involving silane fragments. Examining the reaction from the perspective of the substrate will provide complementary information on the intermediates involved in the coupling steps of the reaction which were not observable in the methodology used here. Also, it is apparent that the role of water in this mechanism needs to be more fully investigated. The intentional addition of varying amounts of water to the reaction should give insight into the consequence of its presence. Even though great care was taken here to exclude moisture from the system it is clear that efforts to exclude unwanted moisture must be bolstered in order to obtain reliable data given the sensitivity of the species involved.

At the conclusion of this project a general methodology for the investigation of catalytic processes has been established. The strength of the technique lies in the fast and continuous nature of data collection, from which information on a multitude of individual species can be extracted. Future researchers in the McIndoe group have a reliable starting point to develop procedures that best fit the particular systems that will be investigated.

References

(1) Dempster, A. J. *Phil. Mag.* **1916**, *31*, 438-443.

(2) Bleakney, W. *Phys. Rev.* **1929**, *34*, 157-160.

(3) Tate, J. T.; Smith, D. H. *Phys. Rev.* **1934**, *46*, 773-776.

(4) Munson, M. S. B.; Field, F. H. *J. Amer. Chem. Soc.* **1966**, *88*, 2621-2630.

(5) Harrison, A. G. *Chemical Ionisation Mass Spectrometry*; CRC Press: Boca Raton, 1992.

(6) Hillenkamp, F.; Karas, M. *Int. J. Mass. Spectrom.* **2000**, *200*, 71-77.

(7) Zenobi, R.; Knochenmuss, R. *Mass Spectrom. Rev.* **1998**, 337-366.

(8) Tanaka, K.; Waki, H.; Ido, Y.; Akita, S.; Yoshida, Y.; Yoshida, T. *Rapid Commun. Mass Spectrom.* **1988**, *2*, 151-153.

(9) Dole, M.; Mack, L. L.; Hines, R. L.; Mobley, R. C.; Ferguson, L. D.; Alice, M. B. *J. Chem. Phys.* **1968**, *49*, 2240-2249.

(10) Fenn, J. B.; Yamashita, M. *J. Phys. Chem.* **1984**, *88*, 4451-4459.

(11) Cole, R. B. *J. Mass. Spectrom.* **2000**, *35*, 763-772.

(12) Fenn, J. B.; Mann, M.; Meng, C. K.; Wong, S. F.; Whitehouse, C. M. *Mass Spectrom. Rev.* **1990**, *8*, 37-70.

(13) Smith, R. D.; Loo, J. A.; Ogorzalek Loo, R. R.; Busman, M.; Udseth, H. R. *Mass Spectrom. Rev.* **1991**, *10*, 359-452.

(14) Blades, A. T.; Ikonomou, M. G.; Kebarle, P. *Anal. Chem.* **1991**, *63*, 2109-2114.

(15) Taylor, G. I. *Proc. R. Soc. London. A* **1964**, *A280*, 383-397.

(16) Taflin, D. C.; Ward, T. L.; Davis, E. J. *Langmuir* **1989**, *5*, 379-384.

(17) Cech, N. B.; Enke, C. G. *Mass Spectrom. Rev.* **2001**, *20*, 362-387.

(18) Kebarle, P.; Verkerk, U. H. *Mass Spectrom. Rev.* **2009**, *28*, 898-917.

(19) Schmelzeisen-Redeker, G.; Butfering, L.; Rollgen, F. W. *Int. J. Mass. Spectrom. Ion Processes* **1989**, *90*, 139-150.

(20) Thomson, B. A.; Iribarne, J. V. *J. Chem. Phys.* **1979**, *71*, 4451-4463.

(21) Iribarne, J. V.; Thomson, B. A. *J. Chem. Phys.* **1976**, *64*, 2287-2294.

(22) McQuinn, K.; Hof, F.; McIndoe, J. S. *Chem. Commun.* **2007**, 4099-4101.

(23) Kebarle, P. *J. Mass. Spectrom.* **2000**, *35*, 804-817.

(24) Henderson, W.; McIndoe, J. S. *Mass Spectrometry of Inorganic and Organometallic Compunds*; John Wiley & Sons Ltd: West Sussex, 2005.

(25) Kebarle, P.; Tang, L. *Anal. Chem.* **1993**, *65*, 972A-986A.

(26) Chernushevich, I. V.; Loboda, A. V.; Thomson, B. A. *J. Mass. Spectrom.* **2001**, *36*, 849-865.

(27) Manisali, I.; Chen, D. D. Y.; Schneider, B. B. *Trends Anal. Chem.* **2006**, *25*, 243-256.

(28) Narancic, S.; Bach, A.; Chen, P. *J. Phys. Chem. A.* **2007**, *111*, 7006-7013.

(29) Chen, D. D. Y.; Schneider, B. B. *Anal. Chem.* **2000**, *72*, 791-799.

(30) Chisholm, D. C.; Oliver, A. G.; McInode, J. S. *Dalton Trans.* **2010**, *39*, 364-373.

(31) Henderson, M. A.; Kwok, S.; McIndoe, J. S. *J. Amer. Soc. Mass. Spectrom* **2009**, *20*, 658-666.

(32) Dyson, P. J.; Johnson, B. F. G.; McIndoe, J. S.; Langridge-Smith, P. R. R. *Rapid Commun. Mass Spectrom.* **2000**, *14*, 311-313.

(33) Vicent, C.; Viciano, M.; Mas-Marza, E.; Sanau, M.; Peris, E. *Organometallics* **2006**, *25*, 3713-3720.

(34) Aliprantis, A. O.; Canary, J. W. *J. Amer. Chem. Soc.* **1994**, *116*, 6985-6986.

(35) Sabino, A. A.; Machado, A. H. L.; Correia, C. R. D.; Eberlin, M. N. *Angew. Chem. Int. Ed.* **2004**, *43*, 2514-2518.

(36) Santos, L. S.; Rosso, G. B.; Pilli, R. A.; Eberlin, M. N. *J. Org. Chem* **2007**, *72*, 5809-5812.

(37) Feichtinger, D.; Plattnew, D. A. *Angew. Chem. Int. Ed.* **1997**, *36*, 1718-1719.

(38) Shriver, D. F.; Atkins, P. W. *Inorganic Chemistry*; 3rd ed.; W. H. Freeman and Company: New York, NY, 1999.

(39) Chisholm, D. C.; McIndoe, J. S. *Dalton Trans.* **2008**, *37*, 3933.

(40) Ahrland, S.; Chatt, J.; Davies, N. R.; Williams, A. A. *J. Chem. Soc.* **1958**, 276-288.

(41) Herrmann, W. A.; Kohlpaintner, C. W.; Hanson, B. E.; Kang, X. *Inorg. Synth.* **1998**, *32*, 8-24.

(42) Ding, H.; Bunn, B. B.; Hanson, B. E.; Kohlpaintner, C. W.; Herrmann, W. A. *Inorg. Synth.* **1998**, *32*, 29-36.

(43) Decker, C.; Henderson, W.; Nicholson, B. K. *J. Chem. Soc., Dalton Trans.* **1999**, 3507-3513.

(44) Okano, T.; Harada, N.; Kiji, J. *Chem. Lett.* **1994**, *23*, 1057-1060.

(45) Mohr, B.; Lynn, D. M.; Grubbs, R. H. *Organometallics* **1996**, *15*, 4317-4325.

(46) Adlhart, C.; Volland, M. A. O.; Hofmann, P.; Chen, P. *Helv. Chim. Acta* **2000**, *83*, 3306-3311.

(47) Hinderling, C.; Adlhart, C.; Chen, P. *Angew. Chem. Int. Ed.* **1998**, *37*, 2685-2689.

(48) Adlhart, C.; Chen, P. *Helv. Chim. Acta* **2003**, *86*, 941-949.

(49) Torker, S.; Merki, D.; Chen, P. *J. Amer. Chem. Soc.* **2008**, *130*, 4808-4814.

(50) Farrer, N. J.; McDonald, R.; McIndoe, J. S. *Dalton Trans.* **2006**, *38*, 4570-4579.

(51) Wu, W. Y.; Chen, S. N.; Tsai, F. Y. *Tetrahedron Lett.* **2006**, *47*, 9267-9270.

(52) Wu, X. E.; Ma, L.; Ding, M. X.; Gao, L. X. *Chem. Lett.* **2005**, *34*, 312-313.

(54) Pannell, K. H.; Hambrick, D. C.; Lewandos, G. S. *J. Organomet. Chem.* **1975**, *99*, C21-C23.

(55) Anson, C. E.; Creaser, C. S.; Stephenson, G. R. *J. Chem. Soc.* **1994**.

(56) Anson, C. E.; Creaser, C. S.; Stephenson, G. R. *Spectrochim. Acta Part A* **1996**, *52*, 1183-1191.

(57) Geldbach, T. J.; Brown, M. R. H.; Scopelliti, R.; Dyson, P. J. *J. Organomet. Chem.* **2005**, *690*, 5055-5065.

(58) Brown, W. G.; Letang, N. J. *J. Amer. Chem. Soc.* **1941**, *63*, 358-361.

(59) Alder, R. W.; Bowman, P. S.; Steele, W. R. S.; Winterman, D. R. *Chem. Commun.* **1968**, *13*, 723-724.

(60) Staab, H. A.; Saupe, T. *Angew. Chem. Int. Ed. Engl.* **1988**, *27*, 865-879.

(61) Glowiak, T.; Malarski, Z.; Sobczyk, L.; Grech, E. *J. Mol. Struct.* **1992**, *270*, 441-447.

(62) Wozniak, K.; Krygowski, T. M.; Kariuki, B.; Jones, W.; Grech, E. *J. Mol. Struct.* **1990**, *240*, 111-118.

(63) Truter, M. R.; Vickery, B. L. *J. Chem. Soc. Dalton* **1972**, *3*, 395-403.

(64) Yamasaki, T.; Ozaki, N.; Saiki, Y.; Ohta, K.; Goboh, K.; Nakamura, F.; Hashimoto, M.; Okeva, S. *Chem. Lett.* **2004**, *33*, 928-929.

(65) Alder, R. W. *Chem. Rev.* **1989**, *89*, 1215-1223.

(66) Alder, R. W.; Bryce, M. A.; Goode, N. C.; Miller, N.; Owen, J. *J. Chem. Soc., Perkin Trans. 1* **1981**, *11*, 2840-2847.

(67) Staab, H. A.; Diehm, M.; Krieger, C. *Tetrahedron Lett.* **1994**, *35*, 8357-8360.

(68) Staab, H. A.; Diehm, M.; Krieger, C. *Tetrahedron Lett.* **1995**, *36*, 2967-2970.

(69) Raab, V.; Gauchenova, E.; Merkoulov, A.; Harms, K.; Sundermeyer, J.; Kovacevic, B.; Maksic, Z. B. *J. Amer. Chem. Soc.* **2005**, *127*, 15738-15743.

(70) Caubère, P. *Chem. Rev.* **1993**, *93*, 2317-2334.

(71) Mazaleyrat, J. P.; Wright, K. *Tetrahedron Lett.* **2008**, *49*, 4537-4541.

(72) Chelucci, G.; Thummel, R. P. *Chem. Rev.* **2002**, *102*, 3129-3170.

(73) Kaes, C.; Katz, A. *Chem. Rev.* **2000**, *100*, 3553-3590.

(74) Malkov, A. V.; Kocovsky, P. *Curr. Org. Chem.* **2003**, *21*, 1737-1757.

(75) Rice, R. C.; Onions, S.; Vidal, N.; Wallis, J. D.; Senna, M.; Pilkington, M.; Stoeckli-Evans, H. *Eur. J. Inorg. Chem.* **2002**, *8*, 1985-1997.

(76) Giam, C. S.; Hauck, A. E. *Org. Prep. Proc. Int.* **1977**, *9*, 9-11.

(77) Sheppard, W. A. *Org. Syn* **1969**, *49*, 111.

(78) Charmant, J. P. H.; Lloyd-Jones, G. C.; Peakman, T. M.; Woodward, R. L. *Eur. J. Inorg. Chem.* **1999**, 2501-2510.

(79) Shaw, F. R.; Turner, E. E. *J. Chem. Soc.* **1933**, 135-140.

(80) Merritt, L. L.; Schroeder, E. D. *Acta. Cryst.* **1956**, *9*, 801-804.

(81) *Hydrogen Bonding - New Insights*; Grabowski, S. J., Ed.; Springer: Dordecht, Netherlands, 2006; Vol. 3.

(82) Kayran, C.; Okan, E. *Z. Naturforsch* **2001**, *56*, 218-286.

(83) Hirsivaara, L.; Guerricabeitia, L.; Haukka, M.; Suomalainen, P.; Laitinen, R. H.; Pakkanen, T. A.; Pursiainen, J. *Inorg. Chim. Acta* **2000**, *307*, 47-56.

(84) Baxter, P. N. W.; Connor, J. A.; Wallis, J. D.; Povey, D. C.; Powell, A. K. *Polyhedron* **1992**, *11*, 1771-1777.

(85) Johnson, R.; Madhani, H.; Bullock, J. P. *Inorg. Chim. Acta* **2007**, *360*, 3414-3423.

(86) Braga, S. S.; Coelho, A. C.; Goncalves, I. S.; Paz, F. A. A. *Acta. Cryst. Sect. E* **2007**, *63*, m782-m782.

(87) Clark-Lewis, J. W.; Thompson, M. J. *J. Chem. Soc.* **1957**, 442-446.

(88) Yamanaka, H.; Araki, T.; Salamoto, T. *Chem. Pharm. Bull.* **1988**, *36*, 2244-2247.

(89) Furstner, A.; Leitner, A.; Mendez, M.; Krause, H. *J. Amer. Chem. Soc.* **2002**, *124*, 13856-13863.

(90) Ruiz, A.; Rocca, P.; Marsais, F.; Godard, A.; Queguiner, G. *Tetrahedron Lett.* **1997**, *38*, 6205-6208.

(91) Gunstone, F. D.; Tucker, S. H. *Org. Syn.* **1963**, *4*, 160.

(92) Letinois-Halbes, U.; Hanss, D.; Beierle, J. M.; Collin, J.-P.; Sauvage, J.-P. *Org. Lett.* **2005**, *7*, 5753-5756.

(93) Truong, T.; Alvarado, J.; Tran, L. D.; Daugulis, O. *Org. Lett.* **2010**, *12*, 1200-1203.

(94) Thomas, S.; Roberts, S.; Pasumansky, L.; Gamsey, S.; Singaram, B. *Org. Lett.* **2003**, *5*, 3867-3870.

(95) Hassan, J.; Sévignon, M.; Gozzi, C.; Schulz, E.; Lemaire, M. *Chem. Rev.* **2002**, *102*, 1359-1469.

(96) Bennett, M. A.; Longstaff, P. A. *Chem. Ind. (London)* **1965**, 846.

(97) Young, J. F.; Osborn, J. A.; Jardine, F. H.; Wilkinson, G. *Chem. Commun.* **1965**, 131-132.

(98) Coffey, R. S.; Patent, B., Ed. 1965.

(99) Collman, J. P.; Hegedus, L. S.; Norton, J. R.; Finke, R. G. *Principles and Applications of Organotransition Metal Chemistry*; University Science Books: Mill Valley, CA, 1980.

(100) Hartwig, J. *Organotransition Metal Chemistry*; University Science Books: USA, 2010.

(101) Eaton, D. R.; Smart, S. R. *J. Amer. Chem. Soc.* **1968**, *90*, 4170-4172.

(102) Lehman, D. D.; Shriver, D. F.; Wharf, I. *Chem. Comm.* **1970**, 1486.

(103) Arai, H.; Halpern, J. *Chemical Communications* **1971**, 1571-1572.

(104) Meakin, P.; Jesson, J. P.; Tolman, C. A. *J. Amer. Chem. Soc.* **1972**, *94*, 3240-3242.

(105) Halpern, J.; Wong, C. S. *J. Chem. Soc. Chem. Commun.* **1973**, 629-630.

(106) Halpern, J.; Okamoto, T.; Zakhariev, A. *J. Mol. Catal.* **1977**, *2*, 65-68.

(107) Halpern, J.; Okamoto, T. *Inorg. Chim. Acta* **1984**, *89*, L53-L54.

(108) Brown, J. M.; Evans, P. L.; Lucy, A. R. *J. Chem. Soc., Perkin Trans. 2* **1987**, 1589-1596.

(109) Osborn, J. A.; Jardine, F. H.; Young, J. F.; Wilkinson, G. *J. Chem. Soc. (A)* **1966**, 1711-1732.

(110) Duckett, S. B.; Newell, C. L.; Eisenberg, R. *J. Amer. Chem. Soc.* **1994**, *116*, 10548-10556.

(111) Jardine, F. H.; Osborn, J. A.; Wilkinson, G. *J. Chem. Soc. (A)* **1967**, 1574-1578.

(112) Tolman, C. A.; Meakin, P. Z.; Lindner, D. L.; Jesson, J. P. *J. Amer. Chem. Soc.* **1974**, *96*, 2762-2774.

(113) Duckett, S. B.; Newell, C. L.; Eisenberg, R. *J. Amer. Chem. Soc.* **1993**, *115*, 1156-1157.

(114) Morran, P. D.; Duckett, S. B.; Howe, P. R.; McGrady, J. E.; Colebrooke, S. A.; Eisenberg, R.; Partridge, M. G.; Lohman, J. A. B. *J. Chem. Soc., Dalton Trans.* **1999**, 3949-3960.

(115) Colebrooke, S. A.; Duckett, S. B.; Lohman, J. A. B.; Eisenberg, R. *Chem. Eur. J.* **2004**, *10*, 2459-2474.

(116) Farrer, N. J.; McDonald, R.; Piga, T.; McIndoe, J. S. *Polyhedron* **2010**, *29*, 254-261.

(117) Ercolani, C.; Quagliano, J. V.; Vallarino, L. M. *Inorgan. Chim. Acta* **1969**, *3*, 421-425.

(118) Taylor, R. C.; Keiter, R. L.; Cary, L. W. *Inorg. Chem.* **1974**, *13*, 1928-1932.

(119) Rivera, V.; Gomez, D.; Degil, E. R.; Suarez, T. *Acta. Cryst. Sect. C: Cryst. Struct. Commun.* **1988**, *44*, 277-279.

(120) Fetouaki, R.; Seifert, A.; Bogza, M.; Oeser, T.; Blumel, J. *Inorg. Chim. Acta* **2006**, *359*, 4865-4873.

(121) Farrugia, L. J. *J. Appl. Crys.* **1997**, *30*, 565-565.

(122) James, B. R.; Mahajan, D. *Can. J. Chem.* **1979**, *57*, 180-187.

(123) Schroder, D.; Schwarz, H.; Clemmer, D. E.; Chen, Y. H.; Armentrout, P. B.; Baranov, V. I.; Bohme, D. K. *Int. J. Mass. Spectrom. Ion Processes* **1997**, *161*, 175-191.

(124) Adlhart, C.; Hinderling, C.; Baumann, H.; Chen, P. *J. Amer. Chem. Soc.* **2000**, *122*, 8204-8214.

(125) Chen, P. *Angew. Chem. Int. Ed.* **2003**, *42*, 2832-2847.

(126) Kim, Y. M.; Chen, P. *Int. J. Mass. Spectrom.* **1999**, *185-187*, 871-881.

(127) Volland, M. A. O.; Adlhart, C.; Kiener, C. A.; Chen, P.; Hofmann, P. *Chem. Eur. J.* **2001**, *7*, 4621-4632.

(128) de Charentenay; Osborn, J. A.; Wilkinson, G. *J. Chem. Soc. A.* **1968**, 787-789.

(129) Ojima, I.; Inaba, S.; Kogure, T.; Nagai, Y. *J. Organomet. Chem.* **1973**, *55*, C7-C8.

(130) Toal, S. J.; Sohn, H.; Zakarov, L. N.; Kassel, W. S.; Golen, J. A.; Rheingold, A. L.; Trogler, W. C. *Organometallics* **2005**, *24*, 3081-3087.

(131) Goikhman, R.; Milstein, D. *Chem. Eur. J.* **2005**, *11*, 2983-2988.

(132) Rosenberg, L.; Fryzuk, M. D.; Rettig, S. J. *Organometallics* **1999**, *18*, 958-969.

(133) Chang, L. S.; Corey, J. Y. *Organometallics* **1989**, *8*, 1885-1893.

(134) Brown-Wensley, K. A. *Organometallics* **1987**, *6*, 1591-1593.

(135) Lappert, M. F.; Maskell, R. K. *J. Organomet. Chem.* **1984**, *264*, 217-228.

(136) Reichl, J. A.; Berry, D. H. *Adv. Organomet. Chem.* **1998**, *43*, 197-265.

(137) Gauvin, F.; Harrod, J. F.; Woo, H. G. *Adv. Organomet. Chem.* **1998**, *42*, 363-405.

(138) Corey, J. Y. *Adv. Silicon Chem.* **1991**, *1*, 327-387.

(139) Tilley, T. D. *Comments Inorg. Chem.* **1990**, *10*, 37-51.

(140) Curtis, M. D.; Epstein, P. S. *Adv. Organomet. Chem.* **1981**, *19*, 213-55.

(141) Rosenberg, L.; Davis, C. W.; Yao, J. *J. Amer. Chem. Soc.* **2001**, *123*, 5120-5121.

(142) Jackson, S. M., University of Victoria, 2007.

(143) Jackson, S. M.; Hughes, C. E.; Monfette, S.; Rosenberg, L. *Inorg. Chim. Acta* **2006**, *359*, 2966-2972.

(144) Brown, T. H.; Green, P. J. *J. Amer. Chem. Soc.* **1970**, *92*, 2359-2362.

(145) Esteruelas, M. A.; Herrero, J.; Olivan, M. *Organometallics* **2004**, *23*, 3891-3897.

(146) Peterson, A. A.; Thoreson, K. A.; McNeill, K. *Organometallics* **2009**, *28*, 5982-5991.

(147) Strauss, S. H.; Diamond, S. E.; Mares, F.; Shriver, D. F. *Inorg. Chem.* **1978**, *17*, 3064-3068.

(148) Osakada, K. *J. Organomet. Chem.* **2000**, *611*, 323-331.

(149) Luben, A. T.; McIndoe, J. S.; Weller, A. S. *Organometallics* **2008**, *27*, 3303-3306.

(150) Brook, M. A. *Silicon in Organic, Organometallic, and Polymer Chemistry* United States of America, 2000.

(151) McIndoe, J. S.; Nicholson, B. K. *J. Organomet. Chem.* **1998**, *577*, 181-188.

(152) Chisholm, D. C.; McIndoe, J. S.; Bodizs, G.; Ang, W. H.; Scopelliti, R.; Dyson, P. J. *J. Cluster. Sci.* **2007**, *18*, 303-318.

(153) Hermans, S.; Khimyak, T.; Raja, T.; Sankar, G.; Thomas, J. M.; Johnson, B. F. G. *Nanotech. Cat.* **2004**, *1*, 33-49.

(154) Hermans, S.; Sadasivan, S.; Judkins, C. M. G.; Johnson, B. F. G.; Mann, S.; Khushalani, D. *Adv. Mater.* **2003**, *15*, 1853-1857.

(155) Sheppard, D. S.; Maschmeyer, T.; Johnson, B. F. G.; Thomas, J. M.; Sankar, G.; Ozkaya, D.; Zhou, W.; Oldroyd, R. D.; Bell, R. G. *Angew. Chem. Int. Ed.* **1997**, *36*, 2242-2245.

(156) Wang, L. S.; Wang, X. B. *J. Phys. Chem. A* **2000**, *104*.

(157) Wang, X. B.; Wang, L. S. *Phys. Rev. Lett.* **1999**, *83*, 3402-3405.

(158) Milman, B. L.; Alfassi, Z. B. *Eur. J. Mass Spectrom.* **2005**, *11*, 35-42.

(159) Dyson, P. J.; Khalaila, I.; Luettgen, S.; McIndoe, J. S.; Zhao, D. *Chem. Commun.* **2004**, 2204-2205.

(160) Dyson, P. J.; McIndoe, J. S.; Zhao, D. *Chem. Commun.* **2003**, 508-509.

(161) Bini, R.; Bortolini, O.; Chiappe, C.; Pieraccini, D.; Siciliano, T. *J. Phys. Chem. B* **2007**, *111*, 598-604.

(162) Tsuzuki, S.; Kato, R.; Mikami, M. *Mol. Phys.* **2007**, *106*, 1621-1629.

(163) Tsuzuki, S.; Tokuda, H.; Hayamizu, K.; Watanabe, M. *J. Phys. Chem. B.* **2005**, *109*, 16474 - 16481.

(164) Lide, D. R. *82nd Handbook of chemistry and physics* New York, 2001.

(165) Mann, B. E.; Motterlini, R. *Chem. Comm.* **2007**, 4197-4208.

(166) Johnson, T. R.; Mann, B. E.; Clark, J. E.; Foresti, R.; Green, C. J.; Motterlini, R. *Angew. Chem. Int. Ed.* **2003**, *42*, 3722-3729.

(167) Schmidt, K.; Jung, M.; Keilitz, R.; Schnurr, B.; Gust, R. *Inorg. Chim. Acta* **2000**, *306*, 6-16.

(168) Ott, I.; Kircher, B.; Bagowski, C. P.; Vlecken, D. H. W.; Ott, E. B.; Will, J.; Bensdorf, K.; Sheldrick, W. S.; Gust, R. *Angew. Chem. Int. Ed.* **2009**, *48*, 1160-1163.

(169) Motterlini, R.; Clark, J. E.; Foresti, R.; Sarathchandra, P.; Mann, B. E.; Green, C. J. *Circ. Res.* **2002**, *90*, e17-e24.

(170) Cornils, B.; Herrmann, W. A. *Aqueous-phase organometallic catalysis: concepts and applications*; Wiley-VCH: Weinheim, 2004.

(171) Dyson, P. J., Personal Communication.

(172) Crawford, E.; Dyson, P. J.; Forest, O.; Kwok, S.; McIndoe, J. S. *J. Cluster Sci.* **2006**, *17*, 47-63.

(173) Hermans, S.; Khimyak, T.; Johnson, B. F. G. *J. Chem. Soc., Dalton Trans.* **2001**, 3295-3302.

Appendix 1 Crystallographic details for 3,3'-bis(methylamino)-2,2'-bipyridine (2.3)

The X-ray crystal structure of 3,3'-bis(methylamino)-2,2'-bipyridine (**2.3**) was solved by Dr. Robert MacDonald at the University of Alberta.

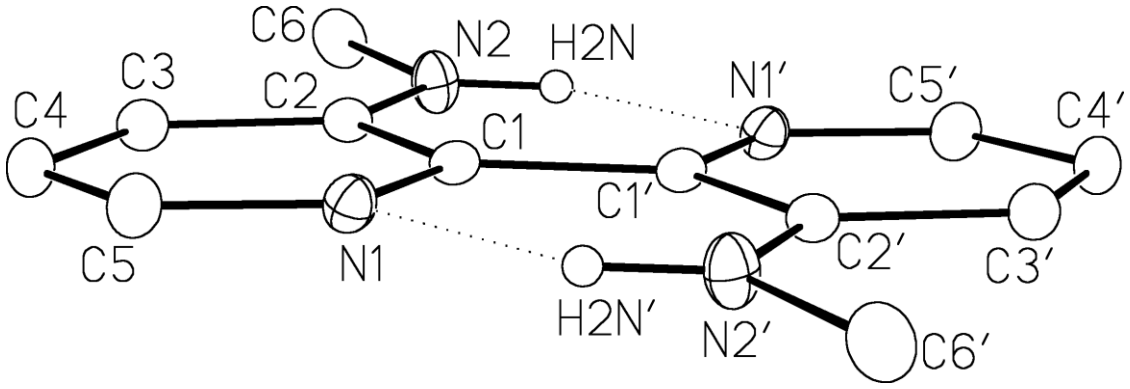

Non-hydrogen atoms are represented by Gaussian ellipsoids at the 20% probability level. Hydrogen atoms are shown with arbitrarily small thermal parameters. Primed atoms are related to unprimed ones vi the crystallographic inversion center ($^1/_2$, 0, $^1/_2$) at the midpoint of the C1–C1' bond. Dotted lines indicate hydrogen-bonded N–H···N interactions.

Appendix Table 1. **Crystallographic experimental details for 2.3**

A. Crystal Data

formula	$C_{12}H_{14}N_4$
formula weight	214.27
crystal dimensions (mm)	0.46 × 0.13 × 0.12
crystal system	monoclinic
space group	$P2_1/n$ (an alternate setting of $P2_1/c$ [No. 14])

unit cell parameters[a]	
a (Å)	7.2033 (8)
b (Å)	7.4226 (9)
c (Å)	10.0292 (12)
β (deg)	98.4133 (18)
V (Å^3)	530.46 (11)
Z	2
ρ_{calcd} (g cm^{-3})	1.341
μ (mm^{-1})	0.085

B. Data Collection and Refinement Conditions

diffractometer	Bruker PLATFORM/SMART 1000 CCD[b]
radiation (λ [Å])	graphite-monochromated Mo Kα (0.71073)
temperature (°C)	–80
scan type	ω scans (0.3°) (20 s exposures)
data collection 2θ limit (deg)	52.70
total data collected	4018 ($-8 \le h \le 8$, $-9 \le k \le 9$, $-12 \le l \le 12$)
independent reflections	1081 (R_{int} = 0.0245)
number of observed reflections (*NO*)	883 [$F_o^2 \ge 2\sigma(F_o^2)$]
structure solution method	direct methods (*SHELXS–86*[c])
refinement method	full-matrix least-squares on F^2 (*SHELXL–93*[d])
absorption correction method	multi-scan (*SADABS*)
range of transmission factors	0.9899–0.9620

data/restraints/parameters	1081 [$F_o^2 \geq -3\sigma(F_o^2)$] / 0 / 74
goodness-of-fit (S)[e]	1.052 [$F_o^2 \geq -3\sigma(F_o^2)$]
final R indices[f]	
R_1 [$F_o^2 \geq 2\sigma(F_o^2)$]	0.0367
wR_2 [$F_o^2 \geq -3\sigma(F_o^2)$]	0.1047
largest difference peak and hole	0.267 and –0.165 e Å^{-3}

[a]Obtained from least-squares refinement of 2055 reflections with 6.54° < 2θ < 52.66°.

[b]Programs for diffractometer operation, data collection, data reduction and absorption correction were those supplied by Bruker.

[c]Sheldrick, G. M. *Acta Crystallogr.* **1990**, *A46*, 467–473.

[d]Sheldrick, G. M. *SHELXL-93*. Program for crystal structure determination. University of Göttingen, Germany, 1993.

[e]$S = [\Sigma w(F_o^2 - F_c^2)^2/(n - p)]^{1/2}$ (n = number of data; p = number of parameters varied; $w = [\sigma^2(F_o^2) + (0.0543P)^2 + 0.1130P]^{-1}$ where $P = [\text{Max}(F_o^2, 0) + 2F_c^2]/3$).

[f]$R_1 = \Sigma||F_o| - |F_c||/\Sigma|F_o|$; $wR_2 = [\Sigma w(F_o^2 - F_c^2)^2/\Sigma w(F_o^4)]^{1/2}$.

Appendix Table 2. **Atomic coordinates and equivalent isotropic displacement parameters for 2.3**

Atom	*x*	*y*	*z*	U_{eq}, Å^2
N1	0.72294(14)	0.08347(15)	0.46500(10)	0.0304(3)*
N2	0.26077(16)	-0.01570(17)	0.27465(11)	0.0354(3)*
C1	0.54217(17)	0.03126(16)	0.44072(12)	0.0250(3)*
C2	0.44136(17)	0.03842(16)	0.30593(12)	0.0267(3)*
C3	0.53934(19)	0.10658(18)	0.20562(13)	0.0321(3)*
C4	0.7220(2)	0.16150(19)	0.23562(14)	0.0354(3)*
C5	0.81122(19)	0.14567(19)	0.36659(13)	0.0353(4)*
C6	0.1613(2)	-0.0170(2)	0.13896(14)	0.0402(4)*

Anisotropically-refined atoms are marked with an asterisk (*). The form of the anisotropic displacement parameter is: $\exp[-2\pi^2(h^2a^{*2}U_{11} + k^2b^{*2}U_{22} + l^2c^{*2}U_{33} + 2klb^*c^*U_{23} + 2hla^*c^*U_{13} + 2hka^*b^*U_{12})]$.

Appendix Table 3. **Selected interatomic distances (Å) for 2.3**

Atom1	Atom2	Distance
N1	N2’	2.6448(15)[a]
N1	C1	1.3463(16)
N1	C5	1.3323(17)
N1	H2N’	1.96[a]
N2	C2	1.3537(17)
N2	C6	1.4422(17)

C1	C1’	1.487(2)
C1	C2	1.4388(16)
C2	C3	1.4050(18)
C3	C4	1.3686(19)
C4	C5	1.380(2)

Appendix Table 4. Selected interatomic angles (°) for 2.3

Atom1	Atom2	Atom3	Angle
C1	N1	C5	121.30(11)
C2	N2	C6	123.26(12)
N1	C1	C1’	116.28(13)
N1	C1	C2	120.08(11)
C1’	C1	C2	123.64(14)
N2	C2	C1	122.85(11)
N2	C2	C3	120.48(11)
C1	C2	C3	116.66(12)
C2	C3	C4	121.16(12)
C3	C4	C5	118.85(12)
N1	C5	C4	121.90(12)
N1’	H2N	N2	133.3[b]

Appendix Table 5. **Torsional angles (°) for 2.3**

Atom1	Atom2	Atom3	Atom4	Angle
C5	N1	C1	C1’	-178.50(13)
C5	N1	C1	C2	1.30(19)
C1	N1	C5	C4	0.7(2)
C6	N2	C2	C1	-176.97(12)
C6	N2	C2	C3	3.5(2)
N1	C1	C1’	N1’	180.0
N1	C1	C1’	C2’	-0.2(2)
C2	C1	C1’	C2’	180.0
N1	C1	C2	N2	178.58(12)
N1	C1	C2	C3	-1.87(18)
C1’	C1	C2	N2	-1.6(2)
C1’	C1	C2	C3	177.91(13)
N2	C2	C3	C4	-179.87(12)
C1	C2	C3	C4	0.57(19)
C2	C3	C4	C5	1.3(2)
C3	C4	C5	N1	-2.0(2)

Primed atoms are related to unprimed ones vi the crystallographic inversion center ($^1/_2$, 0, $^1/_2$). Nonbonded distance. ^{b}Angle includes nonbonded N···H–N interaction.

Appendix Table 6. Anisotropic displacement parameters (U_{ij}, Å^2) for 2.3

Atom	U_{11}	U_{22}	U_{33}	U_{23}	U_{13}	U_{12}
N1	0.0297(6)	0.0351(6)	0.0266(6)	-0.0024(5)	0.0050(4)	-0.0025(5)
N2	0.0338(6)	0.0469(7)	0.0237(6)	0.0056(5)	-0.0015(4)	-0.0067(5)
C1	0.0291(6)	0.0221(6)	0.0235(6)	-0.0021(5)	0.0031(5)	0.0023(5)
C2	0.0331(7)	0.0230(6)	0.0238(6)	-0.0002(5)	0.0027(5)	0.0025(5)
C3	0.0427(8)	0.0306(7)	0.0225(6)	0.0019(5)	0.0034(5)	0.0018(6)
C4	0.0431(8)	0.0352(7)	0.0305(7)	0.0020(6)	0.0141(6)	-0.0032(6)
C5	0.0326(7)	0.0412(8)	0.0332(7)	-0.0025(6)	0.0085(6)	-0.0062(6)
C6	0.0431(8)	0.0444(8)	0.0296(7)	0.0061(6)	-0.0064(6)	-0.0058(6)

The form of the anisotropic displacement parameter is:

$$\exp[-2\pi^2(h^2a^{*2}U_{11} + k^2b^{*2}U_{22} + l^2c^{*2}U_{33} + 2klb^*c^*U_{23} + 2hla^*c^*U_{13} + 2hka^*b^*U_{12})]$$

Appendix Table 7. Derived atomic coordinates and displacement parameters for hydrogen atoms for 2.3

Atom	x	y	z	U_{eq}, Å^2
H2N	0.2011	-0.0519	0.3404	0.042
H3	0.4777	0.1147	0.1154	0.038
H4	0.7864	0.2097	0.1675	0.042
H5	0.9392	0.1801	0.3872	0.042
H6A	0.1569	0.1055	0.1022	0.048
H6B	0.0332	-0.0611	0.1397	0.048
H6C	0.2263	-0.0964	0.0828	0.048

Appendix 2 Crystallographic details for 1-diphenylphosphino-4-benzyldiphenylphosphonium-butane hexafluorophosphate ([3.4]$^+$ PF_6^-)

The X-ray crystal structure of 1-diphenylphosphino-4-benzyldiphenylphosphonium-butane hexafluorophosphate, ([**3.4**]$^+$ PF_6^-) was solved by Dr. Allen Oliver at the University of Notre Dame.

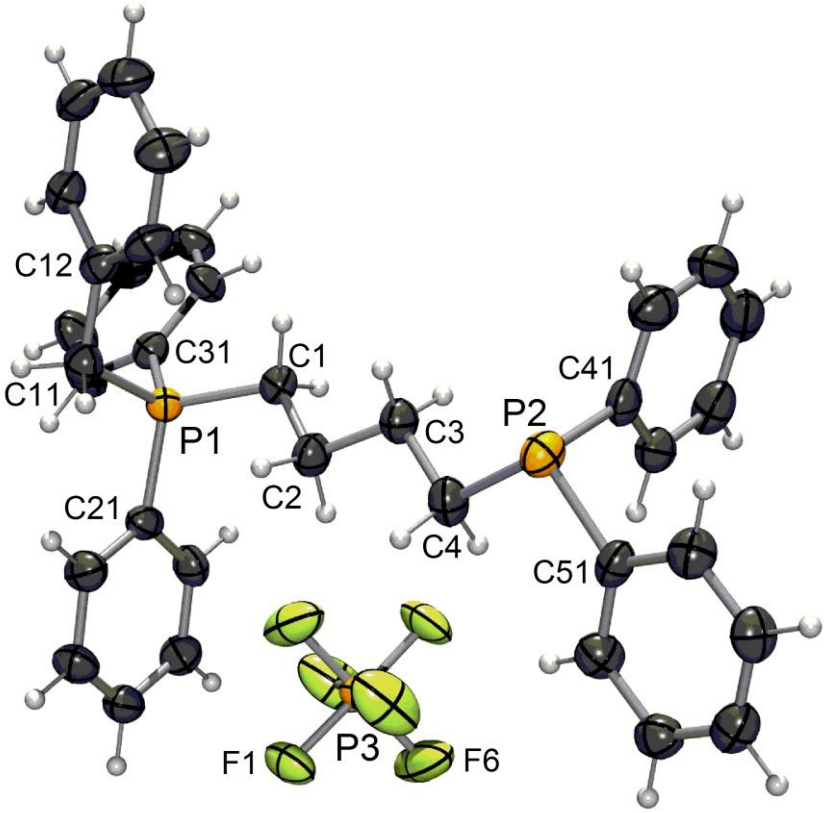

DISCUSSION

The compound crystallizes as colourless block-like crystals. There are four molecules of the phosphine cation and associated PF_6 anion in the unit cell of the primitive, acentric, orthorhombic space group $P2_12_12_1$. This is a chiral space group. The correct

enantiomorph of the space group was determined by comparison of intesities of Friedel pairs of reflections. This resulted in an absolute structure parameter of 0.2 (Flack parameter). This vale is indicative of racemic twinning. A racemic twin law was applied to the refined structure.

The structure of the cation is as expected. The P-C bond distances about P1 are slightly shorter than those around P2 (see Table of Bond Distances). The C-P-C bond angles around P1 are more close to the ideal tetrahedral angle (range is: 107.47(13) to 111.57(13)°), while those about P2 are more constrained and have moved to smaller angles (range is: 99.43(13) to 103.58(13)°, see Table of Bond Angles for details). The remaining bond distances are otherwise unexceptional.

CRYSTAL SUMMARY

Crystal data for $C_{35}H_{35}F_6P_3$; M_r = 662.54; orthorhombic; space group $P2_12_12_1$; *a* = 10.1738(4) Å; *b* = 15.8803(7) Å; *c* = 19.7059(8) Å; α = 90°; β = 90°; γ = 90°; V = 3183.7(2) $Å^3$; Z = 4; T = 100(2) K; λ(Mo-Kα) = 0.71073 Å; μ(Mo-Kα) = 0.247 mm^{-1}; d_{calc} = 1.382g.cm^{-3}; 24326 reflections collected; 6483 unique (R_{int} = 0.0470); giving R_1 = 0.0426, wR_2 = 0.0937 for 5506 data with [I>2σ(I)] and R_1 = 0.0546, wR_2 = 0.1004 for all 6483 data. Residual electron density ($e^-.Å^{-3}$) max/min: 0.407/-0.303.

An arbitrary sphere of data were collected on a colourless block-like crystal, having approximate dimensions of 0.20 × 0.18 × 0.15 mm, on a Bruker APEX-II diffractometer using a combination of ω- and φ-scans of 0.3°. Data were corrected for absorption and

polarization effects and analyzed for space group determination. The structure was solved by direct methods and expanded routinely. The model was refined by full-matrix least-squares analysis of F^2 against all reflections. All non-hydrogen atoms were refined with anisotropic thermal displacement parameters. Unless otherwise noted, hydrogen atoms were included in calculated positions. Thermal parameters for the hydrogens were tied to the isotropic thermal parameter of the atom to which they are bonded (1.2 ×).

Appendix Table 8. Crystal data and structure refinement for $[\mathbf{3.4}]^+ PF_6^-$.

Identification code	$[\mathbf{3.4}]^+ PF_6^-$	
Empirical formula	C35 H35 F6 P3	
Formula weight	662.54	
Temperature	100(2) K	
Wavelength	0.71073 Å	
Crystal system	Orthorhombic	
Space group	P212121	
Unit cell dimensions	a = 10.1738(4) Å	α = 90°
	b = 15.8803(7) Å	β = 90°
	c = 19.7059(8) Å	γ = 90°
Volume	3183.7(2) $Å^3$	
Z	4	
Density (calculated)	1.382 $g.cm^{-3}$	
Absorption coefficient (μ)	0.247 mm^{-1}	
F(000)	1376	

Crystal size	$0.20 \times 0.18 \times 0.15\ mm^3$
ω range for data collection	1.65 to 26.46°
Index ranges	$-12 \leq h \leq 12, -17 \leq k \leq 19, -24 \leq l \leq 24$
Reflections collected	24326
Independent reflections	6483 [$R_{int} = 0.0470$]
Completeness to $\theta = 26.46°$	99.4 %
Absorption correction	numerical
Max. and min. transmission	1.0000 and 0.8915
Refinement method	Full-matrix least-squares on F^2
Data / restraints / parameters	6483 / 0 / 398
Goodness-of-fit on F^2	1.032
Final R indices [$I>2\sigma(I)$]	$R_1 = 0.0426$, $wR_2 = 0.0937$
R indices (all data)	$R_1 = 0.0546$, $wR_2 = 0.1004$
Absolute structure parameter	0.20(8)
Largest diff. peak and hole	0.407 and -0.303 $e^{-}.Å^{-3}$

Appendix Table 9. Atomic coordinates and equivalent isotropic displacement parameters ($Å^2$) for $[3.4]^+ PF_6^-$.

U(eq) is defined as one third of the trace of the orthogonalized U_{ij} tensor.

	x	y	z	U(eq)
P(1)	0.43911(6)	-0.07444(4)	0.39599(4)	0.020(1)
P(2)	0.66646(7)	0.20173(5)	0.63754(4)	0.026(1)
C(1)	0.4454(3)	0.02584(17)	0.43879(13)	0.022(1)
C(2)	0.5707(3)	0.03763(19)	0.48077(14)	0.026(1)
C(3)	0.5564(3)	0.10887(18)	0.53208(14)	0.025(1)
C(4)	0.6895(3)	0.13399(19)	0.56284(14)	0.028(1)
C(11)	0.3929(3)	-0.15446(18)	0.45708(14)	0.025(1)
C(12)	0.2707(3)	-0.13429(17)	0.49698(13)	0.023(1)
C(13)	0.2820(3)	-0.09898(19)	0.56205(14)	0.027(1)
C(14)	0.1726(3)	-0.0832(2)	0.60072(15)	0.032(1)
C(15)	0.0482(3)	-0.1022(2)	0.57601(16)	0.034(1)
C(16)	0.0354(3)	-0.13650(18)	0.51111(16)	0.030(1)
C(17)	0.1460(3)	-0.15234(18)	0.47206(14)	0.027(1)
C(21)	0.5979(2)	-0.10213(17)	0.36331(14)	0.022(1)
C(22)	0.6514(3)	-0.05444(17)	0.31082(14)	0.025(1)
C(23)	0.7763(3)	-0.07162(19)	0.28731(15)	0.029(1)
C(24)	0.8481(3)	-0.13674(18)	0.31585(14)	0.028(1)
C(25)	0.7961(3)	-0.18406(19)	0.36758(15)	0.029(1)

C(26)	0.6703(3)	-0.16720(18)	0.39145(15)	0.027(1)
C(31)	0.3230(3)	-0.06791(17)	0.32780(13)	0.022(1)
C(32)	0.2263(3)	-0.00573(19)	0.32792(15)	0.028(1)
C(33)	0.1358(3)	-0.00202(19)	0.27488(15)	0.029(1)
C(34)	0.1414(3)	-0.05962(19)	0.22335(14)	0.029(1)
C(35)	0.2363(3)	-0.1208(2)	0.22326(16)	0.035(1)
C(36)	0.3289(3)	-0.12475(18)	0.27529(14)	0.030(1)
C(41)	0.5902(3)	0.29445(18)	0.59840(15)	0.026(1)
C(42)	0.4751(3)	0.3245(2)	0.62749(16)	0.033(1)
C(43)	0.4120(3)	0.3950(2)	0.60161(17)	0.038(1)
C(44)	0.4617(3)	0.4359(2)	0.54664(19)	0.041(1)
C(45)	0.5777(3)	0.4062(2)	0.51604(16)	0.036(1)
C(46)	0.6406(3)	0.33610(19)	0.54203(14)	0.028(1)
C(51)	0.8318(3)	0.24425(17)	0.65345(14)	0.024(1)
C(52)	0.9404(3)	0.23186(18)	0.61195(15)	0.028(1)
C(53)	1.0627(3)	0.26680(18)	0.62861(15)	0.029(1)
C(54)	1.0765(3)	0.31335(18)	0.68701(15)	0.029(1)
C(55)	0.9689(3)	0.32657(19)	0.72902(14)	0.028(1)
C(56)	0.8482(3)	0.29167(18)	0.71258(14)	0.029(1)
P(3)	0.82858(7)	0.12914(5)	0.14822(4)	0.025(1)
F(1)	0.92418(17)	0.04997(11)	0.14040(9)	0.041(1)
F(2)	0.73054(18)	0.20635(12)	0.15520(10)	0.047(1)
F(3)	0.8681(2)	0.13496(15)	0.22559(10)	0.066(1)

F(4)	0.7859(2)	0.12172(15)	0.07099(9)	0.060(1)
F(5)	0.71247(18)	0.06754(13)	0.16917(11)	0.056(1)
F(6)	0.94375(19)	0.18987(13)	0.12776(15)	0.078(1)
H(1A)	0.4399	0.0714	0.4046	0.027
H(1B)	0.3682	0.0309	0.4691	0.027
H(2A)	0.5909	-0.0154	0.5051	0.031
H(2B)	0.6451	0.0501	0.4500	0.031
H(3A)	0.4963	0.0909	0.5689	0.030
H(3B)	0.5168	0.1584	0.5095	0.030
H(4A)	0.7422	0.1643	0.5284	0.033
H(4B)	0.7383	0.0827	0.5762	0.033
H(11A)	0.3792	-0.2083	0.4327	0.030
H(11B)	0.4666	-0.1627	0.4892	0.030
H(13A)	0.3666	-0.0859	0.5795	0.033
H(14A)	0.1820	-0.0591	0.6446	0.039
H(15A)	-0.0275	-0.0921	0.6031	0.041
H(16A)	-0.0494	-0.1490	0.4936	0.036
H(17A)	0.1366	-0.1757	0.4279	0.032
H(22A)	0.6018	-0.0100	0.2912	0.030
H(23A)	0.8129	-0.0389	0.2517	0.035
H(24A)	0.9340	-0.1487	0.2995	0.033
H(25A)	0.8461	-0.2284	0.3871	0.035
H(26A)	0.6340	-0.2003	0.4270	0.033

H(32A)	0.2221	0.0339	0.3640	0.033
H(33A)	0.0703	0.0406	0.2745	0.035
H(34A)	0.0792	-0.0572	0.1875	0.034
H(35A)	0.2391	-0.1609	0.1875	0.042
H(36A)	0.3957	-0.1665	0.2745	0.035
H(42A)	0.4390	0.2964	0.6657	0.040
H(43A)	0.3336	0.4148	0.6224	0.046
H(44A)	0.4183	0.4842	0.5291	0.049
H(45A)	0.6129	0.4343	0.4775	0.043
H(46A)	0.7189	0.3162	0.5212	0.034
H(52A)	0.9318	0.1993	0.5718	0.034
H(53A)	1.1360	0.2583	0.5996	0.034
H(54A)	1.1597	0.3365	0.6986	0.035
H(55A)	0.9780	0.3595	0.7690	0.034
H(56A)	0.7754	0.3001	0.7420	0.035

Appendix Table 10. Anisotropic displacement parameters $(Å)^2$ for $[3.4]^+ PF_6^-$.

The anisotropicdisplacement factor exponent takes the form: $-2\pi^2[h^2 a^{*2} U_{11} + ... + 2 h k a^* b^* U_{12}]$

	U_{11}	U_{22}	U_{33}	U_{23}	U_{13}	U_{12}
P(1)	0.0185(3)	0.0203(4)	0.0213(3)	0.0000(3)	-0.0007(3)	0.0002(3)
P(2)	0.0271(4)	0.0289(4)	0.0230(4)	-0.0012(3)	-0.0013(3)	-0.0043(3)
C(1)	0.0225(13)	0.0210(15)	0.0227(14)	0.0010(12)	-0.0001(11)	-0.0023(11)
C(2)	0.0259(14)	0.0235(15)	0.0275(15)	-0.0021(12)	-0.0040(12)	-0.0023(12)
C(3)	0.0275(14)	0.0226(16)	0.0248(14)	-0.0028(12)	-0.0021(12)	-0.0017(12)
C(4)	0.0324(16)	0.0226(16)	0.0286(15)	-0.0021(13)	-0.0052(12)	0.0004(12)
C(11)	0.0266(15)	0.0217(16)	0.0260(15)	0.0022(13)	-0.0007(12)	0.0006(11)
C(12)	0.0222(13)	0.0220(16)	0.0234(15)	0.0058(13)	0.0001(11)	-0.0017(11)
C(13)	0.0189(13)	0.0343(18)	0.0292(16)	0.0025(13)	-0.0037(11)	-0.0045(12)
C(14)	0.0320(15)	0.0414(19)	0.0235(15)	0.0009(14)	0.0050(13)	-0.0022(14)
C(15)	0.0250(15)	0.042(2)	0.0358(17)	0.0067(15)	0.0078(13)	0.0004(13)
C(16)	0.0211(14)	0.0273(17)	0.0413(17)	0.0072(15)	-0.0032(12)	-0.0044(12)
C(17)	0.0268(15)	0.0249(16)	0.0290(15)	0.0008(12)	-0.0022(12)	-0.0042(12)
C(21)	0.0184(12)	0.0243(15)	0.0234(14)	-0.0052(12)	-0.0008(11)	0.0003(10)
C(22)	0.0278(14)	0.0196(15)	0.0279(14)	0.0019(12)	-0.0024(12)	0.0039(12)
C(23)	0.0292(14)	0.0282(17)	0.0302(16)	0.0031(14)	0.0065(12)	-0.0025(13)
C(24)	0.0224(14)	0.0285(17)	0.0319(15)	-0.0049(13)	0.0013(12)	0.0008(12)
C(25)	0.0234(14)	0.0298(17)	0.0349(17)	0.0016(14)	-0.0040(12)	0.0064(11)

C(26)	0.0252(14)	0.0273(16)	0.0295(15)	0.0054(13)	-0.0002(13)	0.0010(12)
C(31)	0.0219(13)	0.0222(15)	0.0206(13)	0.0011(12)	-0.0016(11)	-0.0026(11)
C(32)	0.0254(14)	0.0267(17)	0.0311(16)	-0.0090(13)	-0.0028(12)	0.0061(12)
C(33)	0.0221(14)	0.0309(16)	0.0345(17)	-0.0017(14)	-0.0058(12)	0.0080(12)
C(34)	0.0216(14)	0.0376(19)	0.0268(15)	-0.0001(13)	-0.0031(11)	-0.0008(12)
C(35)	0.0358(17)	0.0336(19)	0.0364(17)	-0.0119(15)	-0.0086(14)	0.0065(14)
C(36)	0.0276(14)	0.0278(17)	0.0333(16)	-0.0041(14)	-0.0061(13)	0.0090(13)
C(41)	0.0288(15)	0.0211(15)	0.0290(16)	-0.0048(13)	-0.0056(12)	-0.0053(12)
C(42)	0.0289(15)	0.039(2)	0.0324(17)	-0.0053(14)	0.0003(12)	-0.0054(13)
C(43)	0.0261(15)	0.040(2)	0.049(2)	-0.0116(17)	0.0017(15)	0.0028(13)
C(44)	0.0306(17)	0.0260(18)	0.066(2)	-0.0025(17)	-0.0163(16)	0.0013(13)
C(45)	0.0376(17)	0.0295(18)	0.0404(18)	0.0034(15)	-0.0087(14)	-0.0090(14)
C(46)	0.0276(15)	0.0285(17)	0.0292(15)	-0.0063(13)	-0.0021(12)	-0.0024(13)
C(51)	0.0251(14)	0.0213(15)	0.0269(15)	0.0019(12)	-0.0065(12)	-0.0047(12)
C(52)	0.0279(14)	0.0313(17)	0.0259(15)	0.0000(13)	-0.0038(13)	0.0025(12)
C(53)	0.0257(14)	0.0289(17)	0.0315(16)	0.0032(13)	-0.0002(12)	0.0021(12)
C(54)	0.0296(15)	0.0273(17)	0.0309(16)	0.0051(14)	-0.0082(13)	-0.0030(13)
C(55)	0.0358(17)	0.0287(17)	0.0199(14)	-0.0028(13)	-0.0051(12)	-0.0009(13)
C(56)	0.0328(16)	0.0290(17)	0.0256(15)	0.0011(13)	0.0005(12)	-0.0021(13)
P(3)	0.0211(3)	0.0281(4)	0.0273(4)	0.0017(3)	0.0012(3)	0.0047(3)
F(1)	0.0370(9)	0.0386(11)	0.0470(11)	0.0071(9)	0.0047(9)	0.0155(8)
F(2)	0.0410(10)	0.0407(12)	0.0604(13)	0.0013(10)	0.0081(10)	0.0214(9)
F(3)	0.0737(15)	0.0814(17)	0.0416(12)	-0.0196(12)	-0.0205(11)	0.0295(13)

F(4)	0.0697(14)	0.0835(17)	0.0267(10)	-0.0036(11)	-0.0049(9)	0.0382(12)
F(5)	0.0286(10)	0.0552(13)	0.0847(16)	0.0323(12)	-0.0052(10)	-0.0042(9)
F(6)	0.0300(11)	0.0471(13)	0.156(3)	0.0421(15)	0.0092(13)	-0.0025(9)

Appendix Table 11. Bond lengths [Å] for $[3.4]^{+}$ PF_6^{-}.

atom-atom	distance	atom-atom	distance
P(1)-C(31)	1.792(3)	P(1)-C(21)	1.794(3)
P(1)-C(1)	1.803(3)	P(1)-C(11)	1.813(3)
P(2)-C(41)	1.834(3)	P(2)-C(4)	1.838(3)
P(2)-C(51)	1.840(3)	C(1)-C(2)	1.531(4)
C(2)-C(3)	1.524(4)	C(3)-C(4)	1.536(4)
C(11)-C(12)	1.506(4)	C(12)-C(17)	1.390(4)
C(12)-C(13)	1.404(4)	C(13)-C(14)	1.372(4)
C(14)-C(15)	1.389(4)	C(15)-C(16)	1.396(4)
C(16)-C(17)	1.387(4)	C(21)-C(26)	1.384(4)
C(21)-C(22)	1.393(4)	C(22)-C(23)	1.380(4)
C(23)-C(24)	1.386(4)	C(24)-C(25)	1.373(4)
C(25)-C(26)	1.390(4)	C(31)-C(36)	1.374(4)
C(31)-C(32)	1.394(4)	C(32)-C(33)	1.394(4)
C(33)-C(34)	1.368(4)	C(34)-C(35)	1.370(4)
C(35)-C(36)	1.393(4)	C(41)-C(42)	1.389(4)
C(41)-C(46)	1.391(4)	C(42)-C(43)	1.387(4)

C(43)-C(44)	1.361(5)	C(44)-C(45)	1.408(5)
C(45)-C(46)	1.382(4)	C(51)-C(52)	1.389(4)
C(51)-C(56)	1.397(4)	C(52)-C(53)	1.401(4)
C(53)-C(54)	1.375(4)	C(54)-C(55)	1.389(4)
C(55)-C(56)	1.386(4)	P(3)-F(6)	1.570(2)
P(3)-F(3)	1.579(2)	P(3)-F(2)	1.5866(18)
P(3)-F(4)	1.5871(19)	P(3)-F(5)	1.5883(19)
P(3)-F(1)	1.5969(18)	C(1)-H(1A)	0.9900
C(1)-H(1B)	0.9900	C(2)-H(2A)	0.9900
C(2)-H(2B)	0.9900	C(3)-H(3A)	0.9900
C(3)-H(3B)	0.9900	C(4)-H(4A)	0.9900
C(4)-H(4B)	0.9900	C(11)-H(11A)	0.9900
C(11)-H(11B)	0.9900	C(13)-H(13A)	0.9500
C(14)-H(14A)	0.9500	C(15)-H(15A)	0.9500
C(16)-H(16A)	0.9500	C(17)-H(17A)	0.9500
C(22)-H(22A)	0.9500	C(23)-H(23A)	0.9500
C(24)-H(24A)	0.9500	C(25)-H(25A)	0.9500
C(26)-H(26A)	0.9500	C(32)-H(32A)	0.9500
C(33)-H(33A)	0.9500	C(34)-H(34A)	0.9500
C(35)-H(35A)	0.9500	C(36)-H(36A)	0.9500
C(42)-H(42A)	0.9500	C(43)-H(43A)	0.9500
C(44)-H(44A)	0.9500	C(45)-H(45A)	0.9500
C(46)-H(46A)	0.9500	C(52)-H(52A)	0.9500

C(53)-H(53A)	0.9500	C(54)-H(54A)	0.9500
C(55)-H(55A)	0.9500	C(56)-H(56A)	0.9500

Appendix Table 12. Bond angles [°] for $[3.4]^{+}$ PF_6^{-}.

atom-atom-atom	angle	atom-atom-atom	angle
C(31)-P(1)-C(21)	109.80(12)	C(31)-P(1)-C(1)	108.86(13)
C(21)-P(1)-C(1)	110.62(12)	C(31)-P(1)-C(11)	111.57(13)
C(21)-P(1)-C(11)	107.47(13)	C(1)-P(1)-C(11)	108.53(13)
C(41)-P(2)-C(4)	100.77(13)	C(41)-P(2)-C(51)	99.43(13)
C(4)-P(2)-C(51)	103.58(13)	C(2)-C(1)-P(1)	112.99(19)
C(3)-C(2)-C(1)	111.7(2)	C(2)-C(3)-C(4)	111.7(2)
C(3)-C(4)-P(2)	110.84(19)	C(12)-C(11)-P(1)	114.3(2)
C(17)-C(12)-C(13)	118.7(2)	C(17)-C(12)-C(11)	121.7(2)
C(13)-C(12)-C(11)	119.6(2)	C(14)-C(13)-C(12)	120.9(3)
C(13)-C(14)-C(15)	120.3(3)	C(14)-C(15)-C(16)	119.4(3)
C(17)-C(16)-C(15)	120.2(3)	C(16)-C(17)-C(12)	120.5(3)
C(26)-C(21)-C(22)	119.7(2)	C(26)-C(21)-P(1)	121.2(2)
C(22)-C(21)-P(1)	119.0(2)	C(23)-C(22)-C(21)	120.1(3)
C(22)-C(23)-C(24)	119.8(3)	C(25)-C(24)-C(23)	120.4(3)
C(24)-C(25)-C(26)	120.1(3)	C(21)-C(26)-C(25)	119.9(3)
C(36)-C(31)-C(32)	119.8(2)	C(36)-C(31)-P(1)	119.9(2)
C(32)-C(31)-P(1)	120.3(2)	C(33)-C(32)-C(31)	119.6(3)

C(34)-C(33)-C(32)	120.1(3)	C(33)-C(34)-C(35)	120.3(3)
C(34)-C(35)-C(36)	120.5(3)	C(31)-C(36)-C(35)	119.7(3)
C(42)-C(41)-C(46)	118.5(3)	C(42)-C(41)-P(2)	117.3(2)
C(46)-C(41)-P(2)	124.2(2)	C(43)-C(42)-C(41)	121.1(3)
C(44)-C(43)-C(42)	120.4(3)	C(43)-C(44)-C(45)	119.5(3)
C(46)-C(45)-C(44)	120.0(3)	C(45)-C(46)-C(41)	120.5(3)
C(52)-C(51)-C(56)	118.2(3)	C(52)-C(51)-P(2)	125.1(2)
C(56)-C(51)-P(2)	116.7(2)	C(51)-C(52)-C(53)	120.8(3)
C(54)-C(53)-C(52)	120.0(3)	C(53)-C(54)-C(55)	120.0(3)
C(56)-C(55)-C(54)	119.9(3)	C(55)-C(56)-C(51)	121.1(3)
F(6)-P(3)-F(3)	91.25(15)	F(6)-P(3)-F(2)	90.96(11)
F(3)-P(3)-F(2)	91.79(11)	F(6)-P(3)-F(4)	90.20(14)
F(3)-P(3)-F(4)	178.55(15)	F(2)-P(3)-F(4)	88.20(11)
F(6)-P(3)-F(5)	179.75(14)	F(3)-P(3)-F(5)	88.54(13)
F(2)-P(3)-F(5)	89.19(11)	F(4)-P(3)-F(5)	90.01(13)
F(6)-P(3)-F(1)	90.24(11)	F(3)-P(3)-F(1)	89.09(11)
F(2)-P(3)-F(1)	178.49(11)	F(4)-P(3)-F(1)	90.89(11)
F(5)-P(3)-F(1)	89.61(10)	C(2)-C(1)-H(1A)	109.0
P(1)-C(1)-H(1A)	109.0	C(2)-C(1)-H(1B)	109.0
P(1)-C(1)-H(1B)	109.0	H(1A)-C(1)-H(1B)	107.8
C(3)-C(2)-H(2A)	109.3	C(1)-C(2)-H(2A)	109.3
C(3)-C(2)-H(2B)	109.3	C(1)-C(2)-H(2B)	109.3
H(2A)-C(2)-H(2B)	107.9	C(2)-C(3)-H(3A)	109.3

C(4)-C(3)-H(3A)	109.3	C(2)-C(3)-H(3B)	109.3
C(4)-C(3)-H(3B)	109.3	H(3A)-C(3)-H(3B)	107.9
C(3)-C(4)-H(4A)	109.5	P(2)-C(4)-H(4A)	109.5
C(3)-C(4)-H(4B)	109.5	P(2)-C(4)-H(4B)	109.5
H(4A)-C(4)-H(4B)	108.1	C(12)-C(11)-H(11A)	108.7
P(1)-C(11)-H(11A)	108.7	C(12)-C(11)-H(11B)	108.7
P(1)-C(11)-H(11B)	108.7	H(11A)-C(11)-H(11B)	107.6
C(14)-C(13)-H(13A)	119.6	C(12)-C(13)-H(13A)	119.6
C(13)-C(14)-H(14A)	119.8	C(15)-C(14)-H(14A)	119.8
C(14)-C(15)-H(15A)	120.3	C(16)-C(15)-H(15A)	120.3
C(17)-C(16)-H(16A)	119.9	C(15)-C(16)-H(16A)	119.9
C(16)-C(17)-H(17A)	119.8	C(12)-C(17)-H(17A)	119.8
C(23)-C(22)-H(22A)	119.9	C(21)-C(22)-H(22A)	119.9
C(22)-C(23)-H(23A)	120.1	C(24)-C(23)-H(23A)	120.1
C(25)-C(24)-H(24A)	119.8	C(23)-C(24)-H(24A)	119.8
C(24)-C(25)-H(25A)	120.0	C(26)-C(25)-H(25A)	120.0
C(21)-C(26)-H(26A)	120.1	C(25)-C(26)-H(26A)	120.1
C(33)-C(32)-H(32A)	120.2	C(31)-C(32)-H(32A)	120.2
C(34)-C(33)-H(33A)	120.0	C(32)-C(33)-H(33A)	120.0
C(33)-C(34)-H(34A)	119.8	C(35)-C(34)-H(34A)	119.8
C(34)-C(35)-H(35A)	119.8	C(36)-C(35)-H(35A)	119.8
C(31)-C(36)-H(36A)	120.1	C(35)-C(36)-H(36A)	120.1
C(43)-C(42)-H(42A)	119.5	C(41)-C(42)-H(42A)	119.5

C(44)-C(43)-H(43A)	119.8	C(42)-C(43)-H(43A)	119.8
C(43)-C(44)-H(44A)	120.3	C(45)-C(44)-H(44A)	120.3
C(46)-C(45)-H(45A)	120.0	C(44)-C(45)-H(45A)	120.0
C(45)-C(46)-H(46A)	119.7	C(41)-C(46)-H(46A)	119.7
C(51)-C(52)-H(52A)	119.6	C(53)-C(52)-H(52A)	119.6
C(54)-C(53)-H(53A)	120.0	C(52)-C(53)-H(53A)	120.0
C(53)-C(54)-H(54A)	120.0	C(55)-C(54)-H(54A)	120.0
C(56)-C(55)-H(55A)	120.0	C(54)-C(55)-H(55A)	120.0
C(55)-C(56)-H(56A)	119.5	C(51)-C(56)-H(56A)	119.5

Appendix Table 13. Torsion angles [°] for $[3.4]^{+}$ PF_6^{-}.

atom-atom-atom-atom	angle	atom-atom-atom-atom	angle
C(31)-P(1)-C(1)-C(2)	-160.38(19)	C(21)-P(1)-C(1)-C(2)	-39.7(2)
C(11)-P(1)-C(1)-C(2)	78.0(2)	P(1)-C(1)-C(2)-C(3)	-163.0(2)
C(1)-C(2)-C(3)-C(4)	-167.2(2)	C(2)-C(3)-C(4)-P(2)	-167.0(2)
C(41)-P(2)-C(4)-C(3)	-64.4(2)	C(51)-P(2)-C(4)-C(3)	-167.0(2)
C(31)-P(1)-C(11)-C(12)	-68.1(2)	C(21)-P(1)-C(11)-C(12)	171.52(19)
C(1)-P(1)-C(11)-C(12)	51.9(2)	P(1)-C(11)-C(12)-C(17)	84.8(3)
P(1)-C(11)-C(12)-C(13)	-97.4(3)	C(17)-C(12)-C(13)-C(14)	0.6(4)
C(11)-C(12)-C(13)-C(14)	-177.3(3)	C(12)-C(13)-C(14)-C(15)	0.2(5)
C(13)-C(14)-C(15)-C(16)	-0.9(5)	C(14)-C(15)-C(16)-C(17)	0.8(5)
C(15)-C(16)-C(17)-C(12)	-0.1(4)	C(13)-C(12)-C(17)-C(16)	-0.6(4)

C(11)-C(12)-C(17)-C(16)	177.2(3)	C(31)-P(1)-C(21)-C(26)	-130.1(2)
C(1)-P(1)-C(21)-C(26)	109.7(2)	C(11)-P(1)-C(21)-C(26)	-8.6(3)
C(31)-P(1)-C(21)-C(22)	53.0(3)	C(1)-P(1)-C(21)-C(22)	-67.2(2)
C(11)-P(1)-C(21)-C(22)	174.5(2)	C(26)-C(21)-C(22)-C(23)	-0.5(4)
P(1)-C(21)-C(22)-C(23)	176.5(2)	C(21)-C(22)-C(23)-C(24)	0.3(4)
C(22)-C(23)-C(24)-C(25)	-0.3(4)	C(23)-C(24)-C(25)-C(26)	0.4(4)
C(22)-C(21)-C(26)-C(25)	0.6(4)	P(1)-C(21)-C(26)-C(25)	-176.3(2)
C(24)-C(25)-C(26)-C(21)	-0.5(4)	C(21)-P(1)-C(31)-C(36)	38.5(3)
C(1)-P(1)-C(31)-C(36)	159.7(2)	C(11)-P(1)-C(31)-C(36)	-80.6(2)
C(21)-P(1)-C(31)-C(32)	-141.9(2)	C(1)-P(1)-C(31)-C(32)	-20.7(3)
C(11)-P(1)-C(31)-C(32)	99.1(2)	C(36)-C(31)-C(32)-C(33)	0.3(4)
P(1)-C(31)-C(32)-C(33)	-179.3(2)	C(31)-C(32)-C(33)-C(34)	0.6(4)
C(32)-C(33)-C(34)-C(35)	-0.5(4)	C(33)-C(34)-C(35)-C(36)	-0.5(5)
C(32)-C(31)-C(36)-C(35)	-1.3(4)	P(1)-C(31)-C(36)-C(35)	178.3(2)
C(34)-C(35)-C(36)-C(31)	1.4(5)	C(4)-P(2)-C(41)-C(42)	129.4(2)
C(51)-P(2)-C(41)-C(42)	-124.7(2)	C(4)-P(2)-C(41)-C(46)	-50.8(3)
C(51)-P(2)-C(41)-C(46)	55.1(3)	C(46)-C(41)-C(42)-C(43)	-0.6(4)
P(2)-C(41)-C(42)-C(43)	179.2(2)	C(41)-C(42)-C(43)-C(44)	0.3(5)
C(42)-C(43)-C(44)-C(45)	0.1(5)	C(43)-C(44)-C(45)-C(46)	-0.3(5)
C(44)-C(45)-C(46)-C(41)	0.0(4)	C(42)-C(41)-C(46)-C(45)	0.5(4)
P(2)-C(41)-C(46)-C(45)	-179.3(2)	C(41)-P(2)-C(51)-C(52)	-97.7(3)
C(4)-P(2)-C(51)-C(52)	5.9(3)	C(41)-P(2)-C(51)-C(56)	83.2(2)
C(4)-P(2)-C(51)-C(56)	-173.3(2)	C(56)-C(51)-C(52)-C(53)	-0.7(4)

P(2)-C(51)-C(52)-C(53)	-179.8(2)	C(51)-C(52)-C(53)-C(54)	0.6(4)
C(52)-C(53)-C(54)-C(55)	-0.8(4)	C(53)-C(54)-C(55)-C(56)	1.0(4)
C(54)-C(55)-C(56)-C(51)	-1.1(4)	C(52)-C(51)-C(56)-C(55)	1.0(4)
P(2)-C(51)-C(56)-C(55)	-179.8(2)		

Appendix 3 Supplementary Spectra

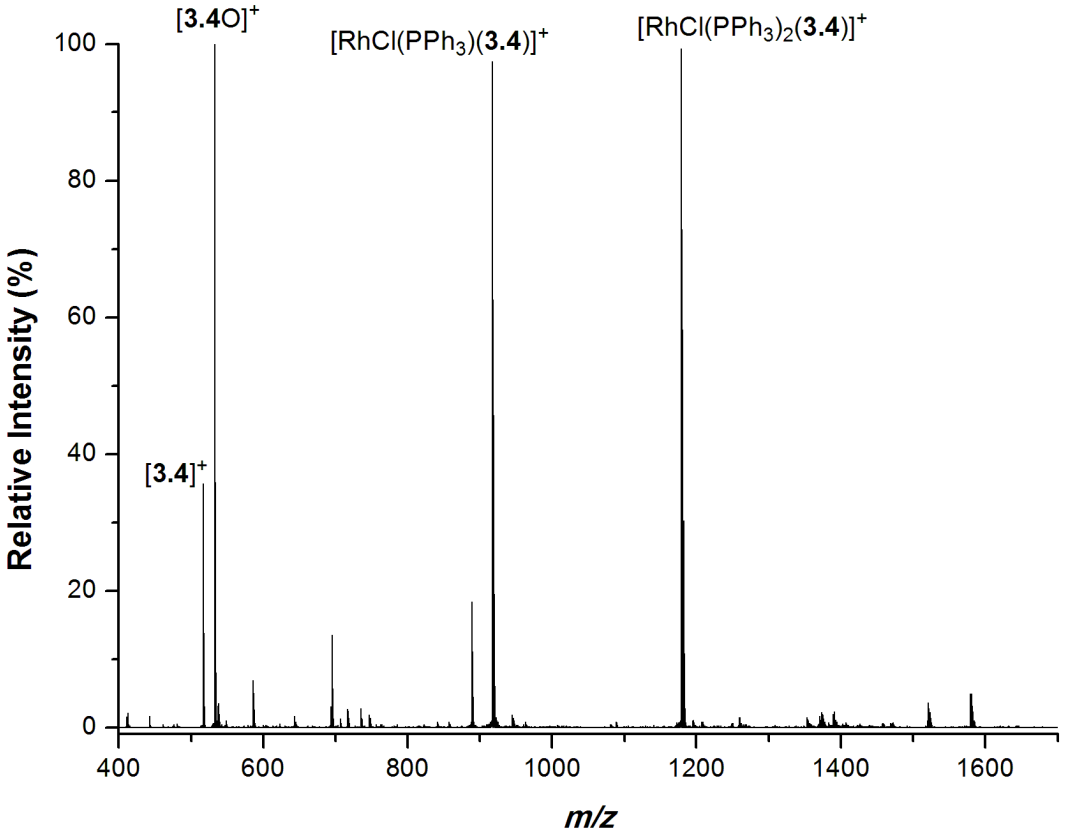

Appendix Figure 1. Positive-ion ESI-MS of [**3.4**]$^{+}$ BF_4^{-} and $RhCl(PPh_3)_3$ in chlorobenzene. Cone voltage = 20 V.

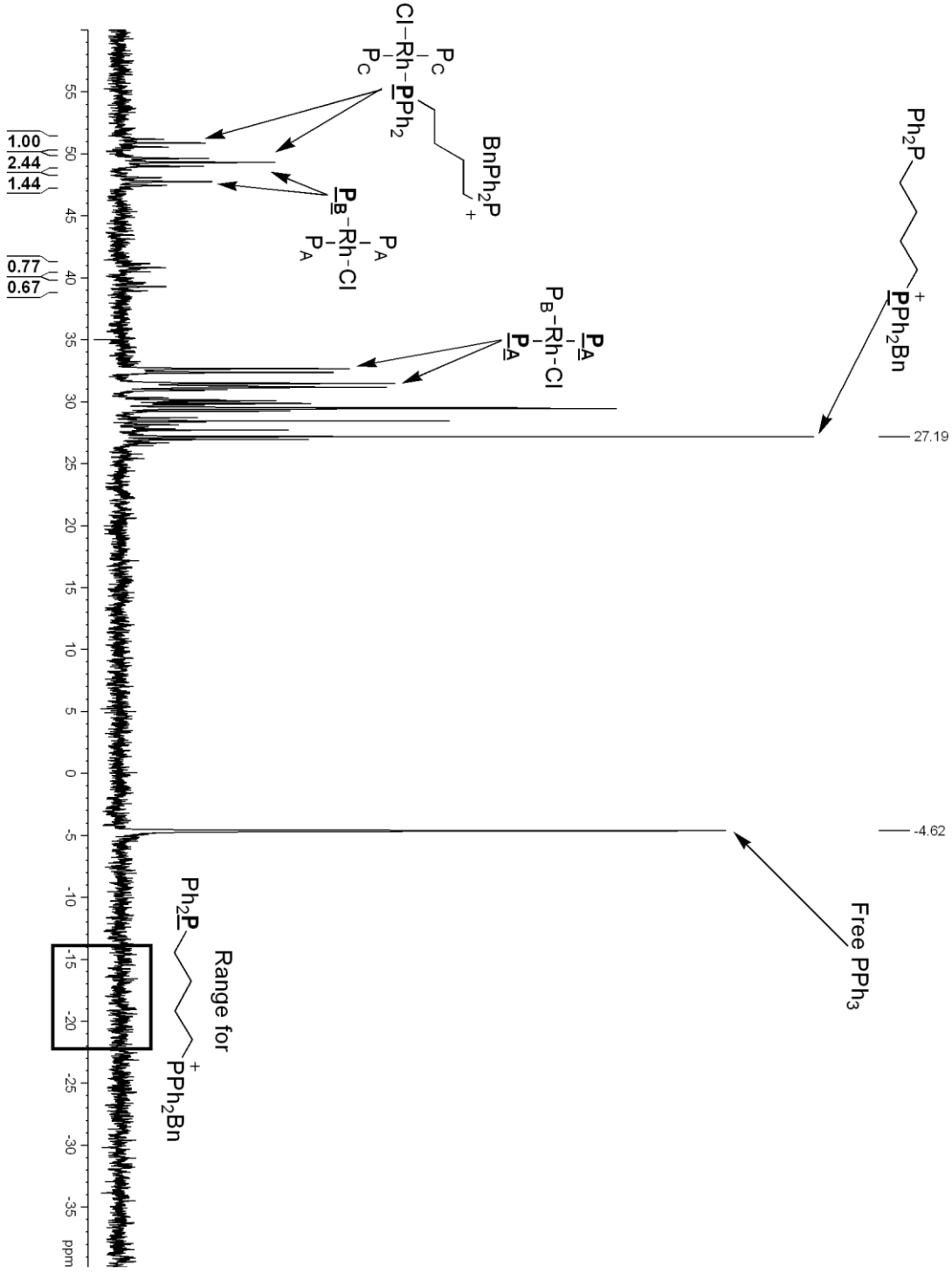

Appendix Figure 2. ^{31}P NMR of 1:1 [**3.4**]$^{+}$ BF_4^{-} in 1:6 d_6-benzene/chlorobenzene

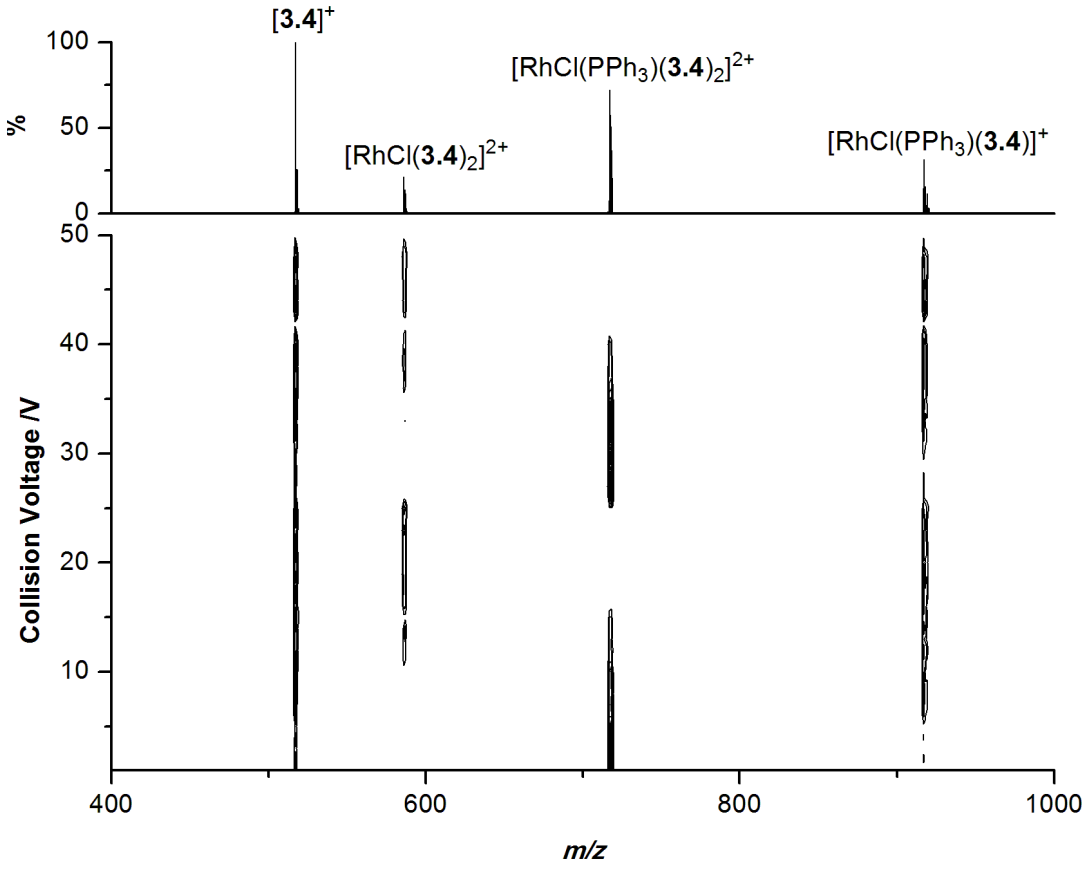

Appendix Figure 3. Positive-ion EDESI-MS/MS of $[RhCl(PPh_3)(\mathbf{3.4})_2]^{2+}$. Cone voltage = 10 V.

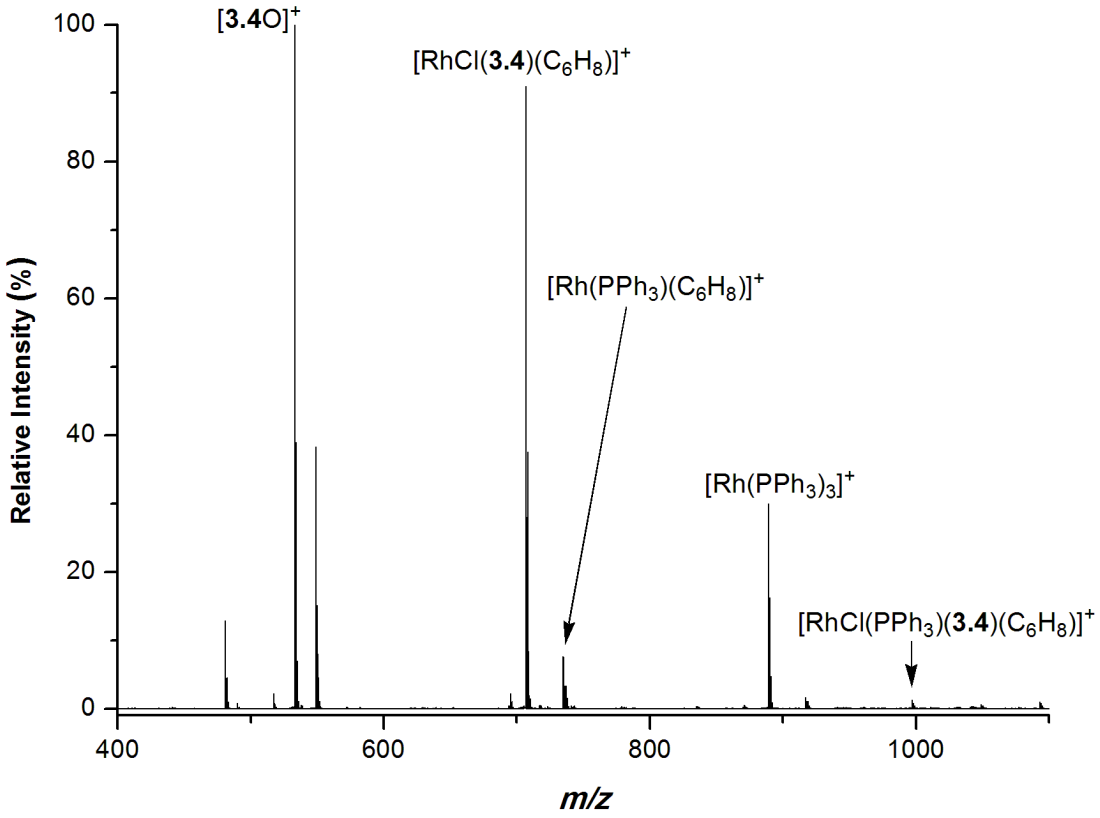

Appendix Figure 4. Positive-ion ESI-MS of [**3.4**]$^{+}$ BF_4^{-} and $RhCl(PPh_3)_3$ in chlorobenzene after the addition of cyclohexene. Cone voltage = 10 V.

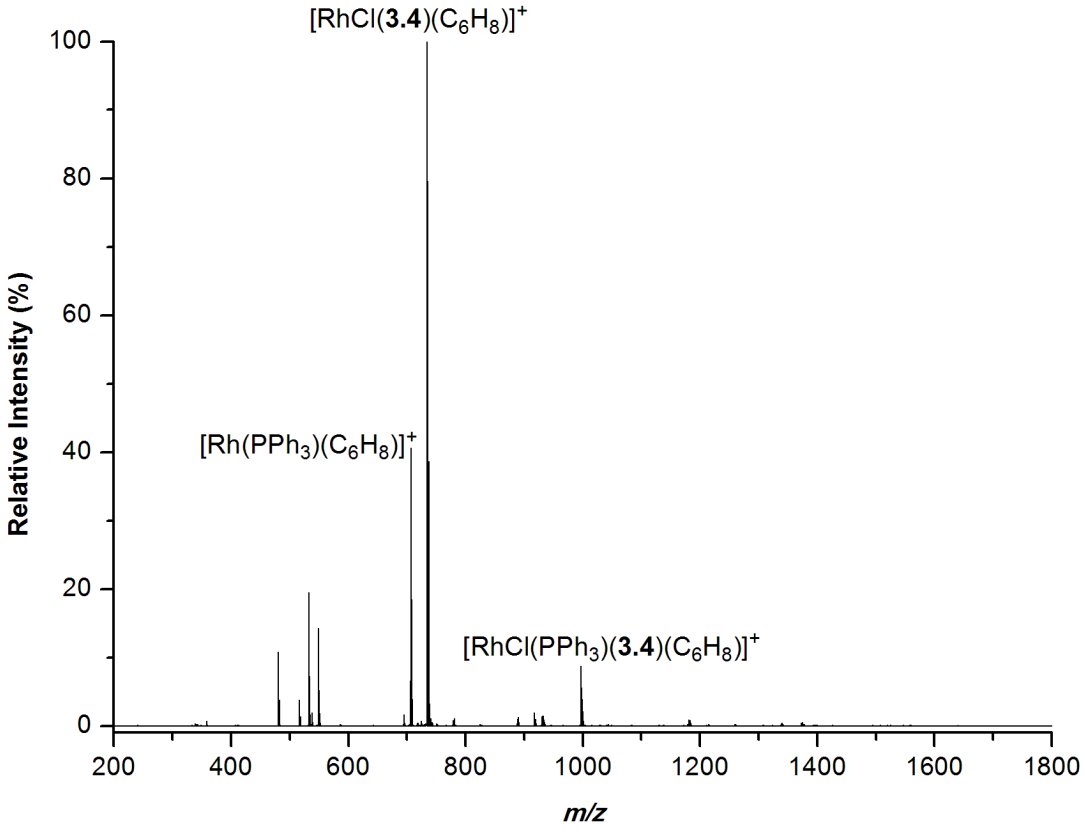

Appendix Figure 5. Positive-ion ESI-MS of [**3.4**]$^{+}$ BF_4^- and $RhCl(PPh_3)_3$ in chlorobenzene after the addition of 1,3-cyclohexadiene. Cone voltage = 10 V.

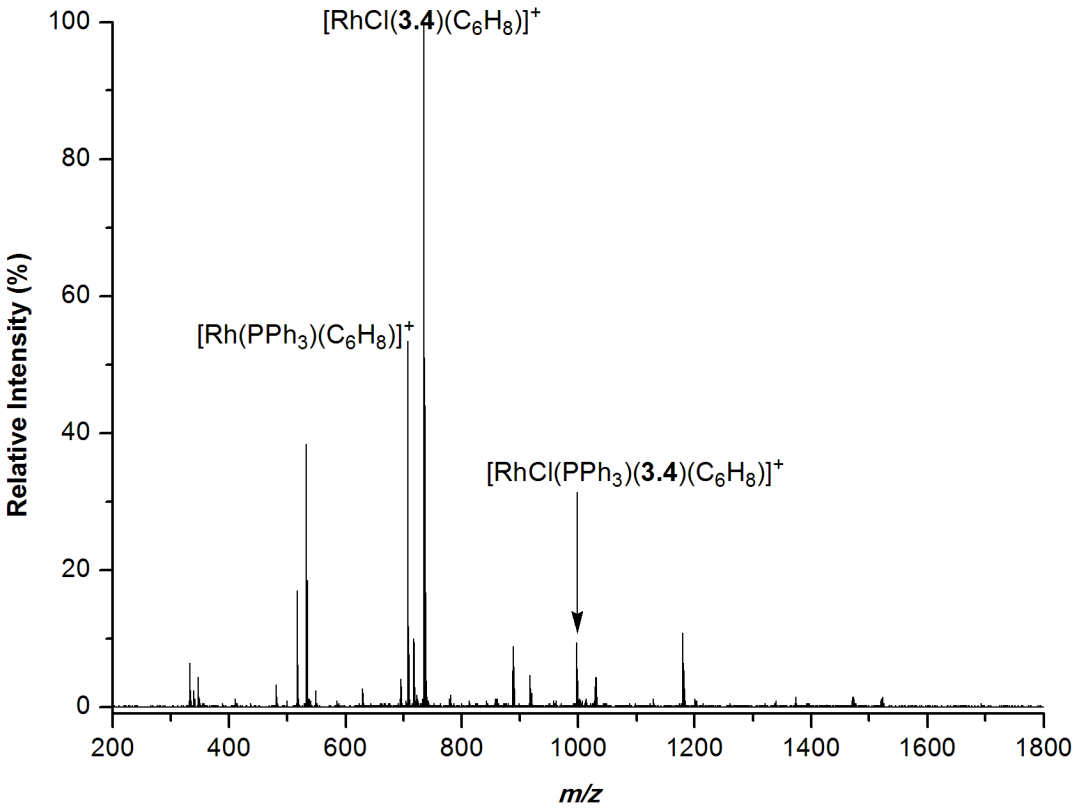

Appendix Figure 6. Positive-ion ESI-MS of [**3.4**]$^{+}$ BF_4^{-} and $RhCl(PPh_3)_3$ in chlorobenzene after the addition of 1,4-cyclohexadiene. Cone voltage = 10 V.

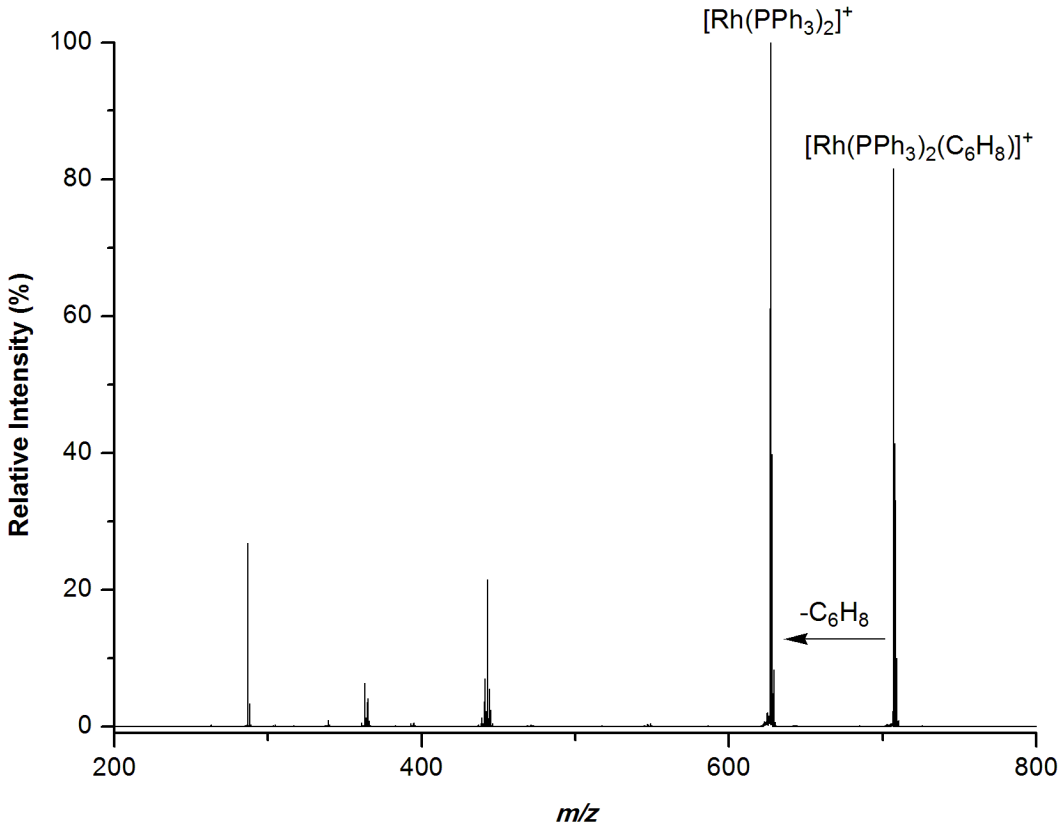

Appendix Figure 7. Positive-ion ESI-MS/MS of $[Rh(PPh_3)_2(C_6H_8)]^+$ from addition of cyclohexene to catalyst solution. Cone voltage = 10 V and collision voltage was increased from 0 to 50 V.

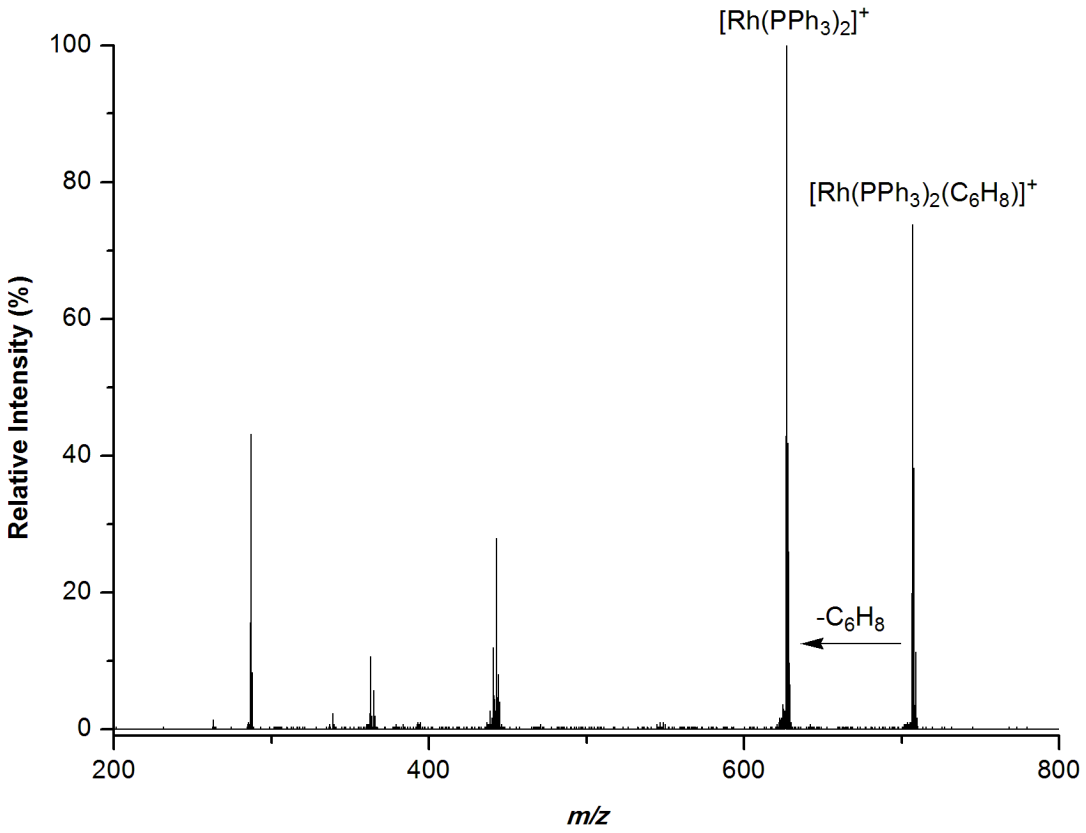

Appendix Figure 8. Positive-ion ESI-MS/MS of $[Rh(PPh_3)_2(C_6H_8)]^+$ from addition of 1,3-cyclohexadiene to catalyst solution. Cone voltage = 10 V and collision voltage was increased from 0 to 50 V.

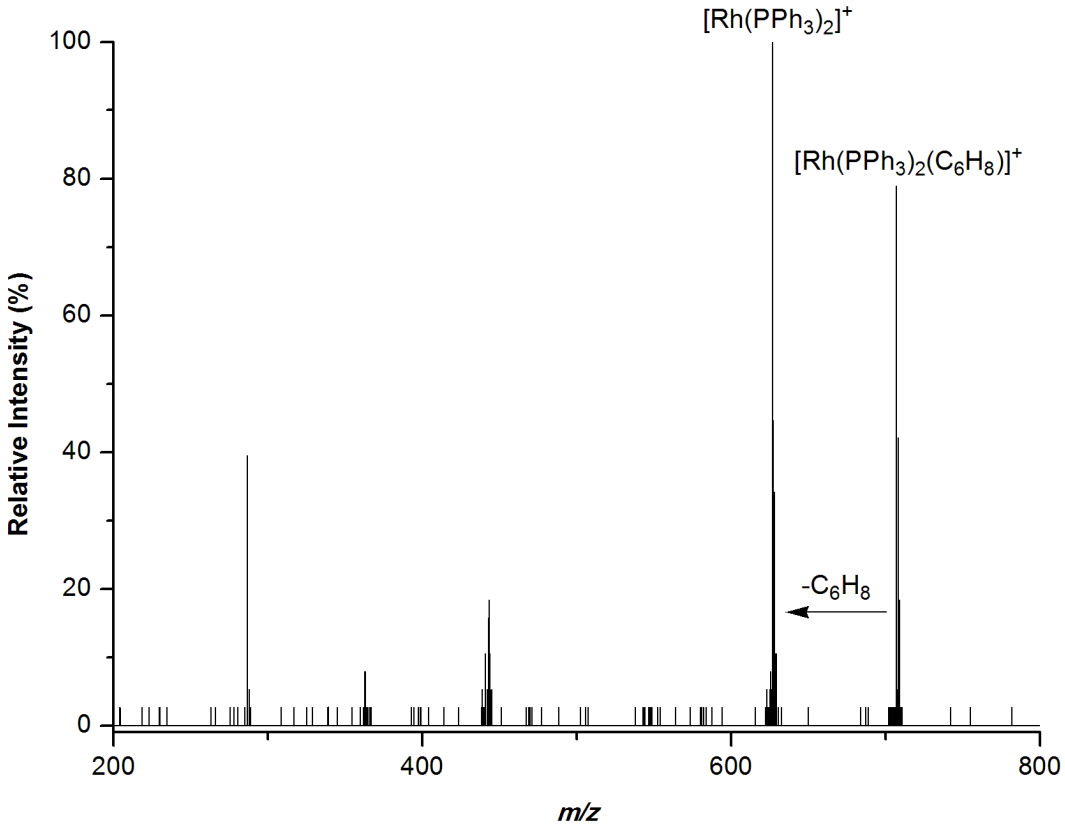

Appendix Figure 9. Positive-ion ESI-MS/MS of $[Rh(PPh_3)_2(C_6H_8)]^+$ from addition of 1,4-cyclohexadiene to catalyst solution. Cone voltage = 10 V and collision voltage was increased from 0 to 50 V.

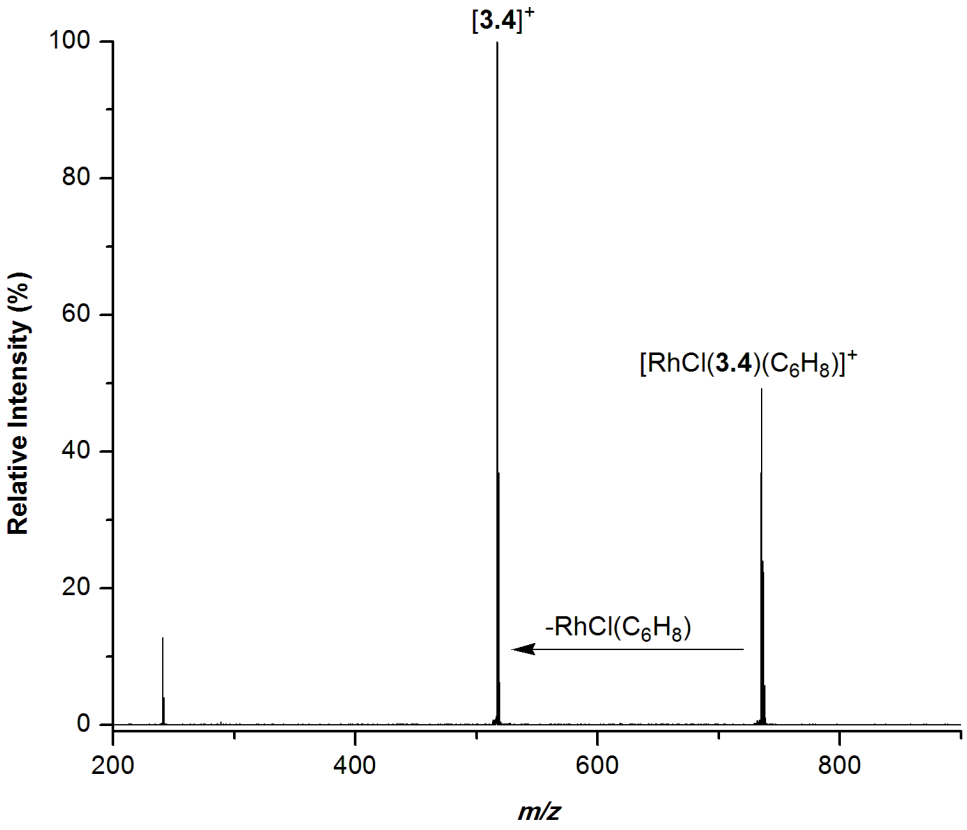

Appendix Figure 10. Positive-ion ESI-MS/MS of [RhCl(**3.4**)(C_6H_8)]$^+$ from addition of cyclohexene to catalyst solution. Cone voltage = 10 V and collision voltage was increased from 0 to 50 V.

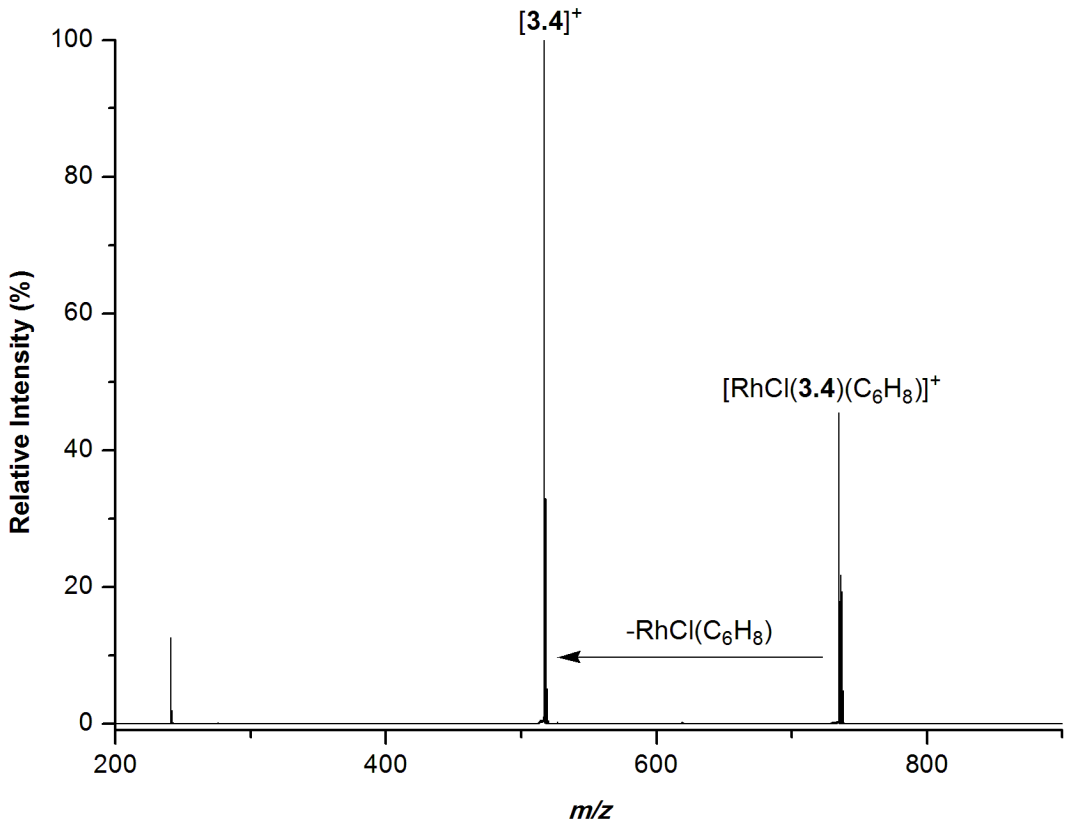

Appendix Figure 11. Positive-ion ESI-MS/MS of [RhCl(**3.4**)(C_6H_8)]$^+$ from addition of 1,3-cyclohexadiene to catalyst solution. Cone voltage = 10 V and collision voltage was increased from 0 to 50 V.

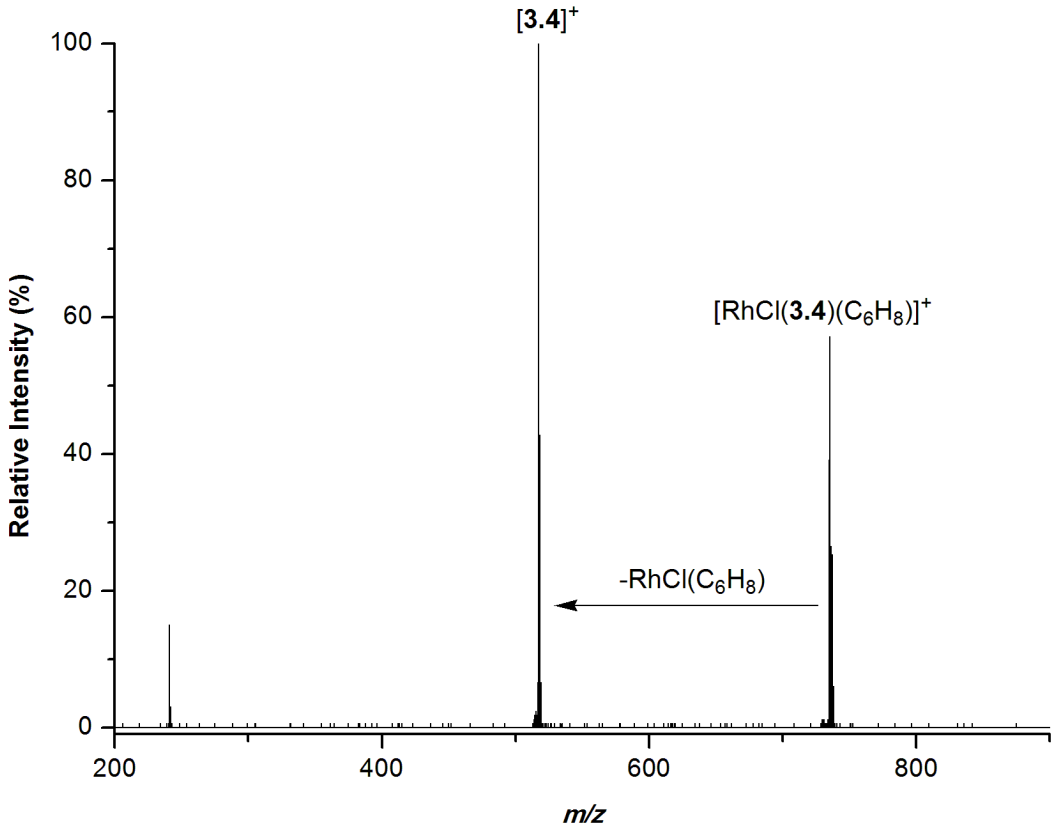

Appendix Figure 12. Positive-ion ESI-MS/MS of [RhCl(**3.4**)(C_6H_8)]$^+$ from addition of 1,4-cyclohexadiene to catalyst solution. Cone voltage = 10 V and collision voltage was increased from 0 to 50 V.

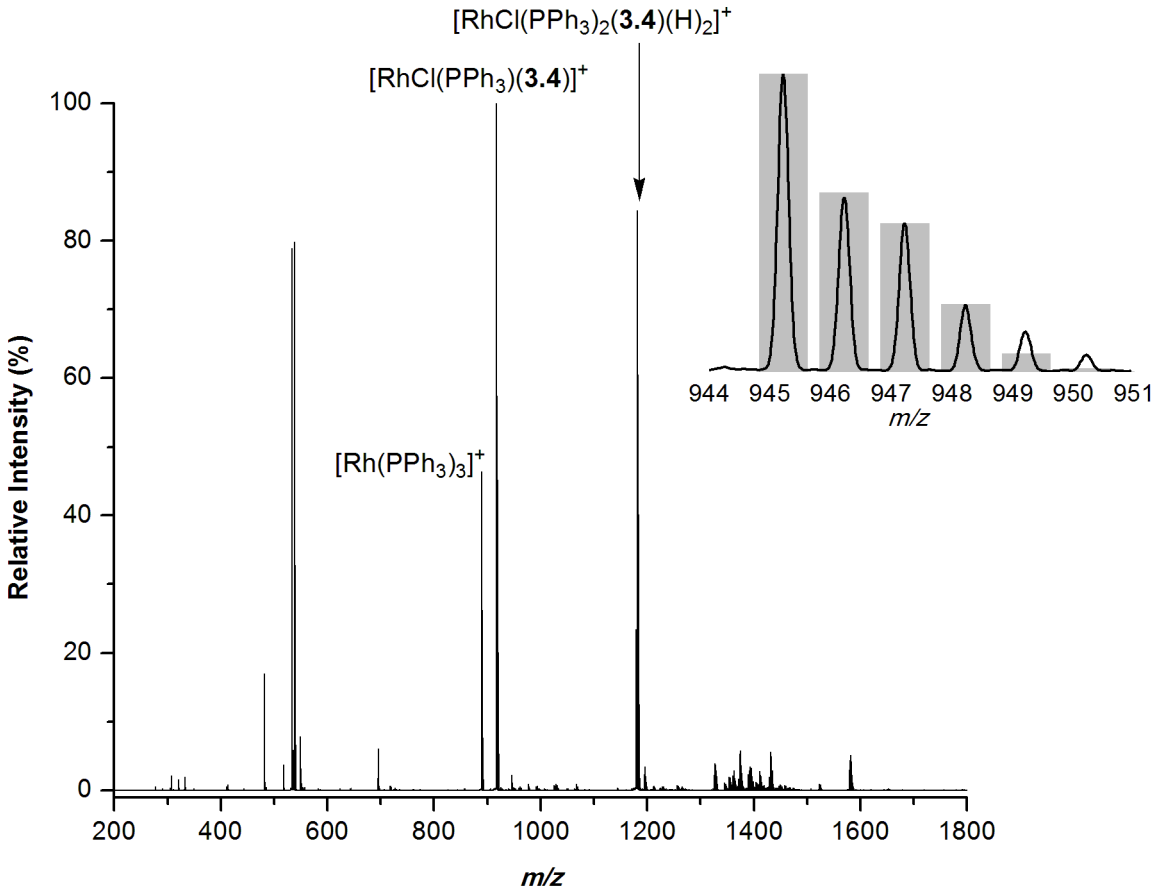

Appendix Figure 13. Positive-ion ESI-MS of the addition of ethylene to a H_2-saturated solution of [**3.4**]$^+$ BF_4^- and $RhCl(PPh_3)_3$ in chlorobenzene. Cone voltage = 10. Inset: isotope pattern for $[RhCl(PPh_3)(\mathbf{3.4})(H_2C{=}CH_2)]^+$ at 945.5 *m/z* present at 2% relative intensity.

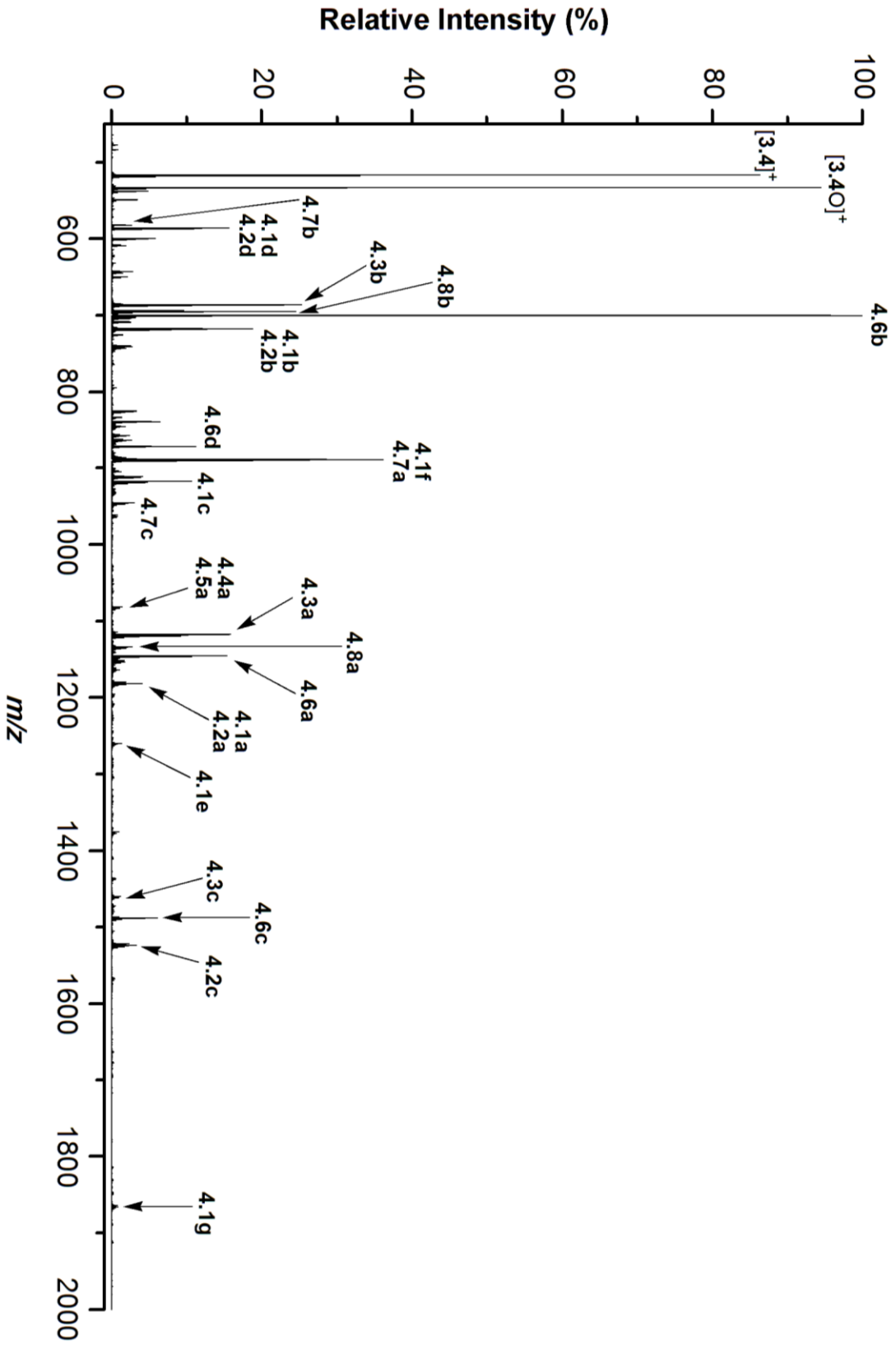

Appendix Figure 14. Positive-ion ESI-MS obtained from a summation of the first five minutes after addition of hex_2SiH_2 to a solution of [**3.4**]$^+$ BF_4^- and $RhCl(PPh_3)_3$. Peak assignments are given in Table 4-1. **4.4b** is visible in the summation of all 144 spectra. Cone voltage = 10 V.

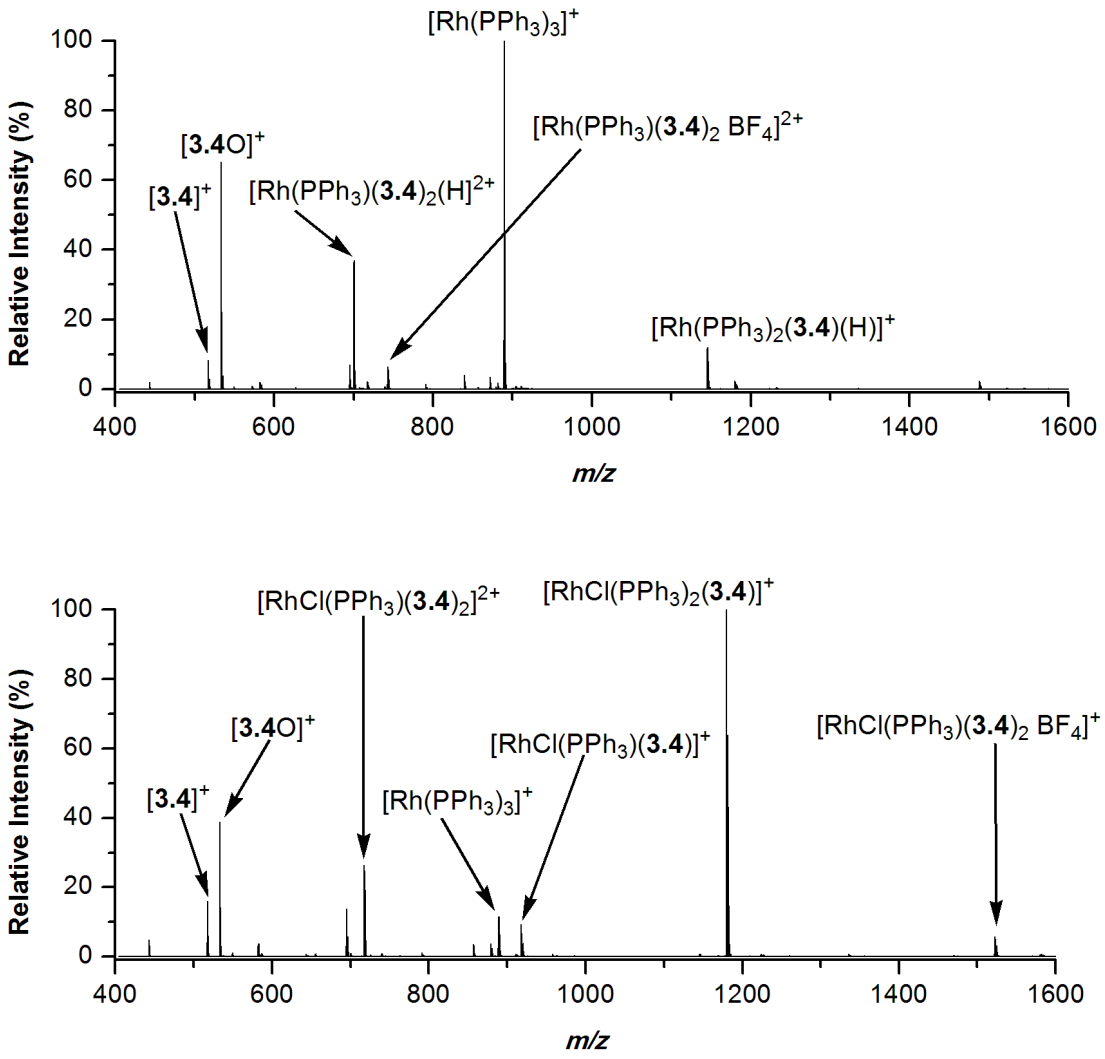

Appendix Figure 15. Positive-ion ESI-MS for [**3.4**]$^{+}$ BF_4^{-} and $Rh(PPh_3)_3(H)$ in chlorobenzene. Cone voltage = 10 V. Top: t = 0; bottom: t = 1 hr.

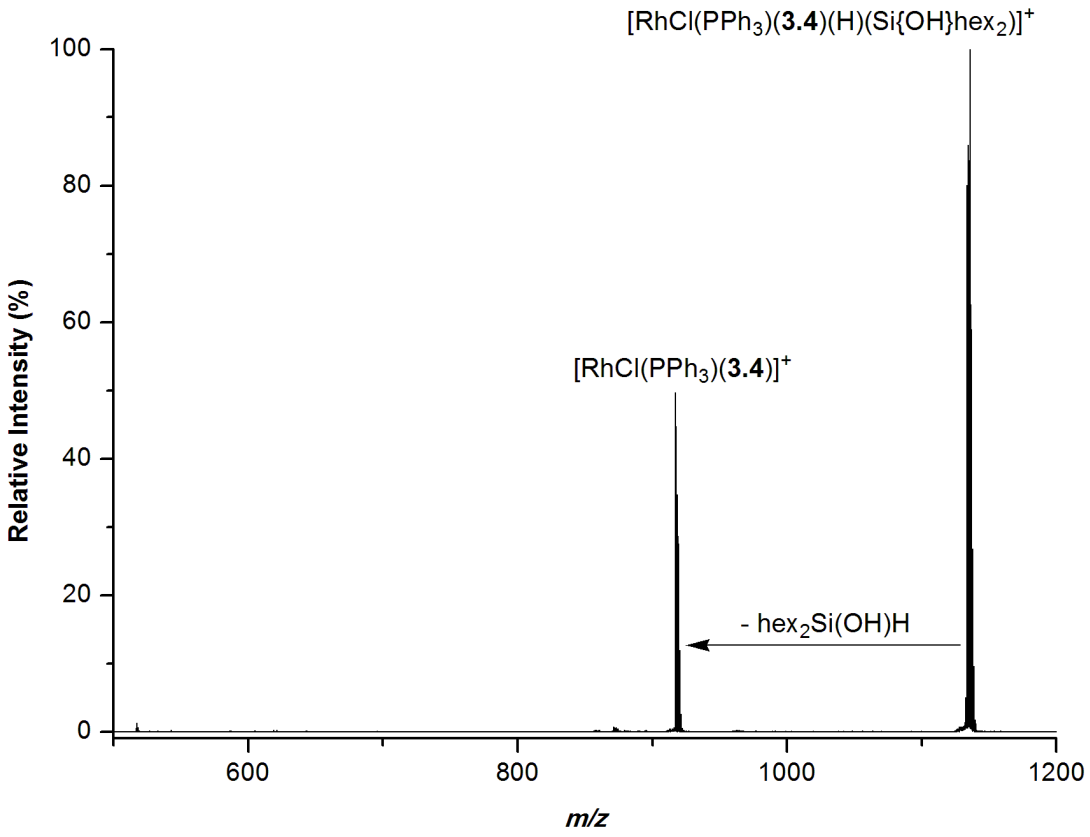

Appendix Figure 16. Positive-ion ESI-MS/MS of $[RhCl(PPh_3)(\mathbf{3.4})(H)(Si\{OH\}hex_2)]^+$. Cone voltage = 10 V and collision voltage was increased from 0 to 50 V.

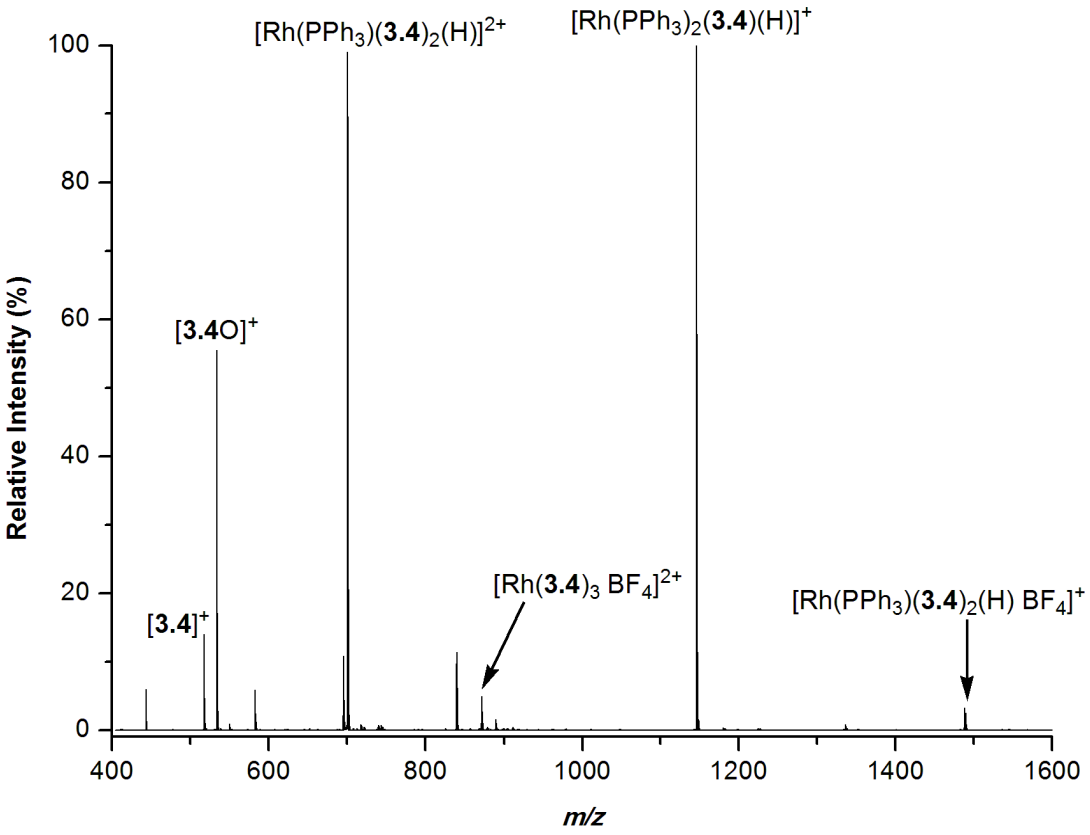

Appendix Figure 17. Positive-ion ESI-MS for $Rh(PPh_3)_3(H)$ and $[\mathbf{3.4}]^+ BF_4^-$ in fluorobenzene. Cone voltage = 10 V.

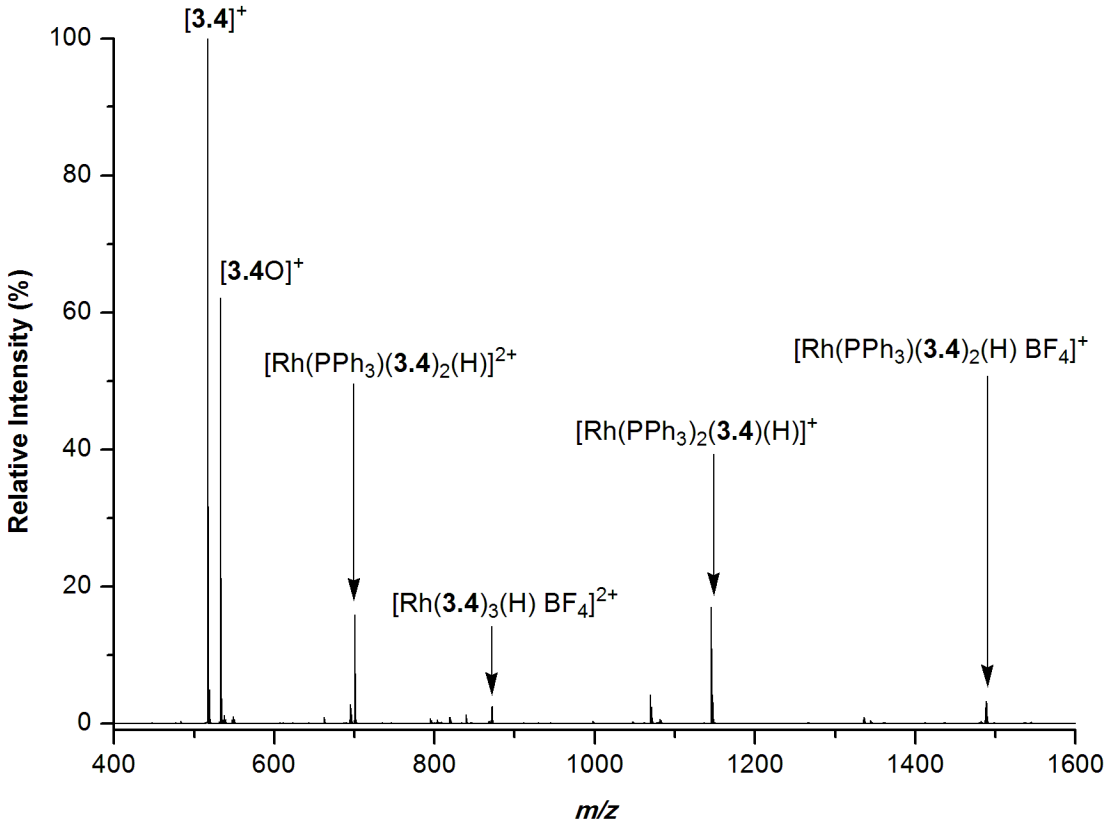

Appendix Figure 18. Positive-ion ESI-MS of the addition of $(hex)_2SiH_2$ to a solution of $[\mathbf{3.4}]^+$ BF_4^- and $Rh(PPh_3)_3(H)$ in fluorobenzene. Cone voltage = 10 V.

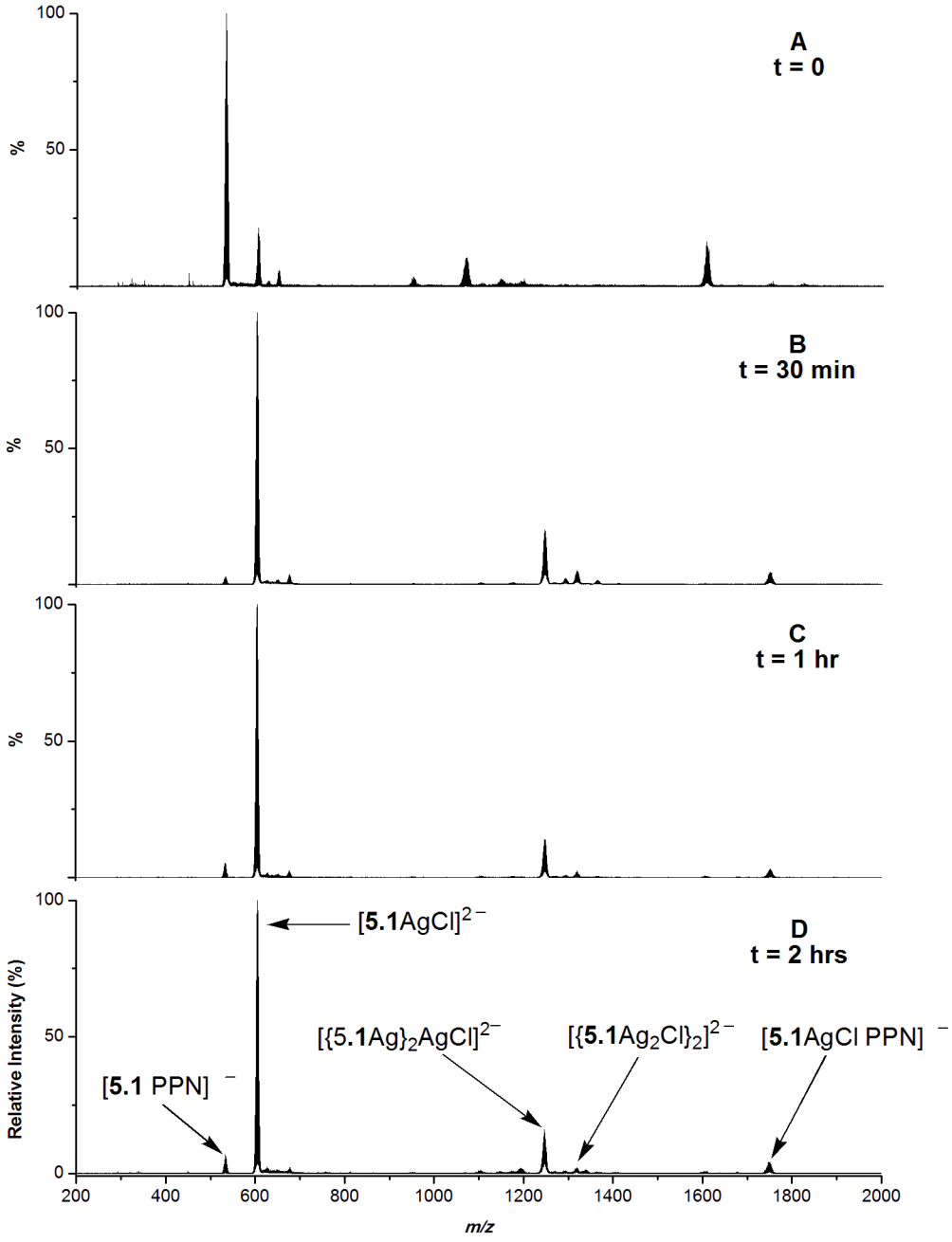

Appendix Figure 19. Reaction profile of [**5.1**]$^{2-}$ and AgCl in THF. ESI-MS spectra were run in CH_2Cl_2. A: t = 0; B: t = 30 min; C: t = 1 hr; D: t = 2 hrs.

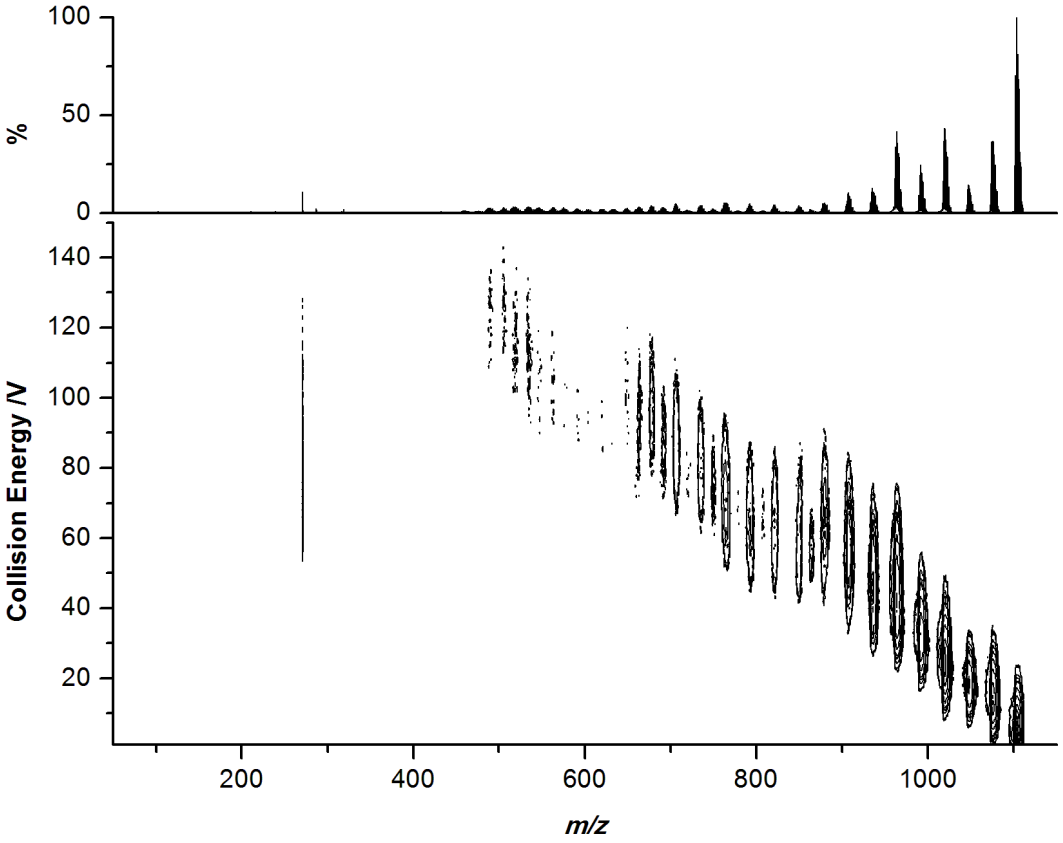

Appendix Figure 20. EDESI-MS/MS for [**5.3** + Na]$^+$ (1103.8 *m/z*) in methanol. Cone voltage = 20 V.

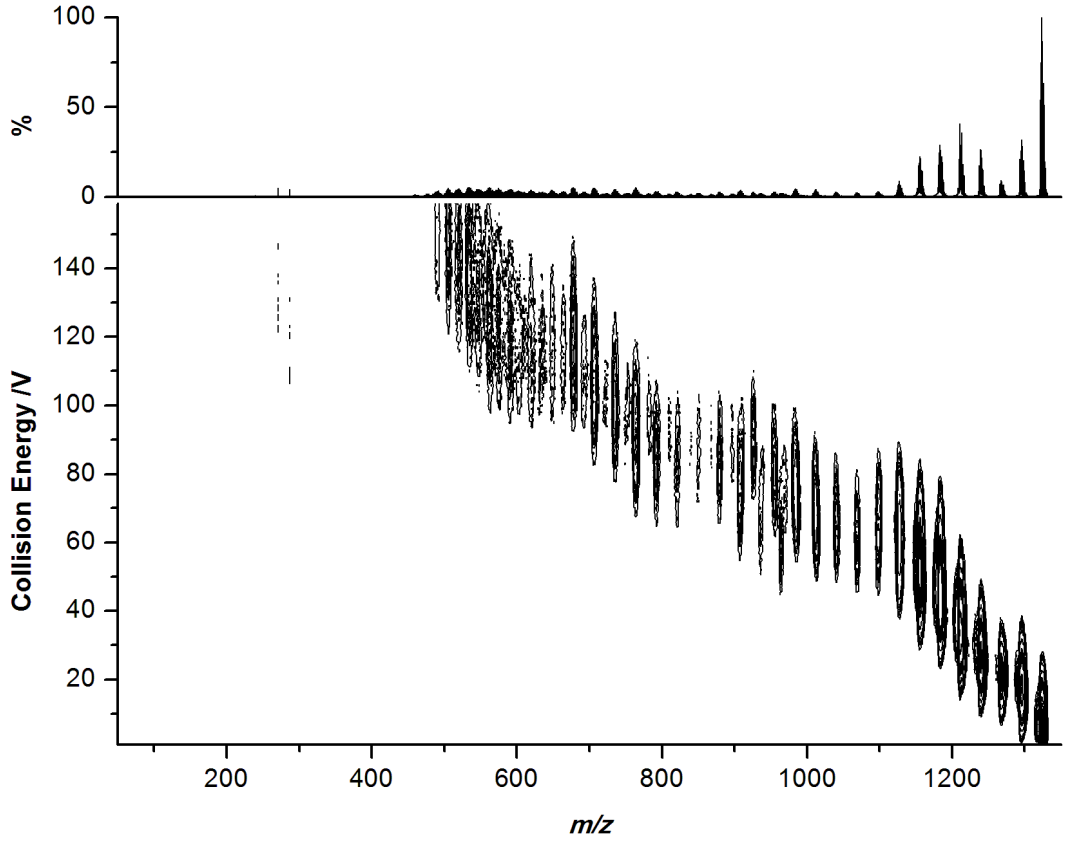

Appendix Figure 21. EDESI-MS/MS for [**5.4** + Na]$^+$ (1323.9 *m/z*) in methanol. Cone voltage = 20 V.